PROGRAMME
FOR
ATMOSPHERIC WATER SUPPLY
(PAWS)

PHASE 2
1987 to 1989
FINAL REPORT

VOLUME 3
Radar Data Interpretation,
Cloud Modelling and
Statistical Considerations

Report to the
Water Research Commission
Pretoria, South Africa

by

CSIR

EMATEK : R C Grosh, G Reuter, M Hodson, C Muller, G Hofmeister

DATATEK: J Galpin

March 1990

133/7/96

ISBN : 0 947447 63 6
SET NO : 0 947447 64 4

CONTENTS

22ga/sgg

1. INTRODUCTION

This report describes the CSIR research contributions to the Programme for Atmospheric Water Supply (PAWS) related to the interpretation of radar data, cloud model output and statistical analyses. A summary of the results of the entire Phase 2 of the Programme can be found in the separate Executive Summary (Volume 1).

II. RAIN MEASUREMENT

Accurate rainfall measurement is crucial to the evaluation of rain stimulation projects. Artificial enhancement of *storm* precipitation is often reported to be on the order of 10 to 20%. Rain measurements that are far more accurate than this figure are obviously desirable, but unlikely to be obtained. Since radar is the main rain measurement tool, the problem is further complicated by the fact that the actual treatment of storms with cloud seeding agents is likely to affect the size distribution and/or phase characteristics of their hydrometeors as radar rain measurement usually assumes a constant drop size distribution (DSD). Consequently, a substantial effort has been made by PAWS to examine the factors which influence radar rain measurement accuracy. These factors include wind, terminal fall speeds, statistical procedures used to relate radar observations to surface rainfall, DSD distribution measurement procedures and gauge sampling requirements. Given that many locations in South Africa and elsewhere have little or no DSD information available a survey and synthesis of existing worldwide DSDs is reported as well. There is also a report describing rainfall in the Carolina study area. This chapter starts with a survey of worldwide reports of radar rain measurement accuracy.

A. RADAR RAIN MEASUREMENT STUDIES

R C Grosh

1. INTRODUCTION

Observations by the PAWS 5 cm radar have provided the most useful means of evaluating the experimental activities. In the future, however, it appears that truly accurate surface rainfall measurements will be required as South African rain stimulation experiments approach a new phase of experimentation; rain measurement over a set area is expected to be necessary shortly. Thus radar rainfall observations must be even more heavily relied on than before and the degree of absolute accuracy available will become much more of an issue. The current report is concerned with the accuracy of typical radar rainfall measurements, such as those suited to determining the hydrologic input to a basin by a horizontally scanning radar.

2. THE ACCURACY OF RADAR RAINFALL MEASUREMENTS

A survey of radar rainfall measurement accuracy from earlier projects was made to provide guidance for what might be expected in an actual field measurement program utilizing conventional weather radars (scanning horizontally). A total of 18 different source articles are summarized in Table 1. Only rain totals for entire storm durations are considered. The number of gauges used for calibration ranged from a few (Wilson, Harrold) to many. (The Florida and Illinois networks each had more than 100 gauges.) The results listed in Table 1 are for both raw measurements (based on only one local Z-R relationship), and for those which have been adjusted by rain gauge measurements from networks of various densities. The results are given in terms of the G/R ratio of gauge (G) to radar (R) rainfall estimates. Absolute values (when available) have been utilized to calculate G/R when the ratio was not given directly in the original article. Absolute values were also used to provide a conservative analysis. Results are intended to depict all important summer rain types. The stratified results of Jatila (1973) and Collier (1983) listed separate

TABLE I RADAR RAINFALL MEASUREMENT ACCURACY ("G/R RATIOS")

	Year	(No Gauges) Z-R	Gauge Adjusted Measurements
1 Aoyagi	1964	1.19	
2 Jones	1966	1.77 (1.39 with 3 Z-Rs)	
3 Huff	1967	1.30	1.12 Adjacent Gauges (AVE)
4 Wilson	1970	1.96	1.59 (1 Gauge) 1.53 (3 Gauges) 1.48 (3G,V)
5 Woodley	1970	1.30 (1.08)	
6 Jatila	1973	1.12 (1.21) Continuous Rain	1.29
		1.43 (0.98) showers	1.25
7 Harrold	1974		1.15 to 1.20 (1 Site, 3 Gauges)
8 Wilson	1974	1.30 (90% of time	
9 "	1975	1.49 with beam <2 km)	1.22 (V)
10 Brandes	1975	1.52	1.18 (Ave G) 1.14 (V)
11 Woodley	1976	1.53 (2.23 showers, 1.69 daily totals)	1.38 (Cluster)
12 Huff	1978	1.55	1.27 (V)
13a Hildebrand	1979	1.87 HIPLEX	1.45 (V) 1.16 (EVAP)
13b	1979	1.37 Illinois	1.15 (V)
14 Wilson	1979	1.63	1.24 (V)
15 Collier	1983	1.33 frontal	.70 (AVE), 1.10 (Domain)
		.79 showers	.63 (AVE), .79 (")
16 Barnston	1983	1.31 Absolute Values (.75 Algebraic Difference)	1.23 (Cluster), .94 (Algebraic)
17 Kiostinen	1984	1.57	1.52 (V)
18 Joss	1984	.86 to 1.17 Best 10 gauges RADAR Albis	
		.66 to 1.45 " " " " Le Dole	
		[.08 to .24 Worst 10 gauges " Albis]	
		[.04 to .31 " " " " Le Dole]	
		Both sites use a vertical projection of ZMAX	
Typically:		-48% Difference 22% N = 19	-25% Difference 20% N = 14

*V = Spatially varying Gauge Calibration used to adjust radar estimate (as opposed to using the average [AVE] of G/R).

ratios for stable rains (frontal/continuous) and showers. Only the case with the largest deviation from 1.0 in each of these two studies were utilized to obtain the average listed at the bottom of the two columns. This was intended to obtain one value thought to best represent showers embedded in stratus as this is most generally representative of heavy summer rains. This was also intended to yield a conservative (high) average value of the ratio.

3. RESULTS

Radars which are uncalibrated via gauges are surprisingly accurate. The average bias is only about 50% ($\pm$20%). Furthermore, rain gauge calibrated radar is within about 25% of the gauge estimates on average ($\pm$20%).

3.1 Cluster Adjustments

The recent thorough analysis by Barnston and Thomas (1983) of the 61 days of FACE data is a good example of the *cluster* calibration approach. The rain data for the six hour period following treatment was the basic analysis unit for their study. The dense (1 gauge per 10 km^2) cluster network of 48 gauges in about 500 km^2 was located within a larger network (13,000 km^2) which supplied final ground truth with another 111 gauges (one every 11.7 km^2). The radar used was a WSR-57 (10 cm wavelength). The use of the cluster of gauges to calibrate the radar lead to a better relationship between the 111 gauges in the network and the radar estimates by improving the slope in the equations relating to two rain measurements from 0.62 to 0.93. The unadjusted radar rain measurements are a bit high for rains below 3 mm, but clearly underestimate the heavier rains. This is probably due to the problem of incomplete beam filling by many relatively small cores and strong rain gradients during the heavy rains. However, the slope approaches one to one with the adjustment, and this problem is largely eliminated by the use of the auxiliary gauges. Thus, the gauge adjustment eliminates the systematic differential bias (underestimates of heavy rains, overestimates of weak rains) from the radar measurements.

Nevertheless, the careful analysis of Barnston and Thomas reveals that the use of the cluster approach to radar gauge calibration actually leads to a slight increase in the random scatter in the relationship between radar and gauge measured rainfall.

This is because when the cluster gauge to radar G/R ratios used to adjust the radar estimates are applied to predict the G/R ratios for the network as a whole, only about 20% of the total network G/R variation is explained. Since the cluster only represented less than 4% of the larger network area, the low representativeness is not surprising. Part of this problem can be viewed as arising because the G/R ratio increases with R, but the correlation is only 0.57. However, G/R ratios increased with range 66% of the time. Therefore, the range dependent beam filling effect is likely to have played an important role in the increased scatter occurring after cluster calibration. The main influence appears to have been the effect of the unrepresentativeness and random nature of the G/R values from the small cluster compared with the ratios from the much larger network which are at increasing range from the cluster.

3.2 Spatially Varying Gauge Adjustments

Thus, Barnston and Thomas concluded that, in general, it is better to calibrate with the distributed gauges throughout the larger network (Brandes' procedure), a technique they did not use themselves, but which has overwhelming intuitive appeal. Koistenen and Puhakka (1981) describe one of the more thorough methods for applying the variable gauge (or G/R) location calibration technique:

1. Calculate the values of the adjustment factor F_g = (G/R) at each gauge location G by dividing the gauge-measured value G by the corresponding radar-estimated value R.

2. Perform a regression analysis by which the range dependence of $\log(F_g)$ is determined. As a result, a symmetrical range dependent adjustment factor field F(r) is obtained.

3. Check the quality of each G/R value by comparing it with the value predicted by the regression model at the same range.

4. Calculate the spacing of rain gauges D(i,j) at each grid point i,j. Determine the filtering parameter field k(i,j) needed in the objective analysis using D(i,j).

5. Analyse individual adjustment factor values to the final grid by using objective analysis. The quality as well as the actual spacing of the observations are taken into account. As a result, a spatially analysed adjustment factor field F(i,j) is obtained.

6. Combine fields F(r) and F(i,j) to give the final adjustment factor field F(i,j) where the relative weights of the component fields are determined by the spatial representativeness of F(i,j). This is estimated from the observed autocorrelation field.

7. Multiply the raw radar measurement field R(i,j) by the final adjustment factor field F(i,j) to get the adjusted radar rainfall.

8. Substitute the objectively analysed rain gauge field in gridpoints where no radar data are available.

The method is very flexible and can provide solutions which range from the uniform but range dependent correction (using F(i,j) set to zero), to Brandes' method (F(r) is set to zero), to raw gauge values depending on subjective and objective quality control thresholds for G/R (to be accepted the G/R point value must be within +/-2 standard deviations, after the linear range correction is applied) and the weighting given to gauge density.

4. CONCLUSION

Uncalibrated weather radar measurements of summer rainfall are likely to be within about 50% of the actual ground truth (gauge) total. However, gauge calibrated radars will be within about 25% of an accurate gauge network value on average. The best means of radar gauge calibration is with a distributed network of gauges throughout the measurement area. The density of the gauges must be determined empirically for each area, but appears to be about 100 km^2 per gauge for storm rain totals in tropical areas.

REFERENCES

AOYAGI J, 1964. Area rainfall amounts obtained by a 3.2 cm radar and a raingage network. World Conf. Radio Meteor., 11th Weather Radar Conference, AMS, Boston, 116.

BRANDES E A, 1975. Optimizing rainfall estimates with the aid of radar. J. Appl. Meteor., 14, 1339-1345.

BARNSTON A D and THOMAS J L, 1983. Rainfall measurement accuracy in FACE: A comparison of gage and radar rainfalls. J. Clim. and Appl. Meteor., 22, 2038-2052.

COLLIER C G, LARKE P R and MAY B R, 1983. A weather radar correction procedure for real-time estimation of surface rainfall. Q. J. Roy. Meteor. Soc., 109, 589-608.

HARROLD T W, ENGLISH E J and NICHOLASS C A, 1974. The accuracy of radar-derived rainfall measurements in hilly terrain. Q. J. Roy. Meteor. Soc., 100, 331-339.

HILDEBRAND P H, TOWERY N and SNELL M R, 1979. Measurement of convective mean rainfall over small areas using high-density raingages and radar. J. Appl. Meteor., 18, 1316-1326.

HUFF F A, 1967. The adjustment of radar estimates of storm mean rainfall with raingauge data. J. Appl. Meteor., 6, 52-56.

HUFF F A and TOWERY N G, 1978. Utilization of radar in operation of urban hydrologic systems. Preprints: 18th Conference on Radar Meteorology. AMS, Boston, 437-441.

JONES D M A, 1966. The correlation of raingage network and radar detected rainfall. Proceedings: 12th Conference on Radar Meteorology, AMS, Boston, 204-207.

JOSS J and KAPPENBERGER G, 1984. Quantitative measurement of precipitation with radar in an alpine country. Preprints: 22nd Conference on Radar Meteorology. AMS, Boston, 270-275.

KOISTINEN J and PUHAKKA T, 1981. An improved spatial gauge-radar adjustment technique. Preprints: 21st Radar Meteorology Conference, AMS, Boston, 179-186.

KOISTINEN J and PUHAKKA T, 1984. Can we calibrate radar by raingages. Preprints: 22nd Conference on Radar Meteorology. AMS, Boston, 263-267.

JATILA E and PUHAKKA T, 1973. Experiments on the measurement of areal rainfall by radar. Geophysica, 141-149.

WILSON J W, 1970. Integration of radar and raingauge data for improved rainfall measurement. J. Appl. Meteor., 9, 489-497.

WILSON J W and POLLOCK D M, 1974. Rainfall measurements during hurricane Agnes by three overlapping radars. J. Appl. Meteor., 13, 835-844.

WILSON J W, 1975. Radar-gage Precipitation Measurements during the IFYGL. CEM Rept 4177-4546. The Centre for the Environment and Man, Hartford, Conn., 121pp.

WOODLEY W L, 1970. A raingauge evaluation of the Miami reflectivity rainfall rate relation. J. Appl. Meteor., 9, 242-257.

WOODLEY W L, OLSEN A R, HERNDON A and WIGGERT V, 1975. Comparison of gage and radar methods of convective rain measurements. J. Appl. Meteor., 14, 909-928.

06/22ga/sgg

B. RADAR RAIN MEASUREMENT, FALL SPEED AND WIND EFFECTS

M Hodson

1. INTRODUCTION

The objective of the work undertaken in this study was to examine quantitatigvely the meteorological components which degrade radar rainfall measurements. This report is a continuation of that presented in December 1988. It has four sections. The first describes the theoretical effect of different drop terminal velocities and horizontal winds on rainfall rates in a rain shaft. The second section describes some results obtained from a numerical model based on this theory. The third section discusses some of the measurements that were made on rainfall and shows how these related to the numericalk model. The final section summarised those factors which degrade radar rainfall measurements and discusses the requirements for more accurate radar rainfall measurements.

2. THEORY

There are several factors which affect the comparison between radar derived rainfall measurements and those made using rain gauges. The most important of these are as follows:

a. The radar reflectivity rainfall relationship, that is, the Z-R relationship.

b. Evaporation.

c. The downdraught in the rain.

d. The terminal fall velocity of the raindrops, either on their own or combined with a horizontal wind.

We shall deal with the first three of these in the final section of this report. The effect of the fourth is dealt with in the remaining sections of the report.

2.2 No Horizontal Wind

In order for rain to have the same drop size distribution at all altitudes in a rain shaft, the drop size distribution at the top of the rain shaft must remain the same through the fall time of the smaller drops to the ground. Because this is of the order of many minutes, it is unlikely to occur in rain. Any change in the rain rate at the top of the rain shaft takes many minutes to propagate throughout the rain shaft, therefore a uniform drop size distribution is unlikely to occur in rain. We look at the mathematics that describes the changes in the rainfall rate with altitude in this section assuming that there is no horizontal wind.

Atlas and Ulbrich (1974) have published a mathematical expression for the rainfall rate assuming an exponential drop size distribution. We have assumed a drop size distribution of the form

$$N = f(D) \quad , \tag{1}$$

where D is the drop diameter and N is the number of drops per cubic metre. We assume that drops of diameter larger than D_{max} break up. Then the rainfall rate obtained by substituting this in the expression given by Atlas and Ulbrich is

$$R = (\pi/6 \times 10^{-6}) \times 3600 \times \int_0^{D_{max}} D^3 \times f(D) \times V(D)dD \ , \tag{2}$$

where V(D) is the drop fall velocity as a function of diameter. This equation assumes that no vertical air currents are present. If the drops fall from heights H (metres), then the time t (seconds) for a drop of diameter D_i to reach the ground is

$$t = H/V(D_i) \quad . \tag{3}$$

Consider the case when there is a sudden onset of rain, namely a step function at time t_0 and at height H. Before time t_0 there is no rain and after this time the rain is given by Equation (2). At time t_0 there are no drops at the ground. Because the largest drops have the greatest fall speed, the first drops to reach the ground do so at the time given by

$$t = t_0 + H/V(D_{max}) \quad . \tag{4}$$

Drops of smaller diameters begin to reach the ground together with the larger drops at the time given by

$$t = t_0 + H/V(D_i) \quad . \tag{5}$$

This gives a drop spectrum at the ground that ranges from diameters D_i to D_{max}. The corresponding rainfall rate at the ground, R_{gp}, is then

$$R_{gp} = (\pi/6 \times 10^{-6}) \times 3600 \times \int_{D_i}^{D_{max}} D^3 \times f(D) \times V(D)dD \quad . \tag{6}$$

D_i can be obtained as a function of time from Equation (5). Then integration of Equation (6) will give R_{gp} as a function of D_i. Eliminating D_i from these two relationships we get the rainfall rate at the ground as a function of time. Because the drop velocity tends to zero as the diameter tends to zero, R_{gp} will tend to equality with R as t becomes larger.

If we consider a negative step change aloft arising from the sudden cessation of the rain, the maximum drop diameter after the step will be D_i and the minimum will be 0. When there is no horizontal wind, the rain rate at the ground is, using equation (6),

$$R_{gn} = (\pi/6 \times 10^{-6}) \times 3600 \times \int_{0}^{D_i} D^3 \times f(D) \times V(D)dD \quad . \tag{7}$$

A pulse of rain (a sudden onset, a steady rate then sudden cessation) will be completely described at the ground by equations (6) and (7) during its three stages.

The rain accumulated over the complete duration of precipitation at the ground (T_R) is

$$\int_0^{T_R} R_{gp}dt + \int_0^{T_R} R_{gn}dt = \int_0^{T_R} Rdt \tag{8}$$

These two integrals can be evaluated via Equations (6) and (7) to obtain the total rainfall aloft. This shows that the accumulated rain at the ground equals that aloft provided there is no horizontal wind.

2.2 The General Case

In general, the horizontal wind changes with time and height. The horizontal distance travelled by a drop as it falls to the ground is no longer independent of time, therefore the drop numbers at each point on the ground do not have a fixed temporal and spatial relationship to the step function change aloft. The rain rate at the ground will be different along the direction of the wind, and can only be obtained if the horizontal wind speed is known as a function of time and height. Accumulating the rain at the ground at a point no longer makes it equal to the accumulated value aloft. The only way to capture all the drops aloft and equate them to all the raindrops at the ground is to accumulate the areal rain aloft and at the ground over an area large enough to account for the variability in the horizontal wind.

3. NUMERICAL MODELS

We have used a simple numerical model to illustrate further the "smoothing" effects of the different terminal velocities on the difference in rainfall rates aloft and at the ground. As an example let us take some rainfall rates that occurred 7 minutes after the start of a record that was taken on 22 January 1988. These have been plotted in Figure 3 in last year's report, and have been applied as input to our model. The model input rainfall at 600 m altitude as well as the resultant rainfall rates at the ground are shown in Figure 1. This comparison indicates that differential terminal velocities have reduced the peak rain rate at the ground by 19% compared with the input. If this pattern of input rainfall

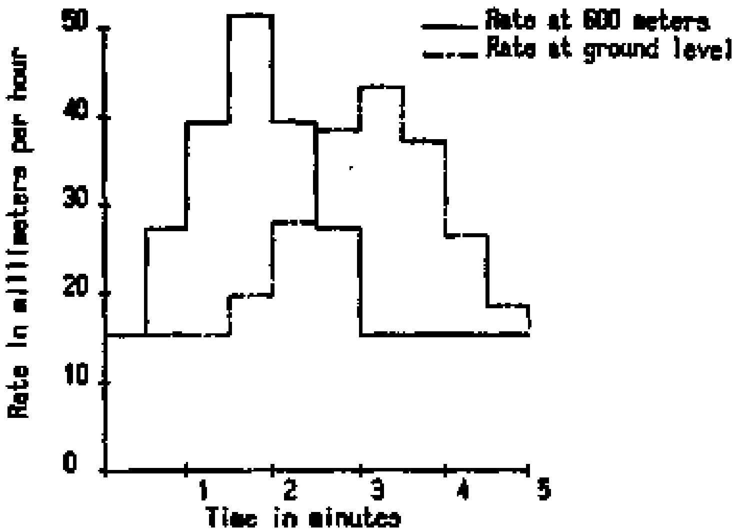

Figure 1 The effects of differential drop velocity on rain rates and reflectivity for rain falling from 600 meters with no horizontal wind.

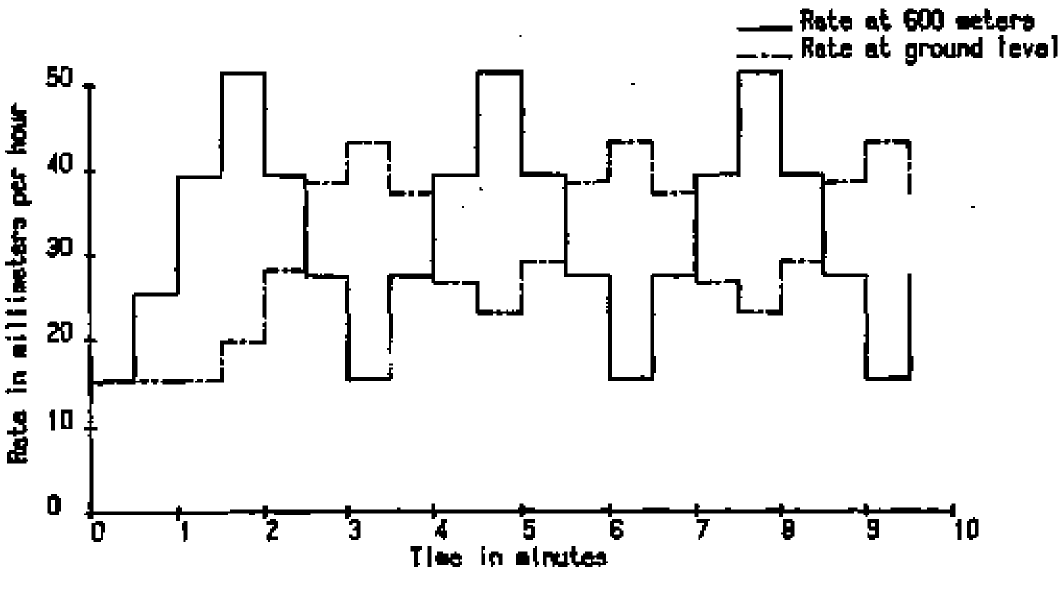

Figure 2 The effects of differential drop velocity on rainfall rates at the ground with the repetitive rainfall rates shown as the input at 600 meters.

were repetitive, then we would obtain the rainfall plotted in Figure 2. Here, the minimum value of the rainfall at the ground is 50% greater than the minimum measured aloft.

If the rainfall did vary in space and time as shown in Figure 3 for example, then very different results would have been obtained at the ground as Figure 4 shows. Here, the drop diameter groups would have been completely separated in space and time at the ground. This shows how difficult it is to sample the rain at the ground adequately with a single rain gauge under these conditions.

With rainfall aloft varying in time and along the direction of the wind, a numerical model would obtain the resultant rainfall at the ground if the horizontal and vertical wind speeds are known. When the wind is variable, integration would have to be done in time and along the direction of the wind to ensure that the same groups of raindrops are being compared. In practice, with winds varying in two horizontal dimensions, comparisons should be done by integrating in time and over an area.

4. EXPERIMENTAL RESULTS

The equipment we used for our experimental work restricted the rainfall records we could use when making comparison between gauge and radar measurements. Figure 5 illustrates the effects of strong horizontal winds on the rain we measure aloft, causing it to fall well outside the small area at the ground where the gauges were situated. We present two records here, one with a low horizontal wind speed and the other with a high wind speed.

The rainfall record taken on 9 February 1988 had a low enough horizontal wind speed (<10 km/hr) to enable it to be used for radar and rain gauge rainfall comparisons. Figure 6 shows the wind speed and direction during the record. Figure 7 is a plot of the high resolution rain gauge measurements at the ground and the radar rainfall measured at 360 m altitude. This result clearly demonstrates the smoothing effect of the raindrop terminal velocities on the rain rate at the ground.

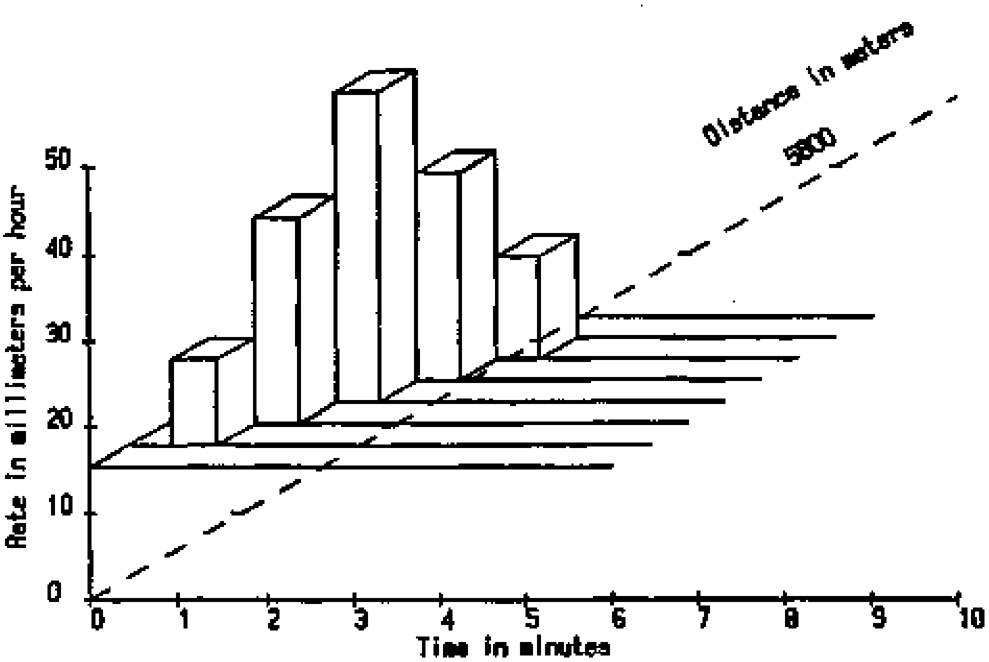

Figure 3 Rainfall input surface for an 8 meter per second horizontal wind - rainfall varies with position and time.

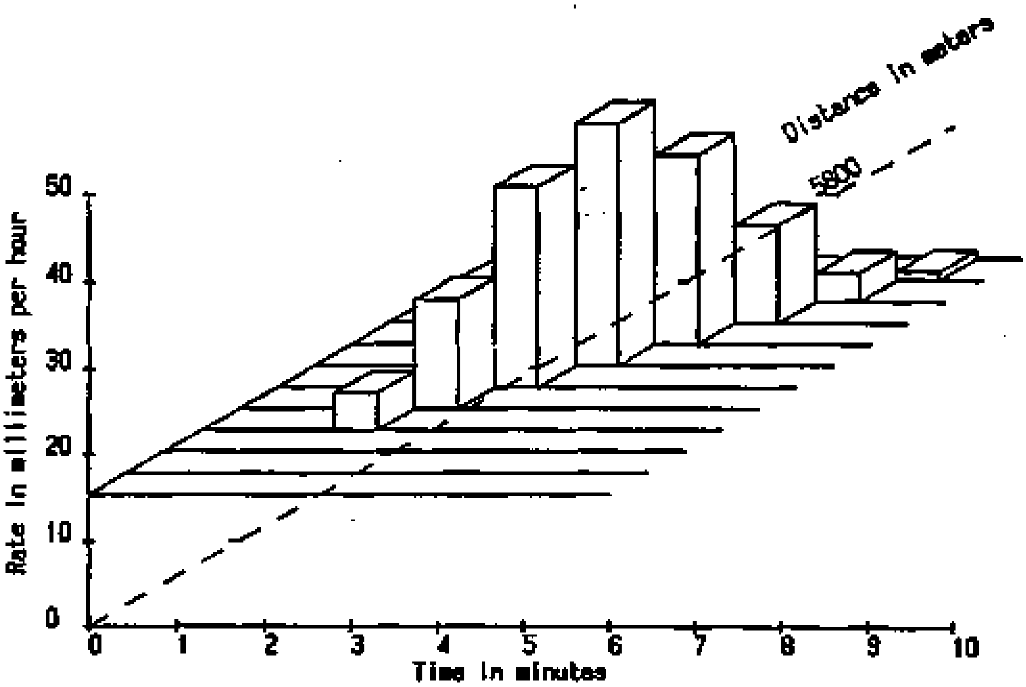

Figure 4 Rainfall output surface for the input given in figure 3.

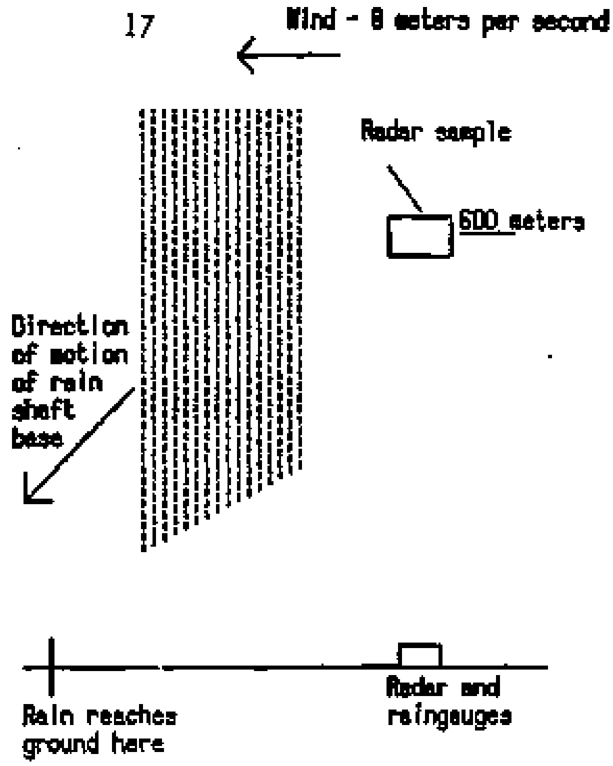

Figure 5 Direction of movement of rain shaft over the radar when there is a horizontal wind present.

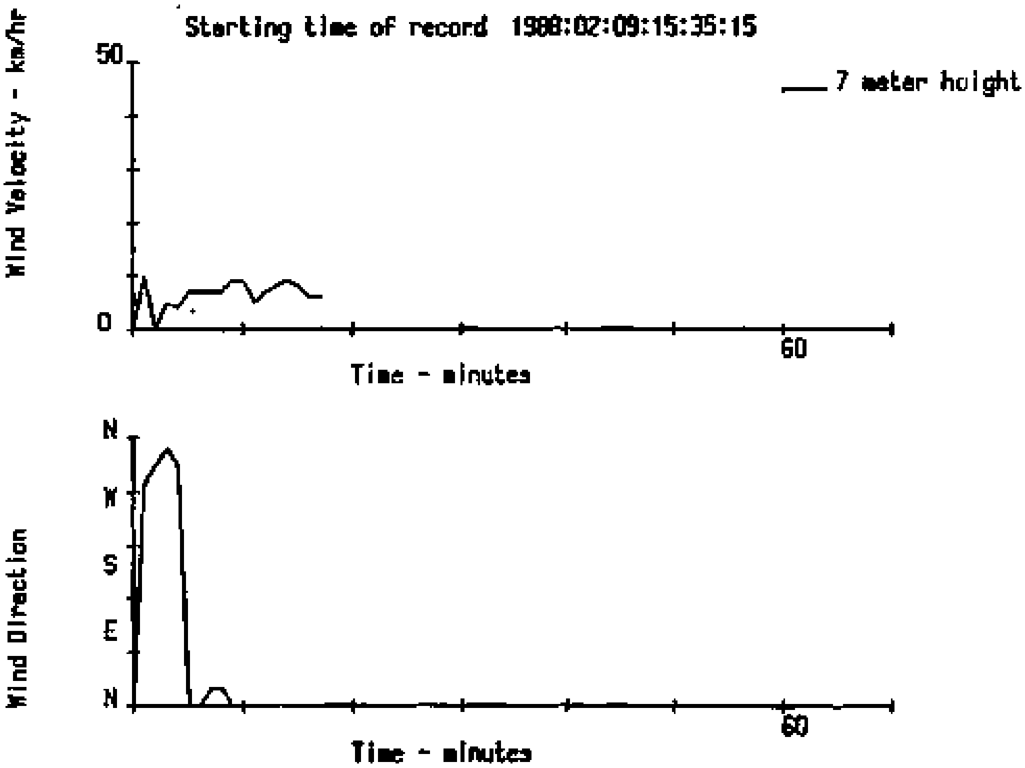

Figure 6 Wind velocity and direction for 9th February 1988.

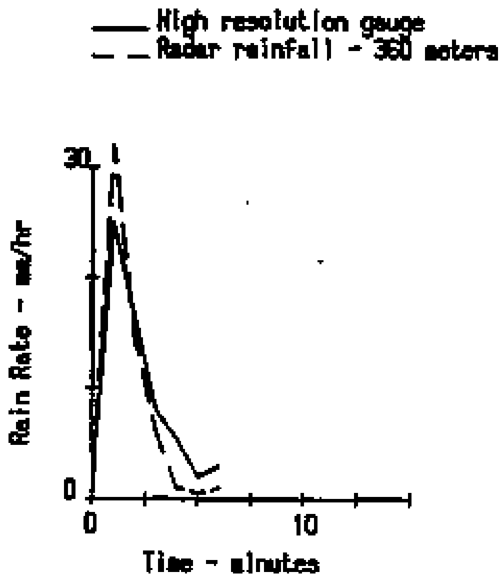

Starting time of record 1988:02:09:15:35:15

Figure 7 A comparison of gauge measured rainfall with radar rainfall at 360 meters altitude for 9th February 1988.

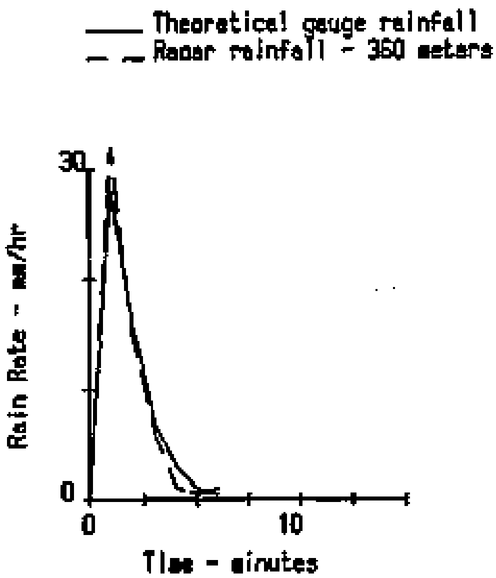

Starting time of record 1988:02:09:15:35:15

Figure 8 A comparison of theoretical values of rain at the ground with radar rainfall at 360 meters altitude on 9th February 1988.

Figure 8 also shows the smoothing. Here the rate expected at the ground was derived from the drop size distributions at 360 m altitude via the model. The rates have been corrected for the measured downdraught. When we accumulate the rainfall over the 6 minutes of the record, we get 1 mm for the gauge value and 0.94 mm for the radar record.

A record taken on 22 January 1988 is used to illustrate the effect of a strong horizontal wind on the comparison of radar and gauge measurements. Figure 9 is a plot of the rainfall measured at the ground during this recording period and Figure 10 is a plot of wind speed and direction at 7 m altitude. To summarise the many drop size distributions obtained during this record, the rainfall rate aloft is plotted from them in Figure 11. For the purposes of discussion, this is divided into three time periods. During period A, the radar showed a burst of very heavy rainfall lasting 1.5 minutes with a peak of 66,8 mm per hour. Very little rain fell into the gauges during this period, some of the gauges registering a rate of 6 mm per hour. This shows that the rain moved through the radar beam and reached the ground outside the gauge network.

During period B, the radar and the gauge records showed considerably better agreement. In the last half of period C, there was fairly steady rainfall of 25 mm per hour with different gauges showing some fluctuation about this value. The radar records had an average value which was lower than this. Here it seems as though the radar was recording the edge of a rain shaft and the gauges were measuring in the rain shaft.

Accumulating the rainfall over the total time of the record, we get values of 11.68 and 11.9 mm for altitudes 360 and 600 m, respectively. The rain gauge records for gauges 5, 6 and 7 have 8, 8.4 and 8 mm, respectively. Accumulating the rainfall amount aloft in the peak at the beginning of the storm gives values of 1.7 and 2 mm, respectively. This accounts for a considerable portion of the difference between the accumulated values for the gauges and the radar.

5 COMMENTS AND CONCLUSIONS

A. The theoretical and experimental results described in the report show the effect of the drop velocity and horizontal winds on the comparison

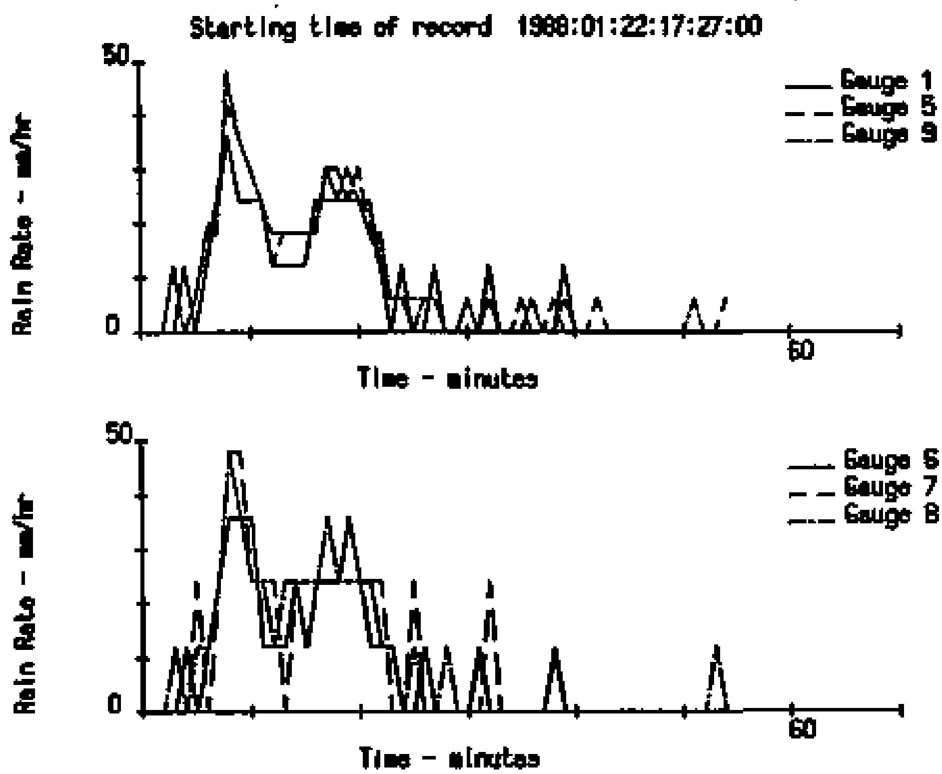

Figure 9 Tipping bucket rainfall records for 22nd January 1988.

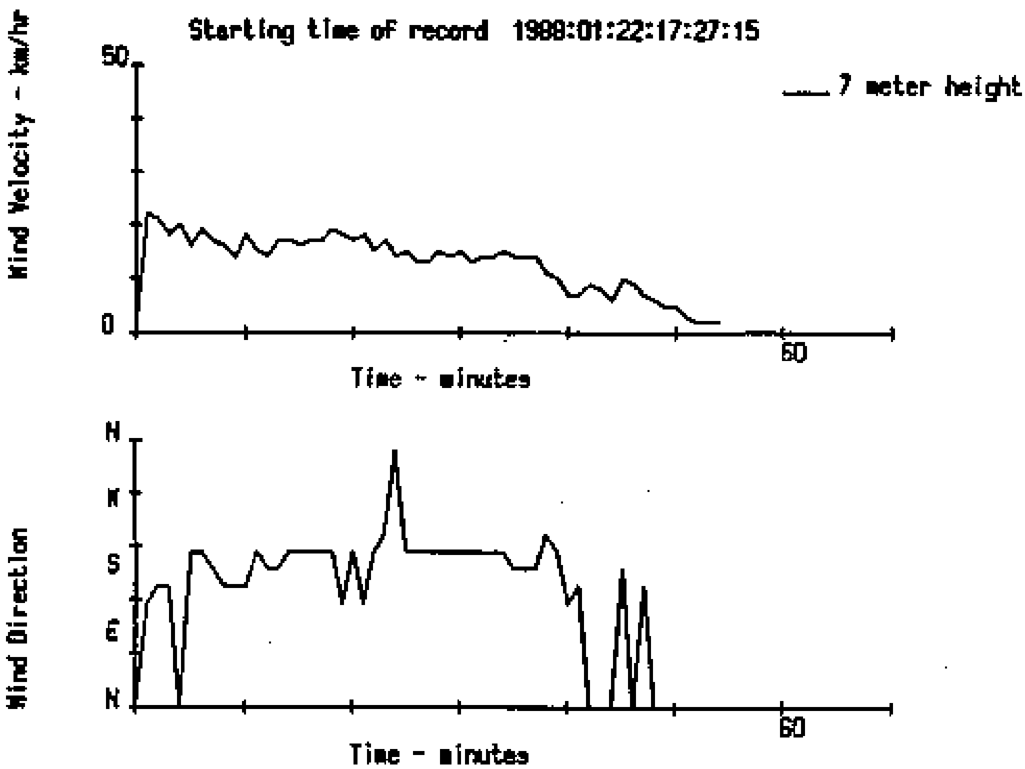

Figure 10 Wind velocity and direction for 22nd January 1988.

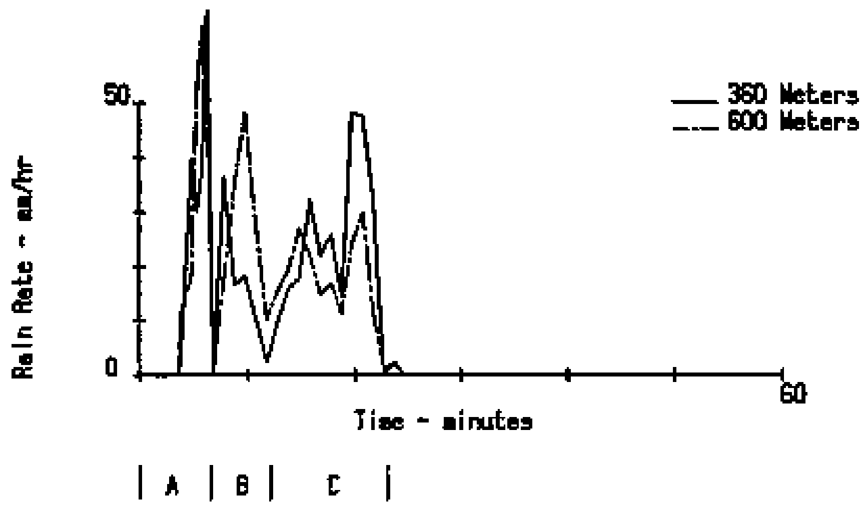

Figure 11 A plot of the rainfall rate at 360 and 600 meters altitude for 22nd January 1988.

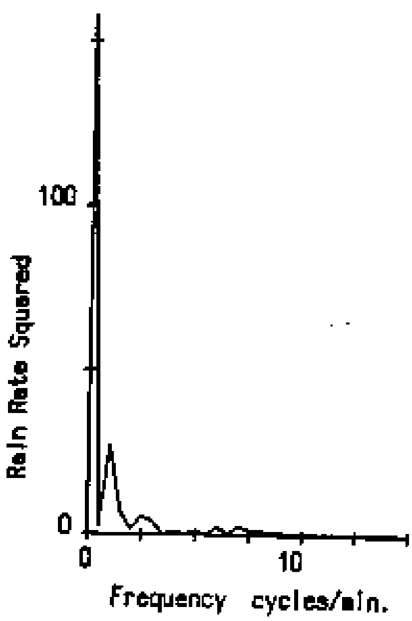

Figure 12 Frequency spectrum of rain rate values derived from figure 13.

of rainfall measurements aloft and at the ground is essentially a smoothing (i.e. ground peaks and valleys are reduced). They also show that the time integral of the rain rates at the ground and aloft are equal under special conditions. However, in the most general case complete theoretical agreement between radar measurements aloft and gauge measurements at the ground is only possible when the time-area integral of the rain is compared aloft and at the ground.

B. If we are to compare the time-area integrals aloft and at the ground, several problems relating to this comparison must be addressed. These are:

a. What is the smallest area that can be compared successfully?
b. How often should the rainfall be sampled by the radar?
c. What should the spatial resolution of the radar be in order to obtain the most accurate rainfall measurements?

Closely related issues have been studied by Zawadski (Calheiros and Zawadski, 1987). If we calculate the trajectory of a raindrop as it falls from 600 m altitude with an 8 m per second horizontal wind then, in the worst case, only 50% of the rainflux through a 2 km square at this altitude falls on a corresponding 2 km square at the ground. Conclusions based on such conditions require that we compare results over 36 km^2 if 85% of the rainflux aloft is to fall on the same area at the ground. Under less severe conditions the area can be considerably reduced and where the horizontal winds are less than 5 km per hour, a single rain gauge is adequate.

The radar measured rates in Figure 11 for 360 m altitude have been used as input to a Fourier transform to obtain the spectrum shown in Figure 12, in which the square of the rate is plotted against frequency in cycles per minute. This figure has a dominant harmonic at 1 cycle per minute. On this evidence, the Nyquists theorem indicates that this particular record should be sampled every half minute. However, this record was taken over an area of 3600 square metres and it is possible that a larger area could tolerate a greater time interval. Again, this should be subjected to experimental verification.

The best possible spatial resolution for the radar should be used in order to obtain good integrated values of rainfall over the areas being compared and to minimise the effect of inadequately filled radar beams.

C. If we eliminate sampling errors arising from horizontal winds and drop fall speeds when comparing gauge and radar measurements by comparing areal rainfall, there still remains the sources of degradation in the radar measurements mentioned in section 2a, b and c. Corrections for evaporation can be made if the temperature and humidity of the atmosphere in the vicinity of the rainfall is known. The downdraught in the rainfall cannot be measured by a conventional radar but requires a multiple Doppler system. Estimating corrections for this requires further investigation.

6. REFERENCES

ATLAS D and ULBRICH C E W, 1974. The physical basis for attenuation-rainfall relationships and the measurement of rainfall parameters by combined attenuation and radar methods. J. Rech. Atmos., 8, 275-278.

CALHEIROS R V and ZAWADSKI I, 1987. Reflectivity-rain relationships for radar hydrology in Brazil. J. Clim. Appl. Meteor., 26, 118-132.

C. THE HIGHLY NON-LINEAR ASPECTS OF Z-R AND VT-Z CAUSED BY RAINDROP TERMINAL FALL SPEEDS

R C Grosh

ABSTRACT

The standard relationships which have been widely used in the past to apply radar measurements of reflectivity (Z) to estimate rainfall rate (R) and the terminal fall speed (VT) of ensembles of raindrops are essentially incorrect. This is because both are theoretically derived from an overly simplified relationship relating the terminal fall speed of individual raindrops ($V_t(D)$) and their diameter (D). Furthermore, an infinite drop size distribution (DSD) is assumed. Thus, when regression is applied to obtain empirical relationships between Z and R or VT, such as when measurements of the DSD from an experiment are integrated, it is standard procedure to seek only simple log-log relationships. For example, the classic Z-R relationship is in the power law form, $Z = aR^b$, with a and b constants. The most well-known Z-R case, that of Marshall and Palmer, $Z = 200R^{1.6}$, was obtained by regression, essentially (MP, 1948). The most well-known VT-Z case, $VT = 3.8Z^{1/14}$, was obtained via a theoretical derivation utilizing a crude power law for $V_t(D)$ (Rogers, 1964). However, more recent empirical analyses such as those utilizing radar and rain gauge cumulative distributions have found that the Z-R relationship may be very highly non-linear in log-log coordinates (Calheiros, 1987).

The present paper theoretically demonstrates that a strong form of non-linearity is introduced into the relationships with Z as soon as $V_t(D)$ is correctly specified. In particular, the slope of the Z-R relationship (in log-log coordinates, b) is not constant, nor are the slopes of the VT-Z relationships. Explicit regression and theoretical forms are derived from the more realistic non-linear cases. Furthermore, the additional non-linearity which enters the problem when the DSD is truncated to reflect even more realistic conditions is also described.

1. INTRODUCTION

Most earlier research on the Z-R and VT-Z relationships has focused on the impact of differences in the observed DSD (Aoyogi, 1968; Joss and Waldvogel, 1968; Fujiwara, 1965; Mueller 1966; Ulbrich, 1983; Willis, 1984). For example, Battan (1973) lists about 70 empirical Z-R relationships based on different DSDs, all published before 1971. These are all in the simple power law form, which in turn implicitly assumes a power law form for $V_t(D)$, and it is this which will be shown to be erroneous. However, much of the difference between these "linear" Z-R relationships appear to be mainly the result of sampling problems in estimating the DSD. More recent investigations have explored the possibilities of fitting gamma functions to the observed DSD and investigated the affect of truncation of the DSD on the associated Z-R relationship (Ulbrich, 1983), but once again only the power law form for Z-R and $V_t(D)$ were examined so Ulbrich does not show the impact of the non-linear aspects of $V_t(D)$ in log-log coordinates. Another reason for taking a different approach from Ulbrich and the earlier researchers, however, is the finding of Joss and Gori (1978) that when DSDs are integrated over a sufficient volume of data (about 500 minutes of distrometer observations or a sample volume of about 1000 m^3) that an inverse exponential DSD is closely approached. Thus, the simple Marshall and Palmer (1948) form for the DSD has stood the test of time because it has usually appeared to be essentially accurate (Merceret, 1974; Joss and Gori, 1978). Though variations in the small drop region are often observed (Mueller, 1966; Srivastava, 1967) these are usually not of great importance to most radar calculations. Nevertheless this will be re-examined here also. However, the impact of the largest drops will be shown to be the most dramatic.

It should also be noted that recent research has suggested that above a liquid water content of about 1 g/m^3 that some important details of the Marshall-Palmer DSD formulation may be in error (Srivastava, 1971; Hodson, 1986), i.e. it appears that the slope of the DSD may be constant for high liquid water contents (and not a function of R). This would require that VT also be constant (e.g. with respect to LWC) for these conditions. However, further observations appear to be required to confirm Hodson's finding, particularly for the rarer high liquid contents.

Consequently, it is assumed here that the inverse exponential DSD function popularized by Marshall and Palmer is basically correct and that the primary variations from it are usually in the form of missing drops at either the small or large drop end of the spectrum.

There appear to have been only a few explicit attempts at non-linear description of radar relationships for R and VT (in log-log coordinates), and these attempts are mostly not in the widely available refereed journals. These attempts also do not explicitly identify the cause of the severe non-linearity as being attributable to V_t (e.g. Jones, 1956). Consequently, this topic, in spite of its fundamental importance, has received little attention.

The earliest report to refer to strong Z-R non-linearity appears to have been the well-known but in-house research report made by Jones in 1956 at the Illinois State Water Survey. This shows erroneous overestimates of R would result from the use of a "linear" Z-R relationship ($Z = 398R^{1.35}$) fit to his data when compared to his more accurate quadratic fit, $\log Z = 2.569 + 1.317 \log R + 0.072(\log R)^2$.

For first order (over-)estimates of R = 1, 10, 25, 50, 100 and 150 mm/hr, the corresponding more accurate non-linear estimates were 1, 9.7, 22.5, 40.9, 75.0 and 104.8 mm/hr Thus, the error becomes significant (>10%) for R = 25 mm/hr and exceeds 40% for R over about 100 mm/hr. Jones made the second order fit after plotting his DSD observations of Z and R on a log-log graph and noticing that the relationship appeared to curve. He did not investigate the cause of the curvature and a decade later there was still no comment on the cause of this complication when Fujiwara (1965) summarized the massive body of DSD observations accumulated at the Illinois State Water Survey and elsewhere. The measurement of the DSD was then the principal focus of attention (Mueller, 1966; Diem, 1966) and this trend continues through the present (Joss and Waldvogel, 1968; Knollenberg, 1976; Willis, 1984; Cunning and Sax, 1977; Jatila and Harju, 1975; Breuer and Kreuels, 1976; Jorgensen and Willis, 1982; and Ulbrich, 1983). Occasionally, subsequent Z-R investigations to Jone's reported either different Z-R relationships for different ranges of Z (or R), (e.g. Shupiaskii, 1957; Doherty, 1963; Cunning and Sax, 1977; Austin, 1981) or would list corresponding averages (or distributions) of Z and R pairs that were clearly not linear when plotted (Diem, 1966; Breuer and Kreuels, 1976; Stout and Mueller, 1968; Calheiros, 1982), but there was a distinct lack of discussion regarding the cause. However, even by 1966 the need for a highly non-linear fit for $V_t(D)$ was beginning to receive some attention from the radar community (Clark and Moyer, 1966; Imai, 1964). Later, the microphysics community provided highly accurate fits for $V_t(D)$ (Foote and du Toit, 1969), but these tended to be clumsy and it was only in 1968 and 1971 that Aoyagi and Lhermitte derived highly non-linear expressions for VTZ (as functions of Z/N_c or Z) which were caused by an accurate fit to $V_t(D)$ and still much later (1981) when the crucial Z-R relationship was finally dignified with an explicitly severe non-linear expression by Uplinger. However, the papers of Aoyagi and Lhermitte were not very explicit on the form of the VTZ relationship, perhaps because of the more complicated algebra required to deal with the multi-term $V_t(D)$ laws they were applying. Worse yet, Uplinger's Z-R paper, though based on an accurate and far more convenient single term $V_t(D)$ expression, had several glaring errors in both logic and the choice of constants and came to an erroneous conclusion. Moreover, these three papers were never published in the refereed literature. It therefore remained for Willis (1984) to explicitly derive an accurate highly non-linear expression for VTZ which accounted for $V_t(D)$ properly. However, in the light of Uplinger's failure, neither a proper expression nor derivation appears to have been presented for the highly non-linear Z-R relationship. Also, the severe effects of truncating the DSD on the non-linear forms of all these equations has remained unexamined.

2. NON-LINEAR ASPECTS

Two approaches were utilized to investigate the true relationships between VT, R and Z, numerical and analytic integration.

Numerical Integration

Numerical integration was applied to calculate Z, R and the reflectivity and mass weighted terminal fall speeds (VTZ and VTM). Integration steps were $\Delta D = 0.5$ mm. Liquid drops were assumed to be distributed in an

inverse exponential form similar to that found by Marshall and Palmer (1948) $N(D) = N_o e^{-\lambda D}$, with $N_o = 0.08$ cm^{-4}.
The variables are theoretically given by

$$Z = \int N(D)\, D^6\, dD \quad (1a)$$
$$R = \int V_t(D)\, N(D)\, D^3\, \pi/6\, dD \quad (1b)$$
$$VTM = \int V_t(D)\, N(D)\, D^3\, dD/\ N(D)\, D^3\, dD \quad (1c)$$
$$VTZ = \int V_t(D)\, N(D)\, D^6\, dD/Z \quad (1d)$$

with the integrations assumed to extend from $D = 0$ to ∞. Rayleigh scattering is also assumed. Under these conditions analytic solutions in terms of the gamma function and λ may be obtained for each of the integrals and thus R, VTM and VTZ can all be given as functions of Z (after substitution), if an integrable analytic function is used to represent $V_t(D)$. In the past this has usually taken the form, $V_t(D) = c\, D^d$, a crude approximation irrespective of the values of the constants. In the present work, therefore, tabular values obtained directly from the measurements of Gunn and Kinzer (1947) and Beard (1977) were applied in the numerical integrations. Above D = 6 mm, these papers uggest that $V_t(D)$ is about 9.2 mps for sea level conditions, and this has been assumed in the calculations.

Eight different concentrations of drops form the basic data set from which values of Z versus R, VTZ and VTM were plotted (Figures 1-3). The eight basic cases correspond to eight different slopes of the DSD (in semi-log coordinates) specified by the nominal rainfall rates (R_n) of 1, 5, 10, 25, 50, 100, 200, and 400 mm/hr via $\lambda = 44.0\ R_n^{-0.21}$. The λ-R relationship is consistent with both Merceret's (1975) and Jatila's (1973) N_o constrained regressions for λ and also with the Spilhaus (1948) constants for $V_t(D)$, $c = 1420$, $d = 1/2$, with D in cm units. The eight basic cases are identified on the graphs by their nominal rainfall rate (1 to 400) even though the rain rate, R, calculated by substituting the linear λ-R_n regression relationship (in log-log coordinates) for λ usually does not produce an R exactly equal to R_n in the analytic equation for $R = f(\lambda)$. Furthermore, when the assumed DSD is truncated there will be additional and often much more significant discrepancies between the calculated R and the nominal value (R_r) which determines the slope of the DSD.

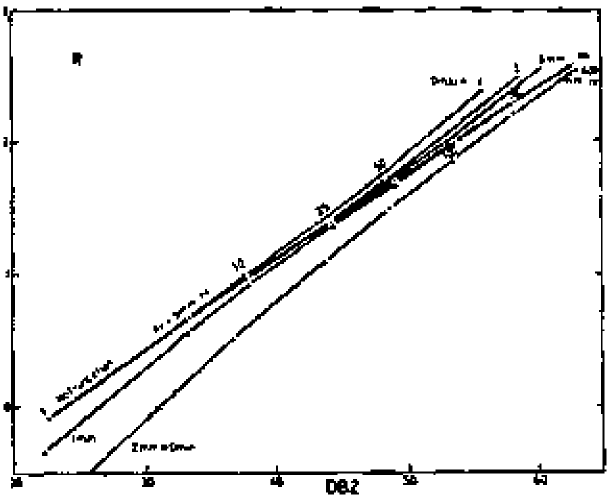

Figure 1: Z-R relationships from nuerical integration, with various truncations.

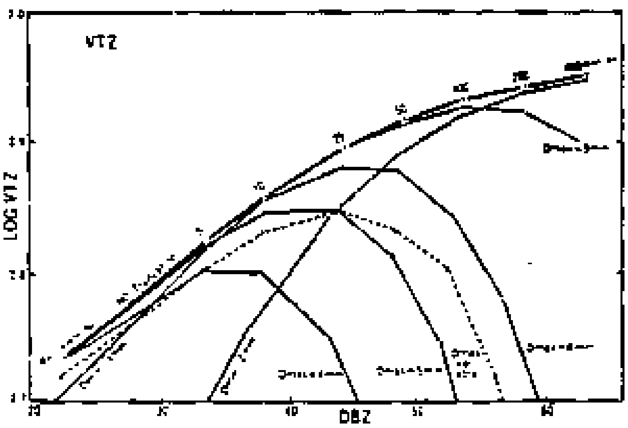

Figure 2: VTZ-Z relationships from nuerical integration, with various truncations.

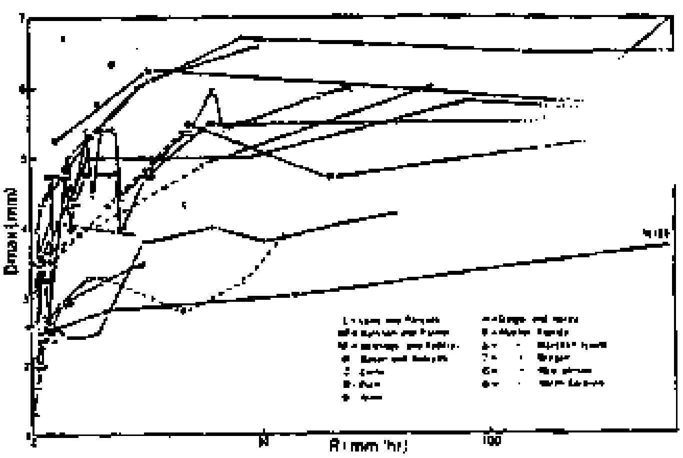

Figure 4: D_{max} as a function of R as observed at 14 locations.

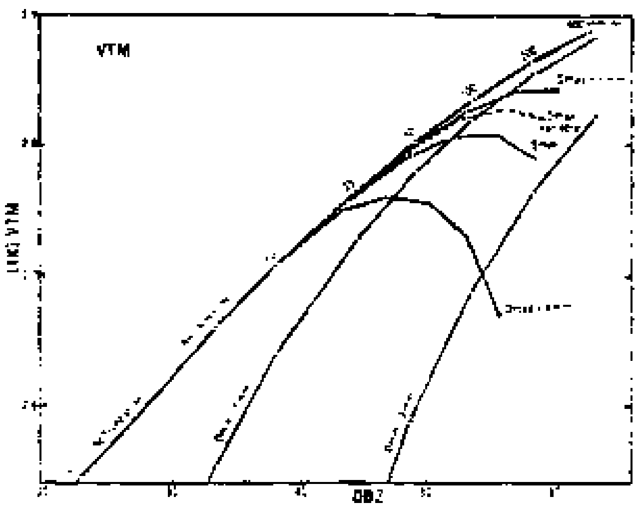

Figure 3: VTM-Z relationships from nuerical integration, with various truncations.

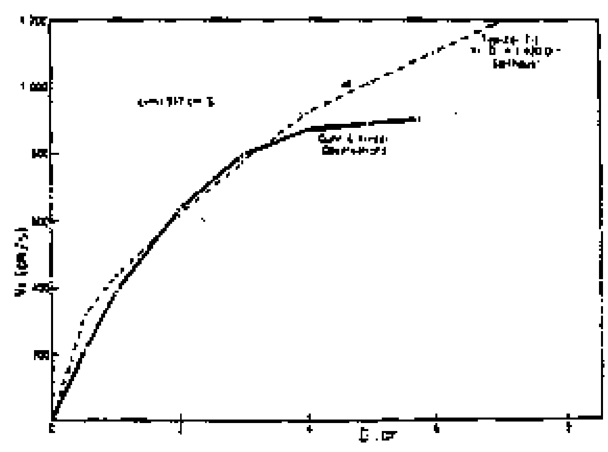

Figure 5: $V_t(D)$ as observed and as fit by a single term power law.

Truncations

To show the possible range of effects of finite DSDs on the three Z relationships, the calculations of all four variables (R, Z, VTZ and VTM) were repeated for all R_n for six cases in which the DSD was truncated either above D = 4, 5, 6 or 9 mm, and/or below D = 1 or 2 mm. For each case the slope of the DSD in semi-log coordinates, λ, remains constant during truncation.

Often there is an observed deficiency of small drops (less than about 1 mm and especially less than 1/2 mm) compared to the strict Marshall- Palmer DSD. This may be the result of selective evaporation of the small drops and/or capture of them by larger drops. Thus, the assumed extreme truncation for drops less than 2 mm is intended to show the maximum likely extent of the effect of such a potential small drop deficiency, while the 1 mm truncation shows the more typical effect.

At the other extreme, 9 mm represents the probable absolute maximum drop size likely to be present. Drops larger than this do not appear to have been observed and the existing theories of drop stability, though crude also find 9 mm to be about the maximum size which can be sustained (Pruppacher and Klett, 1978). Thus, the truncation of drops larger than 9 mm from the DSDs also represents a very realistic minimum constraint on the large drop end of the spectrum. In addition, it is known that large isolated drops become progressively more unstable above diameters of about 5.0 $\pm$ 0.5 mm (Alusa and Blanchard, 1973). Drop breakup is enhanced by turbulent air, but collision induced breakup appears to be the main disintegration mechanism. Thus, drop breakup is very frequent in high liquid water content regions. Consequently, drops larger than about 5 mm tend to be transient with shorter lifetimes in heavy rains. However, Blanchard and Spencer (1971) observed drops of nearly 9 mm after water released from a hose had fallen over 60 metres and Waldvogel and Federer (1974, 1975, 1976) have observed natural drops well in excess of 7 mm, usually in association with hail. Therefore, drops larger than about 5.5 mm are observed but are rare and probably reflect the existence of a cold rain process and the proximity to a source region of larger frozen hydrometeors. Unfortunately, it is difficult to theoretically specify the maximum drop size

(D_{max}) likely to be present for a given set of conditions because of the transient nature of drops larger than about 5.5 mm and our ignorance of the details of the breakup process active in clouds. Nevertheless, because the large drops make the strongest impact on radar calculations (e.g. Z is dependent on the 6th power of drop diameter), they require special attention.

As a result of the lack of reliable theory and observations of DSDs, several extensive long-term DSD measurement programs have been undertaken. Early results from a study in Germany showed that drops larger than 3 mm constituted only about 0.1 to 0.2% of all drops (Diem, 1966). Later work showed that the 0.1% figure held up fairly well for warm season conditions, but may be too large by a factor of 10 for cold season rainfalls (Breuer and Kreuels, 1976). Diameters over 4 mm were observed for only about 0.001 to 0.01% of the drops. In terms of the individual spectra determined from exposures of 1 to 60 seconds, Diem shows that only about 3.3% and 10.3% of spectra have drops over 3 mm in Germany, and equatorial East Africa, respectively. Consequently, it is difficult to obtain reliable statistics on the occurrence of large drops in most climatic zones (Cornford, 1968; Smith, 1976; Gertzman and Atlas, 1972; Mueller and Sims, 1966).

In light of the uncertainty in the growth and breakup of large drops, and since rain showers and continuous rain are expected to have smaller D_{max} than thunderstorms, the truncation of drops over 4, 5 and 6 mm are shown (light solid lines) to depict the range of effects which might be possible under various conditions.

A final more complex truncation which is rain rate dependent was also examined. To get a better idea of the relationship between rainfall rate and D_{max}, the DSD observations from 10 authors in 14 locations were plotted on a graph of D_{max} versus R for convective storms (Figure 4). The data were chosen to be free of the affects of observational limits on the upper end of the DSD and rich in large drops associated with thunderstorms and high rainfall rates. That is, results of camera and filter paper observational techniques were emphasized, while distrometer and airborne measurements were de-emphasized. Some hail was reported to have occurred during the observations of two of the more pertinent studies (Waldvogel and Federer, 1975 and Carte, 1971). Therefore, rain processes in the subfreezing zone were obviously represented. The extensive multi-location data of Mueller (1966) was very helpful. The results showed great sampling variations, but after the most obvious outliers were ignored in some of Mueller's spectra (for R <20 mm/hr) a consensus or midpoint of the D_{max} vs R trends seemed to emerge:

R (mm/hr)	1	5	10	25	50	100
D_{max} (mm)	3.0	4.0	4.5	5.0	5.25	5.5

The range of the observed D_{max} about the listed values for each R was about ± 1 mm. Dashed lines connect the less certain data points for a given author or location. Above 100 mm/hr, D_{max} can be assumed to be about 5.5 mm (in agreement with the independent observations of Fletcher (1969) and Alusa and Blanchard).

These somewhat conservative restraints on D_{max} were then used to truncate the assumed DSD for each of the eight values of R_n in the numerical calculations of R, Z VTM and VTZ (dashed lines in Figures 1-3). In the light of the severe impacts which result, it is noted that even more conservative D_{max} versus R relationships have been proposed for R<50 mm/hr (D_{max} = $.23R^{.213}$, Stephens, 1964; and D_{max} = $(10/\lambda)(1.18)^K$, with K = 0 to 2, Le Grone *et al.*, 1968).

Analytic integration

Analytic expressions for the untruncated relationships between Z and R, VTZ and VTM were also obtained, by using either of two convenient and very accurate fall speed laws:

$$V_t(D) \equiv V_o D e^{-\alpha D} \quad \text{(Uplinger, 1981)}$$

or

$$V_t(D) \equiv V_1 - V_2 e^{-\delta D} \quad \text{(Imai, 1964).}$$

Cgs units are used for these functions. Thus, for Uplinger's function = 1.95 and V_o = 4854.1 give $V_t(D)$ accurate to within about 7%

for D between 0.05 and 0.6 cm. V_1 = 965 cm/s and V_2 = 1030 cm/s in the second expression give $V_t(D)$ to within 2% for the same range for the Imai function. The very convenient single term Uplinger function is usually accurate, being within about 1.3% of the true values in this range except very near 0.5 mm, where even the strong weighting of drop frequency is usually not enough to cause a significant amplification of error in the calculation of the radar variables. However, above D = 6 mm, where the radar variables are very sensitive, other $V_t(D)$ errors begin to approach 20% and the Imai function is more accurate. For D of 9 mm, the Imai function is only 4.7% above the apparent true $V_t(D)$ value (9.2 m/s).

3. RESULTS AND DISCUSSION

The numerically determined relationships between Z and the dependent variables (R, VTM, VTZ) for the untruncated DSDs are shown by the heavy solid line in each of the Figures (1-3).

All three untruncated relationships are clearly curved downward on the log-log plots.

This reflects the highly non-linear downward curvature of $V_t(D)$ as also seen in the two analytic $V_t(D)$ relationships (e.g. at large D, $V_t(D)$ approaches an asymptote of about 9.2 m/s, after rapid changes at small D (Figure 5)). In the most important of these three $V_t(D)$ dependent relationships, Z-R, the resulting deviation from the near linearity at low Z can result in an error of over 120 mm/hr in R at high Z (Figure 1)!

The reflectivity weighted terminal fall speed is given by the integral of $V_t(D)N(D)^6$ integrated from D equal zero to infinity. This flux of reflectivity is then divided by the total reflectivity, Z, to obtain the normalized fall speed, VTZ (Figure 2). Consequently, VTZ is strongly affected by large drops because of the D^6 weighting and most closely approaches the $V_t(D)$ asymptote (9.2 m/s), reaching a speed of 8.9 m/s for the largest R_n examined (400 mm/hr).

In VTM, $V_t(D)$ is weighted by only D^3 and normalized by the liquid water content, (which is proportional to the integral of $N(D)D^3$). Because of the more moderate D^3 weighting, VTM is not as strongly influenced by large drops, only reaches a maximum speed of 7.7 m/s for R_n = 400 mm/hr and is not closely approaching an asymptote (Figure 3). Consequently, VTM is also not as obviously curved as VTZ vs Z.

Because R contains D^3 weighting also, it is closely related to VTM (R = VTM x rain water contents), and the Z-R relationship (although unnormalised), is similar to the VTM-Z relationship, being moderately non-linear in log-log coordinates. Nevertheless, if the linearity suggested by the lowest two or three Z-R values is extrapolated to the largest Z value, 63 dbZ, the indicated rainfall rate would be about 500 mm/hr compared to the actual (non-linear) value of 380 mm/hr (R_n = 400 mm/hr). Of course, these more extreme errors also indicate a distinct non-linear aspect to the relationship that is not well described by a simple power law. However, this is far more true for the Z relationship with VTZ, which is highly non-linear throughout the entire range of likely Z values.

Much more extreme errors (-500%) would occur for VTZ linearly extrapolated from the lowest Z values. Errors for VTM are more moderate (~20%) but still indicate a strongly non-linear relationship that is not well described by a simple power law.

Non-linear regression on the logarithms of the numerically calculated variables shows that these untruncated relationships are very accurately described by the following equations:

$$R(mm/hr) = 0.0200\ Z^{.739-.009515 \log Z},$$
$$VTZ(cm/s) = 289\ Z^{.145-.0108 \log Z},$$
$$VTM(cm/s) = 162\ Z^{.167-.0094 \log Z},$$

where Z is in mm^6/m^3 units.

If drops less than 1 mm are not present in the volume observed by a radar, the concave downward curvature of the Z-R relationship is enhanced below about 53 dbZ (Figure 1). Even stronger and more pervasive effects occur for truncation below 2 mm. However, most studies show that it is drops less than about 1 mm which are most likely to be deficient compared to a Marshall-Palmer DSD (Mueller, 1966). Thus, the less severe truncation is most likely to represent actual conditions.

Truncation of large drops act to reverse the curvature at the high Z end of the Z-R relationship, and may even cause a concave upward curvature in the most severe truncations (see curves, labelled for 4 and 5 mm truncations). One very interesting result of truncating large drops is the 6 mm truncation curve for the log-log plot of Z-R. It is nearly linear! Thus, Marshall-Palmer DSDs with largest drops of around 6 mm will be accurately depicted by the older linear Z-R relationships. Since 6 mm is near the likely upper bound for D_{max}, it appears that earlier results which tended to confirm "linear" Z-R relationships were to some extent serendipitous. Nevertheless, in many cases only smaller drops will be present.

However, the normalized VT-Z relationships are never subjected to similar simplification by truncation at either end of the DSD. All truncations result in non-linear VT curves, and particularly in the most sensitive case, VTZ, the curvature is usually severely exacerbated by truncation.

The truncation effect of drops over 9 mm is hard to detect in the Z-R and VTM-Z relationships which are so close to the untruncated relationships that this truncation is not plotted on these two Figures (1-2).

However, the 9 mm truncation has a relatively pronounced affect on the VTZ-Z relationship. This is an important case of truncation because drops larger than 9 mm probably do not exist. Thus, the 9 mm truncation closely approximates the <u>minimum</u> effect likely to be imposed by the actual finite nature of DSDs.

For VTZ even the minimum realistic upper end truncation has a significant impact.

The 5 and 6 mm truncations represent the more typical effect of finite

DSDs and show that while a linear Z-R relationship in log-log coordinates may actually be appropriate for at least some real situations, this is never true for VTM and VTZ! In fact, with these more realistic conditions, VTM is now in a near asymptotic condition (but only to at most 7 mps) and VTZ is so seriously distorted (doubly defined), even at moderate reflectivities, that it may be of dubious utility for some applications (e.g. VTZ cannot be used to determine Z. However, using Z to establish VTZ still is valid).

The curves for the more complicated truncations identified on the figures as "D_{max} Variable" and described in the D_{max} versus R table usually coincides with the untruncated Z-R and VTM-Z curves for low Z and, as expected, lays between the 5 and 6 mm truncations in the higher Z range where the impact of the missing large drops is significant.

However, this possibly most realistic depiction of finite DSDs in thunderstorms greatly distorts VTZ throughout the entire Z range. The truncated VTZ curve hardly even approaches the untruncated VTZ curve. It is therefore clear that the sensitivity of VTZ-Z to large drops must always be given strong consideration for real situations with finite DSDs. While the impact of truncation on the Z-R and VTM-Z relationships also requires consideration, this is mainly for the higher reflectivities.

4. CONCLUSION

When an accurate depiction of the terminal fall speed of raindrops is included in the theoretical derivation of relationships relating radar reflectivity to rainfall or to the average terminal fall speed of the hydrometeors, it causes the relationships to be non-linear, even in log-log coordinates. This non-linearity may be considerably enhanced if the distribution of drop sizes is not infinite.

However, in the case of one realistic truncation of drops larger than about 6 mm, the deletion acted to remove the curvature from the calculated Z-R relationship and in general the loss of large drops acts to reverse the curvature of Z-R.

However, when small drops are eliminated from the calculations, the downward curvature of Z-R is always enhanced.

Also, the ensemble terminal fall speed-reflectivity relationships are in all cases further distorted by truncation and show no subsequent approach to linearity. These relationships are always extremely non-linear, and in the presence of realistic truncations of the large drop end of the DSD become almost bizarrely contorted, even at moderate Z, (e.g. VTZ is doubly defined!).

These considerations have recently become more pertinent with the advent of more accurate radar rain measurements through ground truth calibration in near real time, as well as through the more common usage of long wavelengths which are less subject to attenuation and non-Rayleigh scattering. The old rule of thumb factor of two accuracy quote for radar rain measurements is no longer generally applicable. Errors on the order of 20% are now being reported frequently (e.g. Collier, 1975; Grosh, 1990).

However, it has been shown here that if the linear trend of the untruncated Z-R relationship at low Z is extended to higher values, errors in R of over 100 mm/hr can occur compared to the non-linear Z-R relationship which accurately accounts for the strong curvature of the terminal fall speed relationship of individual drops. For both VTM-Z and, especially, VTZ-Z large errors will also occur for similar extrapolations, but even worse errors occur for relationships for truncated DSDs compared with those for infinite DSDs. In some of these cases the errors may be severe also.

In light of the above noted effects of $V_t(D)$ and DSD truncation, it is concluded that the basic meteorological radar theory needs to be re-examined. The equations and graphs shown here are a step in this direction.

ACKNOWLEDGEMENT

This paper was presented, in slightly altered form, at the 24th Radar Meteorology Conference of the American Meteorological Society.

REFERENCES

Alusa A L and Blanchard D C, 1973. Drop size distributions produced by the breakup of large drops under turbulence. J. Rech. Atmos., 7, 1-9.

Aoyogi J, 1968. Mean Doppler velocities of precipitation near the ground. Preprints: 13th Radar Meteorology Conference. AMS, Boston, 22-25.

Austin P M, 1981. On deducing rainfall from radar reflectivity measurements. Preprints: 20th Radar Meteorology Conference, AMS, Boston, 200-208.

Battan L J, 1973. Radar Observation of the Atmosphere. U. Chicago Press, 324pp.

Beard K V, 1977. Terminal velocity adjustments for cloud and precipitation drops aloft. J. Atmos. Sci., 34, 1293-1298.

Blanchard D C and Spencer A T, 1971. Experiments on the generations of raindrops-size distribution by drop breakup. J. Atmos. Sci., 27, 101-108.

Breuer L J and Kreuels R K, 1976. Seasonal variations of precipitation parameters. Preprints: 17th Radar Meteorology Conference. AMS Boston, 423-438.

Calheiros R V, 1982. Ph.D. Thesis, Sao Carlos Engineering School, University of Sao Paulo, EECS/USP 230 pp.

Carte A E, 1971. Raindrops spectra in Pretoria. S. Afr. Geogr., 53, 100-103.

Clark R A and Moyer V S, 1966. Some theoretical considerations of the Z-R relationship. Proceedings 12th Radar Meteorological Conference, AMS, Boston, 245-249.

Collier C G, 1975. Rainfall measurement by radar. Proceedings Symposium on Weather Radar and Water Management. Water Research Center, Medmenham, Paper 1.

Cornford S G, 1968. Sampling errors in measurements of particle size distributions. Meteor. Mag., 97, 12-16.

Cunning J B and Sax R I, 1977. A Z-R relationship for the GATE b-scale array. Mont. Weath. Rev., 105, 1330-1336.

Diem M, 1966. Rains in the Arctic, Temperate and Tropical Zones. Scientific Report, European Research Office, United States Army, 93 pp.

Doherty L H, 1964. Z-R relationships deduced from forward scatter Doppler measurements. J. Atmos. Sci., 21, 683-697.

Fletcher N H, 1969. The Physics of Rain Clouds. London, Cambridge University Press.

Foote G B and du Toit P S, 1969. Terminal velocity of raindrops aloft. J. Appl. Meteor., 8, 249-253.

Fujiwara M, 1965. Raindrop size distribution from individual storms. J. Atmos. Sci., 22, 585-591.

Gunn R and Kinzer G D, 1947. The terminal velocity of fall of water droplets in stagnant air. J. Meteor., 6, 243-248.

Gertzman H S and Atlas D, 1977. Sampling errors in the measurement of rain and hail parameters. J. Geophy. Res., 82, 4955-4966.

Grosh R C, 1990. Radar rain measurement studies. This volume, 3-9.

Imai I, 1964. A fitting equation for raindrop size distributions in various weather situations. Preprints: 11th Radar Meteorology Conference, AMS, Boston, 149 A-D.

Hodson M, 1986. Raindrop-size distribution. J. Clim. Appl. Meteor., 25, 1070-1074.

Jatila E J, 1973. Experimental study on the measurement of snowfall by radar. Geophysica, 141-149.

Jatila E J and Harju A E, 1975. The calibration of radar by measuring the flux density or maximum size of raindrops. Preprints: 16th Radar Meteorology Conference, AMS, Boston, 484-487.

Jones D M A, 1956. Rainfall Drop Size Distribution and Radar Reflectivity, Res. Rep. No. 6. Urbana, Illinois State Water Survey.

Jorgensen D P and Willis P T, 1982. A Z-R relationship for hurricanes. J. Appl. Meteor., 21, 356-366.

Joss J and Waldvogel A, 1968. The variation of raindrop size distributions at Locarno. Preprints: Int. Cloud Physics Conference, 369-373.

Joss J and Gori E G, 1978. Shapes of raindrop size distributions. J. Appl. Meteor., 17, 1054-106.

Knollenberg R G, 1976. Three new instruments for cloud physics measurements. Proc. Int. Conf. Cloud Physics. AMS, Boston, 554-561.

Le Grone A, Fowler M S and Dean A P, 1968. Drop size distributions in a rain. Preprints: 13th Radar Meteorology Conference, AMS, Boston, 158-164.

Marshall J S and Palmer W M, 1948. The distribution of raindrops with size. J. Meteor., 5, 165-166.

Merceret F J, 1975. A note on the vertical size distribution of raindrop-size spectra in tropical storm Felice. Meteor. Magazine, 103, 358-361.

Merceret F J, 1975. A comment on "The N_o jump of raindrop spectra". J. Atmos. Sci., 32, 652-654.

Mueller A E, 1966. Radar Cross Sections from Drop Size Spectra. Ph. D. Thesis, University of Illinois, Urbana, 84 pp.

Mueller A E and Sims A, 1966. The influence of sampling volume on raindrop size spectra. Preprints: 12th Radar Meteorology Conference, AMS Boston.

Pruppacher H and Klett, 1978. Microphysics of clouds and precipitation. Reidel Co. Boston, 714pp.

Shupiaski A B, 1957. Radar measurement of precipitation by means of reference a target (in Russian). Trudy Tsentral Aero Obs., Moscow, No. 22.

Smith P, 1976. Comments. J. Appl. Meteor., 15, 189-192.

Spilhaus A, 1948. Drop size intensity and radar echo of rain. J. Meteor., 6, 161-164.

Srivastava R C, 1971. Size distribution of raindrops generated by their breakup and coalescence. J. Atmos. Sci., 28, 410-415.

Srivastava R C, 1967. On the role of coalescence between raindrops in shaping their size distribution. J. Atmos. Sci., 24, 287-292.

Stephens J J, 1964. On the applicability of Rayleigh scattering in radar meteorology. J. Appl. Meteor., 3, 211-212.

Stout G E and Mueller E A, 1968. Survey of relationships between rainfall rate and radar reflectivity in the measurement of precipitation. J. Appl. Meteor., 7, 465-474.

Ulbrich C W, 1983. Natural variations in the analytic form of raindrop size distribution. J. Clim. Appl. Meteor., 22, 1764-1775.

Uplinger W G, 1981. A new formula for raindrop terminal velocity. Preprints: 20th Radar Meteorology Conference, AMS, Boston, 389-392.

Waldvogel A and Federer B, 1976. Large raindrops and the boundary between rain and hail. Preprints: 17th Radar Meteorology Conference, AMS Boston, 167-172.

Waldvogel A and Federer B, 1975. Raindrop spectra in severe local storms. Preprints: Severe Local Storms Conference, AMS Boston, 431-435.

Waldvogel A, 1974. The N_o jump of raindrop spectra. J. Atmos. Sci., 31, 1067-1078.

Willis P T, 1984. Functional fits to some observed drop size distributions. J. Atmos. Sci., 41, 1648-1661.

D. STATISTICAL Z-R RELATIONSHIPS

R C Grosh and C Muller - CSIR

An additional statistical Z-R study was undertaken with the Nelspruit radar data. There were two reason for this study. First, the use of the "statistical" approach to obtaining Z-R relationships has led to unusual highly non-linear relationships (Calheiros and Zawadski, 1988) which require further investigation, particularly in the light of tools which have recently been assembled for the investigation of non-linear Z-R aspects related to truncated drop size distributions and raindrop fall speeds (Grosh, 1989). In particular, the statistical approach usually relies on non-simultaneous observations of Z and R and is thus always open to a degree of uncertainty. The present study was undertaken as the first check on the statistical method using simultaneous observations. Also, the first PAWS study using the Badplaas rain gauge network can be criticised due to the use of conditional probabilities (Calheiros and Zawadski, 1987) and the unfortunate location of the rain gauges south of the radar behind the tallest terrain obstructions to radar viewing (Mather *et al.*, 1987). This led to partial blockage of the lowest radar beam, that which supplied the observations used in the earlier correlations.

In order to obtain simultaneous observations of Z and R independent observations were utilised from the South African Weather Bureau for two sites to the north of the radar. Two other sites were also considered, but one (Friedenheim) was too close to the radar (and therefore located in a data void), and the other (Skukuza) was too far away (90 km) to provide optimum results (the lowest radar beam is nearly 6 km above the gauge at this range). Table 1 is a list of the sites with usable data and their geographic coordinates. The two stations utilised were at ranges of 62.5 km (Lydenburg) and 63.25 km (Graskop) from the former Nelspruit radar site. Thus, the radar viewed volumes that were at least about 2.8 km above the gauges (as the minimum elevation angle used by the Nelspruit radar was only 3.0°). Although unfortunately high, these viewing conditions represent a considerable improvement on the earlier PAWS study which was based on stations ~4 km below the beam height (Mather *et al*., 1987).

Table 1. Station locations, elevations.

	Latitude	Longitude	Altitude (m)
Nelspruit radar	25°30'10"S	20°54'40"E	884
Lydenburg gauge (from radar: range = 62.5 km, azimuth = 315.5°)	25°6'S	30°28'E	1439
Graskop gauge (from radar: range = 63.25 km, azimuth = 353.5°	24°56'S	30°50'E	1441

2. RANGE GAUGE DATA

Copies of the charts from the rain gauges were obtained. Because of the temporal resolution of the original charts and practical considerations, it was only possible to reduce the gauge data for 15 minute "clock-hour" periods. Although siphon gauges were used, the integrated results were checked against independent measurements and the data included found to be quite accurate. The charts were read to 0.1 mm accuracy.

The rainfall data set of matched radar and gauge observations were obtained from 30 rain days at the Graskop gauge and 38 rain days at Lydenburg. Thus, there were 68 station days contributing data to the main analysis. This amounted to 337 fifteen minute data points (187 + 150) or about 84 hours of data.

3. RADAR DATA

The characteristics of the radar are listed in Table 2.

Table 2. PAWS radar characteristics (measured by Smith, 1984).

Wavelength		5.3 cm	
Beam width		1.85 deg (H)	
		1.5 deg (V)	
Pulse length (long)		2.3 microsec	
PRF		197.5 s^{-1}	
Gain		38.4 dB	
First side lobe		-25 dB	
PROCESSING			
Integration:	Azimuth	: every 1/8 deg into 1 deg wide bins	
	Range	: 4 microseconds	
	Range bins:	600 m	

For this study two additional integrations were undertaken. Given that the effective recorded beam width at the range (r) of Lydenburg, 62.5 km (or of Graskop 63.25 km), contains information observed on either side of the beam axis from up to (1° + 1.85°)/2 away, the actual tangential distance observed by the main lobe of the beam must be considered to be up to at least 2.85/57.3 x 62.5 = 3.11 km (or 3.15 km for Graskop). Although the actual recorded beam width corresponds to 1.09 and 1.10 km at the two ranges, most of the recorded information comes from the region covered by the central beam (1.85°). Thus, 1.85(62.5 km)/57.3 = 2.02 km (or 2.04 km at Graskop) was taken as the typical *effective* beam width dimension and the basic data unit for this study was defined to be the sum of three consecutive range bins (each being 600 m radially x 1 degree wide) as this represents a nearly square region (e.g. 1.8 km x 2.02) of about 3.6 km^2.

Comparisons with the rain gauge data were made for these individual data units and also for averages of the nine similar data units surrounding the gauge location. The nine unit radar analyses represent an area of about 28.6 km^2 (= 3 x 1.8 km x [3° + 1.85°]r/57.3) at Lydenburg's range. The radar data used corresponds to the periods with rain at the gauges.

4. ANALYSIS PROCEDURE

Cumulative frequency distributions are used in the statistical approach for obtaining Z-R relationships. Values of Z and R from the distribution with equal cumulative probabilities of occurrence are then matched to obtain the relationship. In this analysis, values were matched for each 10% interval in the distributions. The 95% and 98% values were included as well.

5. RESULTS

Low Z and R values were relatively frequent. Extrapolation was required to obtain the 10% and 20% R values. Furthermore, 15% of the central radar observations directly over the gauges during rain as well as 6.5% of the 28 km^2 average Zs were found to be zero. The explanation for the zeros comes from the great height of the radar beam (wind drift), the spatial and temporal resolution of the radar observations and their sensitivity, as well as from possible azimuth alignment and gauge sampling problems.

The main results are shown in Figures 1a and b. The two Z-R curves for the combined Lydenburg and Graskop data sets each can be interpreted as having three different slopes. The curve for the radar observations directly over the gauges is slightly smoother than the one for the area averaged reflectivities. In the middle range of the distributions (30% to 95%) both the relationships are essentially linear (in log-log coordinates). However, the higher and lower values are associated with slower increases in R for a given change in Z. The lower (Z, R) pairs are all associated with the low cumulative frequencies of R which had to be obtained by extrapolation and are ignored hereafter. They may well be artifacts of the extrapolation (which extends below the lowest measurable R value). However, the slopes for the high values are thought to be real. Curvature enters the relationship at about the same Z-range (above logZ =4) similar to the curvature reported in Figures 12 and 13 of Calheiros and Zawadski (1987) and Figure 1 of Grosh (1989). Thus, the Z-R curvature may be related to the fact that terminal fall speeds for larger raindrops (associated with higher R and Z) increase more slowly with diameter than for smaller drops (Grosh, 1989). This finding tends to confirm the earlier Z-R analyses of Grosh (1989) and is a critical case for the comparison as the current statistical approach is based on

Figure 1a.

ANALYSIS OF RADAR REFLECTIVITIES AND RAINFALL RATES

AT LYDENBURG AND GRASKOP - RAINFALL SEASONS 84/85, 85/86 AND 86/87

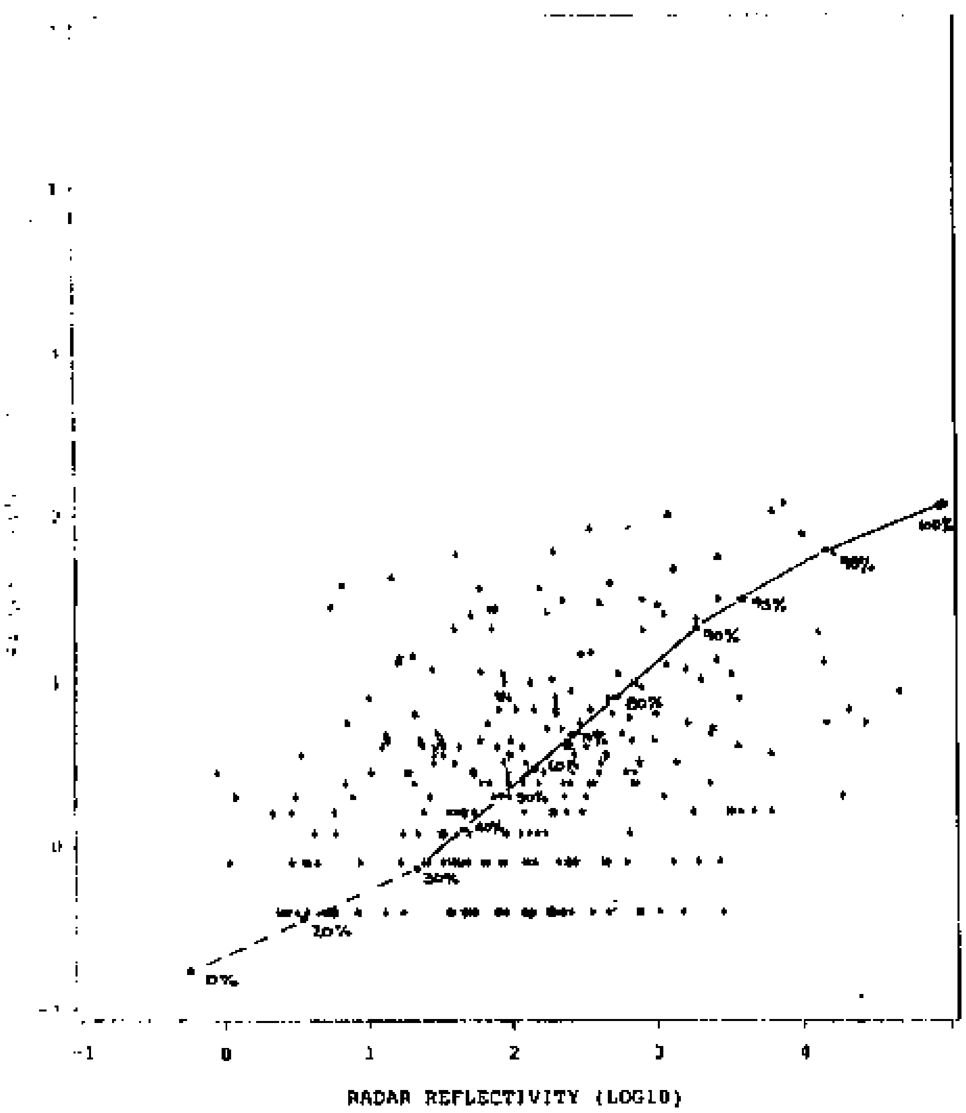

BASED ON RADAR OBSERVATIONS DIRECTLY ABOVE THE RAINGAGE
AVERAGED OVER 15 MINUTE PERIODS AND THREE RANGE BINS

Figure 1b.

ANALYSIS OF RADAR REFLECTIVITIES AND RAINFALL RATES

AT LYDENBURG AND GRASKOP - RAINFALL SEASONS 84/85, 85/86 AND 86/87

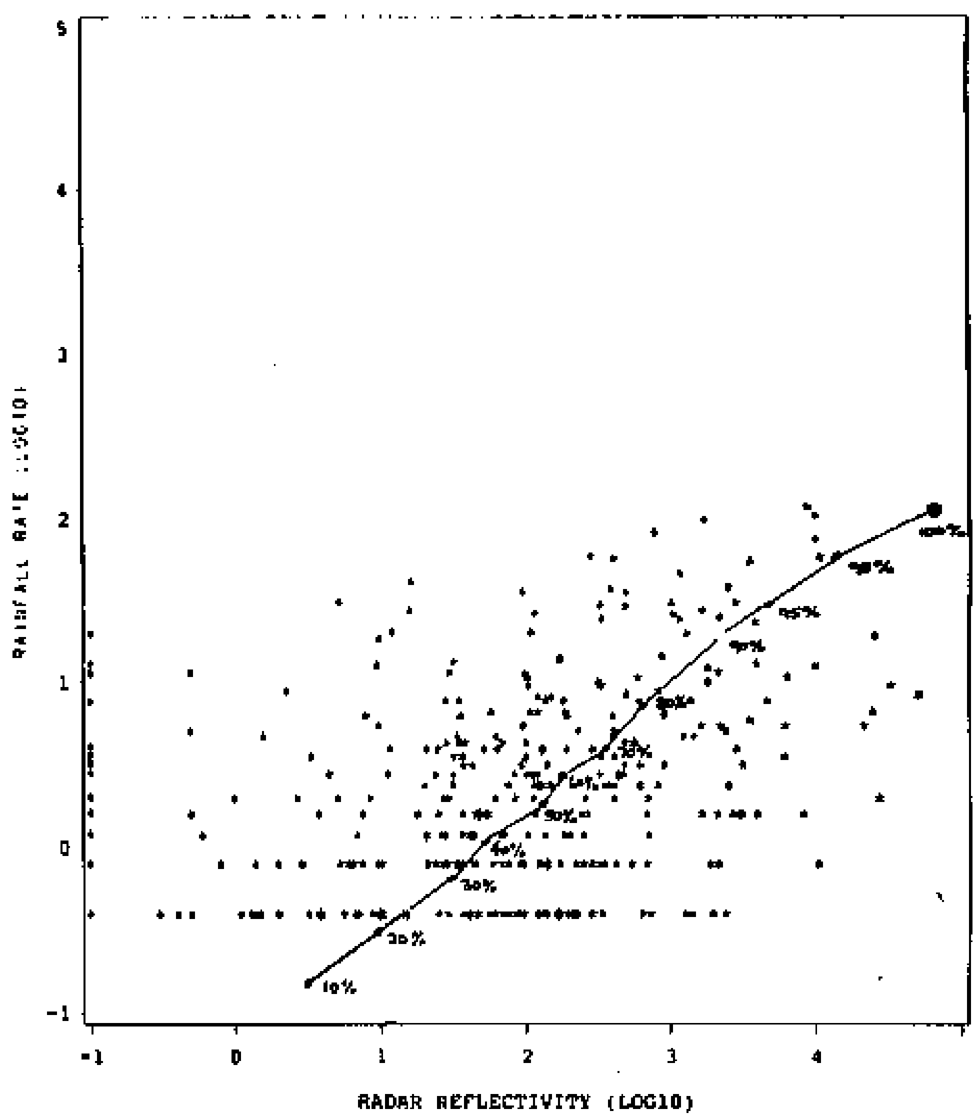

BASED ON NINE RADAR OBSERVATIONS CENTERED OVER THE RAINGAGE
AVERAGED OVER 15 MINUTE PERIODS AND THREE RANGE BINS

simultaneously observed (Z, R) pairs and (nearly) unconditional probabilities. It is therefore recommended that non-linear Z-R relationships such as that reported by Grosh (1989) be used for future PAWS radar calculations when high rain intensities are likely.

As in many other direct Z-R comparisons, the actual correlation of the individual (Z, R) points in the present study is low, ranging from $r = 0.3$ to $r = 0.4$ (if the Z=0 values are ignored). The statistical technique was devised to deal with non-simultaneous observations and the large scatter which often results from radar and rain gauge comparisons. In the present analysis the use of simultaneous (Z, R) observations has shown that the statistical technique can lead to an apparently reasonable Z-R relationship when the individual data points are poorly correlated. This suggests that results based on the statistical technique must be carefully interpreted.

The effect of wind and alignment errors on the correlations must be examined in the future.

ACKNOWLEDGEMENT

R Parsons, CloudQuest, wrote the computer program to average the radar data.

REFERENCES

CALHEIROS R V and ZAWADSKI I, 1987. Reflectivity-rain rate relationships for radar hydrology in Brazil. J. Appl. Meteor., 26, 118-132.

GROSH R C, 1989. The highly non-linear aspects of Z-R and VT-Z caused by raindrop terminal fall speeds. Preprints: Conference on Radar Meteorology, AMS, Boston, 676-681.

MATHER G, MORGAN M and REUTER G, 1987. PAWS Annual Report 1986/87, WRC, Pretoria, 85pp.

SMITH P L, 1984. An evaluation of the Nelspruit C-band Weather Radar System. Memorandum for the Record. CloudQuest, Nelspruit, 15pp.

E. A REVIEW OF RAIN DROP SIZE DISTRIBUTION MEASUREMENTS

R C Grosh

ABSTRACT

Because of its broad viewing capability, weather radar is well suited to the evaluation of rain stimulation experiments and other hydrological situations. Since sampling is a major problem in obtaining the drop size distribution (DSD) information needed to relate the radar measurement (reflectivity, Z) to rain rate (R), a quick but fairly thorough search for all previously observed Z-R relationships for convective weather wa. undertaken. These covered the entire spectrum of "warm" season rain types at geographic locations where both convective and stratiform rains occur simultaneously. For example, recent research shows that about half the rain which falls from tropical cloud clusters and squall lines may be stratiform and that this anvil region may be *much* larger than the convective core (Gamache and Houze, 1983). The goal was, if possible, to synthesize a representative Z-R relationship and DSD and discuss their variability. Thus, an important aspect of the study is the observed variability of the Z-R coefficients a and b for convective rain. Fifty six different relationships which *appeared to have the required general application* were found. Twenty-four of these had sampled air volumes over 200 m^3. The analysis of their characteristics reveals that

$$Z = 260\ R^{1.43}$$

is a representative composite function for DSDs in general convective storms, as the standard deviations for the a and b parameters are moderate, +/-52 and +/-0.10.

1. INTRODUCTION

Z-R relationships are a central issue to radar rainfall rate measurements. Radar rain estimates are often desired in regions where information on raindrop size distributions and/or radar comparisons with rain gauges is completely lacking. For example, radar is receiving rapidly increasing use as a tool to verify weather modification experiments. Also, from the flash flood point of view radar information is particularly important during heavy rains. In the light of the well-known variability of raindrop size distribution measurements and the massive DSD research (Breuer and Kreuels, 1976; Aniol et *al*., 1980; Richards and Crozier, 1983; Jorgensen and Willis, 1982) which has occurred since Battan's review was published (1973), a new review of the situation appeared appropriate. The present study was undertaken with a major goal being to identify the most representative Z-R relationship to assume in areas with insufficient DSD observations such as in Africa. Furthermore, the natural variability of the Z-R parameters (a and b) require study as these might be expected to be altered by cloud seeding activities (Cunning, 1976).

Z-R relationships obtained directly from DSDs are emphasized here, since there are fewer measurement problems than when using radar and rain gauges (the indirect approach). For example, the effects of cloud base altitude must be considered, as evaporation is known to effect the coefficient a. Thus, the directly obtained Z-R relationships contain the more pure meteorological information. In practice, however, equations obtained with radar are obviously more directly applicable to the rain measurement problem. Perhaps most important, radar observations consider large sample volumes. Thus, these Z-R relationships are also discussed.

2. DATA SOURCES

There have been about 10 very strong and/or well-known DSD measurement programs to obtain Z-R relationships. By far the most well-known is the widely referred to study of Marshall and Palmer (MP, 1948). MP made both radar and dual raingauge observations near Ottawa (Canada) to supplement other DSD observations made on "several days by different observers" which included data from Clinton, Ontario (Canada), and some much earlier data of Lenard in Germany. However, MPs results appear to rest most heavily on earlier DSD observations made by Laws and Parsons (LP, 1943) in a warmer climate. The empirical result MP obtained in 1947, $Z = 190 R^{1.72}$, was modified in 1948 to $220 R^{1.6}$ to account for the more comprehensive DSD measurements made about a decade earlier in Washington D C. The LP observations were also used in the original paper to relate radar observations to rain intensity, which was written by Wexler (1947). Later, Wexler (1948) did a more direct least squares regression on the 98 storm spectra that LP obtained and found

$$Z = 214 R^{1.58}.$$

From the magnitude of these parameters it seems clear that the final MP result is strongly influenced by the substantial two year Washington data set of LP. In fact, the "MP" result is usually simplified to

$$Z = 200 R^{1.6}.$$

This compromise between the early MP result and the LP equations obtained by Wexler obviously favours the substantial LP data set.

Therefore, it must be concluded that the main data set from the early analyses is that of LP. It was obtained using the flour technique of Bentley (1904).

Modern DSD Measurement Programs

The first major modern meteorological DSD measurement programs appear to have been conducted at:

(1) The Illinois State Water Survey in the central US (utilizing the famous drop camera of Jones (1956) and Mueller (1966)).

(2) The Technische Hochschulze in Karlsruhe SW Germany (Diem, 1966).

(3) New Delhi and Poona in India (Ramana, Murty and Gupta, 1959; Sivaramakrishnan and Selvam, 1967).

The German and Indian projects used the difficult and now obsolete dye and filter paper technique.

Subsequently, Joss *et al.* (1968) developed the now dominant disdrometer measurement technique in Switzerland. The important newer projects at the University of Bonn in W Germany, in Southern Bavaria and in Canada also utilize the disdrometer (Breuer and Kreuels, 1976; Aniol *et al.*, 1980; and Richards and Crozier, 1983). In addition, Austin and Geotis (1979) utilized disdrometers on ships supplemented by aircraft foil observations during GATE. The last seven groups made primarily local measurements, while Diem and Mueller made world wide observations. Another notable program is the long-term measurement project of the National Hurricane Research Laboratory, usually over the oceans near Miami, Florida (Jorgensen and Willis, 1982).

The estimated total sample volume obtained by these and other qualifying groups are listed in Table 1 to provide a standard for comparisons when considering the stability and significance of the Z-R parameters.

Sample Volume Estimates

The air volume (vol) sampled by a horizontal sensor surface of area A depends on the size of the hydrometeors sampled since raindrop terminal fall speeds $V_t(D)$ are dependent on their equivalent spherical diameter,

$$vol = A\ V_t(D)\ \Delta t.$$

Following Austin and Geotis (1979) disdrometer measurements are assumed to sample about 2 m^3/min, although this is actually dependent on the drop sizes striking the 50 cm^2 sensor. Thus, this calculation requires prior knowledge of the DSD or rain rate. Either of these is equivalent to the assumption of an average drop group fall-speed, which must be 6.7 mps (or a median diameter drop of D_o = 2.1 mm) for the circumstances of Austin and Geotis (1979).

Drop Camera

The camera measurements usually observed about 1 m^3 per spectra and were collected every minute, which is the approximate sampling interval in most ground level DSD studies.

Table 1: Principle Z-R Relationships for All Rains of Convective Season (worldwide).

	a	b	Sample Volume (m^3)	Source
1	220	1.60	~300	MP
2	372	1.47	1,453	Jones
3	286	1.43	2,506	Mueller (Miami)
4	301	1.64	1,703	" (Oregon)
5	221	1.32	2,552	" (Marshall Is.)
6	267	1.54	2,688	" (Alaska)
7	256	1.41	3,147	" (New Jersey)
8	230	1.40	4,804	" (N. Carolina)
9	180	1.26	432	Diem (Karlsruhe)
10	278	1.30	267	" (Entebbe U.)
11	300	1.50*	~50,000	Joss/Waldvogel
12	175	1.33	316,000	Breuer/Kreuels
13	231	1.43	45,440	Aniol/Riedl
14	271	1.57	30,000	Richards & Crozier
15	180	1.35	4,100	Austin & Geotis
16	330	1.41	~1,500	Gorelik (Moscow)
17	298	1.46	~1,500	" (5 km away)
18	238	1.45	260	Jatila
19	310	1.49	308	Geotis
Radar studies				
20	285	1.30	2.5×10^6	Caton
21	244	1.39	400,000	Doherty
22	295	1.43	10^{12}/30,000	Richards & Crozier
Airborne studies				
23	170	1.52	534	Cunning & Sax
24	300	1.35	10,338	Jorgensen & Willis
Mean	260	1.43		* held constant
SD	52	0.10		

Paper and Flour

However, in the flour and dye paper techniques considerable variation in the sample duration is possible, because it depends on how quickly the surface saturates at different rain rates. Thus, duration has usually not been carefully specified in many of these drop studies.

This was particularly true for the duration of the filter paper measurements. However, Ramana, Murty and Gupta show an average Δt value of 2.4 seconds. Others show 2.7 sec for Δt. Consequently, when this information was not included in a report, Δt was assumed to be about 2 seconds.

Although the average terminal fall speed of the drops impinging on the sensor is taken to be a constant 6.7 mps, this may in fact vary. For light rains, smaller drops and slower $V_t(D)$ will be observed and, on occasion, the assumed value of $V_t = 6.7$ mps may be too large by a factor of at least two. For heavy rains, this speed may be too slow. However, for this type of sampling procedure the values of Δt and the average $V_t(D)$ are interdependent. When the drops fall rapidly Δt must decrease or the paper is saturated. Thus, the product $V_t(D)\Delta t$ is approximately constant. Consequently, vol is dependent mainly upon the sample area, A.

Diem apparently used a sampling area of 100 cm^2 (Diem, 1960) for his filter paper studies. Although some researchers report much larger sensing areas (MP, LP, Doumoulin, Best, Anderson), this value was used when in doubt, as many reports claim to follow Diem. The largest A was almost 700 cm^2 (Kelkar, 1959, 1960). Thus, a factor of seven uncertainty in vol may be present from this source of error alone. Nevertheless, it is likely that most unspecified sensing areas did not approach this extreme size. Therefore, the uncertainty in the estimates of these sample volumes is in general probably on the order of 50% or less. Furthermore, in substantial experiments the number of samples (N) will dominate the calculation of the total sample volume (N x vol).

The Disdrometer

The key Swiss disdrometer project based its primary calibration on 48 days of disdrometer measurements between 1 July and 30 November 1967 which totalled 913 mm of rain during 440 hours and included 7.4 million drops (or 80% of all the storms during the period). Using the Austin-Geotis 2 m^3/min sample volume conversion figure, the total sample volume amounts to 52 800 m^3, a volume so large that it seems unlikely for a five month period. Perhaps the 440 hours did not have rain at each minute. The calculated average rain rate, 913 mm/440 hr = 2.1 mm/hr, also suggests that the 2 m^3/min conversion figure is too high for this project as the average terminal fall speed for R = 2 mm/hr is about 3.7 mps (a drop of about D 1 mm). Thus, 25 000 m^3 may be a better sample volume estimate for this project. However, this is a substantial set of observations in any case.

The Swiss disdrometer measurements were supported by four tipping bucket rain gauges (located within 20 metres) and a vertically pointing radar measuring Z at 200 m above the gage/disdrometer site. The daily rainfall totals at the gauges agreed to within a 6% standard deviation, and the disdrometer agreed with them to within 8%. Furthermore, on 46 occasions with uniform rain (temporal variation less than a factor of 2) with an average duration of 14 minutes each, the radar calculated Z values agreed with the disdrometer values to within a standard deviation of 8% (R ranged between 0.5 and 30 mm/hr). Thus, the disdrometer appears a very capable instrument. If the 6% difference between gauges represents sampling error, then the 8% difference between the gauges and the disdrometer indicates an instrument standard error may have been only about 2%!

Airborne Studies

The airborne studies were made at cloud base and employed two measurement techniques, foil and the 2D-P optical array. The sample volume of the 2D-P depends on the air speed, array width (6.2 mm) and depth of field (which depends on the number of diodes occluded). Since the penetrations lasted about 10 seconds and covered about 1.3 km, each 2D-P spectra is based on about 2 m^3. The foil was exposed perpendicularly to the air flow through a 14.5 cm^2 opening at 100 mps for 0.2 seconds. However, the original analysis used 3 km flight segments for each spectra. Thus, the foil derived spectra represented about 1 m^3 each.

Radar Observations

Modern radar rainfall measurement studies often use adjustments based on raingauge measurements to correct the initial radar estimates. Consequently, there has been a minor trend away from reporting new Z-R relationships for some radar rainfall studies. Usually $Z = 200 R^{1.6}$ is used for unadjusted (pure) radar measurements and the percentage improvement shown for various calibration gage densities is reported (Wilson and Brandes, 1979; Grosh, 1984). Furthermore, there has recently been a great deal of discussion about the difficulties in relating radar and raingauge measurements because of their different sample volumes and separation in time and space (Zawadski, 1984). For example, calculations of the evolution of a DSD during a fall of 1 km below cloud base indicates parcel reflectivity may <u>increase</u> up to perhaps 20% (depending on R) while R itself might <u>decrease</u> due to evaporation by a nearly equal amount (depending on R and the relative humidity). Thus, fewer recent reports of these indirectly obtained Z-R relationships are available. Nevertheless, some long term indirect Z-R studies, which appear to supply stable results for their locations, have been conducted recently, and it is clear that the quality of recent studies, as measured by sample size, for example, is much improved.

Canada

One of the best of these is clearly the Toronto study of Richards and Crozier (1983) which employed a disdrometer as well, so that both radar and DSD measurements could be used to supply Z-R relationships. Data was obtained during three warm seasons (over 14 000 minutes of high quality data). They found

$Z = 271 R^{1.57}$ (DSD only)

and $Z = 295 R^{1.43}$ (Radar and DSD),

using seven minute averages of the disdrometer measurements and radar observations made at 5 to 8 minute intervals. The standard-error of the indirect method is much larger than with the disdrometer only (69% vs 39%). The difference between the results of the two methods is most likely due to measurement difficulties with the "indirect" method.

Germany

The German group at Bonn also used radar for two summers of calibration observations with their disdrometer. They found

$Z = 175\ R^{1.33}$ (DSD only)

and

$Z = 175\ R^{1.43}$ (Radar and DSD).

Russia

Another indirect case which appears well established is the result of Berjuljev *et al.* (1966), $Z = 340\ R^{1.50}$, which is based on about one year of data (581 hours, 584 mm) at Valday in the USSR (between Leningrad and Moscow).

Other Studies

Other equations based on combinations of DSD information fine tuned by radar are the equations used by Hudlow and Arkell (1978) for GATE, $Z = 230\ R^{1.25}$, and by Woodley and Herndon (1970) for Miami, $Z = 300\ R^{1.43}$. The last relationship yielded rain total estimates for 50 showers with an average duration of 40 minute (+/-20 min) that averaged within 8% of the single gage values (or within 30% for the average of absolute values).

Special radar measurements have also been used to determine Z-R relationships. Doherty (1964) performed an unusual and very thorough two step project using a modified bi-static radar system which measured scattering at an angle of 60° and Doppler shift information as well. The vertically pointing Doppler radar studies of Caton (1965, $Z = 285\ R^{1.3}$ for several uniform rains adjusted to ground level) and Sekhon and Srivastava (1971; $Z = 300\ R^{1.35}$ in a thunderstorm) are also well-known. Although based on samples of only 17, ten and one storms, respectively, these three studies represent much larger sample volumes than are obtained during the entire duration of most of the disdrometer projects because of the very large volume of the radar beam. Only the disdrometer sample volume obtained by Breuer and Kreuels is of the same order of magnitude as the special radar studies.

The Largest Samples

The table shows that while the well-known direct study of Mueller obtained large sample volumes at many locations, that the Bonn project dominates the single location studies with rather impressive sample volume of about 300 000 m^3. The excellent single site study by Richards and Crozier also deserves special notice, although its sample size trails the German effort by a factor of ten. The sample volumes of the Swiss and the other German disdrometer studies are also of about the same size as the Canadian volume (Joss *et al.*, 1968; Aniol *et al.*, 1980).

3. ANALYSIS

Analyses of average values of a and b were undertaken for both general convective and thunder type storms.

General Convective Storms

Twenty-four of the general summer Z-R relationships, including MP were based on sample volumes well in access of 200 m^3 (Table 1). Since the final MP result appears to have stood the test of time rather well, the 200 m^3 threshold appears reasonable to screen out less substantial studies. The unweighted average parameters of these 24 cases are given by

$$Z = 260\ R^{1.43}$$

where the standard deviations are moderate, 52 (a) and 0.10 (b).

Thunderstorms

Table 2 is a list of the a and b values for 14 additional Z-R relationships obtained primarily during thunderstorm conditions. Note that the Indonesian relationship in Table 2 is for all rains. Thus, it could have been included in Table 1. However, since there are about 320 thunder days per year at the Bogor site, it is best included in Table 2. The average thunderstorm a and b parameters are

$$Z = 385 R^{1.46}$$

The standard deviations are +/-94(a) and +/-0.15(b).

Table 2: Thunderstorm Z-R parameters.

	a	b	Source
1	435	1.48	Jones, 1956
2	290	1.41	Blanchard, 1953
3	450	1.46	Fujiwara, 1965
4	500	1.50*	Joss, 1968
5	224	1.51	Florida: Mueller 1966
6	339	1.64	Oregan: " "
7	311	1.44	Indonesia: " "
8	482	1.30	Kreuels, 1976
9	311	1.38	Aniol/Reidl, 1980
10	430	1.44	Austin/Garrison, 1979
11	417	1.27	Doherty, 1964
12	520	1.81	Foote, 1966
13	300	1.35	Sekhon & Srivastava 1971
Mean	385	1.46	
SD	94	.15	

* Constrained to be constant.

Comparison

Almost none of the individual a and b values listed in Tables 1 and 2 are more than about 1 1/2 standard deviations from the mean. Consequently, the values in each table are mostly not significantly different from other values in the same table.

However, a sample of 14 cases from the convective storm population would be expected to have a standard deviation for a of about 13.9 (= $52/\sqrt{14}$). Thus, there appears to be a truly significant difference (385-260/13.9 = 9 standard deviations) in the coefficients of the Z-R relationships for the convective and thunder rainstorm cases.

4. CONCLUSION

PAWS research on raindrop size distributions should continue, as radar is the main evaluation tool. The present preliminary study indicates that there is some agreement amongst previous research on Z-R relationships and that thunderstorm rains should be analysed with a different Z-R relationship ($Z = 385\ R^{1.46}$) than more typical mixed convective and stratiform rain situations ($Z = 260\ R^{1.43}$). However, further study of these data is required, particularly with regard to sub-cloud relative humidity conditions at the sites within each group of the data.

REFERENCES

Anderson L J, 1948. Drop size distribution measurements in orograpahic rain. Bull. Amer. Meteor. Soc., , 2-366.

Aniol R, Reidl J and Dieringer M, 1980. Meteorol. Rdsch., 3, 50-56.

Austin P M and Geotis S, 1979. Raindrop sizes and related parameters for GATE. J. Appl. Meteor., 69-575.

Austin P M, 1979. Some comparisons of rainfall amounts measured by radar and with rain gauges. Preprints: 19th Conference on Radar Meteorology, AMS, Boston, 431-437.

Battan L J, 1973. Radar Observation of the Atmosphere. U. Chicago Press, 324pp.

Bentley W A, 1904. Studies of raindrops and raindrop phenomena. Mon. Wea. Rev., 32, 450-456.

Beriuliev et al., 1966. The results of radar measurements of areal rainfall. Proc. 12th Conference Radar Meteorology, AMS, Boston, 220-221.

Best A G, 1950. The size distribution of raindrops. Quart. J. Roy. Meteor. Soc., 76, 16-36.

Blanchard D C, 1953. Raindrop size-distribution in Hawaiian rains. J. Meteor., 10, 457-473.

Breuer L J and Kreuels R K, 1976. Seasonal variation of precipitation parameters and a new hydrological field experiment in Western Germany. Preprints: 17th Conference on Radar Meteorology, AMS, Boston, 432-437.

Caton P G F, 1966. Raindrop size distributions in the free atmosphere. Q. J. Roy. Meteor. Soc., 92, 15-30.

Cunning J B, 1976. Comparison of the Z-R relationships for seeded and non-seeded Florida cumuli. J. Appl. Meteor., 15. 1121-1125.

Cunning J B and Sax R I, 1977. A Z-R relationship for the GATE b-scale array. Mon. Weather Rev., 105, 1330-1336.

Diem M, 1960. Concerning the measuring technique of cloud structure and precipitation. Werkzeitschrift, 38, 89-94.

Diem M, 1966. Rains in the Arctic temperate and tropical zones. Sci. Rept. Karlsruhe: Meteorologisches Institut Technische Hochschule.

Doherty L H, 1964. J. Atmos. Sci., 21, 6.

Doumoulin G and Gogombles A, 1966. A comparison of radar values of precipitation intensities and rainfall rate from a rain gauge. Proc. 12th Conference on Radar Meteorology, AMS, Boston, 190-197.

Foote G B, 1966. A Z-R relation for mountain thunderstorms. J. Appl. Meteor., 2, 229-231.

Fujiwara M, 1965. Raindrop size distribution from individual storms. J. Atmos. Sci., 22, 585-591.

Gamache J F and Houze Jr R A, 1983. Water budget of a mesoscale convective system in the tropics. J. Atmos. Sci., 40, 1835-1850.

Gorelik A G et al., 1967. Izvest. Akad. Naak, SSR, Fiz. Atmos i Okeana, Moscow 3:961-966.

Grosh R C, 1984. Radar Meteorology. Working Paper No. 4, NDP/WMO, pp120.

Hudlow M D and Arkell R E, 1978. Effect of temporal and spatial sampling errors and Z-R variability on accuracy of GATE radar rainfall estimates. Preprints: 18th Conference on Radar Meteorology, AMS, Boston, 342-349.

Jatila E and Puhakka T, 1973. Experiments on the measurement of areal rainfall by radar. Geophysica, 103-125.

Jones D M A, 1956. Rainfall drop size distribution and radar reflectivity, Res. Rep No. 6. Urbana, Illinois State Water Survey.

Jorgensen D P and Willis P T, 1982. A Z-R relationship for hurricanes. J. Appl. Meteor., 21, 356-366.

Joss J, Thames J C and Waldvogel A, 1968. The accuracy of daily rainfall measurements by radar. Preprints 13th Conference on Radar Meteorology, AMS, Boston, 448-451.

Kelkar V N, 1959. Size distribution of raindrops - Part I. Ind. J. Meteor. Geophys., 126-136.

Kelkar V N, 1960. Size distribution of raindrops - Part II. Ind. J. Meteor. Geophys., 323-330.

Laws J O and Parsons D A, 1943. The relation of raindrop size to intensity. Trans. Amer.. Geophys. Union., 24, Part II, 452-460.

Marshall J S and Palmer W M, 1948. The distribution of raindrops with size. J. Meteor., 5, 165-166.

Mueller E A, 1966. Radar cross-sections from drop size spectra. PhD Thesis, University of Illinois, 50 pp.

Ramana Murty B L V and Gapta S C, 1959. Precipitation characteristics based on raindrop size measurements at Delhi and Khandala during southwest monsoon. J. Sci. Industrial Res., New Delhi, 18A:352-371.

Richards W G and Crozier C L, 1983. Precipitation measurement with a C-band weather radar in Southern Ontario. Atmosphere-Ocean, 21(2), 125-137.

Sekhon R S and Srivastava R C, 1971. Doppler radar observations of drop size distribution in a thunderstorm. J. Atmos. Sci., 28, 983-994.

Sivaramakrishnon M V and Selvam M, 1967. The relation of raindrop size to intensity of rainfall in different types of tropical rain using a simple raindrop recorder. Ind. J. Meteor. Geophys., 18, 13-26.

Wexler R, 1947. Radar detection of a frontal storm, 18 June 1946. J. Meteor., 4, 38-44.

Wexler R, 1948. Rain intensities by radar. J Meteor., 5, 171-173.

Wilson J W and Brandes E A, 1979. Radar measurement of rainfall - A summary. Bull. Amer. Meteoro. Soc., 60-9, 1048-1058.

Woodley W and Herndon A, 1970. A rain gauge evaluation of the Miami reflectivity-rainfall rate relation. J. Appl. Meteor., 9, 258-264.

Zawadski I, 1984. Factors affecting the precision of radar rain measurements of rain. Preprints: 22nd Conference on Radar Meteorology, AMS, Boston. 251-256.

F. RAIN CLIMATE NEAR CAROLINA

R C Grosh and C Muller

1. INTRODUCTION

The annual cycle of precipitation in the PAWS experimental area is being examined because it is important to understand where and when additional rain would be most desirable, as well as to be familiar with natural variations. The monthly rainfall data from all known sites within 100 km from the new Carolina radar site were obtained and are being analysed to provide this information. The analysis is in terms of annual and monthly mean rainfall and its spatial and temporal variability. Only 12 stations are considered in this preliminary report.

2. DATA

The 12 sites chosen for inclusion in this first look at the data were selected to be representative of the four quadrants about Carolina and because they had long records which would supply stable statistical information (Table 1).

Table 1. Stations examined

Station			height (m)	Length of record (yrs)	Annual rain days	Annual rain (mm)
1	Carolina	(C)	1696	75	92	779
2	Amsterdam	(A)	1239	83	61	843
3	Badplaas	(BS)	1067	76	59	839
4	Belfast	(B)	1970	82	58	795
5	Bethal	(BL)	1663	24	95	724
6	Dullstroom	(D)	2034	81	62	801
7	Ermelo	(E)	1694	64	96	734
8	Machadodorp	(M)	1609	84	97	794
9	Middleburg	(MB)	1447	84	70	691
10	Morgenzon	(MN)	1637	63	57	688
11	Nelshoogte	(NH)	1370	53	99	1109
12	Oshoek	(O)	1370	22	57	897
	Mean		1566	66	75.2	808
	S.D.		283		18.5	114

3. GEOGRAPHY

In general, the network consists of Highveld to the west and Lowveld to the east. There are two main areas of unusually high ground in the network. One ridge line extends northward from Belfast through Dullstroom. Numerous peaks in this line exceed 2 km with the tallest peaks north of Dullstroom. There are also a number of more isolated peaks in a line which begins about 15 km east of Machadodorp and extends northward to beyond the network. Most of these peaks are slightly less than 2 km. Thus, the highest ground tends to be in the centre of the network along a north to south line with the tallest peaks near its northern edge. The Lowveld terrain is considerably more irregular than in the Highveld. Altitudes of the 12 stations range from 1067 m (Badplaas) to 2034 m (Dullstroom) with the mean height being 1566 m ($\pm$283 m).

4. ANNUAL RAINFALL

The mean annual rainfall in the network is about 800 mm (808 mm) with a station to station standard deviation of about 100 mm (114 mm, Table 1). The highest annual rains are in the east (Figure 1). However, strong local variations not noticeable from the 12 station network are to be found near topographic features in more detailed analyses, most noticeably near the southeast boundary.

On average, the rain falls on about 75 days (Table 1). However, there were distinct short distance variations in the number of rain days, also. Carolina had 92 rain days per year while nearby Belfast and Badplaas reported less than 60 rain days per year. The correlation between reported rain days and annual rainfall is very poor ($r = 0.16$).

Annual rainfall for these 12 stations is also poorly correlated with station height ($r = -0.36$). However, if one considers only the seven stations west of the escarpment, the correlation is much improved ($r = 0.87$).

5. MONTHLY RAINFALL

The mean monthly rainfalls for the 12 stations are shown in Figure 2. Obviously, there is a clear seasonal cycle with a distinct rainy season,

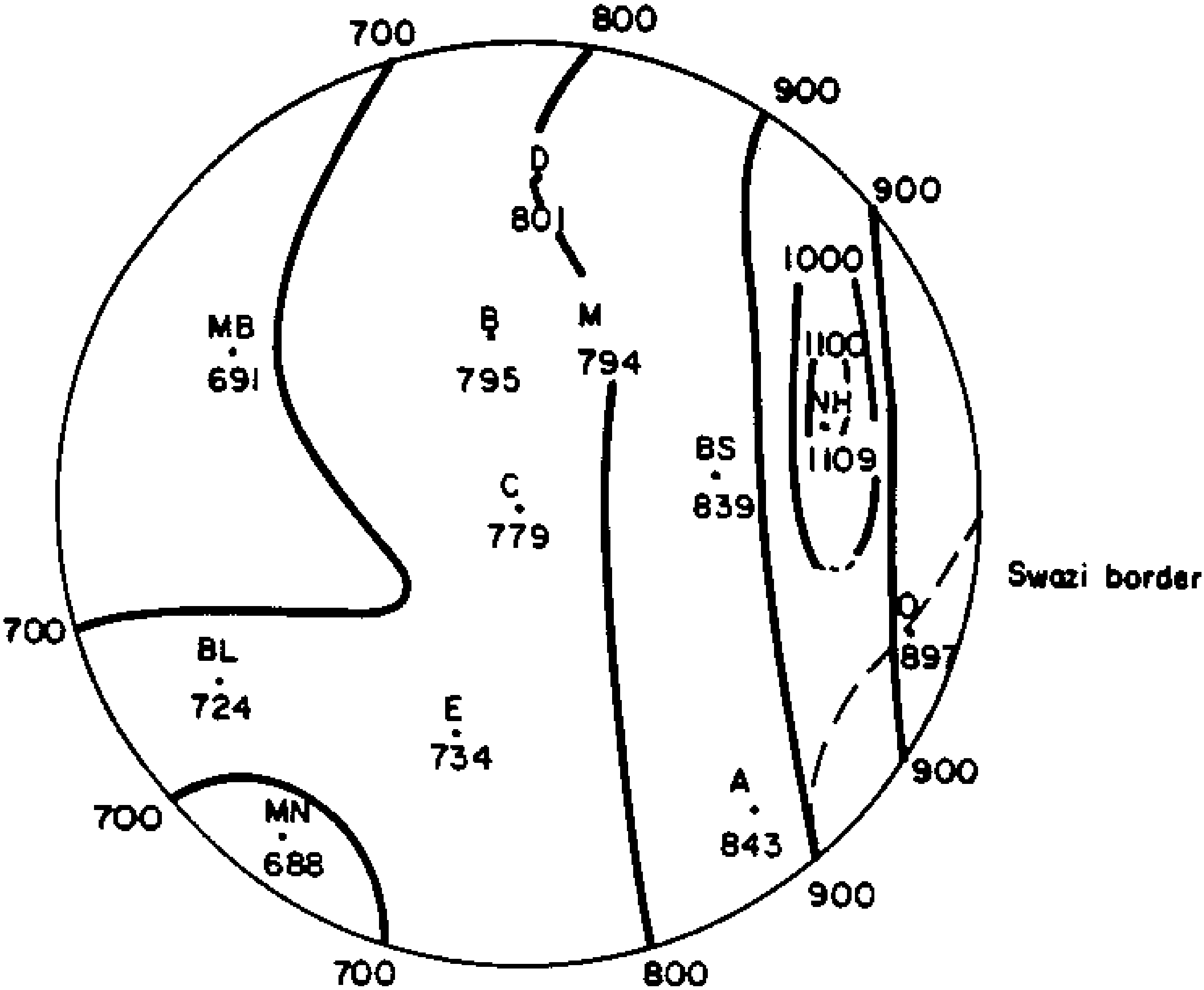

Figure 1. Annual rainfall - Carolina network (mm).

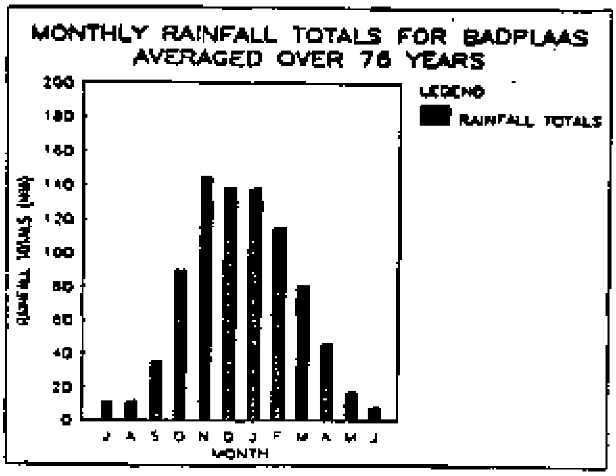

Figure 2a.

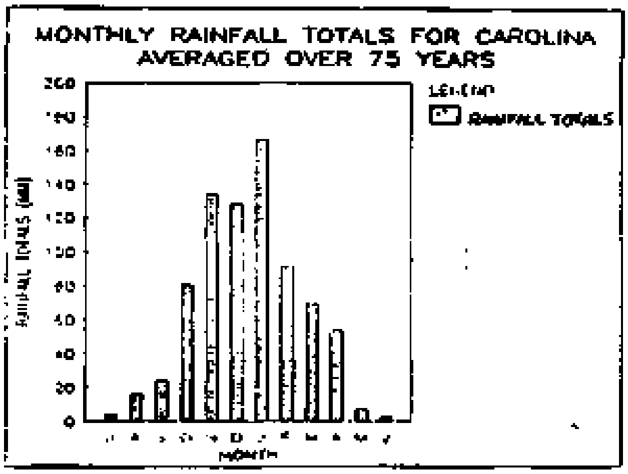

Figure 2b.

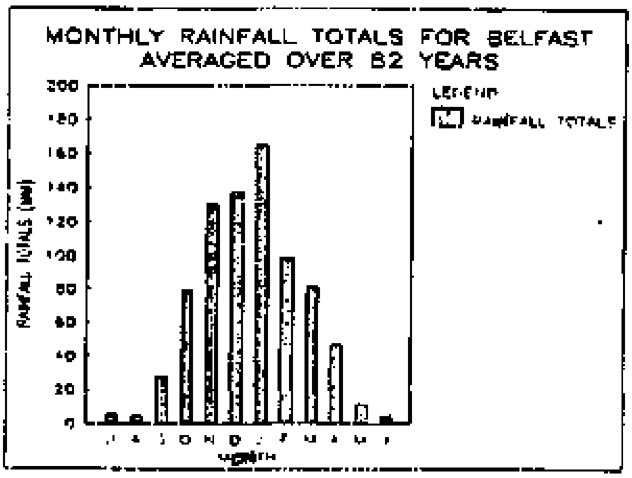

Figure 2c.

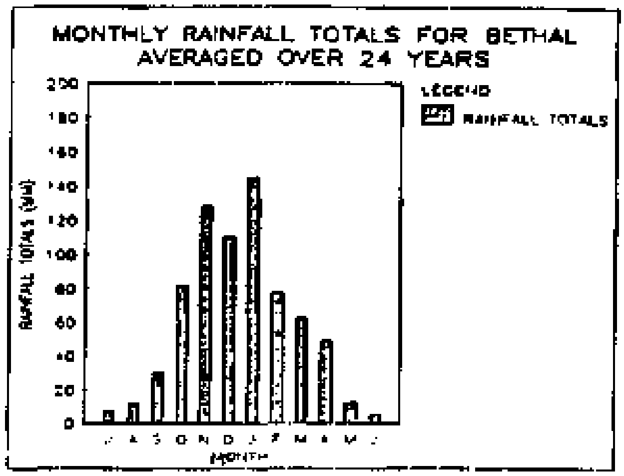

Figure 2d.

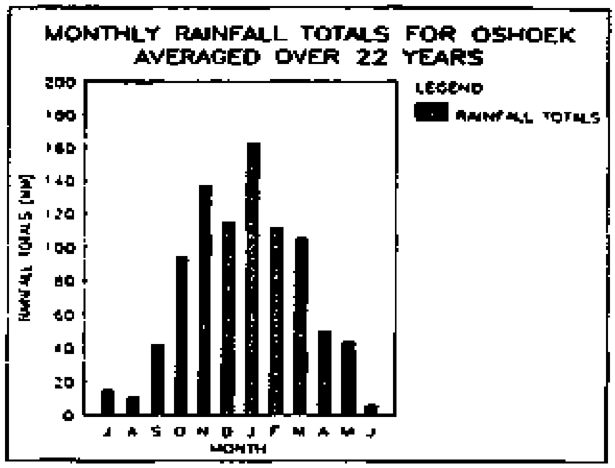

Figure 2e.

primarily from October to March. November, December and January are the three months with the most rain at all 12 stations. However, a few stations (Carolina, Belfast, Bethal and Oshoek) have very pronounced January rainfalls as well (Figures 2b-e).

For the network as a whole, rainfall in January averaged 146 mm with a between stations SD of 21 mm. January is also usually (but not always) the month with the largest standard deviation between years at a given site (Figure 3a with 3b and 3c).

A convenient measure of the relative variability of monthly rainfall is the coefficient of variability, CV. Since CV consists of the SD/mean, the large SDs in months with heavy rainfall are normalised. The graphs (Figure 4) reveal that in CV terms, the relative variability is least during the rainiest months. During the heart of the rainy season, CV - 0.5 at most stations. There is usually a smooth annual trend of CV as well, although occasionally February is slightly anomalous (compare Figure 4a with 4b).

The correlation of January rainfall with altitude was very poor ($r = 0.03$) for the 12 station network, but was greatly improved for the seven western stations ($r = 0.63$).

6. CONCLUSION

The annual rainfall near Carolina is expected to be about 800 mm $\pm$-100 mm. There is a distinct rainy season with heaviest rains in November, December and January. During the wettest month, January, mean rainfall in the network was nearly 150 mm and a standard deviation of over 20 mm can be expected.

Some stations have relatively heavy January rains compared with November and December. The great variability of January and the other wet month rains at the 12 stations is somewhat compensated by the large mean monthly rains. Thus, the coefficient of variability is usually about 0.5 in the heart of the rainy season and varies relatively smoothly throughout the year. February CVs have a slight positive anomaly for about half the sites.

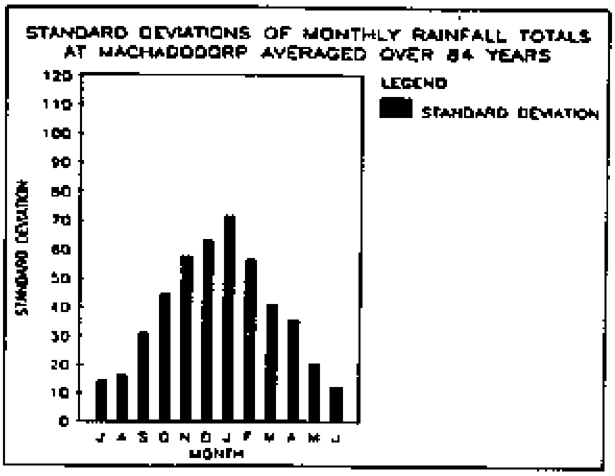

Figure 3a.

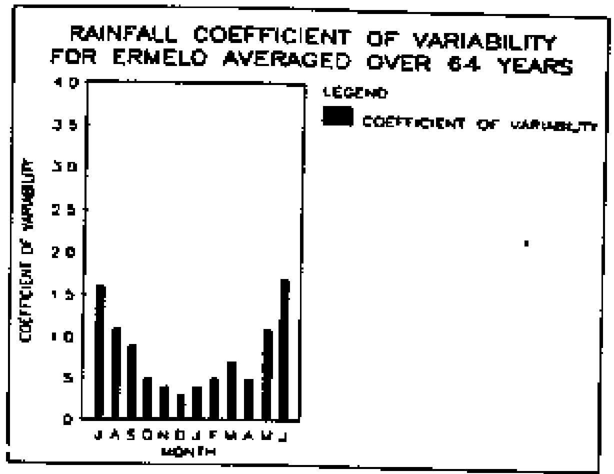

Figure 4a.

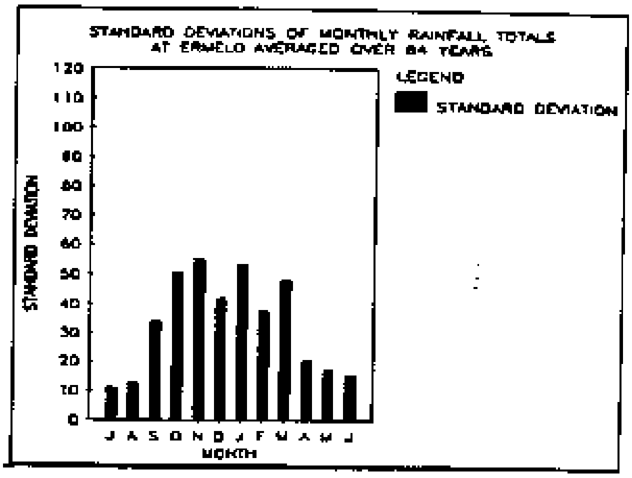

Figure 3b.

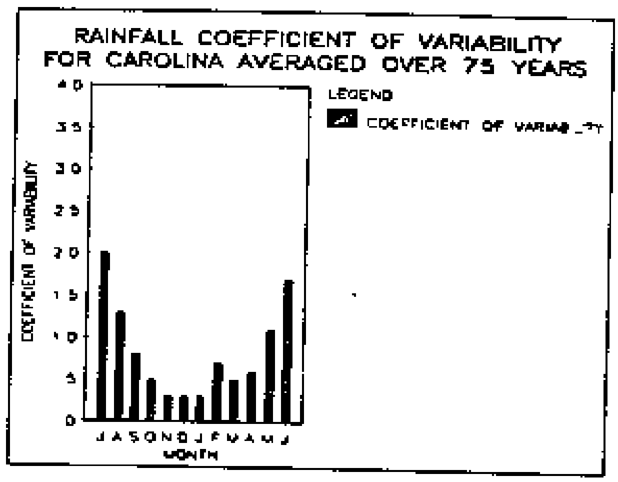

Figure 4b.

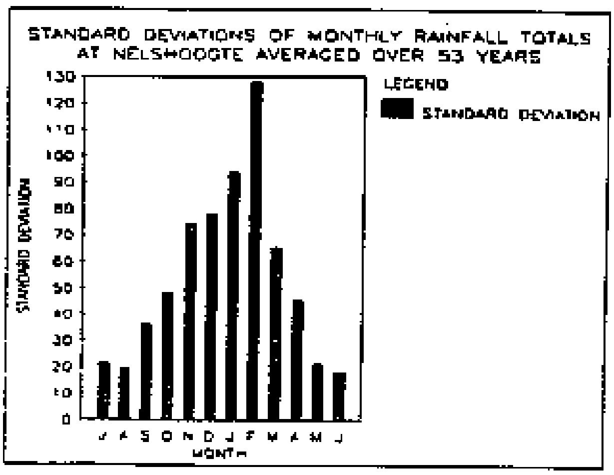

Figure 3c.

The correlation between rainfall and altitude for the entire network was poor on an annual basis and for January. However, this point requires further analysis of wind and terrain effects, as the seven stations west of the escarpment yielded much improved correlations.

G. RAIN SAMPLING FOR RAIN STIMULATION EXPERIMENTS

R C Grosh

1. INTRODUCTION

Radar rainfall estimates are widely accepted as being the best source of areal precipitation information. These estimates are optimised when supported by appropriate auxiliary "ground truth" or calibration observations, as the electronic calibration may drift, and there are some uncertainties in the knowledge of the true raindrop size distribution (Grosh, 1990), as well as in the impact of drop growth, updraughts, wind effects and evaporation. For example, Zawadski (1984) has found that subcloud coalescence can increase radar reflectivity by 20% while evaporation can decrease rain rates by a similar amount and Grosh (1984) shows that effective rain rates are reduced to zero for even the heaviest liquid rain contents if updraughts are over 9.2 mps. On the other hand, most still air rain rates are effectively doubled in downdraughts of about 5 mps. Given that the dimensions of up and downdraughts in convective storms can be as small as a few hundred metres (Ackerman, 1967) and have been repeatedly observed to be typically only one or two kilometres wide since the time of "The Thunderstorm" report, it follows that there may be a need for many ground calibration points if the main small-scale influences are to be accounted for properly.

Calibration with ground truth to reduce the bias of the radar estimates is almost always achieved via rain gauges. The rain gauges are some times in clusters but more often in a nearly uniformly spaced network, as cluster calibration has been found to be of limited utility because storm cases will frequently "miss" the cluster and, in general, the clusters are not representative enough. For example, the use of cluster calibration increased the scatter in the relationship between the radar rain estimates and the true rainfall in FACE (Barnston and Thomas, 1983). However, it is possible that for some applications gauges may not be the best approach to calibration, particularly when storms rarely occur over a ground network. Thus, airborne rain sampling for radar calibration is also considered in this report, in spite of the present uncertain accuracy of aircraft measurements.

The main variables in the problem of determining the rain gauge requirements for a rain stimulation project relying on radar observations for evaluation are the network size, the number and density of rain gauges, the geometric configuration of the network, and the size and shape of the storms. When making comparisons with airborne techniques, it is also necessary to know the volume of air sampled by the ground-based and airborne instruments.

2. NETWORK SIZE

Network size is of fundamental importance, as it controls the number of storms to be sampled. Consequently, this variable is discussed first (Table 1).

Table 1. Number of storms sampled annually by networks of various size for PAWS.

Area sampled (km^2)	Cases
20 000 (nominal)	≈ 50
10 000	25
5 000	12.5
1 250	3.1
1 000	2.5
500	1.2

In the PAWS (the Program for Atmospheric Water Supply) rain stimulation experiment (Morrison *et al.*, 1986; Dixon and Mather, 1986; Grosh, 1988; 1989 and Grosh *et al.* 1989), about 50 storms per year meet the operational decision making requirement for launching the aircraft, two separate 40 dBz precipitation echo centres within 80 km of the radar. The following calculations are based on the current criteria for storm selection. However, the criteria may be subject to change in the future. Also, stratification of the data will effect the effective sample size. Thus, in the 3-year PAWS seeding experiment at Nelspruit, 169 cases actually met the operational decision making criteria, but the number of cases included in most of the final analyses was reduced to about 85. Obviously, the nominal value of 50 cases/year represents a compromise of these extremes. A smaller ground network will only sample a proportional fraction of these cases (Table 1). It follows that a typical network with an area of about 10 000 km^2 (such as the 13 000 km^2 used in FACE) will contain only about half the radar viewing area sample, or about 25 cases per year.

Such statistics suggest that if the spatial distribution of storm tracks is uniform, then an areal rain stimulation experiment must be conducted in an area of at least 10 000 km^2 to obtain a reasonable sample of the selected storms in a limited number of years. Therefore, this report is focussed on networks of 10 000 and 20 000 km^2. Obviously, the larger the network, the quicker an experiment can be completed. Consequently, an area even larger than 20 000 km^2 is preferable. Thus, increasing the useful range of the PAWS radar rainfall measurements by reducing the radar beam width requires immediate serious consideration. For example, if the radar observations could be accurately extended to a range of 106 km (the mean range of the echoes evaluated for FACE) the additional number of storm cases obtained would permit an experiment to be concluded 3.5 times faster than for a 10 000 km^2 network.

However, large networks require many rain gauges. This may become costly and inconvenient. Thus, the number of gauges (or samples) likely to provide calibration information for radar rain estimates for rain stimulation experiments is also discussed.

3. ECHO TRACK AREA

The radar observations of 147 storms included in the earlier three years of PAWS research at Nelspruit show that the maximum instantaneous areas of rainfall for the experimental storm cases have a mean value (aloft) of slightly less than 120 km^2 (117 km^2). Assuming a circular echo, the peak radius (r) is about 6.1 km. The experimental cases also had a mean echo duration of 1.56 hours.

Echo Speed

Several studies have shown that typical echo speeds in the Lowveld near Nelspruit and in the Highveld near Carolina are about 25 km/hr (Mader, 1978; Dixon, 1977; Kelbe, 1984), but may range between 20 and 30 km/hr (Carte and Held, 1978) and are size dependent. In particular, a manual study of computer plotted storm tracks for 50 PAWS *cases* found the average storm speed to be 23.4 (+/-9.7) km/hr (Grosh and Muller, 1990). Thus, the typical path length (l) would be about 39 km for the average storm duration. The echo swath or track area may be estimated by a parallelogram. This shape is based on assumed linear growth and decay before and after the peak echo area is reached halfway through the storm's life cycle. The swath area is then given by A = rl and is typically about 250 km^2 with the likely range being about 200 to 300 km^2 (corresponding to storm speeds of ≈20 to 30 km/hr). Larger and smaller storm sizes are also considered, to provide a spectrum of results in the range likely to be encountered. For example, there is some controversy over the best echo speeds to apply as one report suggests general Nelspruit echoes move at less than 15 km/hr (Mather, 1990). This possibility is also covered, although the median size of the general storms is well below that of the mean experimental cases. If a speed of 15 km/hr is assumed, A will only be about 150 km^2.

4. THEORY

The probability of at least one rain gauge in a network detecting a rainstorm depends on the size, shape and motion of the storm and the density of the gauge network. However, two approaches must be considered when determining the detection probability of a given network with a known number of gauges. The choice depends on the uniformity of the gauge spacing.

Random Spacing

If the gauges are randomly located throughout the network, the probability of one gauge detecting the storm is given by the ratio of the storm area (A) to the network area (Anet), A/Anet. The probability of the storm not being detected is 1 - A/Anet. The probability of two gauges detecting the storm is $(A/Anet)^2$. Thus, Grosh (1977) has shown that the probability of at least one gauge in a network of N gauges detecting the storm is:

$$Pnet = 1 - (1 - A/Anet)^N.$$

This function was evaluated for A between 50 and 400 km^2 and for various Anet(1 000, 2 500, 5 000, 10 000 and 20 000 km^2) and N(20, 50, 100, 200, 300, 400). See Figure 1a.

Uniform Spacing

Networks of gauges with uniform spacing will provide the highest detection probabilities (Grosh, 1977). Pnet must be estimated empirically for the uniform networks. Thus, an experiment based on randomly dropping rectangular paper storms of different sizes and shapes on gridded pages was undertaken to demonstrate the advantages of uniformly spaced networks. The paper experiment simulated storm areas of 50, 100, 200, 300 and 400 km^2 with networks scaled to gauge spacings of 25, 100, 225, 400 and 625 km^2/gauge. Different storm shapes were simulated by using storms with different aspect ratios. 6700 trials were run as up to 450 trials were needed to obtain stable Pnet values for some D and A combinations. The results are listed in Table 2. Since only a limited number of grids can be used, the plotted curves usually required short extrapolation (dashed) to the Pnet = 100% axis (Figure 1b). This was usually done by either simply extending the existing trend for the same A, or by using a parallel line to the curve for the next lower A.

Pnet Stability Analysis

The Pnet values for the uniform network were obtained in sets of 50 trials for each A and D combination considered. The sets of 50 trials were continued until Pnet changed by at most 1% from the sum of the previous trials. In one case (A = 300 km^2, D = 400 km^2/gauge) this required 450 trials, but 200 to 250 trials were typical for most cases where trials were necessary. Storms too large to fit between the gauges in any imaginable alignment were assigned Pnet = 1.0 after a quick

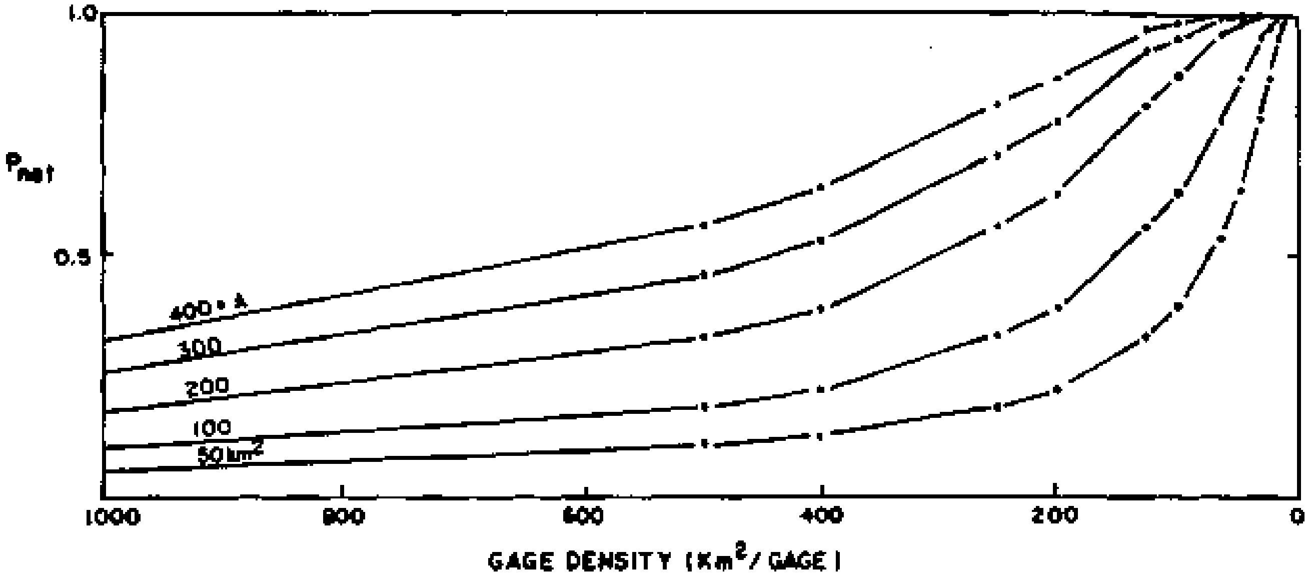

Figure 1a. Pnet for randomly located gauges of various densities (D). Pnet = 1 - (1 - A/Anet)^N.

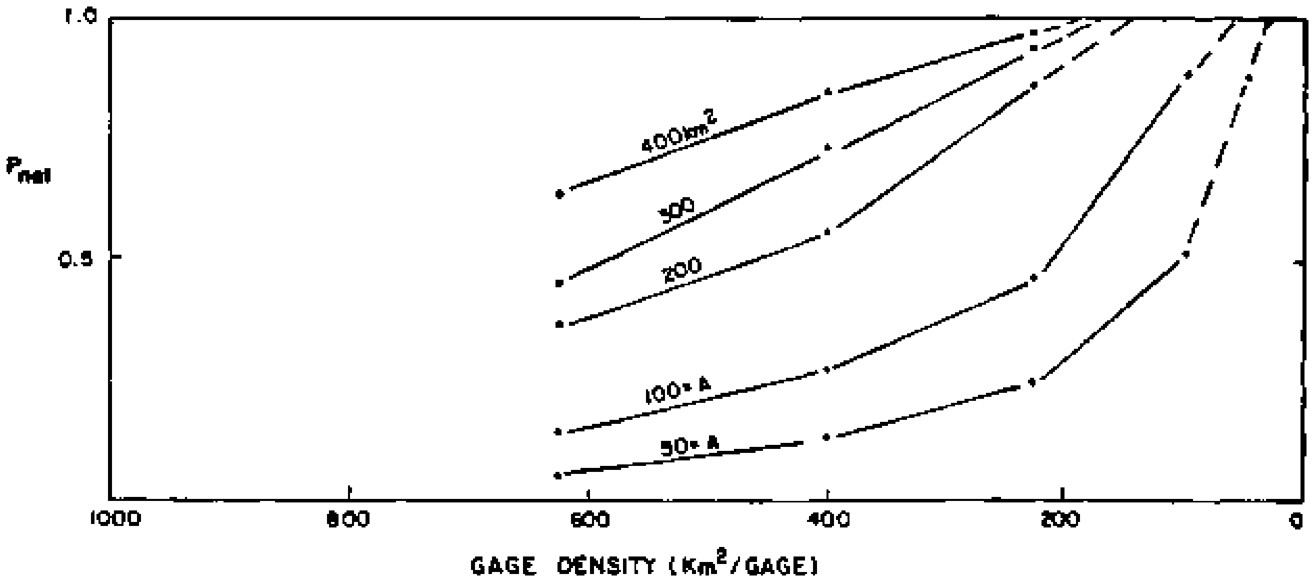

Figure 1b. Pnet as a function of gauge density for uniform gauge networks (simulated storms with various aspect ratios). Pnet determined empirically.

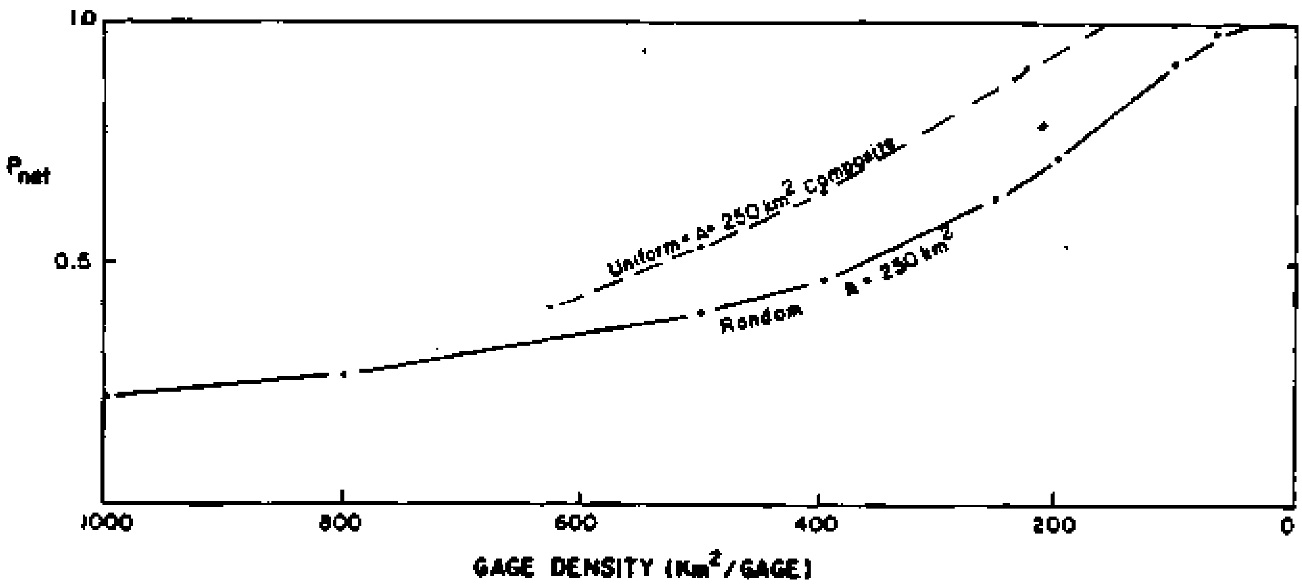

Figure 1c. Comparison of Pnet for random and uniform gauge locations (storm track area (A) = 250 km²). Empirical.

inspection. After Pnet curves had been plotted against D, a few hundred additional trials were run to eliminate the noisy appearance of some neighbouring curves. Of four points checked by this procedure, two required replotting as they varied by 4 and 6%.

Table 2. Pnet for uniform networks of density (D) as a function of swath areal (A).

$A(km^2)$	50	100	200	300	400
	Compact storms (1:1 aspect ratio)				
D (km^2/gauge)					
25		1.0	1.0	1.0	1.0
100	-	0.92	1.0	1.0	1.0
225	-	0.47	0.87	0.97	1.0
400	-	0.27	0.595	0.77	0.92
625	-	0.12	0.38	0.46	0.68
	Line Storms (aspect ratios >1)				
25	1.0	1.0	1.0	1.0	1.0
100	0.51	0.84	1.0	1.0	1.0
225	0.24	0.45	0.85	0.91	0.93
400	0.13	0.24	0.54	0.68	0.78
625	0.05	0.15	0.34	0.44	0.60
	Composite of Compact and Line Storms				
25	1.0	1.0	1.0	1.0	1.0
100	0.51	0.88	1.0	1.0	1.0
225	0.24	0.46	0.86	0.94	0.97
400	0.13	0.26	0.56	0.73	0.85
625	0.05	0.14	0.36	0.45	0.64

Deviate Grids

Both the theoretical and empirical approaches must be considered, as actual gauge networks often deviate considerably from uniform spacing, and it is impossible to anticipate all the possible patterns. Nevertheless, another experiment was conducted to examine the effect of gauge locations deviating slightly from uniform grid points. Thus, a grid with ± 2 km deviations from the uniform 10 km grid was constructed. A pattern of deviations was assumed. At the start of the first originally uniform west to east row of simulated gauge locations the first grid location was displaced 2 km to the north while the second location was moved 2 km to the south. Then two similar east and west (+ then -) deviations were plotted. This pattern repeated itself until the end of the row. In the second row the opposite deviation was assumed for the initial gauge location, but with the south and north deviations still plotted first. At the start of the third and fourth rows both deviations to the east and west were incorporated before the north and south direction was considered. The fifth row was similar to the first row and so forth. Only the 50 and 100 km^2 storms were studied on the deviate network.

5. RESULTS

Gauge Density

The most important variable in the storm detection problem is the density (D) of the raingauge network. Figure 1 contains plots of both the theoretical (random) and empirical (uniform) Pnet calculations as functions of D. The expected increase in detection probability as gauges are placed closer together is quantitatively depicted in the diagrams for both approaches for all storm sizes.

The advantage for uniform gauge locations is greatest for dense networks. This can be seen best in Figure 1c, which is a plot of the interpolated curves for both methods for the assumed typical storm size of experimental seeding cases ($A = 250\ km^2$). The advantage of the uniform network appears to begin at $D \approx 700\ km^2$/gauge and continues to increase as D decreases. Thus, while Pnet for the random network exceeds 90% for $D \approx 100\ km^2$/ gauge, Pnet for the uniform network reaches the same level at $D \approx 200\ km^2$/gauge. Consequently, half as many gauges are needed for uniform networks to achieve the same Pnet.

Of course, there is an obvious limit to the increasing detection advantage of uniform networks at Pnet = 100%. For example, the uniform grid curve in Figure 1c reaches the Pnet = 100% axis at about 200 km^2/gauge. Consequently, the maximum advantage of the uniform network occurs near the

D where Pnet = 100% for the uniform network. The favourable Pnet difference must decrease for closer gauge spacing as Pnet for the random network will continue to improve, while the perfect Pnet (= 100%) result for the uniform network is constant.

It is interesting to note that the D value for the 90% detection level suggested by this study corresponds to about the same as the spacing used between gauges in the large FACE network, 11 km (vs 10 to 14 km in the Eastern Transvaal).

Storm Shape

Compact storms (aspect ratio 1:1) are more efficiently detected by uniform networks than are line storms. The line storms simulated mostly had aspect ratios of 2:1. However, the larger storms (A = 300 and 400 km^2) had 3:1 and 4:1 aspect ratios. The impact of storm shape is most noticeable for the largest aspect ratios, and may actually be more important than storm size in some cases. For example, at D less than about 300 km^2/gauge, the linear 400 km^2 storm was detected less efficiently than the 300 km^2 compact storm (not shown).

If all storms had the same shape, the ratio A/D could be used directly to provide very good estimates of Pnet throughout a large range of A/D. A plot of the empirically obtained Pnet for the uniform networks versus the ratio of the storm track area to the gauge density for storms with 1:1 aspect ratios revealed that up to Pnet = 80 to 90%, A/D describe a 1:1 relationship to Pnet for all the different storm sizes very well (not shown). In fact A/D may be the best estimate of Pnet in this range since the empirical probabilities must be recognised as having been affected by sampling fluctuations to an unknown extent (a few per cent is likely) in spite of the rather stringent stability criterion. However, above Pnet of about 90% there were unmistakable deviations from the linear 1:1 relationship between Pnet and A/D. Above A/D ≈1, the empirical detection probabilities are distinctly less than the 1:1 relationship with A/D would predict. These variations are real and due to the obvious physical possibility for (square) storms with 1:1 aspect ratios to easily fit between the grid points when occurring at an angle to the grid rows.

The empirical Pnet estimates for the lines had similar but even larger deviations from the 1:1 relationship with A/D. The breakdown occurred earlier, at A/D ≈0.7, and the lines with the largest aspect ratios tended to have the lowest probability of detection at large A/D. The decreases in Pnet for lines are associated with the obvious fact that storms with the same area but one long dimension will frequently be aligned parallel to the rows and can more easily occur between gauges. Since storms of various shapes occur in nature, the Pnet for storms of the same area but with different shapes have been combined to produce Figure 2. Because of the stabilising influence of the compact storms, this diagram indicates reduced variability relative to the 1:1 relationship of Pnet with A/D compared with that of the linear storms (not shown).

Effects of Deviations from Uniform Grid

The impact on Pnet of gauge location deviations from uniform spacing depends on the ratio, A/D. When the storm track area is about the same size as the gauge density, detection is clearly hindered by non-uniform locations, as enough extra space between some of the gauges is then available to permit the storm track to be between the gauges more often than is possible in the uniform network which is very efficient at detecting square 100 km^2 storms. Although the decrease in Pnet was small (≈6%), there was no mistaking this impact during the A = 100 km^2 trials.

Number of gauges

Figure 3 has been plotted to aid determining the number of gauges that are required for networks of 10 000 and 20 000 km^2 to detect a spectrum of likely storm sizes at any selected probability level. Both random and uniform networks are considered so that possible location variations may be anticipated when designing a network. Figure 3a is for the average PAWS storm case (A = 250 km^2). For 90% detection and a 20 000 km^2 network, random gauge locations require about 200 gauges, but uniform locations only require about 100 gauges. There is also about a factor of two reduction in the number of gauges required for the uniform 10 000 km^2 network to provide 90% detection. The advantages of uniform networks may therefore provide significant economies for experimental duration, as large areas may be gauged adequately with fewer gauges for the purpose of storm detection.

However, many more gauges may be required for small storms. For example, storms with track areas of 150 km^2 are likely to occur frequently in the PAWS study area. Even the uniform 10 000 km^2 network requires about 100 gauges to detect these storms 90% of the time (Figure 3b).

Storm Size

Figure 4 has been constructed to provide information on Pnet for storms of all likely sizes. Only random and uniform networks with gauge densities of about 100 to 200 km km^2/gauge are considered. The uniform network with D = 100 km^2/gauge detects storms smaller than 100 km^2 with Pnet = 90%, while the corresponding random network reaches the same detection level only for storms well over 200 km^2. The sensitivity to gauge spacing is also very evident, as the uniform network with D = 225 km^2/gauge only crosses the Pnet = 90% level for storms over 300 km^2.

6. RAIN GAUGE SAMPLING

A typical rain gauge has a 400 cm^2 opening. If a typical rain rate is assumed, the air volume sampling rate may be estimated following the approach Austin and Geotis (1979) applied to disdrometer sampling. Recently, Rogers (1989) has shown that an average rain rate of 4 mm/hr can be assumed for the radar echo above the 25 dBz contour. Thus, this crude procedure is not unreasonable. In essence, Austin and Geotis assume that a typical median volume drop falls at a constant fall speed above the 50 cm^2 disdrometer sensor. Thus, a volume of about 2 m^3/min is swept out by such drops falling above the disdrometer. Because of the larger gauge collecting area, the sample volume Austin and Geotis calculated must be increased by a factor of 8 for a rain gauge, or to about 16 m^3/min.

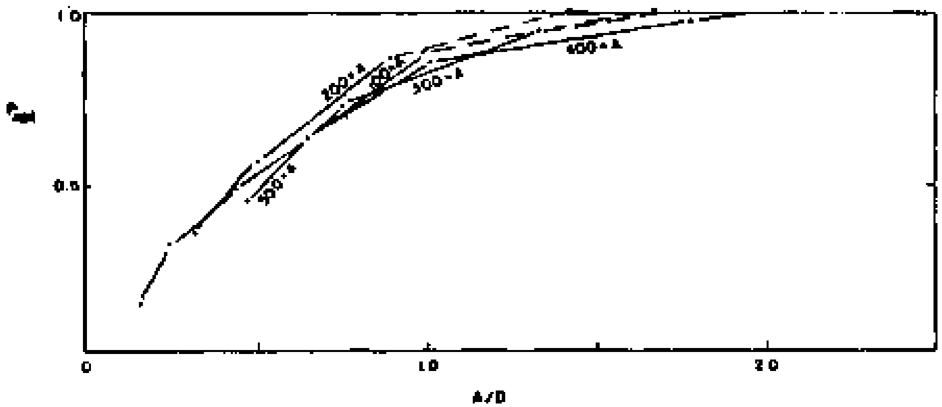

Figure 2. Pnet versus A/D (composite storms).

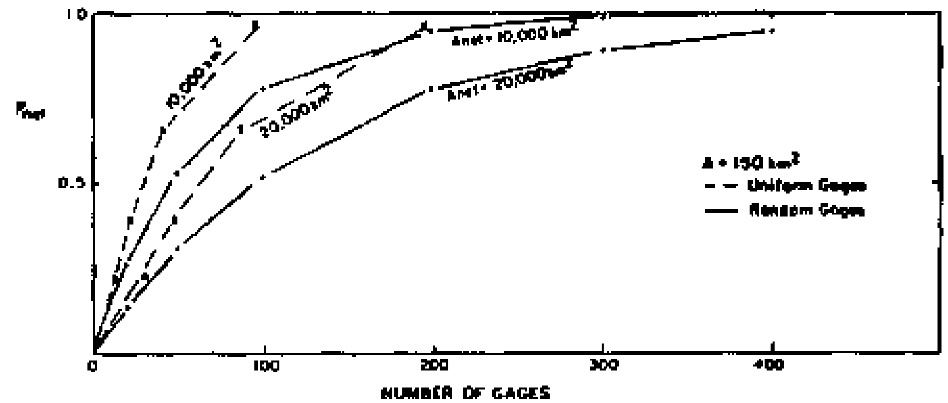

Figure 3b. Pnet versus number of gauges for A = 150 km² and Anet = 10 000 and 20 000 km²

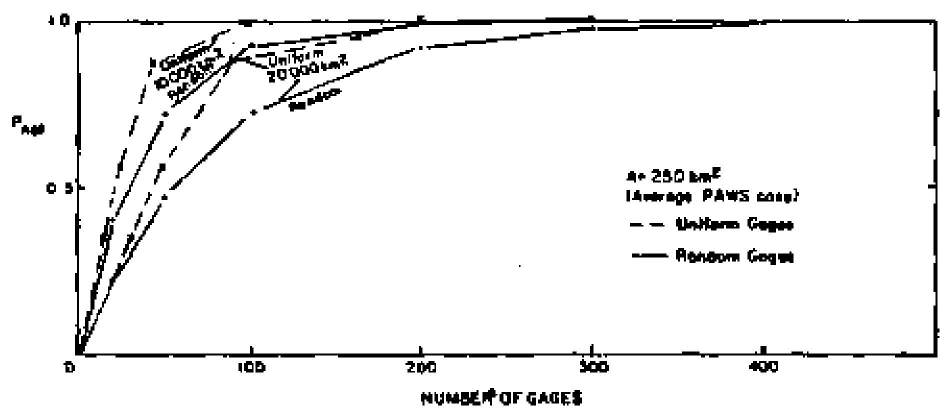

Figure 3a. Pnet versus number of gauges for A = 250 km² and Anet = 10 000 and 20 000 km².

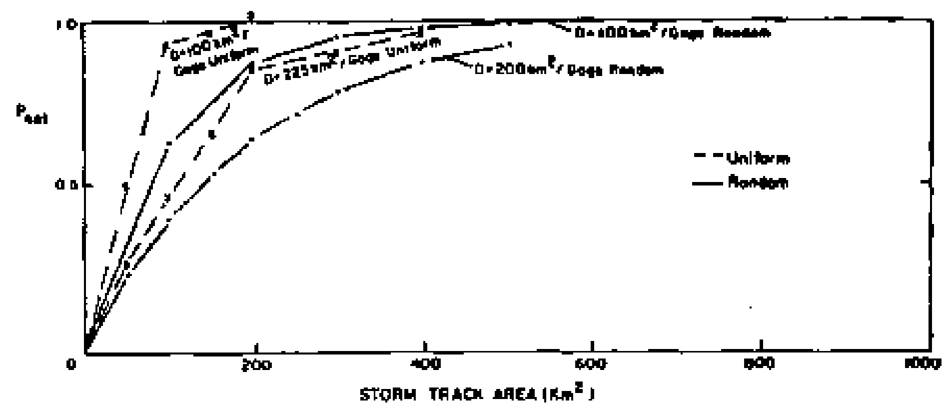

Figure 4. Pnet versus A.

In a network with one gauge every 100 km^2, a 250 km^2 storm track can be expected to intercept about two and a half gauges on average. If the average instantaneous storm area, =50 km^2, is applied to calculate the sample from a gauge crossing at 25 km/hr, a distance slightly less than the actual storm diameter (8 km) must be applied as a direct hit of the gauge is unlikely. The length (L) of storm which affects a rain gauge during a complete overpass will on average be about 64% of the storm diameter (d). The typical distance, L/d (= $2/\pi$), is calculated from the average of the cosine of the azimuth over a 90° quadrant. However, gauges intersected by the middle half of the storm will sample precipitation from an overpass length which exceeds 85% of the storm diameter. Thus, the time over a gauge will be less than the maximum of about 19.2 minutes and the sample volume somewhat less than 307 m^3. However, if all the affected gauges are considered, the sample volume could average two and a half times this, or up to 768 m^3 per case for the rain gauge network. During this 0.8 hour period over the gauges a radar sampling only every 5 minutes could obtain up to ~9 scan measurements for direct comparison with the gages. At slower speeds (e.g. ~15 km/h), the 0.8 h maximum sampling period is unchanged.

7. AIRBORNE SAMPLING

It is also possible to sample rainfall near cloud base by means of low flying aircraft. This technique has the great advantage of being very mobile. Thus, obtaining samples is assured, provided severe weather or terrain problems for airborne operations can be overcome. However, uncertainties in instrument performance and its sampling volume, as well as in the impact of distortion to the air flow about the plane on the air passing through the instrument's aperture are major shortcomings of the airborne approach. There may also be a limit to the maximum drop size measurable, depending on the analysis technique employed for the 2-D probe.

The array of diodes is 6.2 mm wide. If the depth of field is taken as 261 mm (although this actually depends on the number of diodes occluded), a crude estimate of the volume sampling rate can be obtained from the plane's air speed. In the case of the PAWS cloud base plane the speed is nominally 90 mps. Thus, the sampling rate is about 0.15 m^3/sec, and a penetration through a typical cell of about 8 km width (≈90 sec), corresponds to a sample volume of about 13 m^3. If such samples are obtained every six minutes, a potential sample volume of about 200 m^3 might be obtained from a rainstorm lasting about 1.5 hours, as in the case of the typical PAWS experimental unit.

Another problem is that airborne measurements are made well above the surface. Thus they are, to the extent that the small sample volume is representative, indicative of conditions which usually will be much different from those at ground level where the impact of rainfall is most important. However, even the limited representativeness of the measurements is undercut by the navigation accuracy which is only on the order of 1 km. Thus, the airborne approach clearly cannot be relied on as a sole calibration source, and leading authorities strongly recommend the use of rain gauges for radar rain measurement calibration in rain stimulation projects (Changnon, 1989).

8. CONCLUSION

Rain gauge networks on the order of at least 10^4 km^2 are needed to obtain an adequate number of storm cases for weather modification experiments with limited durations. Thus, it is highly desirable to extend the range of high resolution radar observations beyond the current 80 km limit required by the current PAWS radar.

A strong effort should be made to obtain fairly uniform rain gauge locations, as network storm detection will be substantially increased. For randomly spaced networks, gauge densities must be about one per 100 km^2 to detect typical PAWS storm cases (track area ≈250 km^2) 90% of the time. However, to detect smaller storm cases (A = 150 km^2) adequately (90%), densities of order 60 to 70 km^2/gauge may be needed for random networks. In a 10^4 km^2 network this may require over 150 gauges. However, 250 km^2 storms are detected at the 90% level by uniform networks with D=225 km^2/gauge and even storms with only 150 km^2 track areas are detected 90% of the time by uniform networks with D = 150 km^2/gauge.

In the range of storm areas and networks considered likely, it was shown that uniform gauge networks of a given density require about half as many gauges as a random network to obtain the same probability of storm detection.

Slight deviations from uniform gauge locations apparently can have a moderate impact on storm detection probabilities. The most likely result is a decrease in detection rates as storm size approaches the gauge spacing. Fortunately, the effect is small.

Storm shape may have a more dramatic impact on detection probability for uniform networks as line storms are more poorly detected than compact storms. This effect is most distinct when storm size and gauge density are nearly equal, but is also noticeable at most other values of these two variables.

Preliminary calculations suggest that sample volumes obtained by typical rain gauge networks (100 km^2/gauge) may be significantly larger than the optimum airborne sample volume for a typical PAWS storm case being observed with the airborne 2D-P probe. However, the difference derives mainly from the number of gauges likely to be intercepted by a storm in a dense network, rather than an intrinsic sampling advantage to the rain gauge instrument. Nevertheless, the wide spread acceptance of rain gauge measurements, the fact that they make ground-level measurements, and the simple and relatively well-known characteristics of gauge performance give them crucial additional advantages.

Because small storms are frequently present and because it is desired to have a number of gauges detect a storm for radar rain calculation, a uniform network with a density of about 100 km^2/gauge seems a good compromise that is also compatible with feasible logistic and economic conditions. If the entire viewing area of one of the current radars (~20 000 km^2) cannot be gauged, an area of at least 10 000 km^2 selected for highest storm frequency should be gauged, providing radar viewing is not severely affected by terrain. However, a shorter experiment will result if a new radar is obtained with improved beam width characteristics that allow greater areal surveillance and more storms to be included per year.

9. REFERENCES

Ackerman B, 1967. The nature of meteorological fluctuations in clouds. J. Appl. Meteor., 6, 61-71.

Austin P M and Geotis S G, 1979. Raindrop sizes and related parameters for GATE. J. Appl. Meteor., 569-575.

Barnston A D and Thomas J L, 1983. J. Clim. and Appl. Meteor., 22, 2038-2052.

Carte, A E and Held G, 1978. Variability of hailstorms on the South African plateau. J. Appl. Meteor., 17 (3), 365-373.

Changnon S A Jr, 1989. Personal communication.

Dixon M J, 1977. Proposed mathematical model for the estimation of the areal properties of high intensity short duration storms. M Sc Thesis, University of Natal.

Dixon M J and Mather G K, 1986. Radar evaluation of a randomized cloud seeding experiment - some preliminary results. 10th Weather Modification Conference, AMS, Boston, 139-131.

Grosh R C, 1977. Relationships between severe weather and echo tops in central Illinois. Preprints: Severe Local Storms Conference, AMS, Boston, 231-238.

Grosh R C, 1984. Radar Meteorology. WMO Working Paper No. 4, p47.

Grosh R C, 1988. The science of rainmaking, a historical perspective., SASAS Newsletter, September 2-10.

Grosh R C, 1989. Rainmaking - The promise for South Africa. First Biennial Conference of the Water Institute of Southern Africa.

Grosh R C *et al.*, 1989. PAWS Restructured. J. Weather Modification, Weather Modification Association, Fresno, Ca, 94-99.

Grosh R C, 1990. A review of raindrop size distribution measurements. This volume, 45-58.

Grosh R C and Muller C, 1990. Storm speeds. This volume, 180.

Kelbe B E, 1984. Cumulus cloud characteristics of the Eastern Transvaal Highveld. Water SA, 10(2), 81-90.

Mader G N, 1978. Numerical study of storms in the Transvaal. South African Geographical Journal, 61(2), 85-98.

Mather G, 1990. Comparisons of storm statistics - The Nelspruit versus the Carolina radar site. Cloud seeding experiments. Volume 2 of this Report, 81-89.

Morrison B J *et al.*, 1986. Aircraft observations of target turrets on multicellular storms showing radar response to dry ice seeding. 10th Weather Modification Conference, AMS, Boston, 204-209.

Rogers R R, 1989. Average rain rate in a model rainstorm. Preprints: 24th Weather Radar Conference, AMS, Boston, 652-653.

Zawadski I, 1984. Factors affecting the precision of radar measurements of rain. Preprints: Conference on Radar Meteorology, AMS, Boston, 251-256.

05/22gal/sgg

III. CLOUD MODELLING

Because of (1) the extremely complex nature of the interactions between the moisture elements and particles needed to produce precipitation and (2) the need to consider the spatial and dynamic characteristics of clouds and their interaction with the ensembles growing precipitation particles, multi-dimensional time varying numerical cloud models are destined to become increasingly more important to rain stimulation experimentation as these activities develop into more truly scientific endeavours. For a particular case, cloud models can depict both the seeded and the unseeded outcomes and thus the great natural variability of rainfall that statistical approaches must confront is avoided. Considerable savings in terms of experimental duration could be realised with realistic cloud models. Also, there is a great need to better understand the outcome of cloud seeding activities and, within limitations, the detailed and comprehensive output of cloud models is well suited to such analyses. This section contains two summaries of multiple-dimensional time varying cloud modelling activities related to PAWS. A study of the climatic potential for dynamic seeding effects (seeding increased storm heights) and a study of the coalescence time parameter (CTP) are also included, as these two variables derive from numerical and conceptual cloud models and are useful in understanding the nature of cloud alterations in the Eastern Transvaal.

A. REVIEW OF EARLIER PAWS CLOUD MODELLING

G Reuter

1. INTRODUCTION

The goal of the Program for Atmospheric Water Supply (PAWS) is to explore the potential of convective cloud seeding as a possible means for modifying the rainfall over and near the escarpment of the eastern Transvaal. The difficulty of this task lies in determining whether there indeed exists a causal link between seeding and precipitation, and if so, to quantify such a link. This report summarised some highlights of PAWS research on rain drop growth, mixing, storm water budgets and related numerical cloud model development.

2. FORMATION OF RAINDROPS IN TURBULENT AIR

Observations in the PAWS region show that the time between the initial development of a convective storm and the first appearance of precipitation can be as short as 20-30 min. It is necessary to explain the rapid transformation of a cloud droplet population, consisting of on the order of 10^8 droplets (~10 µm in radius) per m^3 into about 1000 rain drops per m^3 (with typical diameters of 1 mm).

Microphysical data sampled with the Learjet suggest that the collision-coalescence mechanism is important for local rain formation, and together with the freezing mechanism coalescence probably yields the primary rain production in the warm based cumulus towers in the moist air over the Lowveld region. Cloud drops collide mainly because of the different fall speeds of drops of different sizes. However, calculations suggest that gravitational collisions cannot occur in significant numbers until some of the drops have grown to a radius of about 20 µm. Thus, initially some other process must account for the production of at least a few droplets (perhaps only 1 in 50^5 droplets, or 1 per litre of cloud volume) as large as 20 µm.

PAWS investigations were focussed on whether small-scale turbulent motions in the clouds can contribute to the initial drop formation. The fact that drops of different sizes respond with different inertia to a fluctuating turbulent velocity field may result in an enhancement of the drop collision rate. In addition, overlapping of turbulent eddies may effect the growth of a cloud droplet population. This mechanism may be of particular interest for the initial stages of raindrop formation as it operates for drops with equal or different sizes.

The first step in dealing with this problem was to consider a single pair of drops and the probability that they collide while falling in a turbulent medium. The results suggested that the magnitude of the collection kernel is increased with increasing intensity of turbulence (Reuter *et al.*, 1988). This study was novel in using stochastic differential equations for modelling the kinematics of the falling drops. As usual with a new approach, there are shortcomings and limitations in the model assumptions and the results should be evaluated against this background (Cooper and Baumgardner, 1989; Reuter, 1989a). The next step was to develop an efficient numerical scheme to solve the collection equation that governs the evolution of the size spectrum of a large population of droplets (Eyre *et al.*, 1988). By combining the turbulent collection kernel with the coalescence equation we could examine the effects of overlapping eddies on the evolution of a realistic drop spectrum (Reuter *et al.*, 1989). The results suggest that a slight broadening of the spectrum can occur when the turbulent intensity is very strong.

3. DOWNDRAUGHTS AND MIXING IN CUMULUS CONGESTUS CLOUDS

The dynamic-mode glaciogenic seeding concept for convective clouds aims at maximising the effect of latent heat release by glaciating cloud updraughts earlier in time and at warmer temperatures that would be accomplished by less efficient natural nuclei. It is hypothesised that the additional freezing of supercooled liquid water causes enhanced buoyancy which may be communicated down to the subcloud layer leading to stronger convergence and possibly merging of neighbouring clouds (Simpson, 1980). Furthermore, Simpson has speculated that downdraughts would act as the primary communication mechanism in this dynamic-mode seeding scenario. Since strong downdraughts are often encountered in convective storms in the eastern Transvaal, it is desirable to investigate their extent and forcing mechanism in natural clouds before the effects of dynamic-mode seeding can be realistically assessed.

Temperature, humidity and liquid water measurements gathered by the Learjet were analysed to determine the source region of the cloudy air in the observed downdraught regions of developing cumulus congestus cloud towers for three case study days. Using the method of Paluch (1979), it was found that in many cases the descending air was composed of a mixture of air, but came primarily from near cloud base. A small fraction of the air also seems to have originated from altitudes close to cloud top (Reuter and Yau, 1987a; 1988).

To further elucidate the nature of downdraughts in developing cloud towers, high resolution numerical simulations were made using a non-hydrostatic deep anelastic time-dependent cloud model (Reuter and Yau, 1987b). To keep the computations manageable a two-dimensional model was used. The model is novel in that a stretched coordinate is incorporated in the horizontal direction. This feature allows a fine resolution in the inner region occupied by the cloud but yet is computationally efficient. The strategy was to perform simulations in both axi- and slab-symmetric geometries to obtain information on the three-dimensional processes occurring in deep convective clouds.

The cloud simulations made for the three case study days displayed highly structured organisation. Downdraughts formed mainly near the cloud boundaries with maximum speeds of up to 10 ms^{-1}. To determine the realism of the simulations, model results were compared with observed data from the Learjet. The results for all three cases indicated that the model had considerable skill in reproducing observed cloud characteristics in terms of vertical velocity, temperature and liquid water content.

The forcing mechanisms of the downdraughts were further investigated by analysing the time history of dynamic and thermodynamic properties along computed parcel trajectories. The results confirm that evaporative cooling contributes to the formation of downdraughts along cloud boundaries.

However, perturbation pressure forces largely influence in the initiation of downward momentum. In the upper regions of rapidly growing cloud towers, the air pressure deviates substantially from its hydrostatically balanced value, and the resulting pressure gradient force is comparable in magnitude to buoyancy.

The slab-symmetric model results show that cloud development is retarded in the presence of vertical shear in the environmental air flow (Reuter and Yau, 1987c). The downshear side near the cloud top becomes more diluted, cooler and has stronger downdraughts than the upshear side. The computed parcel trajectories show that the asymmetric organisation is probably caused by the mixing of horizontal momentum at the cloud top. To study the initiation of downdraughts in mixed-phase clouds, the thermodynamic scheme of the cloud model was extended to include the release of latent heat associated with ice phase processes. A comparison between the simulation results of a mixed-phase cloud and a liquid-phase cloud shows that the downdraught speed is not sensitive to whether the cloud water is in the mixed-phase or liquid-phase (Reuter, 1987).

4. WATER BUDGETS OF CONVECTIVE STORMS

The water budget was investigated using radar observations for three case study days (Reuter, 1990a). The radar measurements were used to compute estimates of the total precipitation content (integrated over the storm volume) as a function of time. Similarly, estimates of the area-integrated outflow of precipitation through the cloud base level were deduced. The nine storms analysed lasted for 1 to 2 h and the total accumulation of rain ranged from 1-10 Tg. During the maturing stage, the storms had precipitation contents of about 0.2-5 Tg and rainfall rates of about 0.302 Ggs^{-1}. The "characteristic" storm updraught, defined as the ratio of the area-averaged rainfall rate to the volume-averaged precipitation content, was close to 4-6 ms^{-1} for all storms during their maturing stages.

Radar observations have the shortcoming that only quantities associated with precipitation size particles can be directly obtained. Furthermore, radar data provide little insight into the quantitative contributions of the various physical processes that act as the sources and sinks in the water budget. A time-dependent three-dimensional cloud model was used as a tool to further study the water budget (Reuter, 1988b). Three-dimensional cumulus modelling requires extensive computing resources. With the facilities available at CSIR, only isolated deep convective clouds could be simulated. As large-scale convergence was not included, only relatively short-lived storms were modelled. The simulation results for all three case study days suggest that the rain is formed mainly by coalescence, while the ice-phase processes were rather limited. This finding has still to be confirmed with a better ice-phase parameterisation scheme.

Numerical experiments with the three-dimensional model were also made to estimate the effects of glacionic seeding on the cloud water budget (Reuter, 1990b). A comparison between the simulated natural and seeded clouds showed no significant differences in terms of rainfall at the ground. Since the model results were in close agreement to observed statistics of radar echoes for the two case study days, it seems reasonable to assume that the simulation results are not far from reality. However, the following article shows distinct seeding signatures aloft in ice mass and occasionally in rain and cloud mass (Reuter, 1990b). Thus, more cases need to be examined.

5. DEVELOPMENT AND ACQUISITION OF NUMERICAL CLOUD MODELS

Numerical modelling of cumulus clouds has become an important area of weather modification research, because cloud models are a useful tool for investigating the complicated interactions of dynamical, microphysical and thermodynamic processes. Not all microphysical and dynamical processes can be included in detail because of the limitations of speed and core memory of existing computers. Therefore, the assumptions to be utilized depend on the purpose of the application of the numerical model. Clearly a set of model assumption that may be adequate for one study, may be inadequate for another. Thus, different cloud models with various degrees of complexities have been acquired and developed during the last five years. The major features of them are briefly summarised here:

TWOCYLINDER (written in FORTRAN), Yau (1979); Yau (1980); Yau and Austin (1979); Asai and Kasahara (1967)

The simplest model that includes a closed formation of the cloud updraught and the interacting environment is the time-dependent two-cylinder model. The cloud and environment are assumed to consist of two concentric cylinders and all quantities are allowed to vary in time. The effect of the perturbation pressure are included. The model includes cloud water, rain and graupel. The growth of cloud droplets are paramaterised. The evolution of particle size spectra for larger hydrometeors and the effects of differential fallspeeds are allowed for the growth of rain and graupel particles in a total of 25 size categories.

The model does not require extensive computer resources and thus may be suitable for some sensitivity studies. However, the oversimplified model geometry requests extreme caution in the interpreting individual results.

CU2D-AXIS (written in FORTRAN), Reuter and Yau (1987b)

Model equations are formulated in cylindrical coordinates, and all dependent variables are assumed to remain constant in the azimuthal direction (i.e. axi-symmetry). The model uses the deep anelastic system of prognostic equations suitable for deep convection. The condensed water is assumed to follow the air flow and there is no precipitation in the present model formulation. A stretched coordinate is used in the radial direction. The model can be run with heat and moisture fluxes at the bottom boundary and trajectory analysis is performed for a set of initial parcels.

The model is suited for simulating some aspects of single-cell convective clouds without (or before) precipitation formation. Effects of environmental wind or cloud-cloud interactions cannot be included. The coding is efficient to allow high-resolution simulations.

CU2D-SLAB (written in FORTRAN), Reuter and Yau (1987c)

The model equations are formulated in cartesian coordinates and the variance in the y-direction are assumed to be zero (i.e. slab-symmetry). Except for this difference in model geometry, the code CU2D-SLAB is very similar to CU2D-AXIS. It is suited for simulating some aspects of two-dimensional cloud bands, allowing for unidirectional vertical shear in the ambient flow.

CU3D (written in PL1), Steiner (1973); Yau (1980); Reuter (1988b)

This three-dimensional model is based on the deep anelastic system of equations. The microphysics is treated using the bulk water technique. Water substance is divided into five categories: vapour, cloud water, rain water, ice crystals and snow. The microphysical processes included are: condensation of vapour to form cloud droplets; autoconversion of cloud water and collection by rain (i.e. coalescence); evaporation of rain water; evaporation of cloud water; nucleation of ice crystals from vapour; depositional growth of ice and snow; sublimation of ice and snow; melting of ice and snow to form rain water; and growth of ice and snow by riming.

This model requires extensive computing time and can thus be run only in fairly coarse resolution. The simulation results, however, are the most realistic of the models discussed, because there are no artificial restrictions imposed on the air flow. The code is complicated because there is extensive transfer of files from disks to core memory. Further development of this code is not encouraged as it was written in PL1 in 1970-1980 and does not take advantage of modern computer architecture such as vectorisation, etc.

6. PAWS PUBLICATIONS DURING 1987-1989

ASAI J and KASAHARA A, 1967. A theoretical study of the compensating downward motions associated with cumulus clouds. J. Atmos. Sci., 24, 487-496

COOPER W A and BAUMGARDNER D, 1989. Comments on "The collection kernel for two falling cloud drops subjected to random perturbations in a turbulent air flow - A stochastic model". J. Atmos. Sci., 46-8, 1165-1167.

EYRE D, WRIGHT C J and REUTER G W, 1988. Spline-collocation with adaptive mesh grading for solving the stochastic collection equation. J. Comput. Phys., 78, 288-304.

MORGAN G, REUTER G W and MATHER G K, 1987. Programme for Atmospheric Water Supply (PAWS). Contract Report to the Water Research Commission, November 1987, Pretoria, 37-42.

PALUCH I R, 1979. The entrainment mechanism in Colorado cumuli. J. Atmos. Sci., 36, 2467-2478.

REUTER G W, 1987. Penetrative downdraughts in mixed-phase clouds: A numerical study. S.A. J. of Physics, 10, 139-145.

REUTER G W and YAU M K, 1987a. Mixing mechanisms in cumulus congestus clouds: Part I. Observations. J. Atmos. Sci., 44, 781-797.

REUTER G W and YAU M K, 1987b. Mixing mechanisms in cumulus congestus clouds: Part II. Numerical simulations. J. Atmos. Sci., 44, 798-827.

REUTER G W and YAU M K, 1987c. Numerical modelling of cloud development in a sheared environment. Beitr. Phys. Atmosph., 60, 65-80.

REUTER G W, 1988a. The effect of turbulence on the collection of cloud drops: A stochastic model. Extended Abstracts of the 10th International Cloud Physics Conference, 15-20 August, Bad Homburg, West Germany, 97-99.

REUTER G W, 1988b. Water budget and kinetic energy transformations of a mixed-phase cumulus cell: Three-dimensional numerical simulation. Beitr. Phys. Atmosph., 61, 30-38.

REUTER G W, DE VILLERS R and YAVIN Y, 1988. The collection kernel for two falling cloud drops subjected to random perturbations in a turbulent air flow: A stochastic model. J. Atmos. Sci., 45, 765-773.

REUTER G W and YAU M K, 1988. Reply to "Comment on 'Mixing mechanisms in cumulus congestus clouds. Part I: observations'". J. Atmos. Sci., 45, 2464-2466.

REUTER G W, 1989a. Reply to "Comment on 'The collection kernel perturbations in a turbulent air flow: A stochastic model. J. Atmos. Sci., 46, 1168-1169.

REUTER G W, 1989b. Radar observations of precipitation production in thunderstorms. Atmosphere-Ocean (submitted).

REUTER G W, WRIGHT C J and EYRE D, 1989. Effects of turbulence on the growth of cloud drop spectrum. J. Atmos. Sci., 46, 1407-1410.

REUTER G W, 1990a. Radar studies. This volume, 142-160.

REUTER G W, 1990b. Modelling of cloud seeding. This volume, 87-94.

SIMPSON J, 1980. Downdrafts as linkages in dynamic cumulus seeding effects. J. Appl. Meteor., 19, 477-487.

STEINER J T, 1973. A three-dimensional model of cumulus cloud development. J. Atmos. Sci., 30, 414-435.

YAU M K, 1979. Perturbation pressure and cumulus convections. J. Atmos. Sci., 36, 690-694.

YAU M K, 1980a. A two cylinder model of cumulus cells and its application in computing cumulus transports. J. Atmos. Sci., 37, 2470-2485.

YAU M K, 1980b. The effects of evaporation, water load, and wind shear on cloud development in a three-dimensional numerical model. J. Atmos. Sci., 37, 488-994.

YAU M K and AUSTIN P M, 1979. A model for hydrometeor growth and evolution of raindrop size spectra in cumulus cells. J. Atmos. Sci., 36, 655-668.

B. MODELLING OF CLOUD SEEDING

G. Reuter

1. INTRODUCTION

Detailed measurements from aircraft and radar of cloud evolution have allowed objective determination of the suitability of a cloud (or system of clouds) for modification by seeding. However, the complexity and natural variability of precipitation systems remain significant obstacles to the assessment of artificial seeding effects. Furthermore, dynamic and microphysical processes interact with each other and seeding generates various feedback effects which are not yet fully understood.

The accumulated knowledge of cloud physics, thermodynamics and fluid dynamics, built up over centuries, makes it possible to describe the various processes in clouds using a large set of mathematical equations. The advent of more powerful computer systems has made it possible to solve these equations accurately. In fact, recent studies have indicated that numerical convective cloud models have significant skill in simulating observed cloud features realistically. The goal of numerical cloud modelling is to obtain quantitative estimates of how the physical processes, such as seeding, interact within the cloud system. Modelling should not be considered a thing apart, but rather as an integral member of the theoretical, laboratory and observational effort to understand rain modification. The following quotation comes from the book 'Precipitation Enhancement - a Scientific Challenge' (Braham, 1986).

> *"It is strongly urged that before we invest in major field experiments to test a weather modification concept, we thoroughly test the concept by computer simulation. We have the computer technology today to thoroughly examine the physical consistency of a concept. This may require several years of computer-code development plus the expenditure of large amounts of computer time, but in this author's opinion, we would be in a much better position to design laboratory and field experiments that can definitely test the concept. It*

should be emphasized that I am not talking about computer models that use simplified physics and dynamics such as we have been forced to use in the past. I am talking about sophisticated models of turbulent transport and diffusion, cloud microphysics and cloud dynamics."

There is actually only one way that models should be used in cloud seeding experiments. They should play a key role in helping to evaluate seeding potential. In particular, model results coupled with observational studies should be valuable in refining a particular seeding hypothesis and putting it on a more quantitative basis. Cloud simulations will clearly identify the critical parameters involved in a seeding hypothesis.

In the past, simple models have been used operationally on a daily basis to predict the possible modification effect, given a particular seeding strategy and the existing atmospheric conditions. However, simple models that run in short time cannot adequately capture the real cloud processes and are thus of limited utility. We believe that models are only valuable in cloud studies if they can simulate nature realistically. And it is a fact of life, that time dependent multi-dimensional cloud scale models that can mimic convection skillfully, use large amounts of computing power and storage and will certainly not run in real-time on present-day computers. Therefore, sophisticated cloud modelling should not be expected to be of any use in field operations. The value of cloud modelling is found in the evaluation of the potential "seedability" of the cloud types that occur within the geographic area of interest.

2. MODEL DESCRIPTION

The three-dimensional cloud model employed in this study has been developed by Steiner (1973), Yau (1980) and Yau and MacPherson (1984). The major features of the model are:

(a) It is fully three-dimensional and time-dependent.

(b) It allows for perturbation pressure effects using the deep anelastic system of equations.

(c) It contains a warm rain parameterisation scheme using autoconversion and accretion (coalescence).

(d) It also contains a cold rain parameterisation scheme using nucleation, deposition, riming and melting.

(e) It includes the effects of turbulent diffusion using a first order turbulence closure scheme with the dispersion depending on deformation shear and local buoyancy.

(f) It is initialise from observations specifying the temperature and moisture stratification and the wind regime.

3. SIMULATION OF ISOLATED CLOUDS

The present study discusses the simulation of isolated cumulus congestus clouds rather than a group of convective clouds or a squall line storm. This choice seems odd because it is well known that most precipitation falls from line storms or multi-cellular cloud systems whereas rainstorms from isolated cumuli is only marginal. However, the limited computer power available has required initial focus to be on single cells. The simulation of a cloud complex would require a model domain of size at least 100 km x 100 km x 15 km. To cover this domain with a net of grid points uniformly spaced 200 m apart, requires a total of 3.8×10^{13} grid boxes. In the model computations at each grid point it is necessary to store about thirty variables and make about two hundred calculations for each time step. The total required memory space and computing time is several orders of magnitude larger than those available on CSIR computers. These severe constraints on computing power have forced the focus to be on the simplest case, a single isolated cloud cell. Once access is gained to generous computing time on super computers the more relevant cases of cloud populations should be considered.

The experimental unit in the field project conducted at Nelspruit has always been active multi-cellular storms that produce significant amounts of rain. In the Bethlehem Precipitation Research Project (BPRP), on the other hand, there has been more experimental interest in isolated cumulus congestus clouds. Environmental conditions for the present cloud simulations are thus taken from observations made in the BPRP area. Three case study days from the 1981 season where fair data coverage was available were selected. The aircraft and radar observations sampled on these days were presented in the doctoral thesis of Hudak (1986). A discussion of the environmental conditions, results of cloud simulations and a comparison of model results with radar observations is given in Reuter (1988, hereafter R88). The interested reader should work through the sections of R88 which focus on the discussion and interpretation of the simulated water budget and kinetic energy transformations. This material provides insight into the precipitation mechanism and convective circulations of a single mixed-phase cumulus cell.

4. SIMULATION OF CUMULUS SEEDING

Modelling of Seeding

Before a model can be used with confidence to examine the potential of rain enhancement by cloud seeding, it is necessary to ensure that natural convection can be simulated realistically. This has been done with the present model for various convective situations in different geographical regions including the following: the tropics (Turpeinen and Yau, 1981), Alberta (Yau and MacPherson, 1984) and Quebec (Yau and Michaud, 1982). In all of these cases, the model results were very similar to observed radar data. The model has also realistically simulated isolated convective cells occurring over the Highveld region in Southern Africa (R88).

Another essential feature of a cloud seeding model is that the actual seeding process is modelled realistically. In this model, we follow the numerical procedure suggested by Orville to simulate the release of silver iodide particles. The method is based on the assumption that silver iodide particles act as deposition or contact nuclei.

The maximum number of ice crystals per litre of air activated under natural conditions is given by Fletcher (1969) as

$$N_n = 10^{-5} \exp(-0.6\ T) \qquad (1)$$

where the given temperature is T(°C). The number of artificial nuclei N_a per litre of air activated by silver iodide particle seeding is given by

$$N_a = \beta \exp [(-0.022\ T - 0.88)\ T - 3.8)] \qquad (2)$$

where β is the number of artificial nuclei per litre of air at -5°C. Equation (2) constitutes the empirical efficiency curve for the combined effect of all nucleation mechanisms active between -5°C and -20°C (Orville and Kopp, 1974). In our simulation experiments, seeding is simulated by specifying a seeding time τ. The maximum number of ice nuclei activated before τ is given by N_n but is set equal to $N_n + N_a$ after τ. Of course, in the event that N ice crystals per litre of air are already present only the excess of $N_n + N_a$ will be nucleated.

Description of Experiments

The effects of seeding were investigated for isolated cumulus clouds over the BPRP area. Numerical experiments were made for the observed environmental conditions occurring on 5 and 22 Feb. 1981. For both cases, two simulated runs were conducted, designated as "natural" (N) and "seeded" (S). Equation (1) is used in experiment N for nucleation under natural conditions while (2) is used in experiment S after the seeding time τ. β is assigned a value of 100 per litre to simulate heavy seeding. τ is set at 15 minutes at which stage the simulated clouds were actively growing with their tops passing through the -10°C level.

Results

The evolution of the convection is described in R88. Here, we focus on the differences between the natural and seeded clouds. In the model, the effects are most significant in the 15 minutes following seeding decision time. Figure 1 compares the structures of the natural and seeded clouds at 30 minutes (i.e. 15 minutes after seeding decision time). The vertical sections passing through the cloud core in the east-west direction are shown. The upper portion compares the precipitation structures. The

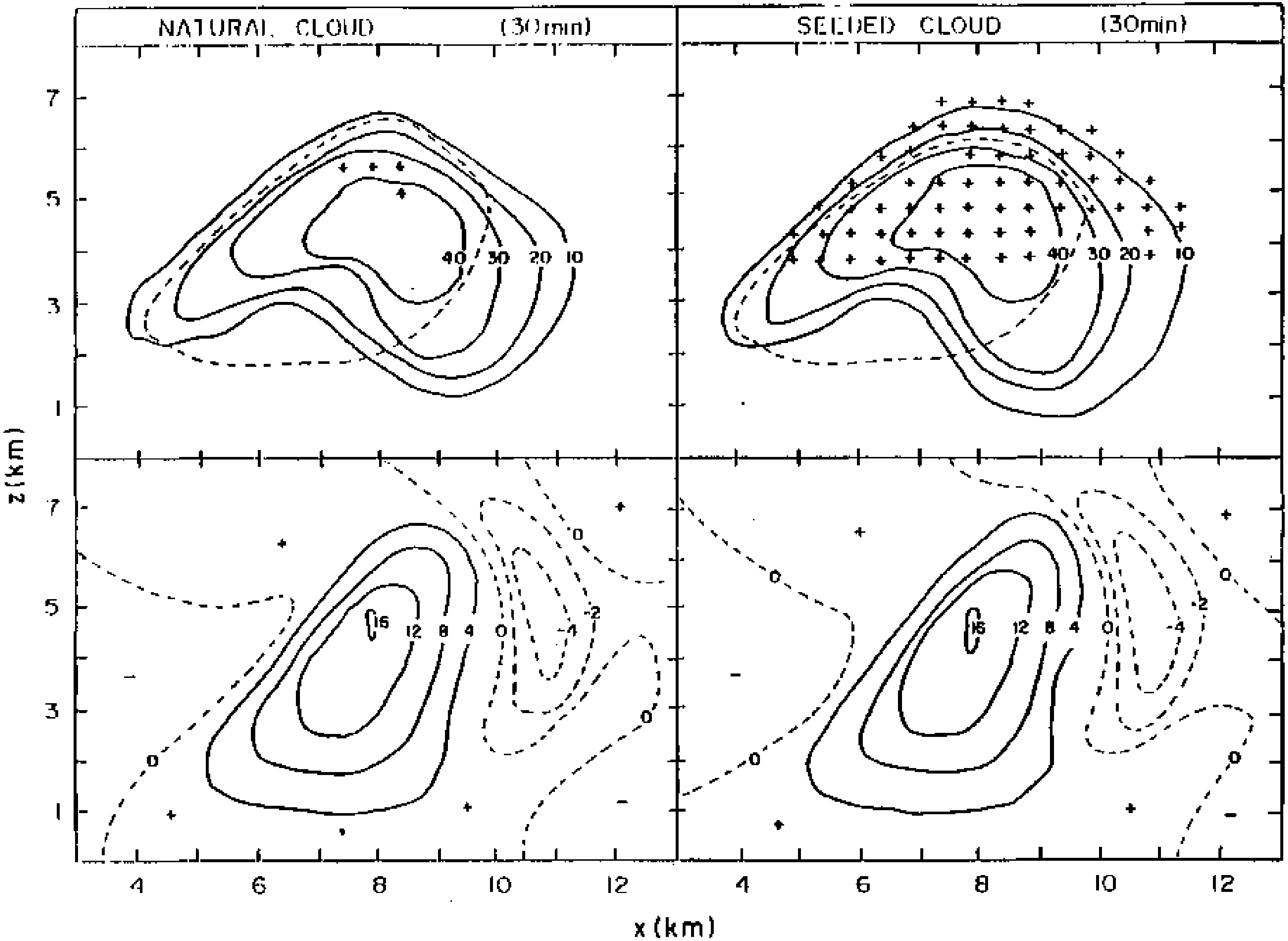

Figure 1. Model results from seeded and unseeded clouds.

solid lines are contours of radar reflectivity factor (in dBz), the dashed line is the 0.1 g kg^{-1} contour of cloud water mixing ratio and the little crosses identify grid boxes that contain ice mixing ratios in excess of 10^{-3} g kg^{-1}. The lower portion compares the vertical velocity structures.

The comparison indicates that seeding results in numerous ice crystals that are not present in the "natural" run. Also, the precipitation field of the "seeded" cloud is slightly more developed and the rain has fallen further down. The effects of seeding on the vertical velocity structure are insignificant. The core updraught is only marginally stronger in the seeded case and the differences in the downdraughts are also small.

To summarise, the qualitative comparison at a single time step suggests that the microphysical processes for rain formation are slightly faster (or more efficient) in the seeded cell. However, there are hardly any differences in the dynamic structure of the natural and seeded cloud cell.

The effects of seeding can be further examined by comparing the instantaneous masses of ice particles, raindrops and cloud droplets integrated over the model domain. Table 1 compares the results for February 5. In the natural case, the integrated mass of ice is small relative to mass of rain. The cloud water reached its maximum mass at 25 minutes, whereafter it decreases gradually as the mass of rainwater increases. The mass of rain that actually reached the surface is only 3.62×10^3 kg during the integration period of 35 minutes In comparison, the seeded cloud contains a substantial amount of ice. The ice crystals grow mainly by riming and the cloud water content is partly depleted though the collection process. In the seeded case, the total mass of rainwater increases faster during the 10 minutes period following seeding. The model results indicate that the accumulated rain on the ground is almost the same for the natural and seeded cases.

On 22 February 1981 the cloud convection was short-lived and no rain reached the ground. The total mass of ice-crystals, rainwater and cloud water are compared for the seeded and natural clouds. Table 2 shows the results for selected times. The qualitative behaviour of the seeding

Table 1 Comparison of total mass of water substances in natural (N) and seeded (S) clouds on 5 February 1981.

Model time (min)		15	20	25	30	35
Mass of ice (kg)	N S	2,47 (-2) 2,47 (-2)	2,02 (0) 4,50 (5)	2,41 (4) 4,98 (6)	4,22 (5) 2,30 (6)	8,66 (5) 3,65 (7)
Mass of rain (kg)	N S	1,01 (2) 1,01 (2)	9,06 (5) 1,47 (6)	1,91 (7) 1,93 (7)	7,60 (7) 7,61 (7)	1,22 (8) 1,13 (8)
Mass of cloud water (kg)	N S	2,52 (7) 2,52 (7)	4,47 (7) 4,65 (7)	5,88 (7) 5,55 (7)	5,37 (7) 4,45 (7)	2,22 (7) 1,79 (7)
Mass of total condensate (kg)	N S	2,52 (7) 2,52 (7)	4,56 (7) 4,84 (7)	7,79 (7) 7,98 (7)	1,30 (8) 1,44 (8)	1,45 (8) 1,68 (8)
Accumulated mass of rainwater at ground (kg)	N S	0 0	0 0	0 0	0 0	3,62 (3) 3,65 (3)

Table 2 Comparison of total mass of water substances in natural (N) and seeded (S) clouds on 22 February 1981.

Model time (min)		15	20	25	30	35
Mass of ice (kg)	N S	4,40 (-2) 4,40 (-2)	6,69 (-1) 4,18 (4)	4,53 (-1) 3,30 (4)	2,23 (-2) 9,23 (2)	7,28 (-4) 2,24 (1)
Mass of rain (kg)	N S	6,16 (2) 1,16 (2)	1,70 (5) 1,73 (5)	5,14 (5) 5,49 (5)	1,50 (5) 1,68 (5)	1,13 (4) 1,32 (4)
Mass of cloud water (kg)	N S	1,53 (7) 1,53 (7)	9,00 (6) 8,98 (6)	6,63 (5) 6,60 (5)	6,54 (4) 6,21 (4)	0 0
Mass of total condensate (kg)	N S	1,53 (7) 1,53 (7)	9,17 (6) 9,19 (6)	1,18 (6) 1,24 (6)	2,15 (7) 2,30 (7)	1,13 (4) 1,32 (4)

effects is similar to the one presented for the other case study day. Again, the seeding results in the rapid formation of ice. Also, the seeded cloud has a larger mass of rainwater suggesting that the presence of ice enhances the production of precipitation particles.

5. CONCLUSION

The work done so far has illustrated the usefulness of cloud simulations by computer to further our understanding of cloud processes and the effects of seeding. We found that a 3-D cumulus model has considerable skill in simulating a

single convective clouds. So far, the simulations have been confined to the simple case where there is no forcing caused by topography or mesoscale convergence. Major changes in the model are needed before these can be included realistically.

The model results indicate that isolated convective clouds are affected by glaciogenic seeding. The seeding causes the formation of more ice crystals than in the natural case. The presence of ice slightly enhances the formation of raindrops. The seeding, however, cannot be traced in the dynamic structure of the clouds, and the size of the cloud is not significantly influenced by seeding. Also, the amount of rain accumulated at the ground is not changed by seeding.

These results have been obtained for two cases of isolated convective clouds in an environment without any large-scale forcing. The results cannot be generalised. In particular, no conclusive statements can be made for precipitation produced by line storms or cumulus complexes. Further work will be pursued to address these cases.

REFERENCES

Braham R R, 1986. Precipitation enhancement - a scientific challenge. American Meteor. Society. Meteor. Mongr. 21, Boston.

Fletcher N H, 1969. The Physics of Rain Clouds: Cambridge University Press, New York, 390 pp.

Hudak D R, 1986. Precipitation processes in natural and seeded cumulus clouds and an assessment of the rain enhancement potential for Southern Africa. Ph D Dissertation, University of Toronto, 190 pp.

Orville H D and Kopp F J, 1974. Numerical simulation of cloud seeding experiments. Preprints Fourth Conference on Weather Modification, AMS Boston, 28-35.

Reuter G W, 1988. Water budget and kinetic energy transformations of a mixed-phase cumulus cell: Three-dimensional numerical simulation. Beitr. Phys., Atmosph., 61, 30-38.

Stiener J T, 1973. A three-dimensional model of cumulus cloud development. J. Atmos. Sci., 30, 414-435.

Turpeinen O and Yau M K, 1981. Comparisons of results from a three-dimensional cloud model with statistics of radar echoes on day 261 of GATE. Mon. Wea. Rev., 109, 1495-1511.

Yau M K, 1980. The effects of evaporation, water load and wind shear on cloud development in a three-dimensional numerical model. J. Atmos. Sci., 37, 488-494.

Yau M K and Michaud, 1982. Numerical simulation of a cumulus ensemble in three dimensions. J. Atmos. Sci., 39, 1062-1079.

Yau M K and MacPherson S, 1984. Numerical simulations of an Alberta hailstorms. Volume of Extended Abstracts, 9th Int. Cloud Physics Conf., Tallin, 585-588.

02/22gal/sgg

C. SOUNDING ANALYSIS

R C Grosh, G Hofmeister

1. INTRODUCTION

It is possible to imagine several sets of conditions which might lead to cloud seeding induced rain increases. The conditions associated with the hygroscopic, static and dynamic seeding hypotheses are well known (Dennis, 1980). The dynamic hypothesis in particular has received a great deal of attention because of Simpson's very promising cloud seeding experiments, and, more importantly, because of her analysis of the atmospheric conditions associated with artificial rain increases from proximal clouds (Figure 1). The model determined potential for additional vertical cloud growth from seeding ("seedability" or "dynamic growth potential" is the preferred term by later researchers) was directly related to observed increased cloud growth and increased rainfall following seeding ($r>0.9$), but there was no significant correlation between model predicted seedability and observed cloud growth and rain flux when the clouds were not seeded ($r\sim0$). This powerful inter-relationship has received a great deal of attention, since it verified the theoretical foundation for dynamic seeding alterations in Florida (Smith *et al.*, 1986; Stith, 1983).

Another form of sounding analysis has also been applied in an apparently very successful effort for PAWS. Mather *et al.* (1986) have shown that, when the coalescence-time parameter, CTP (the ratio of the cloud base temperature, CBT, to the 500 mb thermal buoyancy, $\Delta T5$), is greater than a critical threshold, there is a high probability of finding liquid water amongst the larger droplets at the seeding level (-10°C). High values favour coalescence drop growth because rising currents should be relatively slow and adequate time available for frequent drop collisions. CTP also appears to be very effective in identifying clouds which are susceptible to positive glaciogenic seeding effects (Morgan *et al.*, 1987; Grosh and Mather, 1988) and it is clearly desirable to continue to expand our understanding of this ratio. Therefore, cloud models can be used to:

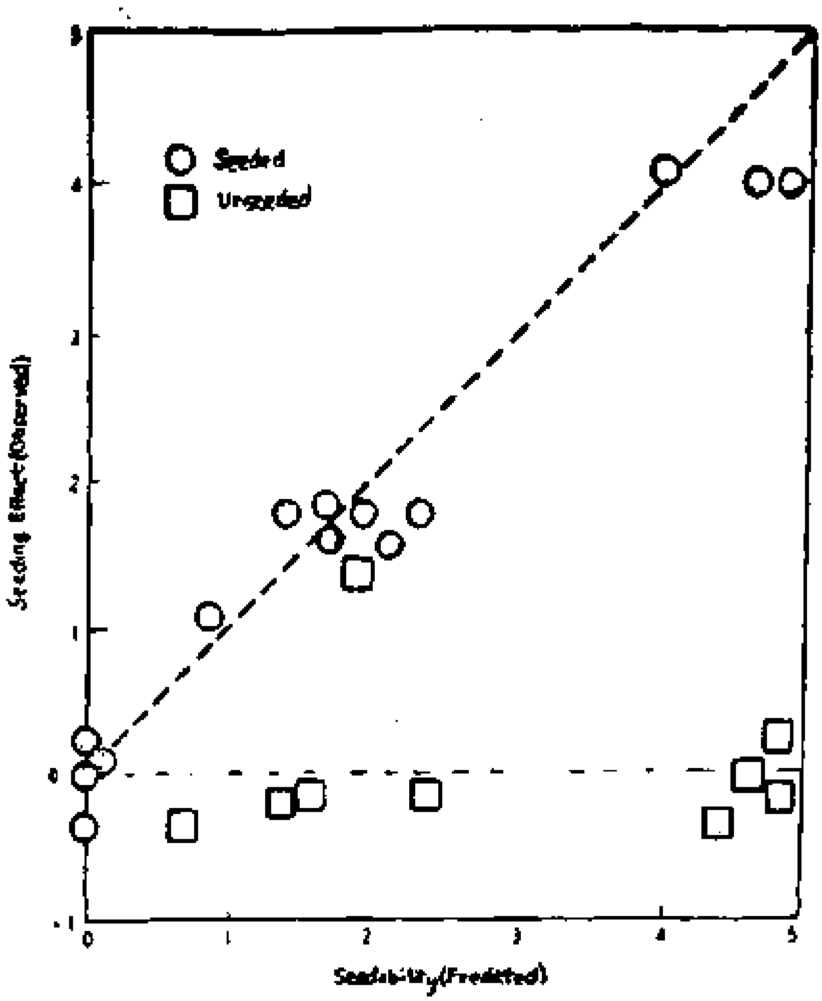

Figure 1 Seedability versus seeding effect for the 14 seeded (circles) and 9 control (squares) clouds studied in 1965. Note that seeded clouds lie mainly along a straight line with slope 1 (seeding effect is close to seedability) while control clouds lie mainly along straight horizontal line (showing little or no seeding effect regardless of magnitude of seedability). Units of each axis are in kilometers (Simpson and Dennis, 1974)

(1) Clarify the relationship of CTP to other sounding variables such as classical seedability,

and

(2) Fine tune the specification of the vertical velocity component of CTP which is currently represented by a surrogate (thermal buoyancy) defined by only a point value (at 500 mb) while the model vertical integration can provide a more representative vertical velocity value, or even a direct estimate of the rise time.

2. CLOUD MODELS

All present frequently used numerical cloud models have highly unrealistic aspects - regardless of their apparent sophistication. In particular, the 1985 International Cloud Modeling Workshop reported that "simulated rates of micro-physical processes in numerical cloud models commonly did not adequately match the observed rates" (Bulletin of AMS, 1988). Worse yet, the best performances of dynamics in non-steady multi-dimensional models require previous ad hoc calibration runs with the same input data but altered kinematics (Orville, 1988). Thus, it is crucial to carefully consider the application intended for a model run to assure a truly valuable conclusion can be drawn from the output.

Thus, except when used with a very close proximity sounding and measured cloud radius and base, 1-D steady state results certainly cannot be related to individual cloud performance and this is not the present intention. More information on the local *climatic* potential for dynamic modification of cloud growth is needed in the Eastern Transvaal. If seedability is not present frequently, new seeding hypotheses may need to be developed for PAWS.

Mathews (1981) has succinctly described the application of 1-D cloud models to determine seedability:

"One-dimensional steady-state parcel models provide an objective analysis of basic thermodynamic features which affect the potential for convective cloud growth. They quantify the manual analysis of positive area above the convective condensation level (CCL) found on a thermodynamic diagram. This highly simplified, fast, numerical simulation of parcel buoyancy provides a systematic measurement tool to determine the relative potential for convective cloud growth and its intensity. These characteristics of convection are diagnosed by the model ... using the radiosonde data for model initialization. These data are analyzed in terms of cloud properties such as cloud-base height, cloud-top height, maximum vertical velocity of the parcel and other quantitative properties which may be compared for different soundings and locations to describe the natural variability of potential for convective cloud growth. Due to the simple and incomplete microphysics and dynamics of these models, care must be taken in the interpretation of results. Meaningful comparisons between model diagnosed cloud properties and those of a specific observed cloud are difficult, if not impossible, due to the complex three-dimensional time-dependent nature of cloud growth. Nevertheless, useful thermodynamic characteristics of individual clouds within a field of clouds may be obtained from model analyses which quantify the potential for convection in a given area and time. Such results may be interpreted as general thermodynamic characteristics which may be useful for examining the natural variability of convective potential.

The atmosphere's capacity to support convective cloud development, as defined by the cloud depth diagnosed by the model, is probably the most useful information available from one-dimensional, steady-state cloud models (Silverman, 1976). This "dynamic potential" for convective cloud growth is directly related to the positive area observed on a thermodynamic diagram. Due to the limited ability of one-dimensional steady-state models to correctly diagnose precipitation (Sax, 1972; Weinstein, 1972b), this study focuses on the model's strength in diagnosis of the dynamic potential for convective cloud growth (Sax, 1969; Marwitz *et al.*, 1970; Simpson and Dennis, 1974).

...comparison(s) between model and aircraft observations ... indicate that the model is able to diagnose basic cloud properties such as base height and cloud-top height which can be used to broadly classify the potential for convective development from a local radiosonde. Hence, the model is viewed as a more comprehensive Showalter (1953) or Totals Totals Index of convective development to examine the natural variability of thermodynamics related to convective cloud development..."

Simpson's seedability concept, as verified in her correlation approach (Figure 1) and also later by Dennis *et al.* (1975) and others, is the most widely recognised scientific theory which has had apparent success in confronting the rain stimulation problem. It attempts to identify atmospheric conditions when the artificial cause (seeding) will have the desired effect (increased vertical cloud growth and rainfall). Thus, 1-D steady state models may supply useful cost effective climatic information for relating potential causes to effects in cloud seeding. The 1-D steady state model approach is very crude, but that is why it has been useful. It examines a single and simple but fundamental climatic issue, the potential for vertical growth of individual convective bubbles or jets of a given size in the study region. Its realism is not over-extended to details of individual cloud growth or temporal effects. It purports to answer only one of many possible questions, but it does supply a reliable answer. The Florida cloud top height calculations from the EMB 1-D steady state model were on average within <u>50 meters</u> of actually measured proximal cumuli tops (Simpson and Wiggert, 1971). Dennis, et. al. (1975) applied a slightly different 1-D SS model and used soundings which were not nearly as close to the cloud cases as Simpson's soundings but, on average predicted cloud tops to within 200 meters of radar tops. These studies and three others (Weinstein and MacCready, 1969; Sax, 1967; Mathews, 1981) found good correlations ($r = 0.9$) between model and observed tops. Finally, using Illinois soundings much later, Wiggert *et al.* (1982) also concluded that "the (Florida) model's predictions are realistic and ... can discriminate between broadly different weather situations". If frequent seedabilities >1 km are found in a region, there may be potential for seeding-enhanced rainfall via the dynamic hypothesis. If the seedability is weak or infrequent, other concepts have to be drawn in. Thus, this type of sounding analysis is an essential first step in understanding regional potential for rain augmentation.

A myriad of recent and past articles point to the high frequency with which many other knowledgable atmospheric scientists overseas have drawn this same conclusion (e.g. Ackerman & Sun, 1985; Mathews, 1981; Smith *et al.*, 1986; Stith, 1983; Hudak and List, 1988; Sax, 1972; Simpson and Wiggert, 1971; Weinstein and MacCready, 1969; Dennis *et al.*, 1975; McCarthy, 1972; Semonin, 1977; Simpson and Brown, 1978; Wiggert *et al.*, 1982).

Weinstein and MacCready described the situation which prevailed before the 1-D SS models were applied:

> "The principal reason for the inconclusive results obtained in many of the previous isolated cumuli seeding experiments was a poor choice of test clouds. Clouds which could not have possibly responded appreciably to seeding treatment were seeded along with those which could, and did, respond. When cloud top and precipitation increases for all of the clouds were combined, the negative, or no-increase, cases masked the favorable cases and the results were inconclusive."

The concept of seedability, as revealed by the 1-D SS Model studies changed all this. These studies show that the Florida climate has significant seedability (over 1 km) present on about 90% of summer days. In other climates (Virginia, the High Plains, Arizona, Illinois) seedability is much less frequently observed (only ~50 to 70% of the time). Worse yet, a study of 39 days in North Dakota showed only two had seedabilities over 1.2 km and only six had seedabilities over 0.5 km. For this and other reasons, it was concluded that only microphysical seeding effects were likely in that climate. Thus, seedability is a key climatic variable for rain stimulation research, and is particularly important to consider in the Eastern Transvaal where many seeded clouds do not show obvious seeding effects.

In addition, the crude 1-D steady state model output rain estimates were one of the most valuable <u>covariates</u> in the FACE rain enhancement analysis (Flueck *et al.*, 1986).

Finally, it should be recognised that these simple model runs are <u>very</u>

<u>inexpensive</u>, and that steady state cloud assumptions have been used recently in another application by an eminent atmospheric scientist because it is believed that the best approach is to use the simplest possible model. It is still necessary to learn "how simple a model can be and still remain useful" for explaining observations (Knight, 1987).

3. DATA

In the present study, December, January and February morning soundings for the 3-year Nelspruit phase of the PAWS project (1984-87) are analysed for their seedability and other cloud modification potential. The morning data set was selected for primary analysis because it was nearly complete, and because the balloon soundings were taken at about the same time each day (~0800 SAST). The later soundings made by the Learjet upon take off or near cloud cases at the end of operations are also of great value, and will be examined later. However, since these required a plane flight, were not time synchronous and were much less frequent (~22% of the days) they are not as suitable for a full climatology.

Unfortunately, most of the Nelspruit soundings were terminated at levels above 200 mb (<12.4 km). Temperatures at 50 mb intervals from nearby Pretoria have been substituted for the missing data above 200 mb.

4. THE GPCM

The Great Plains Cloud Model (GPCM, Mathews, 1981; Hirsch, 1971) was selected for use because it appears to be more accurate than the well-known 1-D model of Simpson and Wiggert (Ackerman, Grosh and Sun, 1979; Ackerman and Sun, 1985). The GPCM is less likely to over-estimate cloud top heights. The GPCM computer program has two basic functions: to determine the in-cloud thermodynamic and dynamic structures.

The thermodynamic calculation to determine the in-cloud lapse rate is:

$$\frac{dT}{dZ} = -\left[\frac{g}{c_p}\left[1 + \frac{qL_e}{RT}\right] - \mu(T - Te) - \frac{\mu L_e}{c_p}(q - q_e)\right]\left[1 + \frac{\varepsilon L_e^2 q}{c_p R T^2}\right]^{-1} \qquad (1)$$

A set of assumed freezing functions simulates natural (-20 to -40°C) and modified glaciation (-5 to -25°C).

The dynamic equation governing the vertical cloud motion (w) is

$$\frac{1}{2}\frac{dw^2}{dZ} = g[\frac{T_v - T_{ve}}{T_{ve}} - Q] - \mu w^2 \quad . \tag{2}$$

This dynamic calculation is made to determine the vertical air velocity, based on environmental and in-cloud virtual temperatures (T_{ve}, T_v), the water loading (Q), and the assumed mixing process. The cloud top height is defined by w = 0. The calculations are terminated when w = 0. This is a steady state equation with no horizontal advective terms included and is the source of the models name, "one-dimensional steady state". Thus, this equation is obviously also the source of many of the models most noticeable shortcomings, such as the lack of larger scale forcing for example.

A number of mixing calculations are performed to account for entrained momentum, moisture and energy. The basic expression for the fractional mixing rate (μ = (1/m)(dm/dz)) of the mass flux (m) depends on the cloud radius (R) according to μ = 0.15/R. Small clouds are severely diluted in calculations for deep ascents (~10 km) and approach the environmental conditions but larger clouds may be diluted by only ~25% for the assumed mixing function.

A set of bulk moisture balance equations are solved to account for the formation and partitioning of liquid and frozen water into cloud, rain, ice and graupel components via condensation, freezing, auto-conversion and accretion. Equations are used for rain and graupel collecting cloud water, rain water and cloud ice. Graupel is allowed to form between -8°C and the glaciation temperature. The fractional precipitation fallout is calculated to be the ratio of the time for the parcel to rise through the vertical height step over which the integration is performed to the time the volume mean diameter particle requires to fall through one cloud bubble radius.

The program calculates the moist adiabatic ascent and mixing separately for each 200 m height step. The moist adiabatic values at the new height, T_1 and q_1, are adjusted for mixing with the environment (e) via

$$T_2 = \frac{T_1 + T_e \, \mu\Delta Z}{1 + \mu\Delta Z}$$

and

$$q_{s2} = \frac{q_1 + q_e \, \mu\Delta Z}{1 + \mu\Delta Z} \quad .$$

T_3 and q_3 are the final in-cloud values after resaturation and are determined via successive approximation with

$$T_3 = T_2 - \frac{L}{C_p} (q_{s3} - q_2) \quad .$$

The cloud water and ice contents mixing ratios (Q_c and Q_i) linearly vary in reverse direction over the freezing interval chosen. The temperature change resulting from the partial freezing is given by

$$\Delta T = \frac{Q_J}{Q_l} \quad \frac{Q_J L_f + \dfrac{\epsilon L_s}{p} (\bar{e}_w - e_i)}{C_p + q_e \, C_p + \dfrac{\epsilon L_s^2 \, e_i}{P R_w T^2}}$$

where Q_l is the total amount of liquid available for freezing and Q_J is the amount of liquid to be frozen. $\bar{e}_w$ is the weighted mean of e_w and e_i.

Sensitivity - Cloud Base Conditions

The cloud base conditions (height, updraught dimension and speed) need to be determined for each model run. The cloud base height is determined in the model pre-processing of the sounding. Various updraught radii between 500 to 6000 m are assumed for each sounding. The initial cloud base updraught speed is assumed to be 2.5 mps. The model is sensitive to all of these inputs, but probably least so to the cloud base updraught speed.

5. RESULTS

Seedabilities

234 soundings were examined. These represent 87% of the possible morning soundings for December, January and February 1984-87.

Only about 9 to 15% (depending on the subcloud mixing depth used) of these 234 days had seedabilities (S) over 1 km for at least one of the assumed input cloud radii (0.5 to 6 km) for the runs with 60 and 100 mb mixing depths, respectively. The 100 mb mixing depth produced seedabilities over 1 km on 60% more days than the 60 mb mixing depth. Although 43 to 50% of the days had seedabilities greater than zero, only S>1 km cases are considered physically meaningful (Mathews, 1981).

Flight operations leading to successful case identification for inclusion in the PAWS experiment occurred on about 22% of the 234 days with morning soundings. However, these cases coincided with seedability over 1 km for only about 4 to 5% of the total study period. Thus, most (~75%) of the operationally active 22% of the days had morning soundings with S<1 km. However, 56 to 63% of the case days did have S>0 on the morning sounding.

The largest seedabilities at Nelspruit were over 8 km. The average value of the maximum seedabilities which were over 1 km is a substantial 4.1 km. Thus, when present, dynamic effects are expected to be strong in the Eastern Transvaal.

Seeding Windows

About half (46 to 51%) of the days with soundings indicated that natural clouds would rise above the -10°C level for at least one of the assumed cloud radii between 0.5 and 6 km. Of these days, again about half (45 to 50%) appeared to be quite promising candidates for rain stimulation through glaciogenic seeding because their natural tops were not predicted to pass above the -20°C level and they would not be expected to have a great amount of natural glaciation. Thus, about a quarter (21 to 25%) of all the days at Nelspruit have soundings which favour positive glaciogenic seeding effects. About 43 to 60% of these days (9 to 15% of the total number of days) have seedabilities greater than 1 km and thus hold the further promise of relatively well understood dynamic effects on rainfall in the Eastern Transvaal.

Model Accuracy

Since experimental cloud cases had to have towers penetrating the -10°C level, they provide rough quality control information. The 1-D model analyses of the morning soundings indicate that 63% of the natural experimental cases should have had towers reaching the -10° level. Given that some previous 1-D cloud model studies in other climates have shown that mesoscale variability of seedability may be great (Cotton and Tripoli, 1980), that morning soundings will obviously underestimate afternoon convective potential (and seedability) and that the actual cloud cases were obtained for the experiment in mid-afternoon about 6 hours after the morning soundings, the 63% figure suggests that accurate local model performance has been obtained.

CTP

The coalescence time parameter (CTP) is by definition an inverse buoyancy index intended to provide a measure of rise rates in clouds. The present discussion focuses on the precision of the relationship between $\Delta T5$ and the actual updraught speed. Since the updraught speed may be expected to follow the vertically integrated buoyancy from Equation (2), the use of a point value to represent the buoyancy can be expected to give a far less than perfect correlation with either model or actual updraught speeds. The model values of $\Delta T5$ and W at 500 mb are both known and their correlation is plotted in Figure 2. The correlation coefficient is about 0.8 regardless of whether the comparison of w is with $\Delta T5$ or $(\Delta T5)^{1/2}$. The correlation is based on model runs for an assumed cloud radius of 6 km (minor entrainment), with the rising air "parcel" defined by the average of the lowest 100 mb of the atmosphere. Thus, although there is good correlation between the point values of $\Delta T5$ and the vertically integrated values of w, there is still a substantial amount of unexplained variance in the relationship (~40%) which it might be very

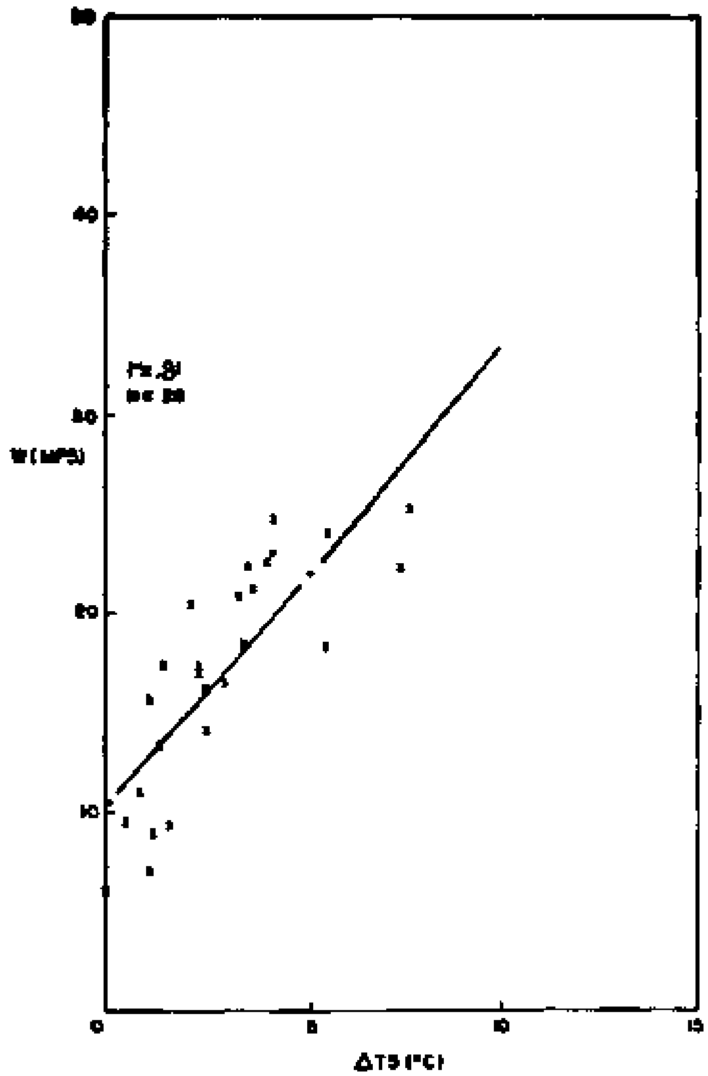

Figure 2a. Correlation of model output W(500) and ΔTS.

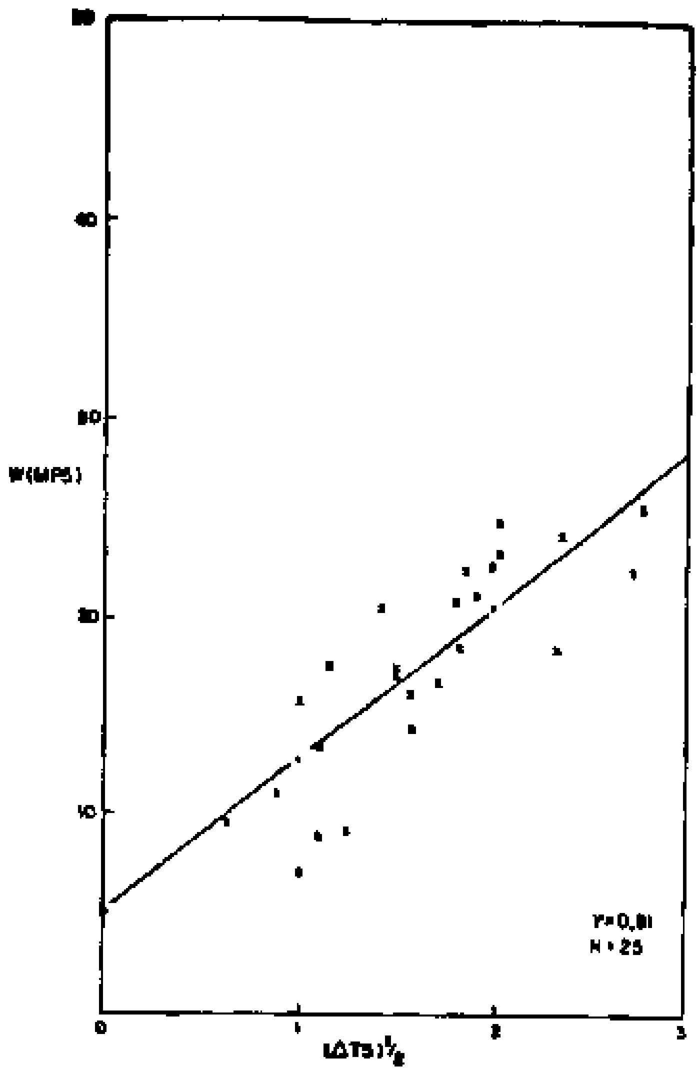

Figure 2b. Correlation of model output W(500) and $(\Delta TS)^{1/2}$.

useful to reduce as this could lead to a more efficient stratification parameter.

6. CONCLUSION

Using either 60 mb or 100 mb mixed layers for averaging the sub-cloud inputs of thermal and latent energy suggests that only about 9 to 15% (respectively) of the morning soundings at Nelspruit would be associated with promising clouds for rain stimulation activities based on the dynamic modification hypothesis. Thus, the main conclusion of this study is that the frequency of good potential for dynamic seeding in the morning at Nelspruit is much less than in most other locations where 1-D cloud models have been applied. For example, Florida, Arizona, Illinois and Virginia have seedabilities over 1 km on between about 90 and 50% of the rainy season days On the other hand, a South Dakota study found significant seedabilities which were both much less than the Nelspruit enhanced growth projections and occurred less frequently (on only about 5% of the study days).

However, there are caveats. It is important to recognise that at Nelspruit there were many more operational days than days with morning values of S>1 km as there were airborne experiments on 22% of the days with morning soundings. Furthermore, about 21 to 25% of the days at Nelspruit appear suitable for some type of glaciogenic seeding, as natural cloud tops are expected between -10°C to -20°C and about 43 to 60% of these window days have S>1 km. Finally, about 56 to 63% of the operational days were associated with S>0 for the morning soundings and there probably were important destabilising changes of the thermodynamic structure of the atmosphere during the course of the operational days. Although in some cases seedability probably improved significantly, it nevertheless seems likely that many of the actual case days were not closely associated with significant seedabilities. Thus, dynamic seeding enhancement, as described by Simpson *et al.* may not have been active on a large number of the PAWS case days. The afternoon soundings will be examined to clarify this point. Since PAWS cloud enhancements have been reported, an important conclusion is that other seeding enhancement mechanisms may be active and require exploration.

In spite of the above, a dynamic effect may well be expected to be present in many of the positive seeding results from PAWS, as 43 to 60% of the days in the seeding window (-10°C to 20°C cloud tops) have S>1 km, and when present, the dynamic effect is expected to be strong as the average of the maximum seedability for cases with S>1 is 4.1 km. Furthermore, given the fact that seeding signatures are often not apparent in seeded storms, it may be that dynamic effects are the main enhancement to PAWS clouds. Case studies will be continued to determine the relationship between seedability and apparent seeding signatures.

Model output has also been used to suggest ways to improve the coalescence time parameter as a stratification variable.

REFERENCES

ACKERMAN, B, R C GROSH, R Y SUN, 1979. Assessing Midwest Cloud Characteristics for Weather Modification. Final Report ENV77-11527 to NSF. Illinois State Water Survey, pp128

ACKERMAN, B and R Y SUN, 1985. Predictions by two one-dimensional cloud models: a comparison. J. Clim. Appl. Meteor., 24, 617-628.

Bulletin of American Meteorological Society, 1988: Vol. 69, p996.

COTTON W R and TRIPOLI G J, 1980. A numerical investigation of several factors contributing to the observed variable intensity of deep convection over South Florida. J. Appl. Meteor. 19, 1037-1063.

DENNIS, A S, A KOSCIELSKI, D E CAIN, J H HIRSCH and P L SMITH, 1975. Analysis of radar observations of a randomized cloud seeding experiment. J. Appl. Meteor., 17, 897-908.

DENNIS, A S, 1980. Weather Modification by Cloud Seeding. Academic Press, 267pp.

FLUECK, J A, W L WOODLEY, A G BARNSTON and T J BROWN, 1986. A further assessment of treatment effects in the Florida Area Cumulus Experiment through guided linear modeling. J. Clim. Appl. Meteor., 25, 546-564.

GROSH R C and MATHER G, 1988. 1987/88 PAWS Report, WRC, Pretoria, pp199.

HIRSCH, J H, 1971. Computer modelling of cumulus clouds during project Cloud Catcher. Report 71-7, Institute of Atmospheric Sciences, South Dakota School of Mines and Technology, Rapid City, South Dakota, 61PP.

HUDAK, D R and R LIST, 1988. Precipitation development in natural and seeded cumulus clouds in Southern Africa. J. Appl. Meteor., 27, 734-756.

KNIGHT, C A, 1987. Precipitation formation in a convective storm. J. Atmos. Sci., 44, 2712-2726.

MARWITZ, J D, J R MIDDLETON, A H AUER and D L VEAL, 1970. The dynamics of updraft vaults in hailstorms as inferred from the entraining jet model. J. Atmos. Sci., 27, 1099-1102.

MATHER G, MORRISON B J and MORGAN G M Jr, 1986. A preliminary assessment of the importance of coalescence in convective clouds in the Eastern Transvaal. J. Clim. Appl. Meteor., 25, 1780-1784.

MATHEWS, D A, 1981. Natural variability of thermo-dynamic features affecting convective cloud growth and dynamic seeding: A comparative summary of three high planes sites from 1975 to 1977. J. Appl. Meteor., 20, 971-996.

McCARTHY, J, 1972. Computer model determination of convective cloud seeded growth using Project Whitetop data. J. Appl. Meteor., 11, 818-822.

MORGAN G, REUTER G and MATHER G, 1987. 1986/87 PAWS Report, WRC, Pretoria, pp85.

ORVILLE, H D, 1988. Personal Communication.

SAX, R I, 1967. Natural and artificial glaciation of tropical cumuli. M.S. Thesis, Pennsylvania State University, University Park, Pennsylvania, 85pp.

SAX, R I 1969. The importance of natural glaciation on the modification of tropical maritime cumuli by silver iodide seeding. J. Appl. Meteor., 8, 92-104.

SAX, R I, 1972. Comments on "Ice phase seeding potential for cumulus cloud modification in the Western United States". J. Appl. Meteor., 11, 1017-1018.

SEMONIN, R G, 1977. Seeding opportunities as indicated by a 1-D model. Preprints: Sixth Conference on Planned and Inadvertent Wea. Mod. AMS, Boston, 266-269.

SILVERMAN, B A 1976. Use of models in weather modification - solution or confusion? J. Wea. Mod. 2, 33-41.

SIMPSON, J and B G BROWN, 1978. Potential of summer rain augmentation by cloud seeding in the mid-Atlantic states. Va. J. Sci.,29, 146-156.

SIMPSON, J and V WIGGERT, 1971. Models of precipitating cumulus towers. Monthly Weather Review, 97, 471-489

SIMPSON, J and A DENNIS, 1974. Cumulus clouds and their modification. Weather and Climate Modification, W N Hess Editor, Wiley and Sons 229-279.

SMITH, P L, J R MILLER, J H HIRSCH and H D ORVILLE, 1986. Dynamical versus microphysical effects of seeding: Some cloud model and radar observations. Preprints: 10th Conference on Weather Modification. AMS, 175-178.

STITH, J I, 1983. Limitations to dynamic seeding of North Dakota Summer Clouds. J. Weather Modification, WMA, 28-33.

WEINSTEIN, A I and P B MACCREADY, 1969. An isolated cumulus cloud modification project. J. Appl. Meteor. , 8, 936-947.

WEINSTEIN, A I, 1972. Reply (to Robert Sax). J. Appl. Meteor., 11, 1018.

WIGGERT, V, R I SAX and R L HOLLE, 1982. On the modification potential of Illinois summertime convective clouds with comparison to Florida and FACE observations. J. Appl. Meteor., 21, 1293-1321.

D. THE COALESCENCE TIME PARAMETER

R C Grosh

1. INTRODUCTION

The coalescence time parameter (CTP) has not received adequate attention. This concept has been found to be useful in identifying cloud conditions which are likely to be associated with high liquid water contents in the larger cloud drop sizes (Figure 1) and thus appear to be susceptible to some type of glaciogenic seeding induced rain alterations (Mather *et al.*, 1986). The purpose of this note is to stimulate further exploration of this interesting concept through the presentation of related PAWS data and some speculative calculations.

The parameter is defined by the ratio of the cloud base temperature (CBT) to the 500 mb buoyancy ($\Delta T5$)

$$CTP = CBT/\Delta T5 \quad . \qquad (1)$$

$\Delta T5$ is determined by the temperature difference between the environment at 500 mb and a parcel rising adiabatically to that level from the 60 mb layer nearest the surface. When the ratio is large, liquid droplets are more likely and when $CBT/\Delta T5>2$ current results also suggest that glaciogenic seeding is most effective in rain stimulation (Grosh and Mather, 1988). This last condition corresponds to the points above the 2 to 1 line in Figure 2. The plotted data points are from the Nelspruit experimental cases obtained by PAWS.

The flight level serves as a constant reference level (-10°C). Thus, the cloud base temperature (and in-cloud lapse rate) determines the distance the growing drops must rise before they reach the seeding and/or sampling level for PAWS airborne operations. The vertically integrated true buoyancy of the rising air parcel determines how rapidly it actually

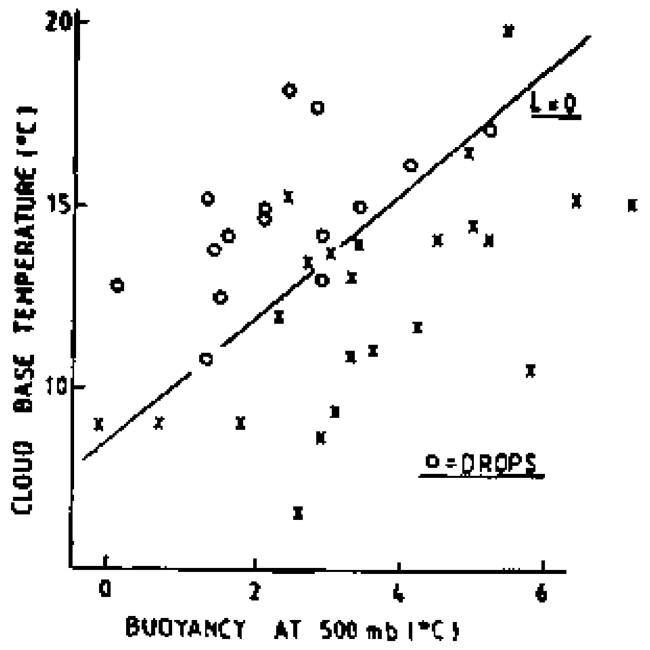

Figure 1. Plot of cloud base temperatures (CB.) vs potential buoyancy at 500 mb (ΔT_{500}) for the storms in this study. Those cases in which clear images of cloud drops >300 μm were encountered are plotted as open circles (O). The oblique line in the figure is the discriminant function plotted for L = 0 (Mather *et al.*, 1986).

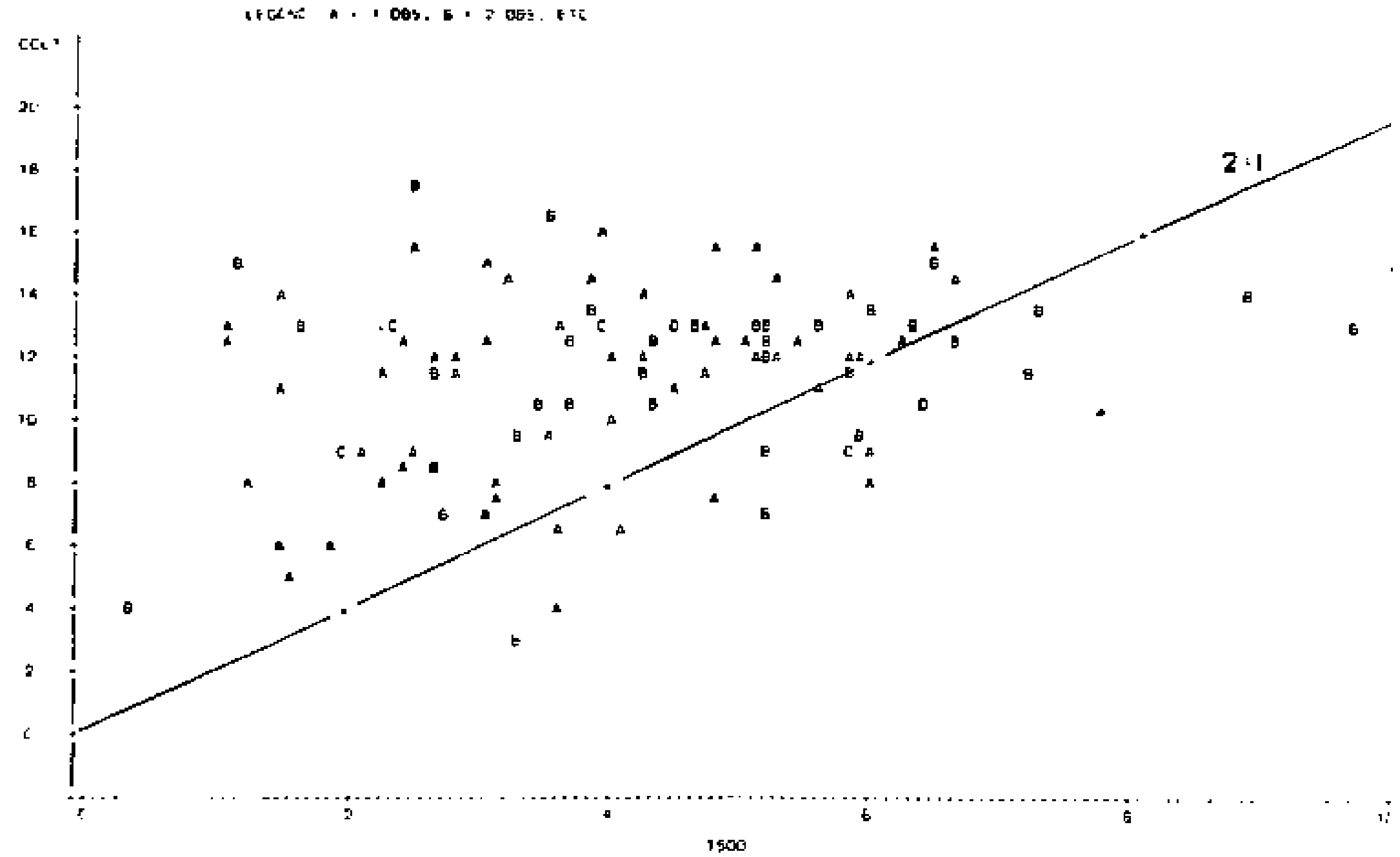

Figure 2. Cloud base temperature versus 500 mb buoyancy for Nelspruit PAMS cases (N = 107)

rises. The 500 mb point value of ΔT serves as a crude estimate of the true parcel buoyancy. Together with the CBT, the buoyancy information provides an index of the time required for the parcel to reach the constant reference level height. This is also the time available for drop growth via, for example, coalescence. Thus, the ratio is referred to as the coalescence time parameter.

In the mean Nelspruit PAWS case, CBT is 11.4°C (with a standard deviation of ±2.9°C). The 500 mb thermal buoyancy for the 147 cases is 4.3°C, on average (±1.9°C). The frequency distributions of both CBT and $\Delta T5$ are shown in Figures 3 and 4 (the bars represent an interval one unit wide starting with the number below each bar). Based on the average $\Delta T5$ and CBT, the mean CTP from the PAWS data set is 2.65, with variations of 1.98 to 3.33 associated with the SD of the CBT and with variations of 1.84 to 4.75 associated with the SD of $\Delta T5$. Thus, it appears that CTP is more sensitive to buoyancy alterations. If this were true, CTP might be reducible to a simple stability index. Furthermore, it appears that the actual time available for drop growth is related to CTP by a non-linear function. Thus, the actual growth time could be even more drastically affected by the relative variations of CBT and $\Delta T5$. A preliminary investigation of these possibilities follows.

2. TIME FOR DROP GROWTH

The actual time available for any mechanism to act on the droplets as they rise from ground base to the observation level (at temperature = TREF = -10°C) can be estimated by

$$CT = \frac{\dfrac{TREF - CBT}{-\gamma_c}}{W} \quad . \qquad (2)$$

Here, W is the mean updraught velocity. W depends on the average parcel buoyancy, B ($-\Delta T5/T$), and the radius of the current, r. According to Scorer and Ludlam (1953), $W = c(gBr)^{1/2}$, with c = 1.2. The in-cloud lapse rate (γ_c) is taken to be 5.5°C/km, and $\Delta T5$ is assumed to be representative for lower altitudes as well. Thus, the approximate nature of CT must be immediately recognised.

Figure 3.

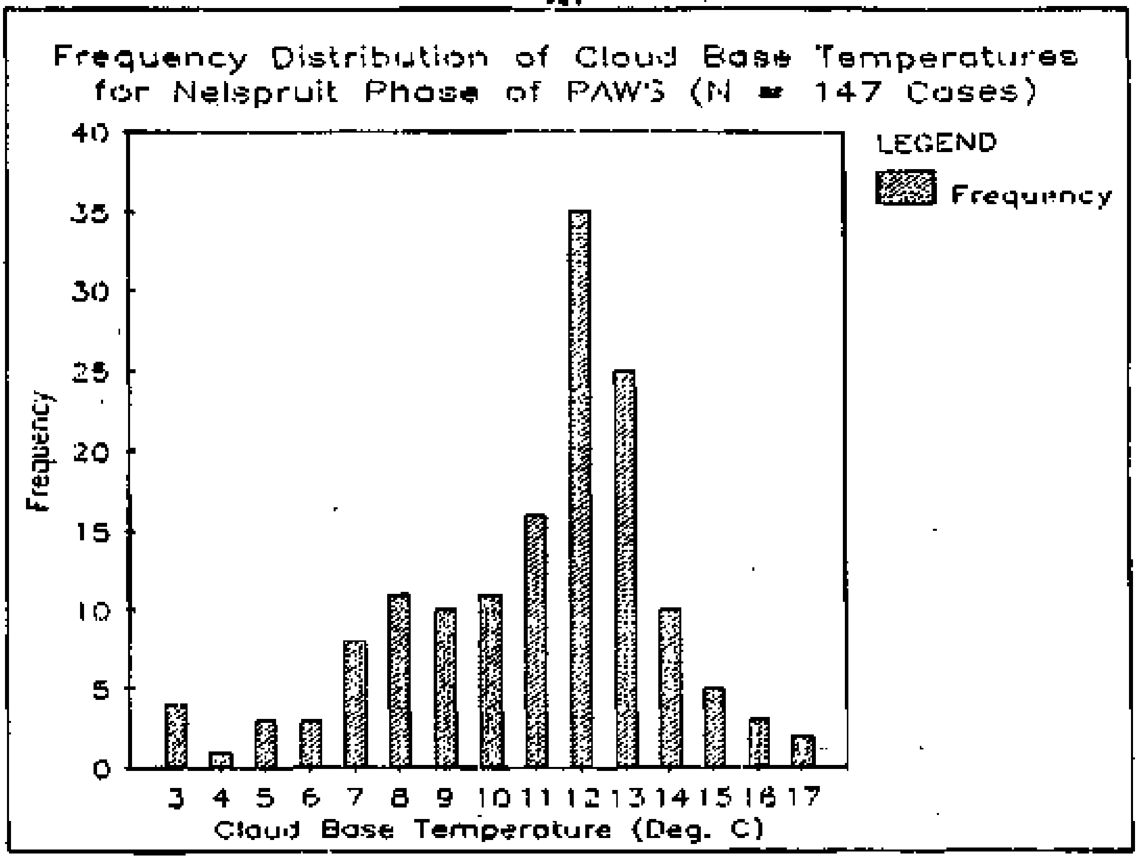

Figure 4.

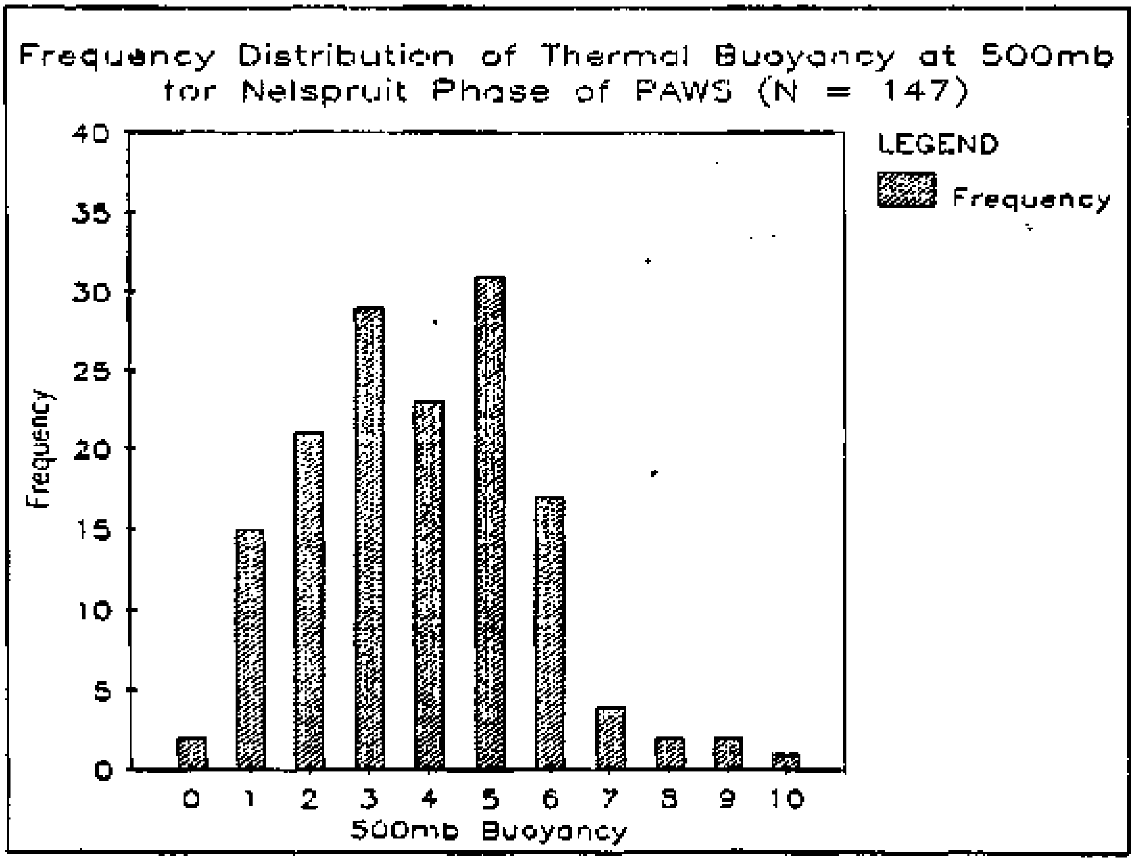

Analytic manipulation quickly reveals that because W is taken to be proportional to $(\Delta T5)^{1/2}$, CT is related to CTP via non-linear equations such as

$$CT = \frac{301}{(\Delta T5)^{1/2}} + 30.1 \times CTP(\Delta T5)^{1/2} \qquad (3a)$$

or

$$CT = 301\ (CTP/CBT)^{1/2} + 30.1(CTP)^{3/2}/CBT^{1/2}. \qquad (3b)$$

However, CT is more conveniently obtained directly from CBT and ΔT5,

$$\begin{aligned} CT &= 301/(\Delta T5)^{1/2} + 30.1\ CBT/(\Delta T5)^{1/2} \qquad (3c) \\ &= (301 + 30.1\ CBT)/(\Delta T5)^{1/2} \quad . \end{aligned}$$

The distance travelled between cloud base and the -10°C level is on average about 3.9 km (=(-10°C-11.4°C)/-5.5°C/km). Fluctuations in the travel distance associated with the observed standard deviation of CBT, 2.9°C, are between about 3.4 to 4.4 km.

If the average updraught of PAWS storms is about 5 mps as suggested by the general radar analyses of Reuter (1990), the time available for raindrop growth is on average about 780 seconds with variations due to CBT fluctuations between about 680 to 880 seconds. Small thermal bubbles (r ~110 m) must be associated with these velocities given the strong mean buoyancy (4.3°C). However, if the average of the maximum in-cloud updraught velocities (~12.5 mps) measured at Nelspruit by Morrison *et al.* (1986) are taken to be representative of the central convection, more realistic large bubbles are permitted (r ~680 m) and CT is about 310 seconds with an approximate 270 to 350 second range of variations caused by the CBT variations.

The range of variation of W associated with the observed standard deviation (SD) in ΔT5, ±1.9°, is calculated with the W equation to be 9.4 to 15.0 mps (for the same large r). This W range is similar to the observed variation between the "worst" and "best" cases averaged by Morrison *et al.*, 11 to 14 mps. Thus, variations in CT associated with buoyancy fluctuations are calculated to be between about 260 to 410 seconds. Consequently, the buoyancy variations also appear to play a slightly stronger role in determining CT than the cloud base temperature variations.

The above calculations are summarised in Table 1 and indicate that the actual drop growth time as the core of the rising air ascends the nearly 4 km distance above cloud base to the flight level is most likely to be about 4 to 7 minutes. However, CT may be over 15 minutes for cases with W ~5 mps. The key variable not well specified from measured data is the updraught radius, as this may dominate the calculations. Nevertheless, the main conclusion is that both CTP and CT are more strongly influenced by buoyancy than by the cloud base temperature variations.

The relative variation of CT is smaller than that of CTP. Over the range of the PAWS data set a factor of 10 change in CTP corresponds to only a factor of ~3 change in CT (Figure 5). Another important result is that a linear function fits the observed (CT, CTP) data points very well (r = .99). Thus, in the present theory, the relationship between the index and the actual time available for growth appears to be relatively simple. Furthermore, the data points in Figure 5 reveal that the time available for droplet growth that corresponds to CTP = 2 is ~250 seconds. However, at this point the true importance of ΔT5 compared with CBT is somewhat difficult to determine, particularly for the more realistic case of simultaneous ΔT5 and CBT variations.

Table 1: Fluctuations in the coalescence time parameter and the coalescence time due to variations in cloud base temperature and buoyancy for PAWS cases.

	Ave	CBT(11.4±2.9°C)		ΔT5(4.3+/-1.9°C)	
		+1SD	-1SD	+1SD	-1SD
CTP	2.65	3.33	1.98	1.84	4.75
ΔZ (km)	3.9	4.4	3.4	(3.9)	(3.9)
W (mps)	12.5	(12.5)	(12.5)	15.0	9.4
CT (sec)	311	353	269	259	414

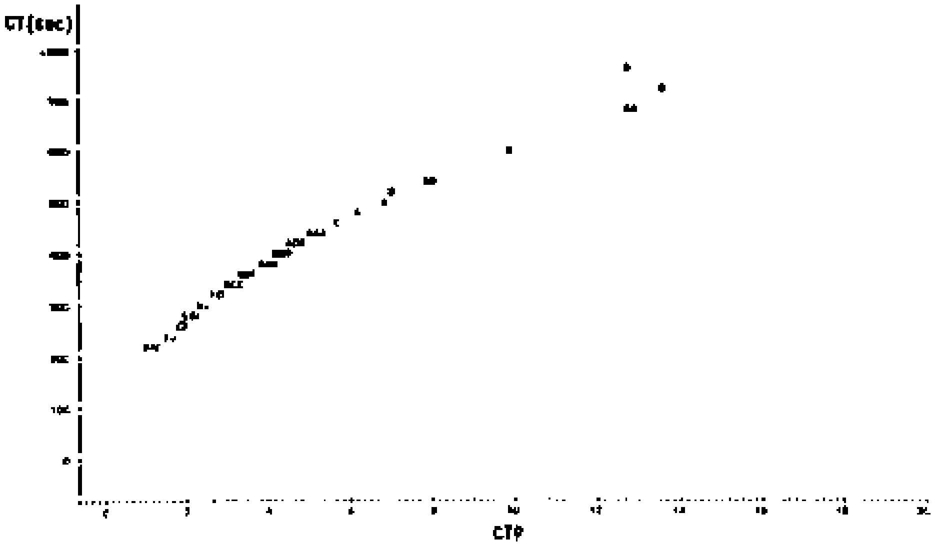

Figure 5. Relationship between CT and CTP (γ = 5.5°C/km, W = c/gθr).

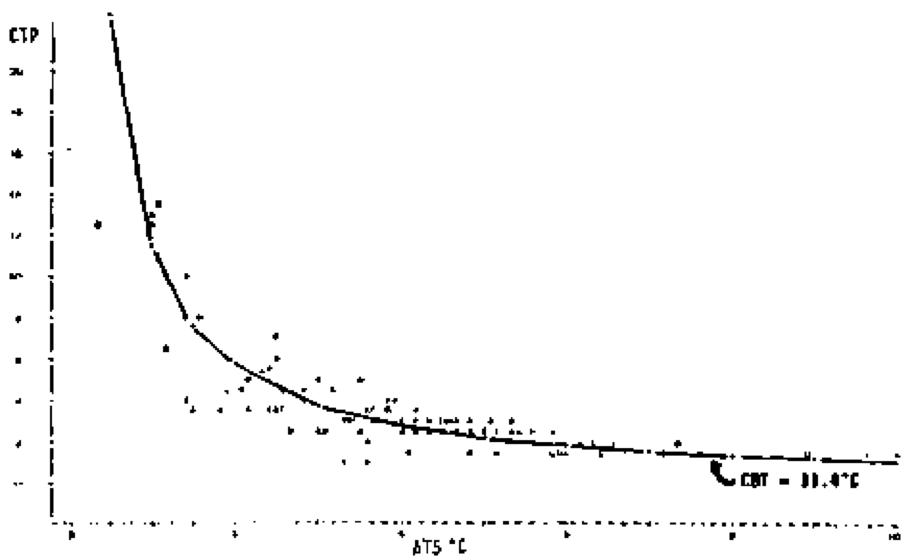

Figure 6a. CTP as a function of ΔTS (Nelspruit PAWS data).

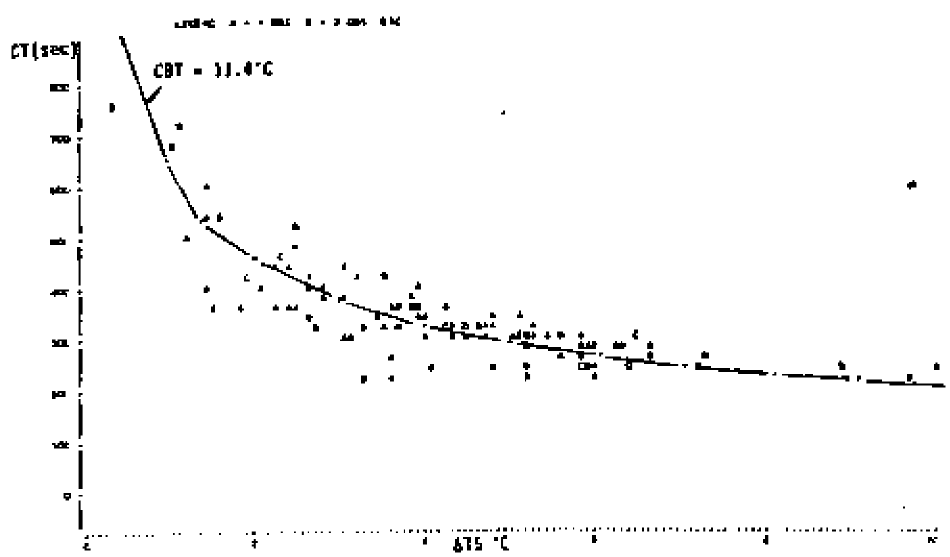

Figure 6b. CT as a function of ΔTS (Nelspruit PAWS data).

The relationships that CTP and CT have with their independent variables (CBT and ΔT5) are revealed by the plots in Figures 6 and 7. The substantial ranges of variation in both CTP and CT associated with changes in ΔT5 are evident, but the bulk of the variations is associated primarily with only a few small ΔT5 observations. On the other hand avoiding cases with the ratio greater than two eliminates the strongest buoyancies (Figure 6a). There is far more scatter of CTP and CT over the range of CBT (Figure 7). This is partly because CBT and ΔT5 are poorly correlated (Figure 2). However, the expected increasing linear relationships would be better supported by the data if two cold CBT (-4°C) data points from one day were not present.

3. MATHEMATICAL ANALYSIS

The best means of analysing the variations of CTP and CT with simultaneous variations of both ΔT5 and CBT is probably via the total differential. The total differential is often applied in error analysis. The total differential of a function (f) is given in terms of the partial derivatives with respect to the related independent variables (e.g. x, y),

$$df = f_x\,dx + f_y\,dy, \qquad (4)$$

where f_x and f_y are the partial derivatives of f. For the case of f = CT (or f = CTP), the most obviously related variables are CBT and ΔT5. However, it may be important to recognise that other variables correlated to the independent variables may make substantial contributions to the variation of CTP and CT. Nevertheless, the analysis here considers only the CBT and ΔT5 contributions, and is therefore only a relative comparison of the importance of these two variables. Thus,

$$d[CTP] = \frac{1}{\Delta T5}\,d[CBT] - \frac{CBT}{(\Delta T5)^2}\,d[\Delta T5] \quad , \qquad (5)$$

and

$$d[CT] = \frac{30.1}{(\Delta T5)^{1/2}}\,d[CBT] - \frac{1/2(301 + 30.1\ CBT)}{(\Delta T5)^{3/2}}\,d[\Delta T5] \quad . \qquad (6)$$

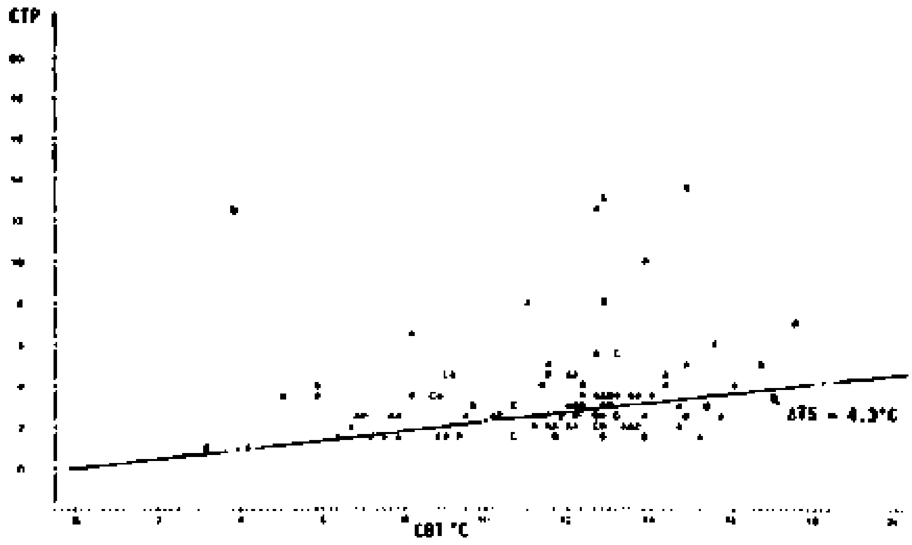

Figure 7a. CTP as a function of CBT (Nelspruit PAWS data).

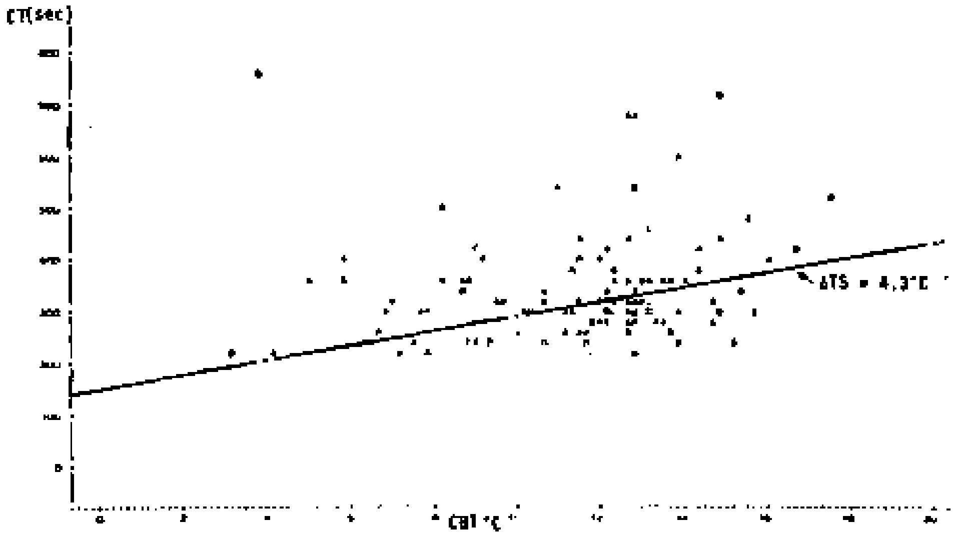

Figure 7b. CT as a function of CBT (Nelspruit PAWS data).

Using the mean values for CBT (11.4°C) and ΔT5 (4.3°C) to evaluate the partial derivatives and the observed standard deviations (2.9 and -1.9°C, see Table 1) for the independent variable differentials (the d[CBT] and d[ΔT5] terms) yields

$$
\begin{aligned}
d[CPT] &= 0.233\,[2.9] - 0.617\,[-1.9] \\
&= 0.67 + 1.17 = 1.84 \\
&(\text{or } 36\% + 64\% = 100\%)
\end{aligned}
$$

and

$$
\begin{aligned}
d[CT] &= 14.5[2.9] + 36.1[1.9] \\
&= 42.1 + 68.6 = 110.7 \\
&(\text{or } 38\% + 62\% = 100\%).
\end{aligned}
$$

Since positive deviations from the mean CBT and negative deviations from the mean ΔT5 both increase CTP and CT, it is appropriate to compare the impact of positive CBT deviations with negative ΔT5 deviations. The above numerical calculations are similar to the results in Table 1 (divided by 2) and indicate that CBT and ΔT5 contribute 38% (= 42.1/110.7) and 62% of the total variation in CT, respectively. Similarly, CBT and ΔT5 contribute 36% and 64% of the CTP variation.

4. CONCLUSION

In spite of the fact that the theoretical relationship between the coalescence time parameter and the estimated actual time available for drops rising in convective currents to grow is non-linear, the actual data points are very well fit by a linear function. Thus, the impact of buoyancy and cloud base temperature on CT is not greatly distorted compared with their impact on CTP. Consequently, the buoyancy contribution to both the estimated droplet growth time and to CTP accounts for slightly more than 60% of their total variations as determined by differential calculus. Furthermore, the CTP = 2 threshold eliminates all the strongest buoyancy cases and thus acts something like a buoyancy threshold. However, the cloud base temperature still makes a substantial contribution to the total differentials of both CT and CTP and obviously can not be overlooked in either case. The PAWS data can also be used to crudely estimate the time available for droplet growth. It is estimated for example, that a duration of ~250 seconds corresponds to CTP = 2. Therefore, a droplet growth time of more than four or five minutes appears to favour positive seeding results in the Eastern Transvaal, although more data is desirable.

5. ACKNOWLEDGEMENTS

Comments by G Mather, B Foote, P Grosh and J Gertenbach led to substantial improvement in this text.

6. REFERENCES

GROSH R C and MATHER G K, 1988. 1987/88 PAWS Report. CSIR/WRC, Pretoria, 199pp.

MATHER G K, MORRISON B J and MORGAN G M, 1986. A preliminary assessment of the importance of coalescence in convection clouds in the Eastern Transvaal. J. Clim. Appl. Meteor., 25, 1780-1784.

MORRISON B J, MATHER G K and MORGAN G, 1986. Aircraft observations of target turrets on multicellular storms showing radar response to dry ice seeding. Preprints: 10th Weather Modification Conference. AMS, Boston, 204-209.

REUTER, G W, 1990. Radar observations of precipiation production in PAWS storms. This volume, 152-170.

SCORER, R S and LUDLAM, F H, 1953. The bubble theory of penetrative convection. Quant. J. Roy. Meteor. Soc., 79, 94, 315.

0/22gal/sgg

IV. CASE STUDIES

Examination of the observations from individual cases from the PAWS data set was undertaken to determine the nature of seeding effects on storm processes and to better understand the moisture processing mechanisms of thunderstorms in the Transvaal.

A. SEEDING EFFECTS

R C Grosh, C Muller

1. INTRODUCTION

An integral part of many weather modification projects has been the detailed examination of a few individual experiments to better link cause and effect (Grosh and Semonin, 1973; Farley, 1987). Thus, a number of case studies of seeded PAWS storms which appear to have responded have been initiated to improve our knowledge of cloud processes at Nelspruit and Carolina. These storms were selected from the summary radar histories for each of the PAWS storms.

Previous research on seeding induced storm alterations through the study of radar rain echo evolution and cloud photographs has shown:

1) Storms treated with large doses of seeding material within five minutes of echo development may be by far the most effected storms (Gagin *et al.*, 1986).

2) In the forty minutes following the start of treatment, seeded PAWS storms tend to initially have more rapidly growing echo centroid heights, followed by more intense reflectivities and, finally, greater areal expansion and increased rainflux than their untreated counterparts (Mather *et al.*, 1988). Simpson and Dennis (1974) describe a similar two step process of visually observed seeded cloud growth, vertical tower development followed by areal expansion with both phases being accomplished in about 20 minutes.

3) Updraught stimulation due to artificial glaciation is quickly observed and glaciogenic seeding at the 6 km level can cause precipitation effects which may reach the lower region of individual cloud in about 10 minutes (Simpson, 1970). Grosh *et al.* (1985) show that there may be rapid (~5 minute) communication between cloud top and the rainout level. Nevertheless, in area experiments the net rainfall enhancement from seeding may only become apparent after about an hour (Woodley, *et al.*, 1982).

4) Another important aspect of rain enhancement is cloud mergers. Simpson (1980) suggests that these may be induced via enhanced low-level convergence which is thought to be associated with updraughts and/or downdraughts stimulated via glaciogenic seeding under the "dynamic" seeding hypothesis. Induced cloud mergers are viewed as being very important to rain stimulation efforts as merged clouds are known to produce much more rain than the sum produced by their constituent clouds before merger.

The case studies have also been undertaken to discover any similarity between the earlier findings and the individual PAWS cases. Two sets of case studies are discussed. These consisted of six Nelspruit and two Carolina experiments.

2. NELSPRUIT CASE STUDIES

The radar observed cloud evolution of six Nelspruit cases is depicted on the "Storm Time History" profiles (Figures 1a to 1d). Cases with rainflux or other echo properties increasing within about 20 minutes of seeding activities were selected for further study. Only about half of the seeded cases had distinct signs of seeding induced increases on the profiles (note logarithmic ordinates).

Case 40 (23/2/85)

Seeding began early in the echo lifetime of case 40, at 13:15 (SAST), or about 10 minutes after the first echo (FE). A substantial increase in the growth of echo size, height, and rain flux began about 10 minutes after the initial seeding, and was sustained until shortly after the last of the six penetrations (Figure 1a). The growth occurred mainly in the form of two pulses, starting about 10 minutes and 50 minutes after seeding began.

Case 56 (2/11/85)

Seeding of Case 56 started at 12:21, about 35 minutes after the FE (Figure 1b). The first seeding penetration appears to have occurred at about the same time as a distinct increase in the size and rainflux of the echo

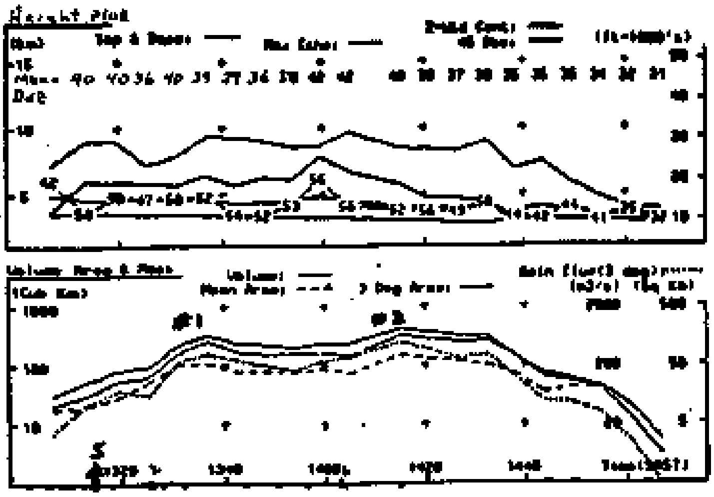

Figure 1a. Storm time history - Case 40.

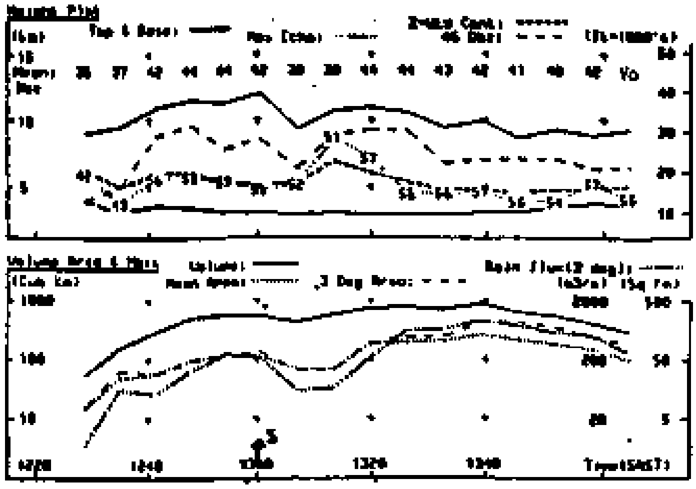

Figure 1d. Storm time history - Case 126.

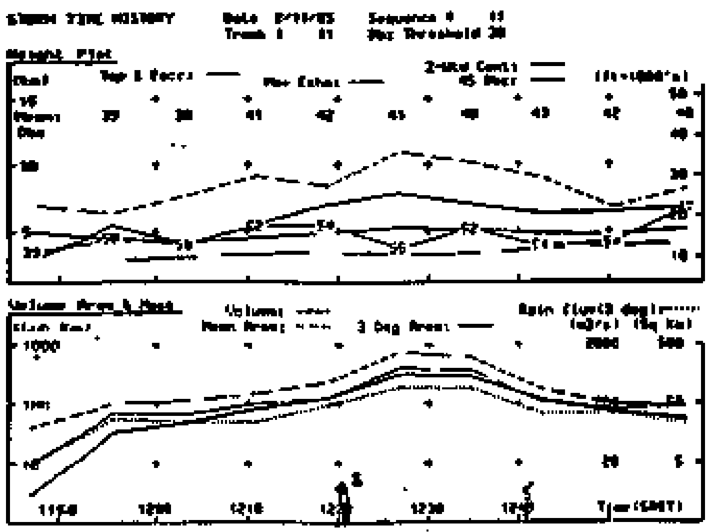

Figure 1b. Storm time history - Case 56.

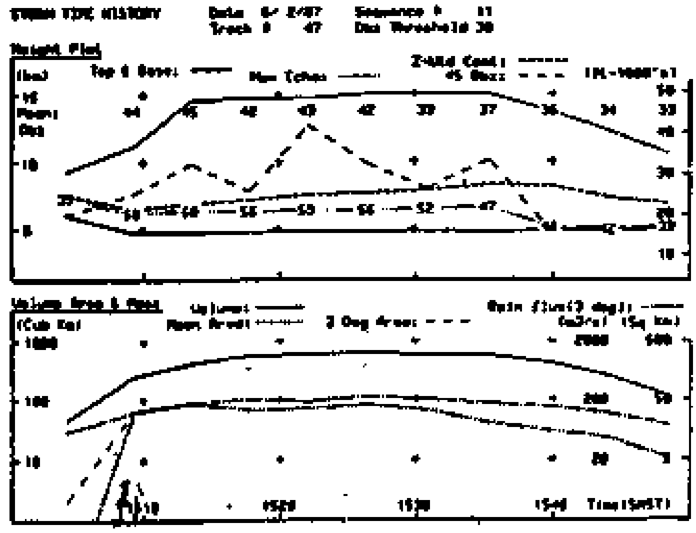

Figure 1e. Storm time history - Case 151.

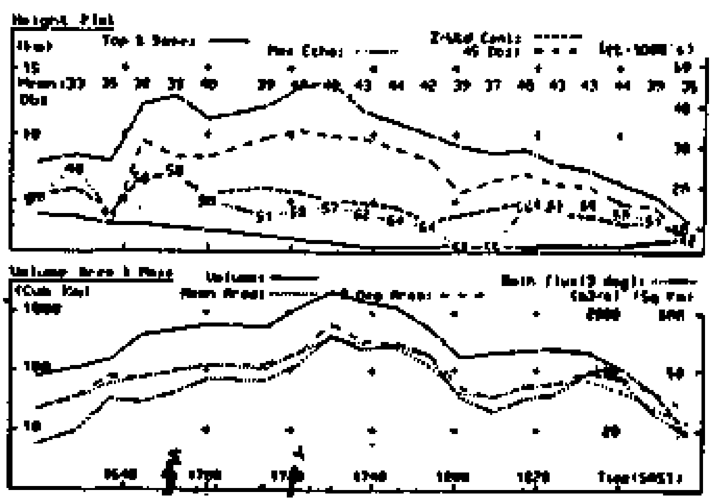

Figure 1c. Storm time history - Case 109.

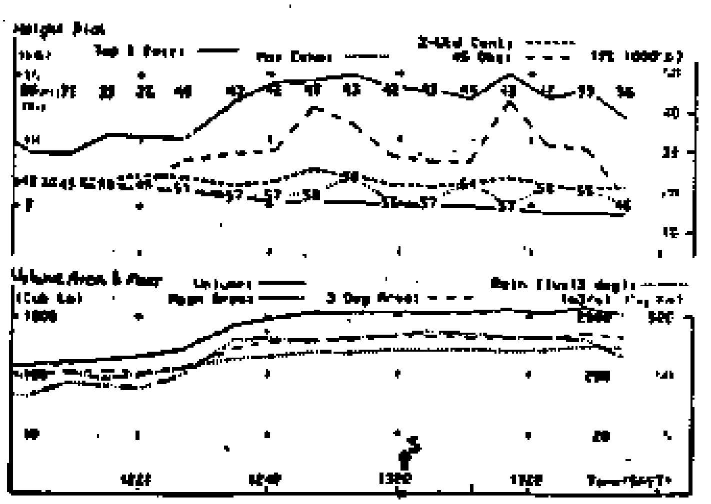

Figure 1f. Storm time history - Case 155.

began. However, given the 7 to 8 minute resolution of the radar volume scans, the precise time of the initial rise of the enhanced echo growth rate is not known. The observed peak was at about 12:26. The increasing trend in top height and rain flux were all underway before the seeding commenced, but at a less intense rate than after the initial seeding. The last of the five penetrations occurred as the echo was well into its decline. Conditions for effective seeding may be assumed to have ended by this time. The fast response to seeding (<5 minutes) seems less likely to be a true seeding effect compared with Case 40 (Figure 1a).

Case 109 (27/10/86)

The first seeding penetration of Case 109 occurred at 16:52, about 30 minutes after the FE (Figure 1c). A very distinct maximum in echo size and rainflux occurred about six minutes after the last of the four penetrations and is reasonably impressive evidence for a seeding effect during a period of generally growing storm conditions and probable low-level air flow convergence.

Case 125 (19/12/86)

The first of the six seeding passes through Case 125 began at about 13:00, about 30 minutes after the FE, and during a period of sharply decreasing rainflux (Figure 1d). This case was included because within 15 minutes the rainflux began a strong comeback and quickly exceeded its earlier peak value by a very substantial amount. This occurred during a period of generally decreasing echo heights. However, top heights also reached secondary maxima within 10 minutes after seeding commenced. A new cell intensifying within the general echo mass seems to be the cause of the new growth, and was doubtlessly associated with a seeded tower. As such, this must be viewed as a promising case for a positive seeding effect.

Case 151 (6/2/87)

The FE of Case 151 formed about 5 minutes before the first seeding penetration at about 15:08 (Figure 1e). The size of this echo was rather uniform with little fluctuation during or after the seeding period. Nevertheless, a detectable increase in rainflux occurred at about 15:14, ~6 minutes after the seeding commenced, but peaked well before the last of the seven penetrations. The quick appearance and moderate amplitude of the rain peak appear somewhat dubious as seeding signatures. In general, this case was not impressive evidence of a seeding effect, but a true effect cannot be ruled out, especially in the light of the very large growth in the echo top and 45 dBz heights shortly after seeding commenced and the large sustained echo volume during the seeding period.

Case 155 (27/2/87)

The seeding of Case 155 began at 13:01, at least 40 minutes after the FE (Figure 1f). Only a very slight increase in the rainflux occurred (a few minutes after seeding), but a dramatic increase (~5 km) in the height of the 45 dBz echo began about 10 minutes after seeding, and was accompanied by moderate rises of the echo top height and centroid. Interestingly, there were only two short penetrations at 13:01 and 13:03 (of 13 and 34 seconds of seeding duration, respectively). The modest increases in echo centroid height and rainflux suggest that the normal seeding signature is only partly present, and may be explained by the decreased dosage (~8.9 kg) and lack of sustained treatment that this case received.

3. CAROLINA CASE STUDIES

The two Carolina cases selected for study were also chosen because of their relatively promising echo profiles for seeding enhancements (Figures 2 and 8). An important difference from the Nelspruit experiments in addition to the drier location at Carolina is that unlimited amounts of seeding material could be released depending only on logistics and the availability of suitable cloud towers.

CAROLINA CASE 6 (26/11/88)

Introduction

The storm on 26 November 1988 was selected for study because it included a merged echo track (Figure 2). This locally intense storm case was located 25 to 40 km north of Carolina and occurred between 12:50 and 14:40 as part

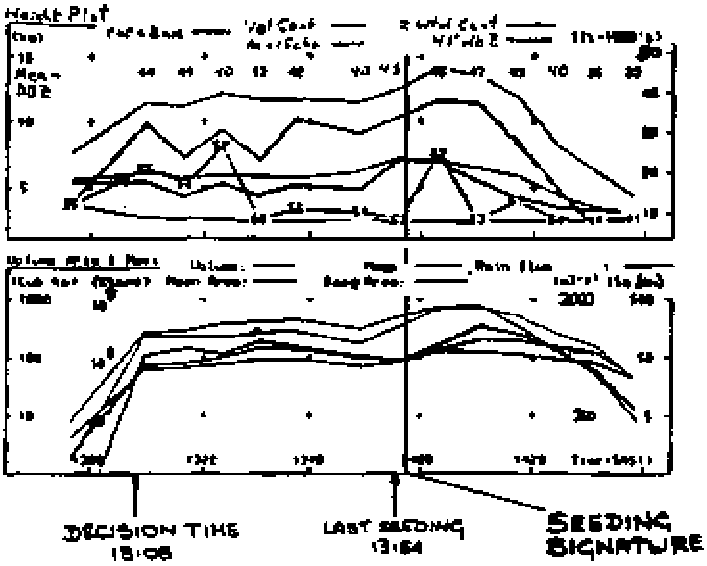

Figure 2. Storm time history.

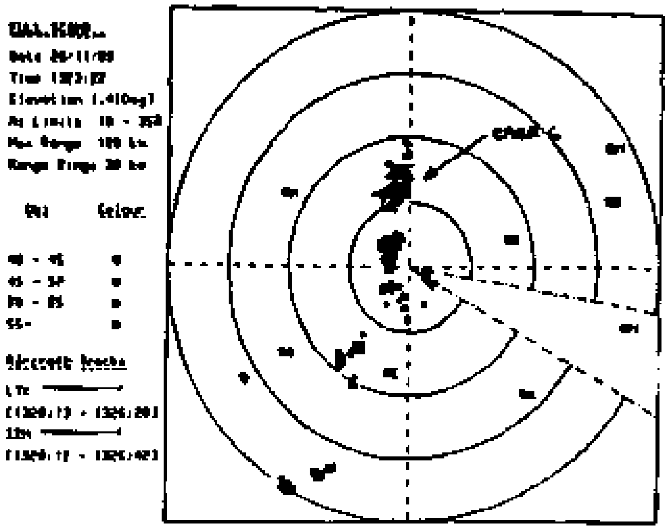

Figure 3. PPI full scan survey (range marks = 30 km).

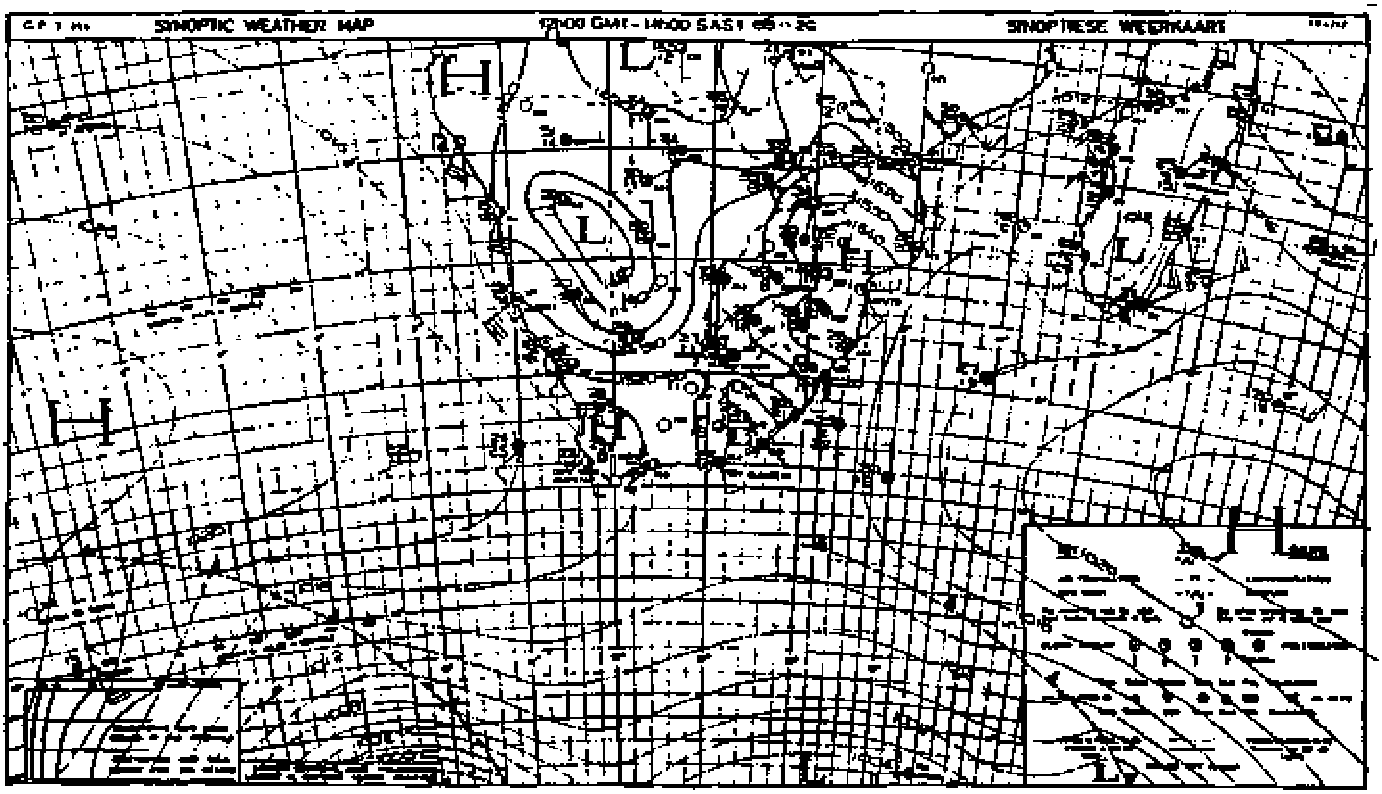

Figure 4. Synoptic weather map (26-11-1988).

of a line of scattered cells from 60 km north to 120 km southwest of Carolina (Figure 3).

Synoptic Situation

The synoptic chart at 14:00 showed moist air east of a trough over the Southern African interior. A surface trough is usually also associated with a well-defined moisture boundary, separating moist air to the northeast from drier air to the southwest. Thunderstorm activity can be expected to develop within a convergence zone 200 to 300 km east of the moisture boundary. However, as the study area was under a region of high pressure, convective activity was somewhat isolated (Figure 4). The maximum temperature near Carolina was about 30°C. The dew point temperature was about 9°C. Nearby rainfall measurements from the synoptic report were between 2.1 to 3.6 mm for Carolina, Ermelo and Piet Retief. No rain was reported at any of the other rain-recording stations in the area.

Storm Echo History

The storm echo top reached to 14 km and with a mean area of 50 km^2 and a volume of over 300 km^3, it classified as a moderate to small storm with a tall top (Table 1). The probability for the presence of hail was high, due to reflectivities being larger than 50 dBz, with the 45 dBz contour extending to almost 12 km. During its ~100 minute lifetime, the storm tracked a distance of 27.2 km.

The seeding signature appeared shortly after the end of the 10 seeding penetrations and about 50 minutes after seeding began at 13:11 (Figure 2). The cumulative seeding time amounted to 215 seconds, a substantial increase over the 120 second (23 kg) limit used in the Nelspruit experiments. The last seeding penetration began at 13:54 and lasted 15 seconds. The growth of the storm size, mass and rain flux commenced at about that time. This suggests the prolonged seeding may have been successful in favourably altering the precipitation process. Since the echo volume and height increased distinctly, the dominance of a dynamic alteration over a static effect seems likely, but is not proven.

Table 1. Echo Characteristics of Carolina Case 6.

Echo top mean	:	10 480 m
Volume mean	:	321 km^3
Total mass mean	:	231 kton
Area 3° mean	:	49.9 km^2
Area cutoff mean	:	37.4 km^2
Rflux 3° mean	:	232 m^3/s
Rflux cutoff mean	:	131 m^3/s
CCL temperature	:	6.0°C
Buoyancy at 500 mb	:	2.3°C
TCCL/DT500	:	2.6

Upper Air Sounding

The earlier of the two aircraft soundings started at 12:24 (Figure 5a). The cloud base temperature was 11.7°C and the average sub-cloud mixing ratio was 10.8 g/kg. One of the main features present was an elevated inversion layer at about 450 hPa. At Pretoria, winds were from the north-west or west between 500 hPa and 200 hPa. Below 500 hPa the wind was weak but consistently from the north. A strong low level inversion and the low mixing ratio were not very promising for a strong convective day. The coalescence time parameter (9), the ratio of cloud base temperature to the 500 mb thermal buoyancy, was well above than the critical value (2). This suggests substantial time was available for rain drop growth in the updraught.

The second sounding was taken during the period of apparent seeding induced rain enhancement at 14:07 (Figure 5b). The 500 hPa buoyancy, though initially small (1.3 °C), was positive and increased with time to 2.3°C. The coalescence time parameter (2.6) had decreased markedly but was still above 2. Although a stabilising change can be seen in the slight decline in height of the upper inversion from the earlier sounding, the dew point temperature near 650 hPa is now approaching the environmental temperature trace. This and the buoyancy trend suggest that instability adequate for substantial vertical cloud growth was now present. The observed cloud growth proves some type of destablising mechanism, like

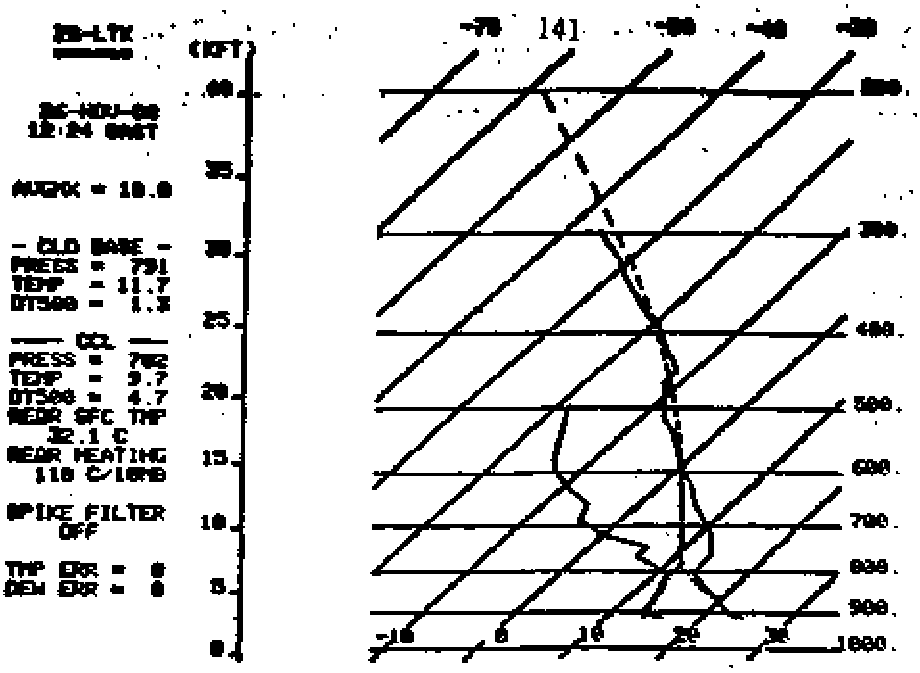

Figure 5a. Nelspruit sounding 12:24 SAST.

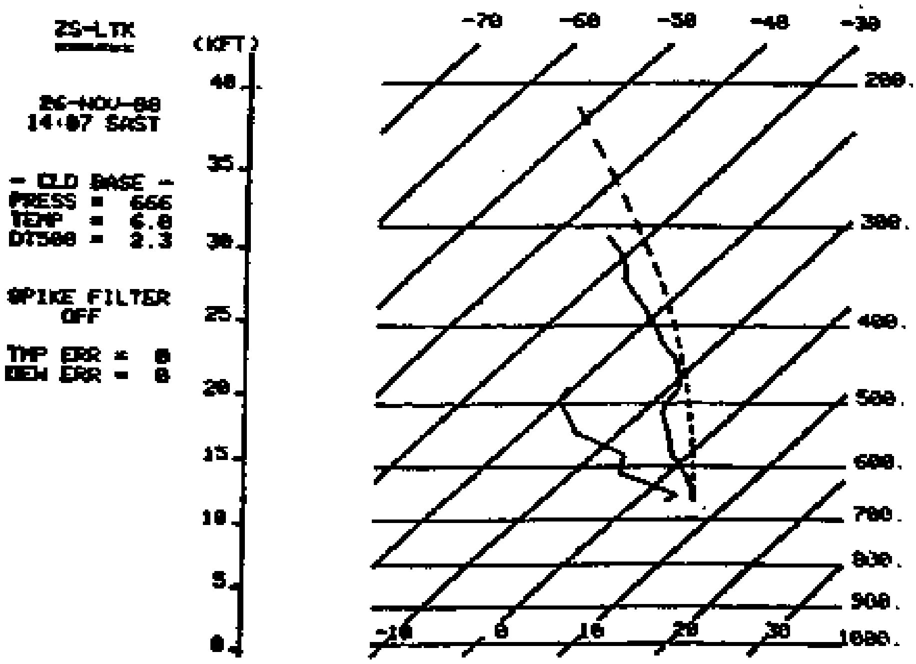

Figure 5b. Airborne sounding 14:07 SAST.

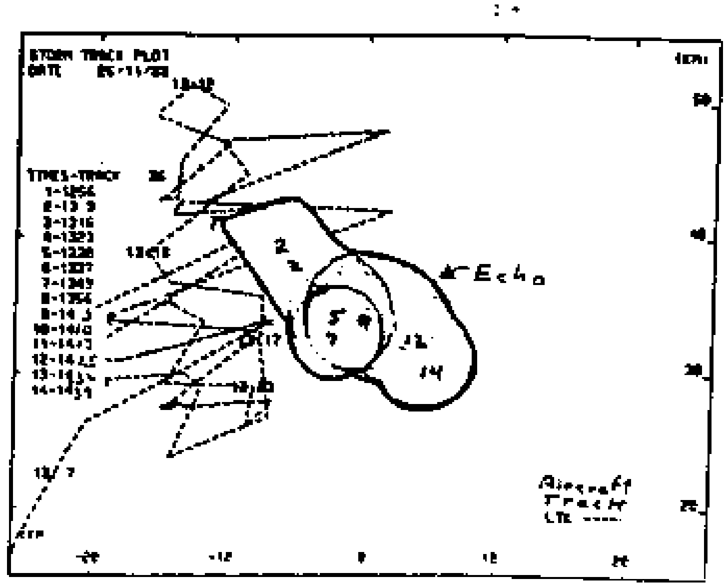

Figure 3.

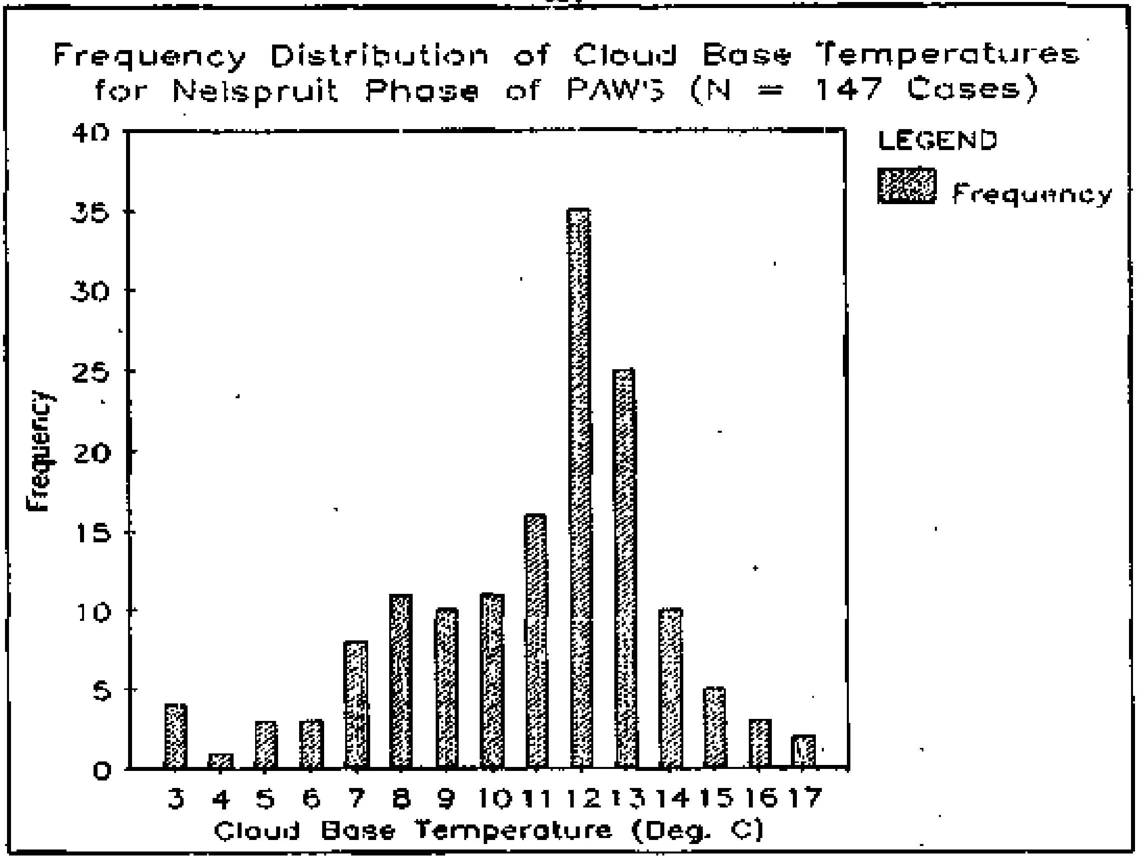

Figure 4.

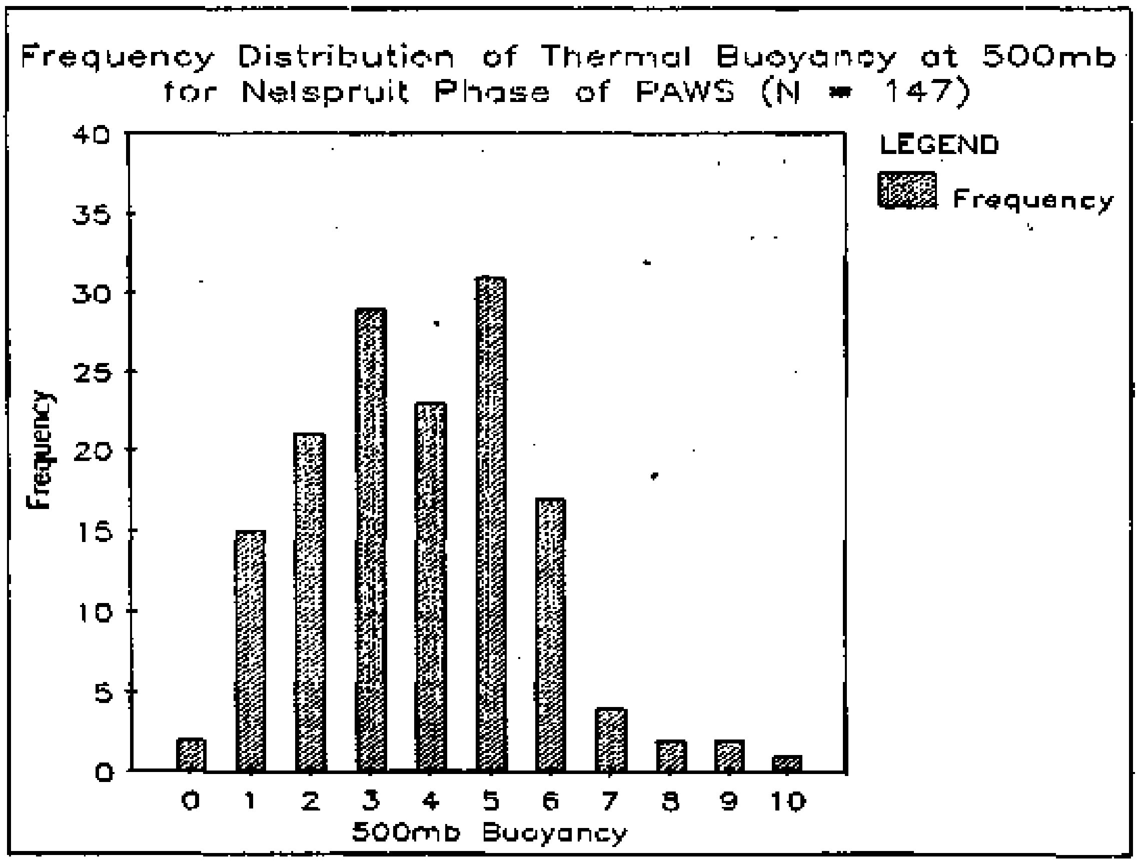

Analytic manipulation quickly reveals that because W is taken to be proportional to $(\Delta T5)^{1/2}$, CT is related to CTP via non-linear equations such as

$$CT = \frac{301}{(\Delta T5)^{1/2}} + 30.1 \times CTP(\Delta T5)^{1/2} \tag{3a}$$

or

$$CT = 301\ (CTP/CBT)^{1/2} + 30.1(CTP)^{3/2}/CBT^{1/2}. \tag{3b}$$

However, CT is more conveniently obtained directly from CBT and ΔT5,

$$\begin{aligned} CT &= 301/(\Delta T5)^{1/2} + 30.1\ CBT/(\Delta T5)^{1/2} \\ &= (301 + 30.1\ CBT)/(\Delta T5)^{1/2} \end{aligned} \tag{3c}$$

The distance travelled between cloud base and the -10°C level is on average about 3.9 km (=(-10°C-11.4°C)/-5.5°C/km). Fluctuations in the travel distance associated with the observed standard deviation of CBT, 2.9°C, are between about 3.4 to 4.4 km.

If the average updraught of PAWS storms is about 5 mps as suggested by the general radar analyses of Reuter (1990), the time available for raindrop growth is on average about 780 seconds with variations due to CBT fluctuations between about 680 to 880 seconds. Small thermal bubbles (r ~110 m) must be associated with these velocities given the strong mean buoyancy (4.3°C). However, if the average of the maximum in-cloud updraught velocities (~12.5 mps) measured at Nelspruit by Morrison *et al.* (1986) are taken to be representative of the central convection, more realistic large bubbles are permitted (r ~680 m) and CT is about 310 seconds with an approximate 270 to 350 second range of variations caused by the CBT variations.

The range of variation of W associated with the observed standard deviation (SD) in ΔT5, $\pm$1.9°, is calculated with the W equation to be 9.4 to 15.0 mps (for the same large r). This W range is similar to the observed variation between the "worst" and "best" cases averaged by Morrison *et al.*, 11 to 14 mps. Thus, variations in CT associated with seeding enhanced downdraughts (or updraught induced surface low pressure areas), must have been acting on the low-level environment of the cloud since the first sounding. However, the nature of the true mechanism is not clear at present and requires further analysis which would have had much more chance of providing a firm answer if it had been supported by Doppler radar observations. The rather isolated activity (Figure 3) is a sign of relatively dry atmospheric conditions, and weak flow dynamics. However, storm motion and height suggest the influence of the northwest winds above the seeding level (-10°C or -500 mb). Thus, it appears seeding enhanced downdraughts may have transferred upper level northwesterly momentum downward and spread out to the southeast at the surface setting up convergence as a propagation mechanism in the lower atmosphere near the storm.

Storm Track

The radar echo track for the seeded cell during the time period 12:56 to 14:37 is depicted in Figure 6. The computer analysed PPI echo area is also shown schematically as a function of time. The rain echo travelled from northwest to southeast at an average speed of 18 km/h. At about 13:30, there was a temporary pause in the storms motion which lasted about a half hour, and was associated with cloud merging.

The Learjet and cloud base plane paths indicate that the seeding took place just to the northwest of the actual rain centre (Figures 6 and 7). Thus, the seeding was upwind from the direction of cell propagation. In the existing air flow, rain cells enhanced by seeding could have contributed to the downdraughts which caused the southeastward propagation of cloud growth and, eventually, merger with another rainstorm to the south.

Detailed PPIs

The first radar echo of the case occurred at 12:56. Maximum reflectivities of 50 to 55 dBz occurred within minutes of the first echo (Figure 7a). At 13:37, thirty minutes after decision time, the storm had expanded and propagated as a small multi-cellular storm about 10 km to the southeast (Figure 7b). In close proximity south of the treated storm is another storm cell, propagating northeastwards.

CASE 6

26-11-88 PPIs at 1.5° Elevation

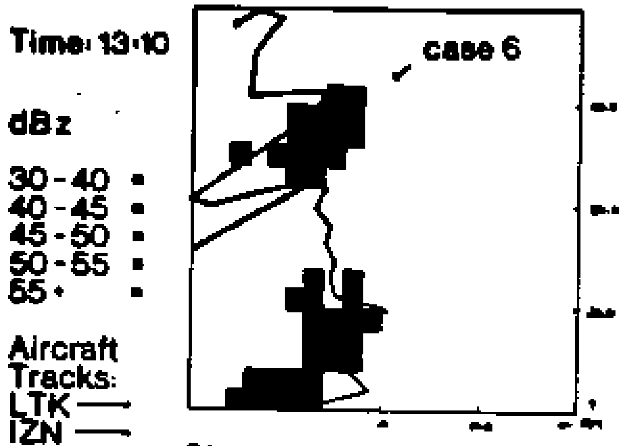

Figure 7a. Carolina Case 6.

N

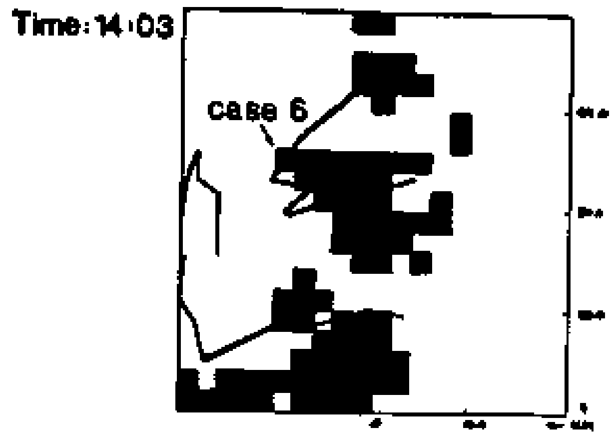

Figure 7d. Post merger consolidation.

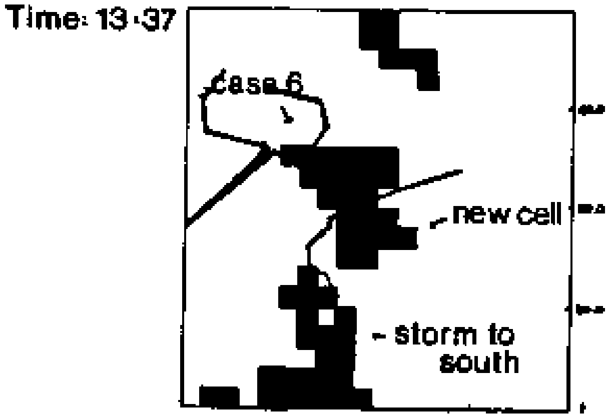

Figure 7b. Case 6 has new element.

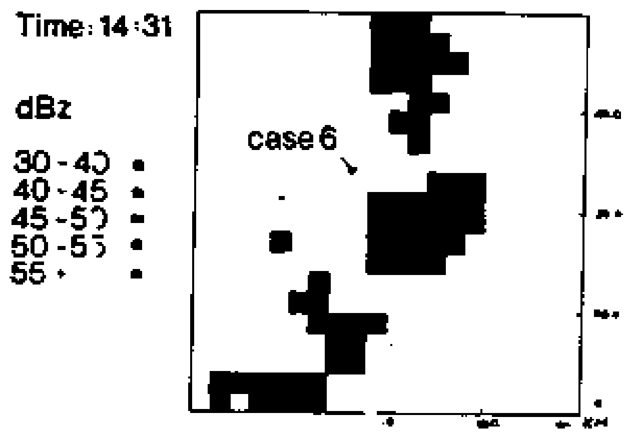

Figure 7e. Case 6 dying.

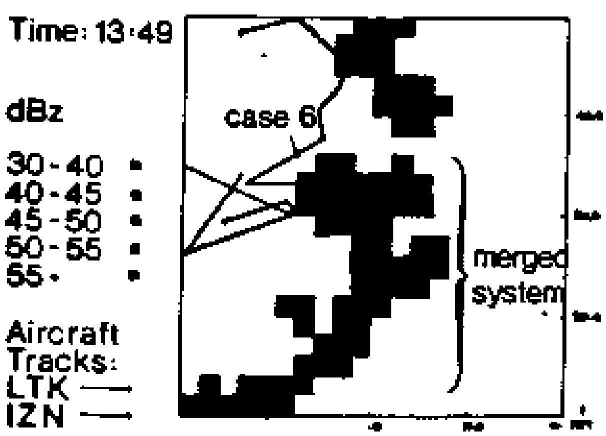

Figure 7c. Case 6 merged with storm to south.

The two rain systems merged about 12 minutes later at 13:49 (Figure 7c). A consolidated storm centre with increased central area, is obvious at 14:03 (Figure 7d). By 14:30, about 20 minutes after the last seeding penetration, the initial storm centre is dying (Figure 7e).

The merging of two separate storm cells can lead to greatly increased rain production. The seeding was also closely associated with the core of the initial storm intensity centre. Thus, the seeding may have led to the merging and subsequent increased rainfall, as suggested in Simpson's hypothesis.

Discussion

Synoptic and environmental conditions are expected to strongly affect storm history, even when seeding is effective. In this case relatively dry, stable atmospheric conditions are associated with generally moderate but locally intense convective activity. The propagation of new cells toward the southwest and the multicellular nature of the storm are probably related to the northwesterly winds in the middle and upper troposphere, and may have been seeding induced.

The entire seeding period lasted 33 minutes with an effective 3 minute 35 seconds of seeding time in the cloud. There is a substantial increase in storm size and intensity variables just before the end of the last penetration. This growth period lasted about 20 minutes and was associated with a 10 000 ft (3 km) rise in storm height, a ~300 km^3 increase in volume, and a ~400 m^3/s increase in rain flux. This might be an indication of a dynamic seeding induced cloud merger. However, an explanation for the slow response of storm rain output to the seeding at earlier times is needed. Furthermore, the pattern of development appears atypical of seeded storms at Nelspruit in that the notable growth in storm size and rainflux occurred over 40 minutes after seeding began.

Doppler radar or other supporting observations would have been very useful in this case, as the present analysis of seeding induced downdraughts which lead to cell mergers is mainly conjecture.

CAROLINA CASE 8 (28/11/1988)

Introduction

A delayed reaction to seeding appeared on 28 November 1988 in a storm to the southeast of Carolina (Figure 8). Thus, this case raises a key issue: "What technique can be used to relate a possible seeding effect occurring with a potentially arbitrary delay to the treatment?"

Another unusual characteristic of this storm was its 80 km long track (Figure 9). The storm first appeared on the radar scope 10 km east of Carolina around 12:40 and dissipated 72 km to the southeast at about 15:00. Other storm activity occurred throughout the entire radar viewing area in the form of scattered storms (Figure 10).

Synoptic Situation

During the afternoon, a cold front moved near Carolina with an anticyclone to the southwest of the subcontinent driving weak southerly flow (Figure 11). Temperatures in the study area ranged up to 27,5°C and the dew point was about 13°C. Under these conditions, convective activity and scattered thunderstorms can be expected over the eastern and northeastern parts of southern Africa. Consequently, widespread rain fell over the radar viewing area with nearly all stations recording substantial amounts over 40 mm.

Storm Echo History

The lifetime of the storm was approximately 140 minutes during which the storm had a mean area of 45 km^2, an echo top height of 6.8 km, and a volume of over 100 km^3. Thus, it was a smaller and shallower storm than Carolina Case 6 (Table 2).

Maximum reflectivities were generally much weaker than in Case 6, typically being about 45 dBz or less. However, reflectivities were highest (57 dBz) just before the seeding and exceeded 50 dBz for about 20 minutes thereafter (Figure 8).

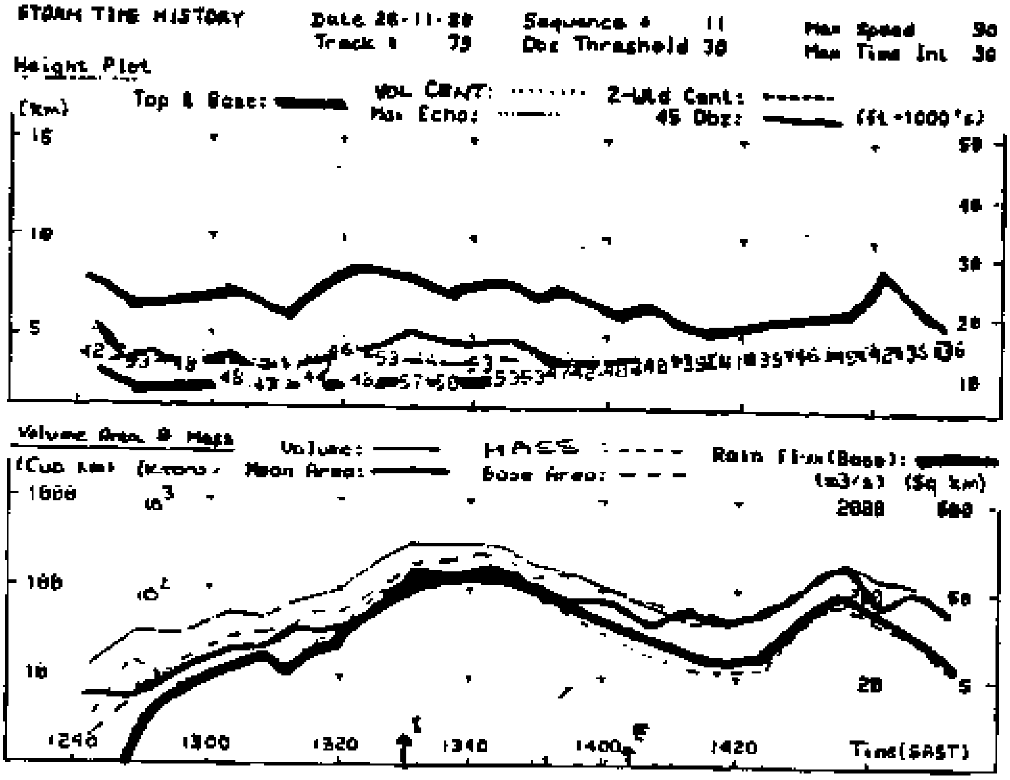

Figure 8. Storm time history.

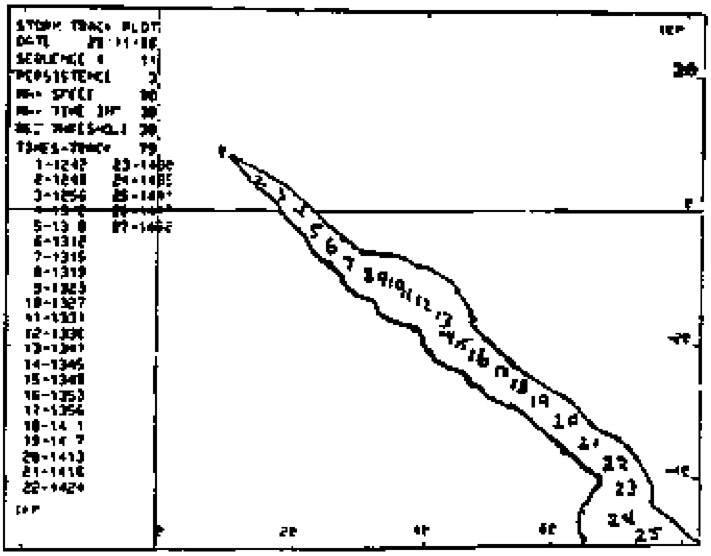

Figure 9. Storm echo track.

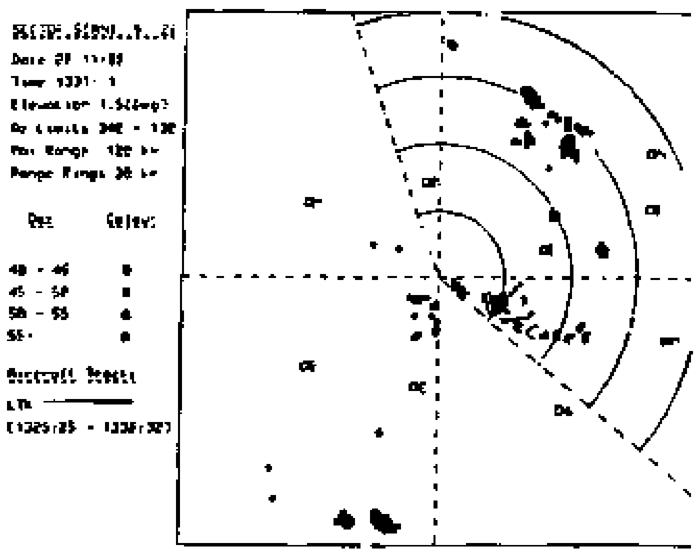

Figure 10. Full PPI scan (range markers = 30 km).

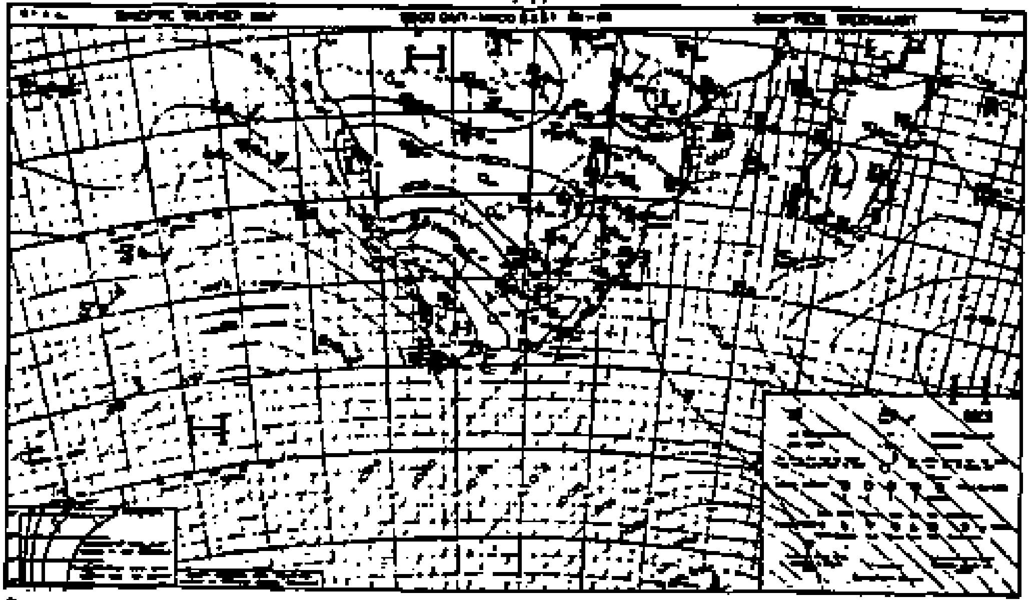

Figure 11. Synoptic weather map (28-11-1988).

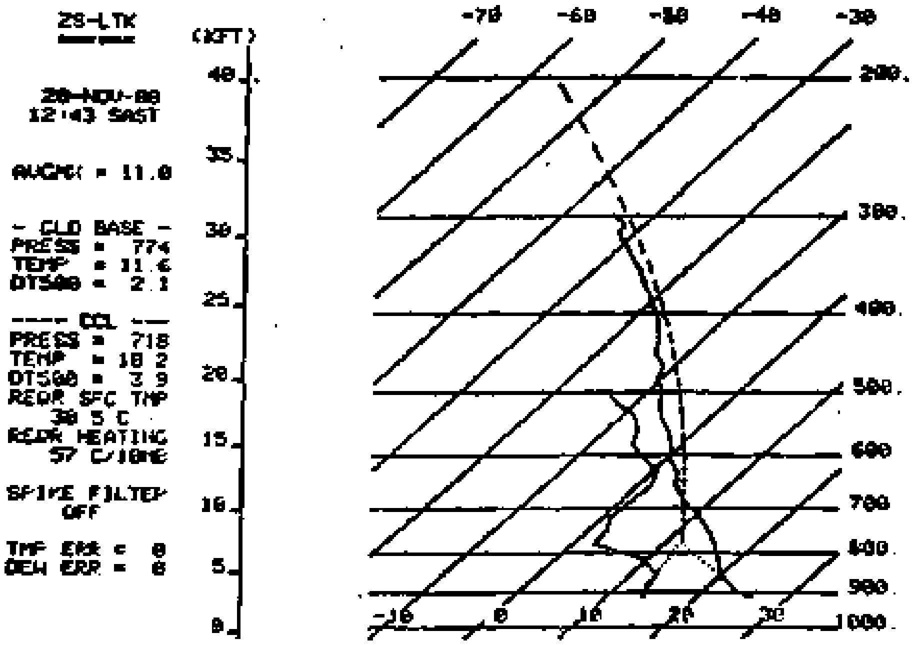

Figure 12a. Nelspruit sounding 12:43 SAST.

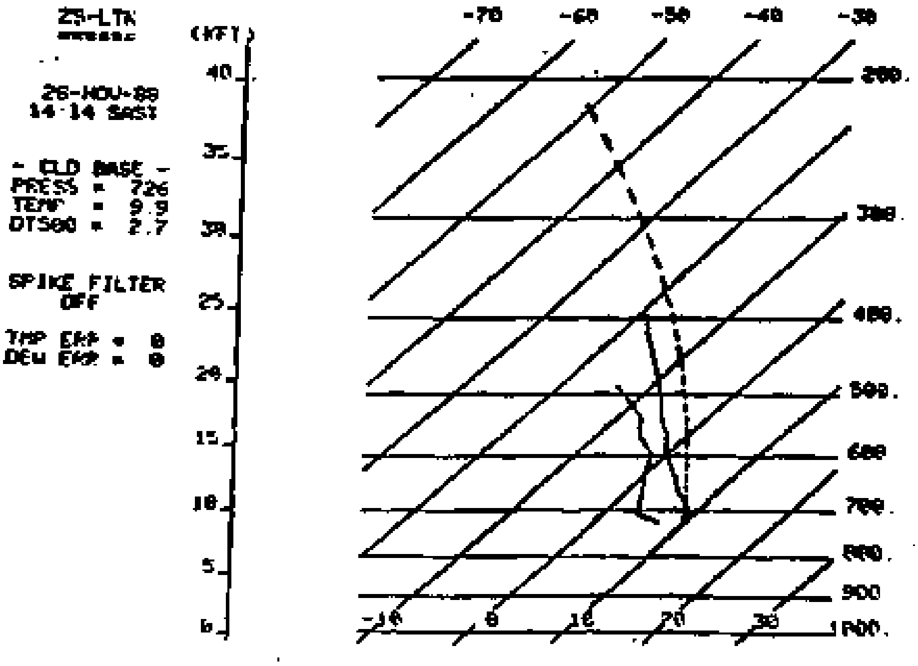

Figure 12b: Airborne sounding 14:14 SAST.

Table 2. Echo Characteristics of Carolina Case 8.

ECHO TOP MEAN:	6778 m
VOLUME MEAN:	115 km^3
TOTAL MASS MEAN:	44 kton
AREA 3° MEAN:	44.5 km^2
AREA CUTOFF MEAN:	8.5 km^2
RFLUX 3° MEAN	91 m^3/s
RFLUX CUTOFF MEAN:	11 m^3/s
CCL TEMPERATURE	9.9°C
BUOYANCY AT 500 mb:	2.7°C
TCCL/DT500	3.7

The first seeding penetration into the cloud occurred at 13:33 (Figure 8). The cumulative seeding time during the eight penetrations into the storm was 120 seconds. After a formerly slow and steady decline of all storm parameters, storm size, mass and rain flux suddenly increased at about 14:24. However, the subsequent rain increase is delayed longer than normal for seeded PAWS storms, as it begins ~50 minutes after seeding commenced compared with the normal 20 to 40 minute lag.

Upper Air Sounding

At the time of the first sounding (12:43), the cloud base temperature and average mixing ratio were 11.6°C and 11 g/kg, respectively (Figure 12a). Upper air wind data for Pretoria showed west to northwest winds up to 100 hPa. Relatively strong northwesterly winds were present near the surface. The occurrence of many scattered cells indicates more widespread instability, and with the lack of a mid-level trapping inversion, the conditions seem more promising for natural cloud growth than on 26 November 1988. However, the echo top of Carolina Case No. 8 never exceeded 10 km. Nevertheless, the 500 mb buoyancy (2.7°) was moderate, and the large CTP (3.7) suggests adequate time for drop growth in updraughts was available during the storm (Figure 12b).

Storm Track

The radar echo followed a long narrow storm track, propagating from northwest to southeast in the direction of the wind but with an average speed of 37 km/h (Figure 9). Seeding occurred west of the fast moving echo centre (Figure 13).

Detailed PPIs

Rapid growth of the storm followed the first radar echo at 12:42. The quick development of new cells was continuous throughout the echo pattern and may have been a seeding effect (Figure 13). However, the overall storm size decreased immediately after the seeding. Nevertheless, propagation of new cells continues until about 14:07, when the storm was near its minimum size. The last seeding penetration occurred at 14:04, and about 20 minutes later, the storm increased in strength reflecting a possible positive seeding effect (Figure 8). If so, the storm life has been prolonged for about 20-30 minutes, resulting in longer rainfall and subsequently increased total rain output.

Discussion

The late peak in the rainflux might indicate a positive seeding effect in this case, although the response appears to be a bit slower than normal. However, without additional observational and/or cloud modelling tools it is impossible to link cause and effect with confidence.

4. GENERAL CONCLUSION

The fact that the search for obvious seeding signatures amongst the PAWS storm radar histories was frequently unsuccessful is of fundamental importance - the integrated properties of many storms do not appear to have been strongly affected by seeding. Furthermore, the storms studied evolved in a variety of different patterns after the seeding. The meaning and importance of this diversity requires further study. The variety of cloud response times suggests different seeding paths and influences. Thus, trajectories of the seeding material and the affected air and precipitation must be known to link cause and effect. This information cannot be obtained without the use of multiple Doppler radar observations or detailed multi-dimensional cloud model calculations. More extensive surface and airborne observations would also have been helpful.

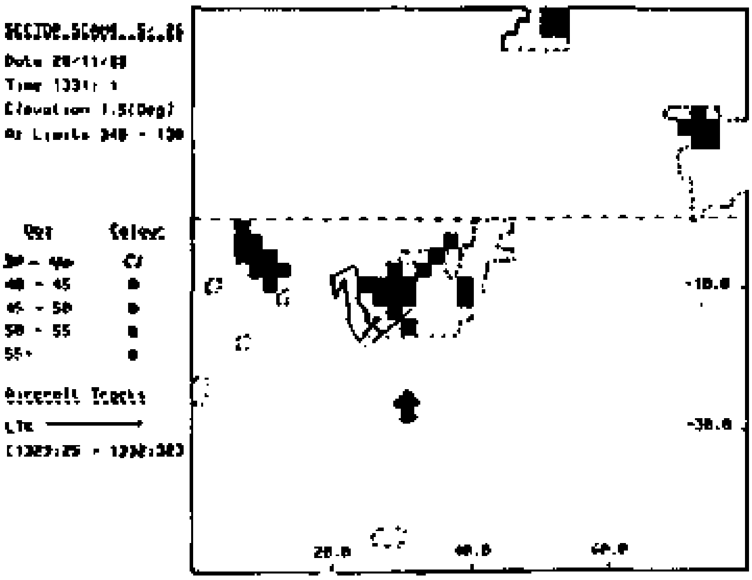

Figure 13a. PPI 13:31.

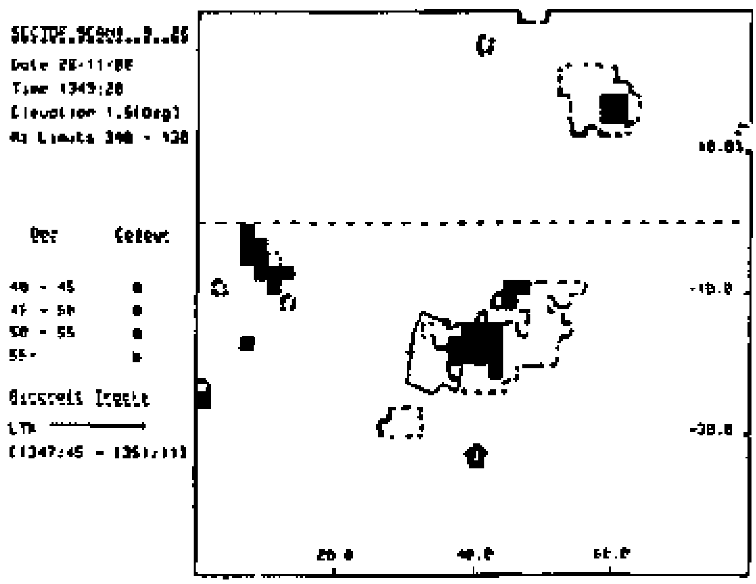

Figure 13b. PPI 13:49.

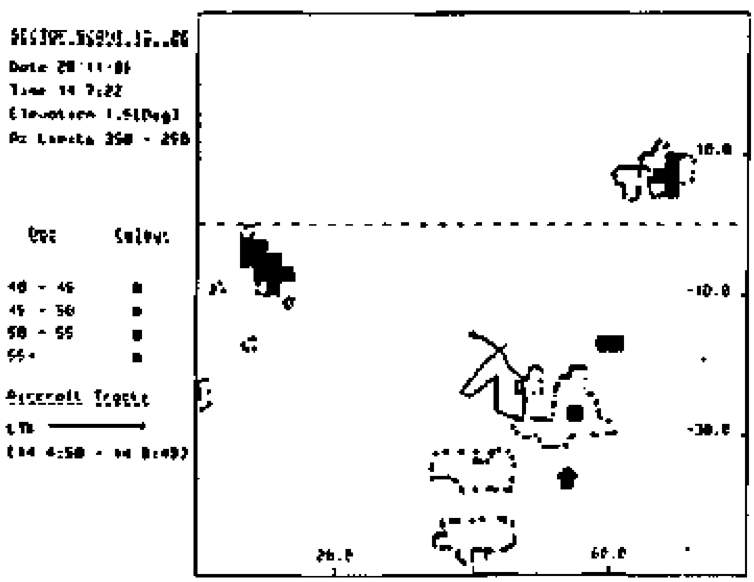

Figure 13c. PPI 14:07.

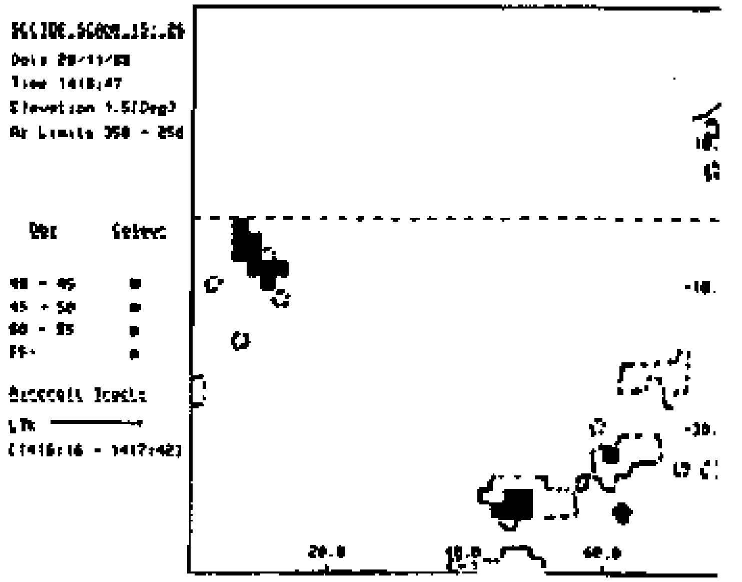

Figure 13d. PPI 14:19.

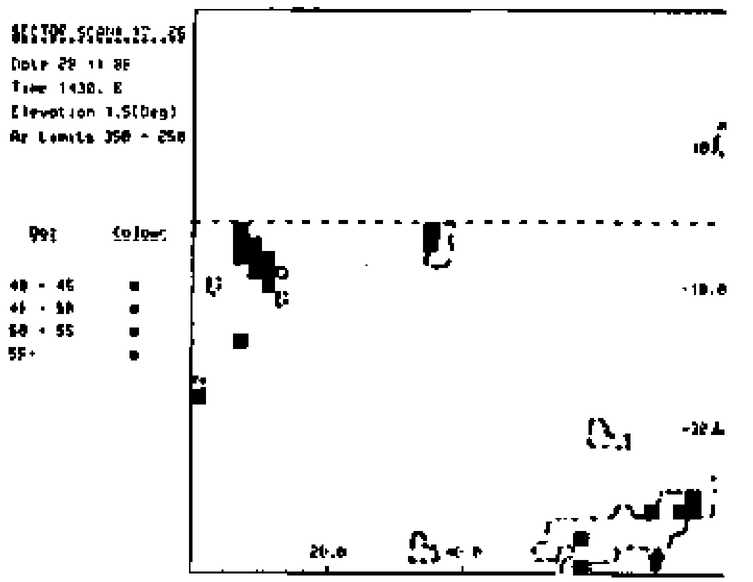

Figure 13e. PPI 14:30.

REFERENCES

FARLEY T D, 1987. Numerical modelling of hailstorms and hailstone growth. Part III: Simulation of an Alberta hailstorm - natural and seeded cases. J. Clim. Appl. Meteor., 27-7, 789-812.

GAGIN A, ROSENFELD D, WOODLEY W L and LOPEZ R E, 1986. Results of seeding for dynamic effects on rain cell properties in FACE-2. J. Clim. Appl. Meteor., 25-11, 3-13.

GROSH R C and SEMONIN R G, 1973. Moisture budgets and wind fields of thunderstorms passing over an urban area in the Midwest. Preprints: Severe Local Storm Conference, AMS, Boston, 130-137.

GROSH R C, MASSAMBANI O and BRIGUENTI Neto J, 1985. Brazilian convective precipitation evolution study with the Bauru radar. Preprints: Conference on Hydrometeorology, AMS, Boston.

MATHER G, MORGAN G and REUTER G, 1988. PAWS Annual Report 1986/87, pp85.

SIMPSON J M, 1970. On the radar measured increase in precipitation within ten minutes following seeding. J. Appl. Meteor., 9, 318-320.

SIMPSON J M, 1980. Downdrafts as linkages in dynamic seeding effects. Journal of Appl. Meteor., 19, 477-487.

SIMPSON J M and DENNIS A S, 1974. Cumulus clouds and their modification in W N Hess (Ed.), Weather and Climate Modification, John Wiley, New York, 229-281.

WOODLEY W L, GORDAN J, BARNSTON A, SIMPSON J, BIONDINI R and FLUECK J, 1982. Rainfall results of the Florida Area Cumulus Experiment, 1976-79. Journal of Appl. Meteor., 21, 139-164.

C. RADAR OBSERVATIONS OF PRECIPITATION PRODUCTION IN PAWS STORMS

G Reuter

ABSTRACT

During the last six years, digital radar data have been recorded at Nelspruit for numerous storms in the PAWS region. The present work synthesizes some of the radar data to obtain estimates of the total amount of precipitation produced in a storm, the rate at which the rain is produced and the total outflow of rain at cloud base. We believe that a careful study of rain production in PAWS storms is mandatory in considering the potential rainfall enhancement by seeding. The major findings are the following:

(a) Precipitation production varies greatly during a storm life cycle.

(b) During the maturing stage, the storms had precipitation contents of about 0.2-5 Tg and rainfall rates of about 0.3-2 Gg/s.

(c) Rain accumulation ranged from about 1-10 Tg.

(d) The precipitation production in Lowveld storms agree well with those reported by others for large thunderstorms in Alberta and New England.

Finding (d) implies that the integral properties of convective storms in different geographical localities are rather similar, in spite of the fact that the microphysics of these storms differ greatly.

1. INTRODUCTION

Most of the rainfall in the tropics and subtropics is produced in cumulus clouds. Organized convection also occurs frequently during the summer in mid-latitudes, and may contribute substantially to regional rainfall.

Precipitation production can be characterized by the time evolution of two storm-integrated quantities: the total precipitation content P(t) within the storm volume at time t, and the instantaneous outflow rate O(t) at the cloud base. Both quantities can be estimated from a series of radar observations of the three-dimensional storm pattern. Using a single relationship between reflectivity factor and precipitation content and integrating over the storm volume provides a crude estimate of P(t) since hydrometeor phase is not considered (Grosh *et al.* 1985). Applying an empirical relationship between reflectivity and rain rate to the data near cloud base, and integrating over area, yields an estimate of O(t).

Estimates of integrated storm parameters have been reported for storms of different intensities occurring at different geographical locations: severe hailstorms in Illinois (Morgan and Grosh, 1972), hailstorms over Alberta (Pell, 1971), a huge convective storm complex over Quebec (Holtz, 1968), a severe local storm over Oklahoma (McLaughlin, 1967), intense thunderstorms over New England (Geotis, 1971), a hailstorm over Oklahoma (Fankhauser, 1971), a thunderstorm of "moderate intensity" over Colorado (Foote and Fankhauser, 1973), large thunderstorms over Alberta (Rogers and Sakellariou, 1986) and air mass storms in Illinois and Missouri (Grosh, 1978). Before reliable radar data were available, integrated storm parameters had been estimated using data from radiosondes and rain gauges (Braham, 1952). Some estimates of precipitation production were also derived from results of numerical cloud models (Sikdar *et al.*, 1974; Reuter, 1988).

Remarkably, the English literature does not contain much information about the magnitudes and temporal behaviour of integrated storm parameters for thunderstorms in regions outside North America, except perhaps Brasil (Grosh, 1985).

The purpose of this study is to analyse precipitation production in convective storms occurring over the Lowveld in South Africa. Using radar observations for three days, the precipitation content P(t) and the outflow rate O(t) are estimated for nine intense thunderstorms, along with the accumulated outflow through the cloud base, the total generation of precipitation, and the characteristic time and updraught for the precipitation process. These estimates will then be compared with those reported for thunderstorms in New England and Alberta.

2 DATABASE

The storm observations used in this study were collected during the 1986/87 field season of the Project of Atmospheric Water Supply (PAWS) in the Lowveld of South Africa. The radar was located at Nelspruit. Most of the annual precipitation in this region falls during the summer from convective storms, often accompanied with hail (Kelbe, 1982). Localized storms over the Lowveld are usually triggered when the easterly low-level moist airflow is able to penetrate the capping inversion typically present in the lee of the escarpment barrier (Garstang *et al*, 1987). Analysis of microphysical measurements indicated that rain is formed mainly by a coalescence-freezing precipitation mechanism (Mather *et al*., 1986).

The Pacer III Radar located at Nelspruit operates at a wavelength of 5.3 cm. It transmits a peak power of 250 W in pulses of 2 μs duration. The pulse repetition frequency is 200 Hz, the horizontal and vertical beamwidths are about 1.6°, and the antenna's gain factor is 40 dB. The antenna rotates in azimuth at a scan rate of 3 rpm and ascends in elevation to 20°. As the Nelspruit radar is surrounded by hilly terrain with mountains to the east, the elevation angle is never lowered beneath 3°. A complete volume scan takes about 8.5 minutes. However, when convection is isolated, sector scanning is employed to improve the time resolution.

Radar data are stored every degree as the mean values from eight returns 0.125° apart in azimuth. In range, data are stored from 10 to 130 km at 600 m intervals. In this study, however,to avoid cases with poorly observed tops or bases, only data within the range 30 to 60 km are examined.

3. METHOD OF ANALYSIS

The method of data analysis follows that of Rogers and Sakellariou (1986). From the observed radar reflectivity value, Z (mm^6m^{-3}), rainfall rate R (mm h^{-1}) is derived using the Marshall-Palmer (1948) relation $Z = 200\ R^{1.6}$. The outflow rate is obtained from an area integration of the rainfall rate R near cloud base level. The reflectivity values are converted to precipitation content values M (g m^{-3}) using the relation of $Z = 20300\ M^{1.67}$, first suggested by Morgan and Mueller (1972) for severe storms. The total precipitation content P(t) is obtained from integration of M over the storm volume. The values of O and P depend slightly on the value chosen for the echo threshold that defines the storm boundary. For the data observed, it was found most appropriate to use a threshold value of 30 dBz, corresponding to a rainfall rate of 2.7 mm h^{-1}. This threshold value was high enough to allow tracking of convective echoes even when they were embedded in layers of nimbus stratus. On the other hand, the threshold value of 30 dBz was also sufficiently low to include almost the entire precipitation region for the integrations.

It is difficult to judge the accuracy of the calculated values of P(t) and O(t). Some errors are likely to occur due to the simple Z-R and Z-M relations that are probably not highly accurate for those regions in the storm that have ice-phase precipitation. Also the choice of the 30 dBz threshold will result in underestimating the actual storm size. Other sources of error may come from partial beam-filling (due to poor radar spatial resolution) and from vertical drafts near the cloud base. The estimated values are probably within a factor of two of their correct values.

There are a number of other variables that can be derived from P(t) and O(t) that further characterize the precipitation production. The accumulated mass of precipitation that has fallen from the storm up to time t can be obtained by integrating the outflow rate O(t). The cumulative amount of precipitation generated G(t) is defined by the mass of precipitation aloft plus the accumulated outflow. Thus G can be written as

$$G(t) = \int_0^t g(t)dt = P(t) + \int_0^t O(t)dt \quad , \qquad (1)$$

where g(t) is the rate of generation of precipitation, i.e. the rate of accumulation aloft plus the rate of outflow. Other quantities that will be examined are the average precipitation content and the average rainfall rate, defined by P/V and O/A where V and A denote the storm volume and base area. Holtz (1968) introduced the concept of the characteristic time, τ, of the precipitation production defined by the ratio

$$\tau(t) = \frac{P}{O} \quad . \tag{2}$$

In periods during which P(t) and O(t) are relatively steady, τ can be interpreted as the time needed for precipitation development. Inspired by the approach of Holtz, we define the characteristic updraught U(t) of a storm by the ratio

$$U(t) = \frac{O/A}{P/V} \quad . \tag{3}$$

In periods during which O/A and P/V are relatively steady, U is the storm updraught required to maintain an average precipitation content of P/V while rain is falling through cloud base at the average rate of O/A.

4. RESULTS

Data were analysed for 2 December 1986, 30 January 1987 and 9 March 1987. The synoptic conditions on the three days were similar. An upper-level trough was moving with the westerly flow over southern Africa. When the flow passed over the mountain barrier in eastern Transvaal, it created a subsidence inversion on the lee side of the escarpment. This subsidence inversion was apparent in the sounding data for all three days, but most pronounced on March 9 (Figure 1). The low-level inversion layer is usually not spatially uniform over the PAWS region (Garstang *et al.*, 1987), but exhibits a detailed structure resulting from differential sinking over the complex topographical shape of the escarpment.

Table 1 summarizes some values derived from sounding data sampled by aircraft rising from Nelspruit when convection started. Since the aircraft did not measure the wind profile and moisture values for temperatures below -12°C, the wind speeds and precipitable water are taken from the radiosonde observations sampled in the morning at Nelspruit. On all days,

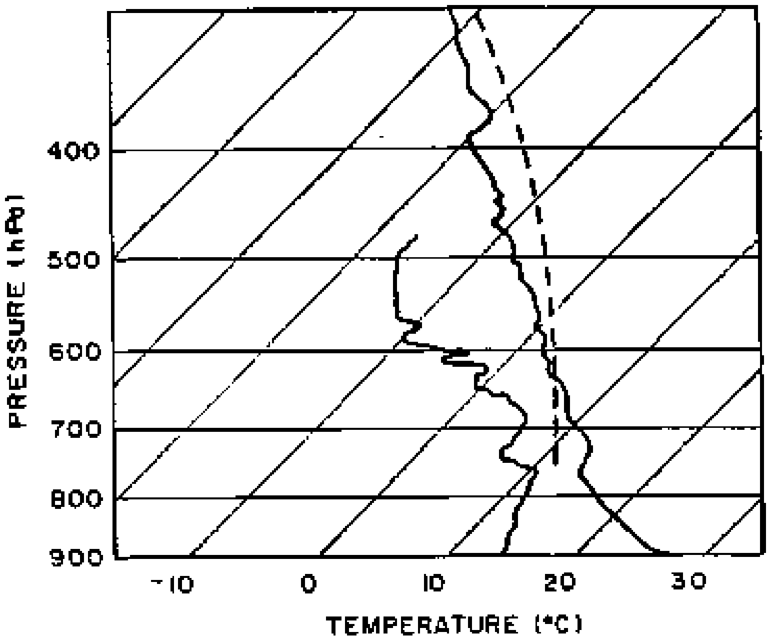

Figure 1. Sounding at Nelspruit on 9 March 1987 plotted on a skew T-log p diagram. The dashed curve denoted the pseudo-adiabat passing through the cloud base.

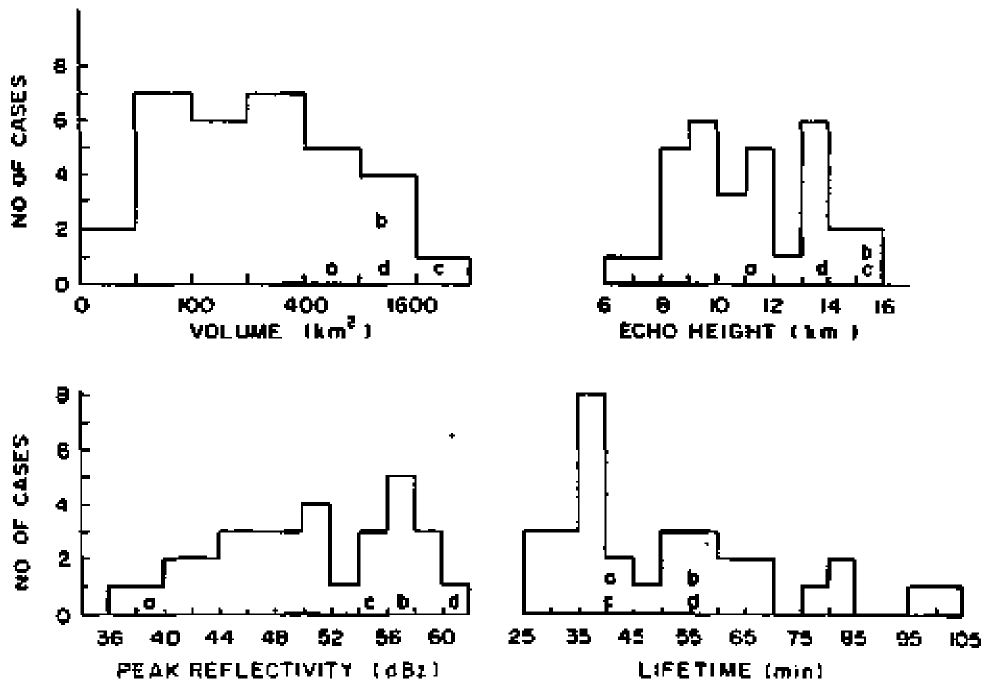

Figure 2. Frequency distributions of maximum volume (km³), maximum echo top height (km AGL), maximum reflectivity factor (dBz) and lifetime (minutes.) for echoes above 30 dBz observed on 9 March 1987.

the surface air was very humid. The values of vapor mixing ratio (averaged over the bottom 60 hPa) ranged from 11.6 to 14.2 g/kg. Moist conditions extended well to mid level layers with values of total Table 1. Parameters derived from observed sounding data for three different days.

Parameter		2 Dec	30 Jan	9 Mar
Surface pressure	(kPa)	91.1	91.3	90.9
Surface temperature	(°C)	29.2	31.1	28.2
Average mixing ratio[1]	(g/kg)	12.9	14.2	11.6
CCL pressure	(kPa)	70.7	70.3	70.5
CCL temperature	(°C)	12.4	13.8	10.4
Precipitable water[2]	(mm)	29.4	23.4	25.9
Showalter stability index	(°C)	-7.0	-9.6	-7.5
Wind speed[2] at 3 km AGL	(m/s)	2.4	7.3	5.2
Wind speed[2] at 6 km AGL	(m/s)	7.9	10.4	2.6
Wind speed[2] at 9 km AGL	(m/s)	17.7	13.5	23.1

[1] averaged over the lowest 6 kPa layer.
[2] from the morning radiosonde observations.

precipitable water ranging between 23.4 and 29.4 mm. The Convection Condensation Level was close to 705 hPa and cloud base temperatures were 14 to 10°C, which is typical to cool for Lowveld storms (Mather *et al*, 1986). On all three days the atmosphere above the CCL was unstable to moist ascent. 30 January had the most unstable air with a Showalter index of -9.6, while 2 December had the weakest potential for severe convection. Consequently, the largest and most severe storms occurred on 30 January, while the convection on 2 December was the weakest. On all three days, the winds were rather calm in the lower and middle levels. Shear was weak and there was also little veering. One of the consequences of such calm wind conditions is that storms are usually short-lived, as there is inadequate shear to separate the cloud updraught from the precipitation generated downdraught.

On 30 January and 9 March, moist convection was triggered throughout the afternoon by surface heating at localized "hot spots" near the foothills of the escarpment. On 2 December, low-level convergence combined with orographic lifting and surface heating to initiate the convection, starting at about 10h00 local time. On each day, a number of convective elements at different stages of their life cycle co-existed at any given time. To examine this variability, we tracked those radar echoes with signals above 30 dBz throughout their lifetime using the tracking method of Mader (1979). For each cell tracked, we obtained the maximum volume, echo height and reflectivity factor during its life cycle. The observed frequency distributions of these parameters are shown for 9 March in Figure 2. There was great variability in storm size, intensity and duration. Small hailstones were reported for some of the more intense storms (typically those with peak reflexivity factors exceeding 58 dBz) but large hail stones were not recorded.

Table 2 summarizes some observed characteristics for nine storms.

Table 2. Estimates of certain thunderstorm characteristics.

Storm	Date	Life-time (min)	Total outflow (Tg)	Maximum volume (km^3)	Maximum area (km^2)	Maximum reflectivity (dBz)
A	9 Mar	75	1100	390	80	59
B	9 Mar	60	1000	1330	170	57
C	9 Mar	90	1700	1590	260	51
D	9 Mar	~120	~8000	4310	580	59
E	30 Jan	~120	~2000	1250	140	55
F	30 Jan	~180	~11000	8930	780	59
G	2 Dec	135	1700	480	130	58
H	2 Dec	130	1780	570	120	57
I	2 Dec	125	1280	420	135	55
Average		~115	~3280	2140	250	57

These nine cases are selected to be representative for the larger, more severe storms observed on the three days. The values listed for maximum volume, maximum area and maximum reflectivity are instantaneous peak magnitudes. Storms D, E and F, were not sampled accurately during their decaying stage as they left the favourable range for good radar observations. Rough estimates of the lifetime and total outflow for these storms however were still made, based on the available data. The peak reflectivity was above 50 dBz in all nine storms. The values for total outflow varied considerably, ranging by a factor of about 10. The four storms of March 9 had the shortest life time, consistent with the very weak wind shear on that day. Remarkably the three storms on December 2 were quite similar in all quantities listed.

For each storm, the time histories of the total precipitation content P(t), the outflow rate O(t), the average precipitation content (P/V), the average rain rate (O/A), the characteristic time $\tau(t)$ and the characteristic updraught U(t) were all obtained. These parameters, averaged over "their maturing stage" are listed in Table 3.

Table 3. Storm parameters averaged for the 20 min when the precipitation content is maximum.

Storm	Date	Rain content (Gg)	Outflow rate (Mg/s)	Average rain content (g/m^3)	Average Rain Rate (mm/h)	Charac-teristic time (min)	Charac-teristic updraught (m/s)
A	9 Mar	290	329	0.79	17.7	15	5.9
B	9 Mar	801	483	0.69	12.9	28	5.2
C	9 Mar	640	529	0.46	8.5	20	5.1
D	9 Mar	2988	1516	0.73	11.3	33	4.3
E	30 Jan	716	518	0.64	18.3	23	4.9
F	30 Jan	5379	1852	0.74	11.7	47	4.3
G	2 Dec	244	348	0.82	12.9	12	5.8
H	2 Dec	267	307	0.57	12.0	14	5.8
I	2 Dec	212	349	0.55	12.5	12	6.1
Average		1282	692	0.67	11.1	23	5.3

The "maturing stage" was taken as the half hour period when the precipitation content values were maximum. During this 30 minute period, P and O remained quasi-steady (see e.g. Figure 3), so that τ may be thought of as the duration for precipitation formation and U provides a rough estimate of the average storm updraught.

The values of rain content and outflow varied greatly between the nine storms. However, the values of the volume average rain content and area average rain rate were uniform, never deviating much from 0.7 g m^{-3} and 11 mm h^{-1}. The characteristic time of the precipitation process varies between 12 and 47 minutes, averaging about 23 minutes. The characteristic updraught is found to be close to 5 m s^{-1}, consistent with

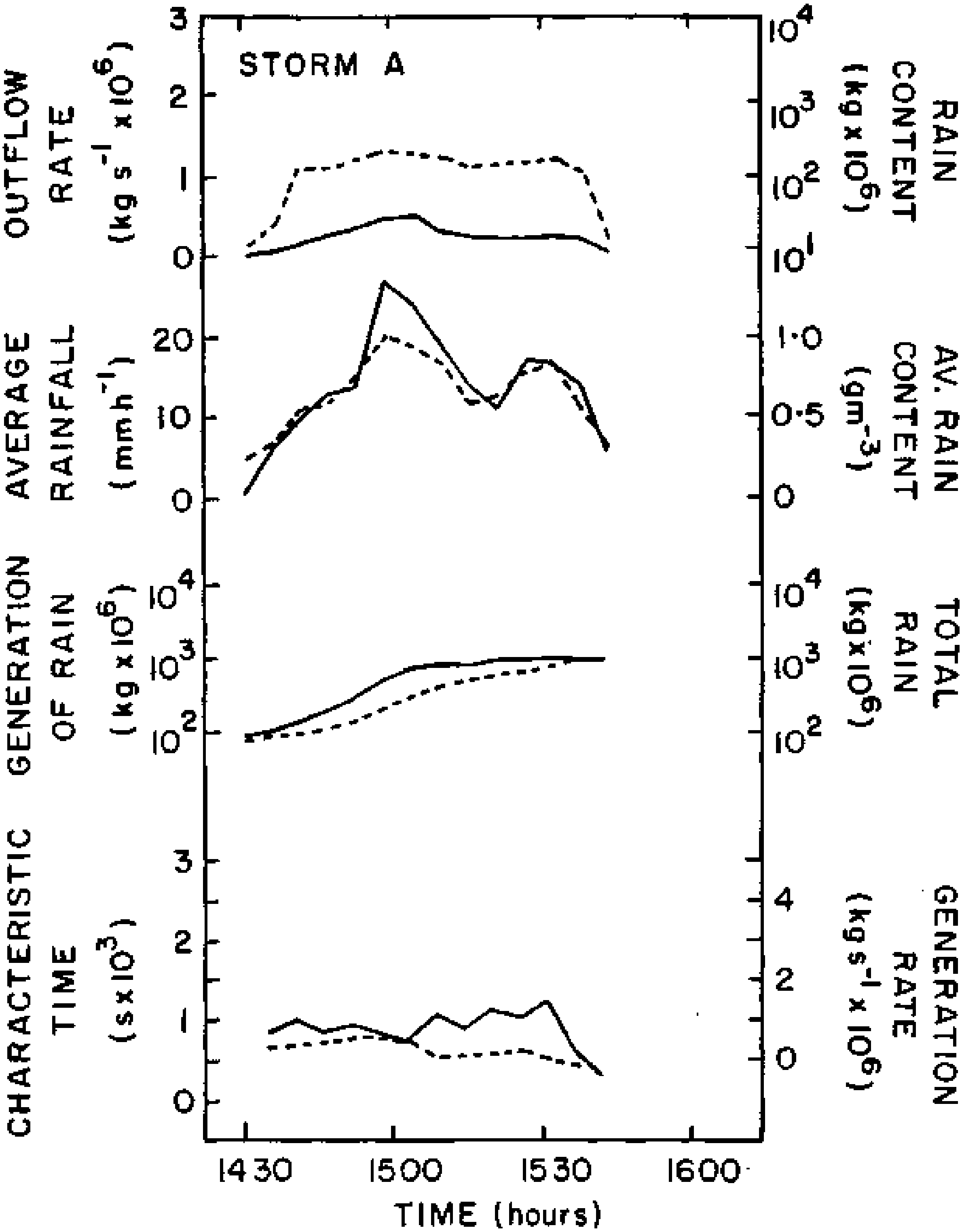

Figure 3. Time variations of storm properties for Storm A. Solid curves (_____) correspond to left side ordinates for outflow rate, average rainfall rate, cumulative amount of precipitation generated and characteristic time. Dashed curves (.....) show rain content, average rain content, accumulated outflow and generation rate.

average draft measurements sampled by aircraft in Lowveld storms (Reuter and Yau, 1987). The larger storms seem to have a slightly weaker average updraught.

Figures 3 to 6 show the evolution of precipitation production in Storms A, D, E and F. Four pair of variables are plotted as functions of time: outflow rate and rain content, area average rainfall and volume average rain content, cumulative amount of rain generated and accumulated outflow, and characteristic time and generation rate. To allow easy intercomparison of different storms, the same ordinate scales are used for all four cases.

The plots indicate that storm properties change considerably during the lifetime of the storms. The values of outflow and precipitation content are closely correlated in Storms A and F, but less in the other two storms. The curves of average rainfall rate often show double maxima, (Storms A, E, and F) and a similar behaviour is apparent in the average precipitation content. Variation in rain production with a period of 30-45 minutes was also recorded in Alberta thunderstorms (Rogers and Sakellariou, 1986).

The accumulated amount of rain generated and the accumulated outflow are rather smooth curves. The vertical separation of these curves shows the instantaneous rain content aloft. Total rain generated over the life of each storm is much larger than the maximum of P(t) present at any stage. The characteristic time of the precipitation process is rather uniform in Storms A and D, but irregular in the other two cases. In Storm F, τ is close to 1000 s for the first 40 minutes, but thereafter it increases with a factor of 3. This jump in τ is caused by the "explosive growth" in P(t) from about 100 to 1200 Gg during the period 15h40 to 16h20. The rate of generation of precipitation exceeds 3 Gg s^{-1} during this period. This large amount of precipitation is formed mainly in the upper portion of the storm, and it takes several minutes before the rain descends to the cloud base where it contributes to the outflow rate. The generation rates in the other three storms are smaller. The peak values found in Storms A, D and E are 0.57, 2.6 and 1.0 Gg s^{-1}, respectively.

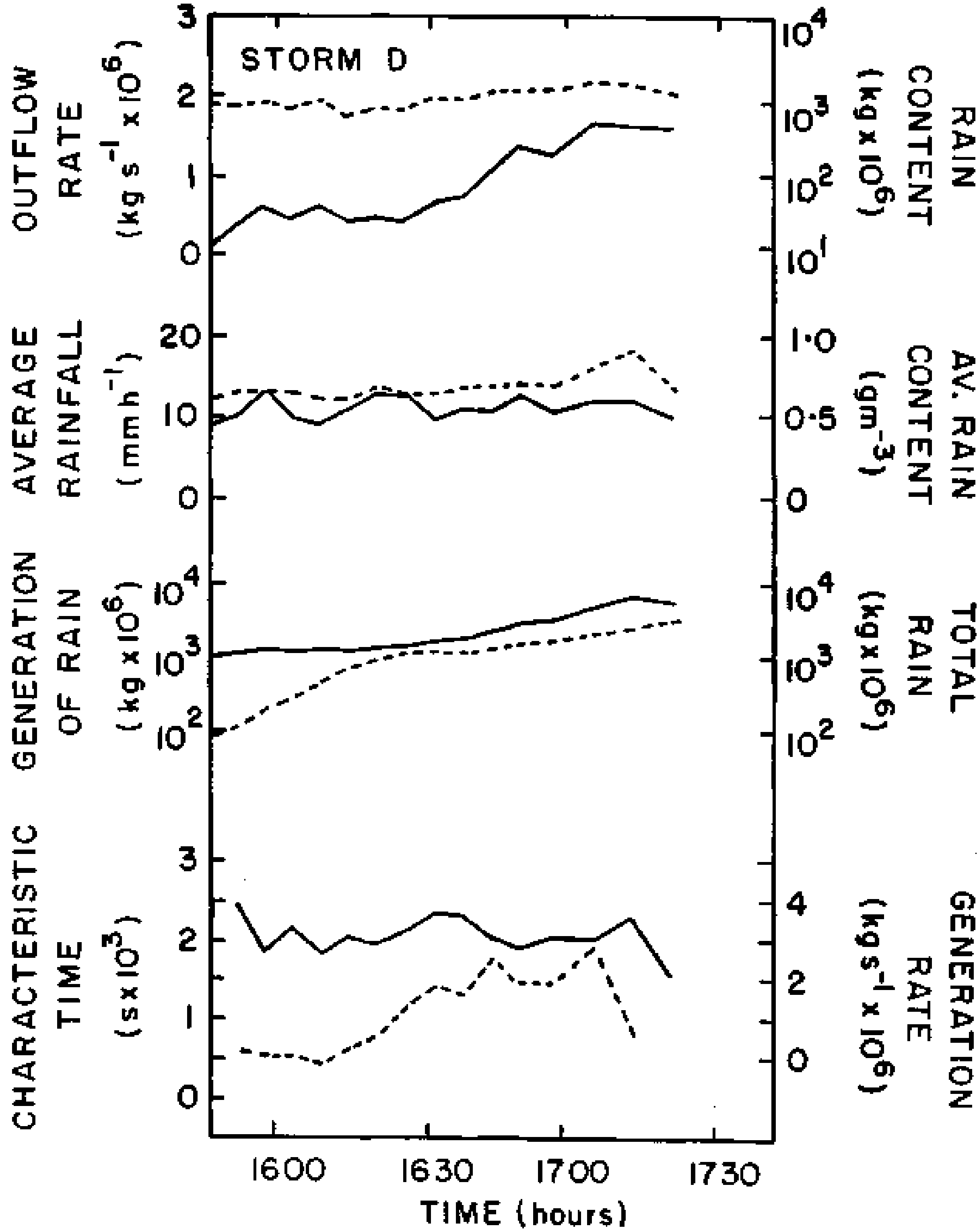

Figure 4. As in Figure 3 except for Storm D.

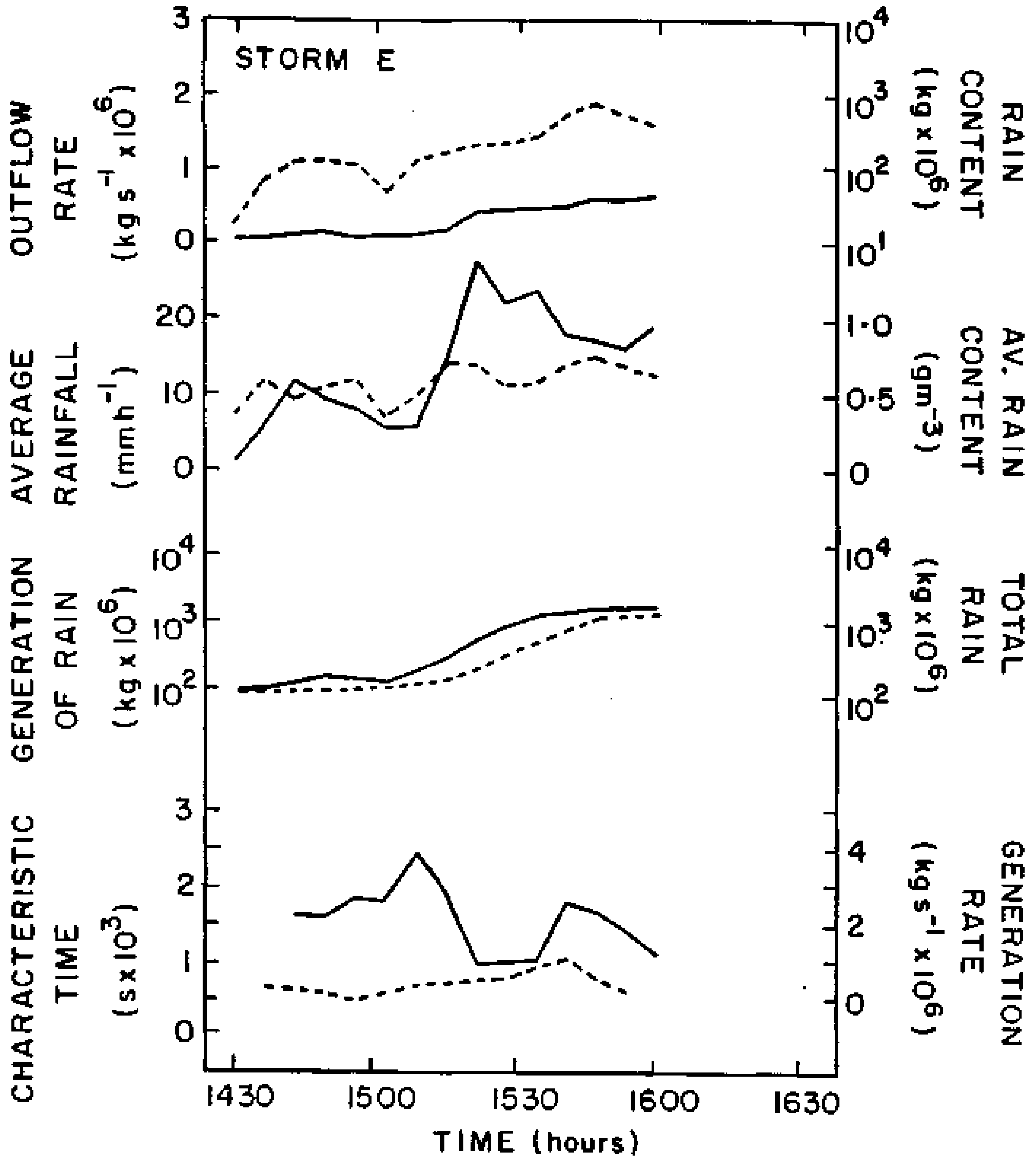

Figure 5. As in Figure 3 except for Storm E.

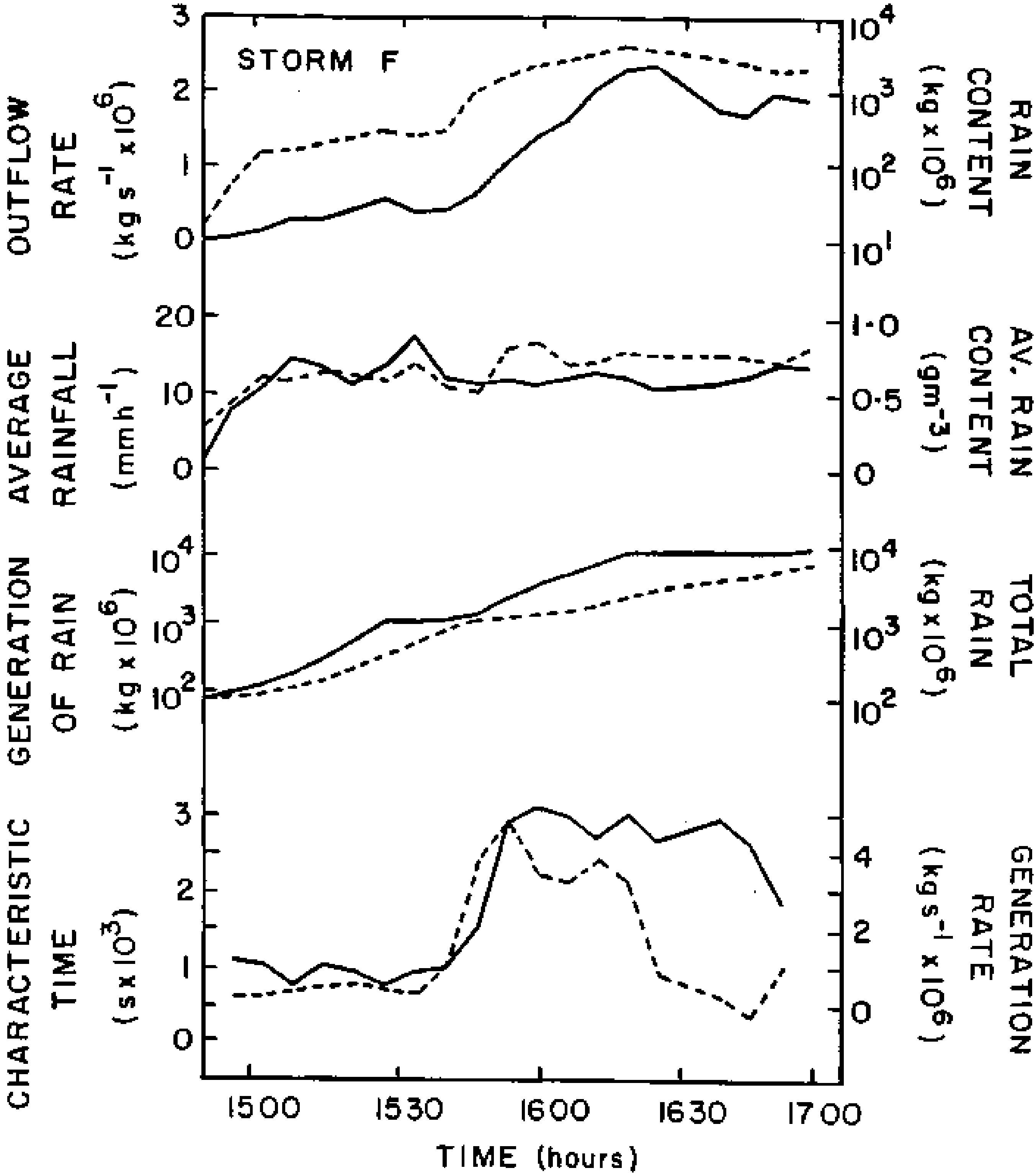

Figure 6. As in Figure 3 except for Storm F.

5. COMPARISON OF RESULTS

The available data reported in the literature concerning precipitation production in thunderstorms have recently been reviewed by Rogers and Sakellariou (1986). The estimates of precipitation content and outflow rate cover a large range of values, resulting from the fact that convective storms vary greatly in size and intensity. This large variability makes it difficult to compare precipitation production in different storms. A comparison becomes even more problematic in that most previous studies dealt only with a single extremely severe storm which might not be very representative.

To attempt to make a meaningful comparison of precipitation production in Lowveld storms with those reported for storms elsewhere, values averaged over many storms are required. Unfortunately only a few are available. Table 4 summarizes average values for Lowveld storms, together with those reported for New England storms (Geotis, 1971) and Alberta storms (Rogers and Sakellariou, 1986).

Table 4. Comparison between averages of storm characteristics.

Location	New England[1]	Alberta[2]	Lowveld
Number of storms used for averaging	8	3	9
Duration (h)	-	4.7	1.9
Accumulated rainfall (Tg)	5.30	4.90	3.28
Rain content at maturing stage (Tg)	1.70	0.78	1.28
Outflow rate at maturing stage (Gg/s)	0.96	0.80	0.69

[1] Taken from Geotis (1973).
[2] Taken from Rogers and Sakellariou (1986).

The values for New England storms represent average values obtained for eight severe thunderstorms observed with an S-band radar. The values for

P and O were computed using smoothed cylindrical representations drawn from RHI photographs. The assumption that the precipitation field is axisymmetric is a gross simplification, and therefore Geotis' values represent only rough estimates. The values listed for Alberta storms show averages for only three large thunderstorms observed with a 10.4 cm radar. The integral storm parameters were calculated as functions of time using the same methods as reported here. Two minor differences, however, are that Rogers and Sakellariou used a different Z-M relation and the echo boundary was taken to be the 20 dBz contour. The "maturing stage" values of P and O for the three Alberta storms represent the maximum hourly-average values. The data for Lowveld storms are averages for the nine storms listed in Tables 2. The "maturing stage" values are taken from Table 3, representing values averaged for the 30 minutes when P is maximum.

Our comparison suggest that the average values for the storms in the three different regions are rather similar. The averaged accumulated outflow values are between 3.2 and 5.3 Tg. The average values of precipitation content and outflow rate for storms in their maturing stage ranged from 0.78 to 1.7 Tg, and from 0.69 to 0.96 Gg s^{-1}, respectively. The most obvious difference between the storms is in their duration. The average lifetime of thunderstorms in the Lowveld is about half of that in Alberta. This finding has also been noted by Admirat et al (1985) in their comparison of hail fall characteristics between storms occurring in Alberta and southern Africa. The shorter duration of Lowveld storms can be attributed to the weaker wind shear compared to Alberta conditions.

Rogers and Sakkelariou also included time history plots of storm parameters. As mentioned earlier, both the Alberta and Lowveld storm samples have two or more peaks in their precipitation production separated by about 30-45 minutes. The values of characteristic time $\tau(t)$ and generation rate g(t) reported for Alberta storms compare well with our estimates. The Lowveld storms have a slightly higher average precipitation content and average rain rate than the Alberta storms. This finding is expected, since Lowveld storms are warmer at cloud base. Also, the troposphere is higher in the Lowveld and this results in taller storms.

6. CONCLUSIONS

Digital radar data were used to analyse the precipitation production in thunderstorms over the Lowveld of southern Africa. Nine convective storms from three different days were selected for case studies. During their maturing stage, the storms had precipitation content values ranging from about 0.2 to 5 Tg and outflow rates between 0.3 and 2 Gg s^{-1}. The total mass of precipitation falling from cloud base was about 1 to 10 Gg.

The nine storms had similar values in volume-averaged rain content (~0.7 g m^{-3}) and area-averaged rain rate (~11 mm h^{-1}) during their maturing stage. The characteristic time for the precipitation process varied from 12 to 47 minutes, with an average of 23 minutes. The characteristic updraught, defined as the ratio of the instantaneous area-averaged rainfall rate to the volume-averaged precipitation content, was close to 4-6 m s^{-1}. The time histories of storm parameters indicate that precipitation production is not a steady process. Some storms show multiple peaks in their activity, typically separated by about half-hourly intervals.

Our estimates of precipitation content and outflow rate, when averaged for the nine Lowveld storms, agree well with estimates reported for intense thunderstorms over New England and Alberta. The time variations of precipitation production in Alberta storms also showed multiple peaks in precipitation production, separated by 30-45 minutes. The sample of Alberta storms, however, differs from the sample of Lowveld storms in that they last longer, consistent with a stronger wind shear over Alberta.

This type of study can be extended in many ways. One useful extension would be to analyse many more storms, and to stratify the cases into different classes according to synoptic conditions and atmospheric stability. With a sufficiently large number of storm cases, one should gain insight in how these environmental factors control the precipitation production in local storms. Another useful extension would be to also examine observations of vapor fluxes. With this additional information, the water budgets in thunderstorms can be derived. This would allow estimates of the efficiency of a storm to convert water vapor into precipitation (e.g.

Fankhauser, 1971; 1988). It would also be useful to compare observational data with results obtained with a numerical storm model (e.g. Reuter, 1988). A combined observational and modelling approach would offer a powerful tool to further understanding of precipitation production in thunderstorms.

7. REFERENCES

ADMIRAT P, GOYER G G, WOJTIW L, CARTE A E, ROOS D vdS and LOZOWSKI E P, 1982. A comparative study of hailstorms in Switzerland, Canada and South Africa. J. Climatol., 5, 35-51.

BRAHAM R R, 1952. The water and energy budgets of a thunderstorm and their relation to thunderstorm development. J. Meteorol., 9, 227-242.

FANKHAUSER J C, 1971. Thunderstorm-environment interactions determined from aircraft and radar observations. Mon. Weather Rev., 99, 171-192.

FANKHAUSER J C, 1988. Estimates of thunderstorm precipitation efficiency from field measurements in CCOPE. Mon. Weather Rev., 116, 663-684.

FOOTE G B and FANKHAUSER J C, 1973. Airflow and moisture budget beneath a northeast Colorado hailstorm. J. Appl. Meteorol., 10, 1330-1353.

GARSTANG M, KELBE B E, EMMITT G D and LONDON W B, 1987. Generation of convective storms over the escarpment of northeastern South Africa. Mon. Weather. Rev., 115, 429-443.

GEOTIS S G, 1971. Thunderstorm water contents and rain fluxes deduced from radar. J. Appl. Meteorol., 10, 1233-1237.

GROSH R C *et al.*, 1985. Brazilian convective precipitation: Evolution study with the Bauru Radar. Preprints: Conference on Flash Floods. Am. Meteorol. Soc., Boston, 6pp.

GROSH R C, 1978. Lightning and precipitation - the life history of isolated thunderstorms. Preprints: Conference on Cloud Physics and Atmospheric Electricity. Am. Meteorol. Soc., Boston, 614-617.

HOLTZ C D, 1968. Life-Cycle of a Summer Storm from Radar Records. Ph.D. Thesis, Dept. of Meteorology, McGill Univ. Montreal, 141pp.

KELBE B E, 1982. Factors Contributing to the Development of Convection over Northeastern South Africa and Swaziland. Ph.D. Thesis, University of Virginia, 261pp.

MADER, G N, 1979. Numerical study of storms in the Transvaal. S. Afr. Geogr. J., 61, 85-91.

MARSHALL J S and PALMER W McK, 1948. The distribution of raindrops with size. J. Meteorol., 5, 165-166.

McLAUGHLIN M R, 1967. The Energy Budget of a Severe Local Storm. Rep. No. 7, Atmospheric Science Group, University of Texas, Austin, 57pp.

MORGAN G M and MUELLER, E A, 1972. The total liquid water mass of large convective storms. Preprints: 15th Radar Meteorology Conference, Champaign-Urbana, Ill., Am. Meteorol. Soc., Boston, 39-40.

MORGAN G M, GROSH R C, ACHTEMEIER G L, STRUEBING W and BRUNKOW D A, 1975. Radar studies of severe storms observed on 3 April 1974 in Central Illinois. Preprint: Conference on Severe Local Storms, Am. Meteorol. Soc., Boston, 278-279.

PELL J, 1966. The use of broad-beam radar for quantitative analysis of severe storms. J. Appl. Meteorol., 10, 1238-1251.

REUTER G W and YAU M K, 1987. Mixing mechanisms in cumulus congestus clouds. Part I. Observations. J. Atmos. Sci., 44, 781-797.

REUTER G W, 1988. Water budget and kinetic energy transformations of a mixed-phase cumulus cell: Three dimensional numerical simulation. Beitr. Phys. Atmosph., 61, 30-38.

ROGERS R R and SAKELLARIOU N K, 1986. Precipitation production in three Alberta thunderstorms. Atmos. Ocean, 24, 145-168.

SIKDAR D N, SCHLESINGER R E and ANDERSON,C E, 1972. Severe Storm latent heat release: Comparison of radar estimate versus a numerical experiment. Mon. Weather Rev., 102, 455-465.

V. STORM TRACKING AND MOTION REVIEW

The analysis of the PAWS radar observations is achieved via a computer program which defines and tracks storm cells based on the centroid within a given intensity contour (usually 30 dbZ), and a maximum permitted displacement between radar scans. The displacement limit is determined by the maximum storm speed allowed, and this is the actual parameter set in the program. A study was made of the effect of setting the maximum permitted speed at a high value, since the maximum value used in practice is much higher than the actual average storm speed of the PAWS cases.

A. MAXIMUM TRACKING SPEED IMPACT ON SEEDING ANALYSES

C Muller, R C Grosh

ABSTRACT

The effect of the maximum speed allowed in a radar echo tracking programme is shown to affect the findings of significant seeding influences on rainstorms.

1. INTRODUCTION

One of the key innovative features of the past PAWS research has been the application of an objective and automated technique to track radar echoes from clouds and thereby define the basic analysis unit for the Lagrangian study of storm histories of rainflux and size characteristics. A large number of different storm tracking procedures exist. Some procedures track echo centroids, intensity maxima and maxima clusters (Brandes, 1972; Crane, 1976; Blackmer and Duda, 1972) while others apply pattern recognition or cross correlation (Bellon and Austin, 1975). Recently, an effort has also been made to study the top heights and rainfall of the smallest echo elements, the towers (cells) of individual rain showers, for weather modification research (Rosenfeld, 1987). Therefore, it is important to understand the characteristics of the tracking programme being applied to the PAWS data, both in terms of the physical storm units which are analysed, and the statistical evaluation which follows.

The PAWS tracking programme follows centroids and is an adaptation of a method originally devised by CSIR (Mader, 1979) which now considers the three-dimensional structure of the echo (Dixon and Mather, 1986). Thresholds of 30 dbZ minimum intensity and 750 km^3 maximum initial echo volume are applied in the programme for the usual statistical analyses, with the maximum translation between images being constrained to be less than an echo speed of 90 km/hr would permit.

It is necessary to reconcile the constraint on the maximum velocity allowed in the tracking programme, with the climatological findings for many South African locals: typical echo speeds calculated from scalar displacements are only 25 to 30 km/hr (Carte and Held, 1977; Mader, 1979; Mason-Williams, 1984; and Dixon, 1977). Mason-Williams suggests that 95% of South African storms move slower than 40 km/hr based on the data of Dixon and Mader. If daily averages or velocities are used, even slower speeds are calculated. Nevertheless, Mader notes geographic variability can be great. Typical Oklahoma (USA) storms move at about 60 km/hr.

This section describes the affect of varying the constraint for the maximum permitted speed, on the resultant echo properties, and their apparent influence on the significance of the analysed seeding effect.

2. DATA

A sample of 50 experimental cases was examined, including 25 seeded cases and 25 cases which were neither seeded nor penetrated by the Learjet, but met the cloud selection criteria. These cases occurred between October 1985 and March 1987, and were selected on the basis of two other criteria. It was intended to only utilise cases on days with many other cells present to provide a good test of the programme. In practice, the criteria adopted required at least 8 other cells to be present. Seeded cases were also selected on the basis of a probable seeding signature being detected by the analyst, a minimum 10% jump in the case rainflux following seeding, as measured by the radar viewing at an elevation angle of 3 . Only 23 unseeded cases met the criteria so they were relaxed to permit two other cases into that subsample. Thus, the selection criteria should favour the finding of significant seed-no seed differences.

The steps in the standard PAWS radar analysis were followed, including tracking, the calculation of physical storm variables and then their statistical analysis via 1000 re-randomizations. However, only 45 of the 250 storm variables were examined, to economise computer usage.

3. RESULTS

The effects of varying the maximum displacement velocity accepted by the tracking programme on the apparent seeding enhancement of the rainflux from the storms (and its statistical significance level) are listed in Table 1a. The rainflux enhancements of the storms calculated for their entire durations range between 11 and 20%, but are not near the normal statistical significance levels. The post-seeding periods of 10, 20, 30 and 40 minutes have enhancements of 11 to 38%, none of which approached significance either. However, these enhancements show strong evidence of increasing with the maximum velocity accepted by the tracking programme. This is also found for the three ten-minute time windows listed at the bottom of the table. Even more important, true statistical significance (~90%) is approached in the 20 to 30 minute time window and exceeded in the 30 to 40 minute window. The seeding enhancements in the last window are also much larger, 53 to 112%. The peak seeding enhancement of rainflux is indicated at 90 km/hr.

Table 1a: Effect of maximum tracking velocity on rainflux at 6 km (% seeding increase/significance probability level).

Speed (km/hr)	60	80	90	100	120
Period (min)					
0 - 10	14/47	14/52	-	14/50	17/46
0 - 20	11/37	18/39	-	18/42	22/40
0 - 30	13/37	21/42	-	22/41	26/45
0 - 40	22/45	33/49	-	34/54	38/55
Entire life	20/36	15/37	11/31	12/33	14/29
10 - 20	15/31	28/50	-	28/52	33/55
20 - 30	15/67	33/76	-	38/79	38/79
30 - 40	53/90	93/94	112/99	101/96	112/98

The percentage seeding enhancement usually increases with the maximum permitted tracking velocity up to about 90 km/hr for the multi-dimensional radar variables, except for the entire life time duration category (Table 1b). The increase is most noticeable for the 30 to 40 minute time window, as "statistically significant" seeding induced increases begin to be suggested above 80 km/hr for echo area and, it appears, at lower velocities for the other variables which are more complicated than simple length. Seeding induced increases in the "multi-dimensional" variables of over 100% are usually calculated for velocities above 80 km/hr. In the case of rainflux, this threshold is reached at 90 km/hr (Table 1a).

Table 1b: Effect of increasing maximum tracking velocity on "multi-dimensional" radar variables (% seeding increase/significance probability).

Speed (km/hr)	60	80	90	100	120
Period (min)					
Volume 0 - 10	25/59	26/63	-	25/64	27/52
0 - 20	18/53	29/63	-	29/62	31/51
0 - 30	23/57	34/64	-	34/64	37/58
0 - 40	37/70	52/75	-	52/78	56/70
Entire life	35/61	32/59	23/50	25/55	27/40
10 - 20	18/51	37/78	-	38/78	41/73
20 - 30	31/79	51/85	-	57/88	55/85
30 - 40	101/92	137/96	160/99	148/98	161/99
Mass 0 - 10	33/63	30/65	-	30/64	33/59
0 - 20	24/54	29/58	-	28/58	32/54
0 - 30	24/57	30/61	-	30/59	34/59
0 - 40	33/68	44/70	-	45/73	49/69
Entire life	31/56	24/51	17/44	19/49	21/38
10 - 20	22/51	33/74	-	33/75	38/75
20 - 30	13/77	37/84	-	43/86	42/82
30 - 40	53/93	107/97	128/99	117/9	129/99
Area 0 - 10	19/73	23/77	-	22/78	24/81
(6 km) 0 - 20	14/68	27/79	-	27/79	29/80
0 - 30	16/70	29/79	-	29/78	33/82
0 - 40	25/78	41/87	-	42/88	46/89
Entire life	22/73	23/74	17/72	18/72	20/77
0 - 20	14/67	36/82	-	36/85	40/88
20 - 30	22/69	39/83	-	44/86	44/88
30 - 40	78/89	111/97	131/99	120/98	131/99

The 30 to 40 minute time window for echo top height also shows these trends with statistical significance being indicated at and above 90 km/hr where a 16% enhancement is calculated (Table 1c).

Table 2 is a list of the number of variables for which a significant seeding effect was found (at the 90% level or above) as a function of the maximum permitted tracking velocity. Again, the positive affect of the maximum tracking velocity is revealed. The main effect is seen in the 30 to 40 minute time window after seeding, where the number of significant variables increases from 20 for 60 km/hr to 39 at both 100 and 120 km/hr

Table 1c: Effect of maximum tracking velocity on echo top height (% seeding increase/significance probability level).

Speed (km/hr) Period (min)	60	80	90	100	120
0 - 10	-2/38	-3/32	-	-3/30	-3/32
0 - 20	-3/32	-3/26	-	-3/29	-4/29
0 - 30	-3/34	-3/31	-	-3/33	-3/33
0 - 40	-1/47	-1/40	-	-1/46	-1/46
Entire life	-4/25	-5/18	-6/15	-6/15	-6/13
10 - 20	-4/27	-4/29	-	-4/32	-3/33
20 - 30	-2/40	0/51	-	1/53	1/58
30 - 40	10/79	13/88	16/95	15/92	17/96

maximum permitted velocities. The effect is also apparent in the 20 to 30 minute window, the only other case with a noticeable number of significant variables. However, in this window the peak number of significant variables occurs at 100 km/hr.

Table 2: Number of variables with significant seeding effect (at the 90% level) for five different maximum permitted tracking velocities. A total of 45 variables were examined for each velocity.

Velocity	60	80	90	100	120
Period					
Entire life	5	4	4	4	4
0 - 10	0	0	-	0	0
10 - 20	0	1	-	3	0
20 - 30	4	6	-	10	7
30 - 40	20	35	38	39	39

The 45 variables examined are listed in Table 3. Significant variables and their seeding enhancements for the 80 km/hr maximum permitted velocity are also identified.

4. CONCLUSION

Apparently significant seeding effects on radar storm observations are indicated for all the speeds examined, although mostly for the 30 to 40 minute time window after treatment decision. However, even at a maximum

Table 3. Variables tested, with % seeding increase (D) and probabilities (P) for cases significant at 90% level (for maximum permitted tracking velocity of 80 km/hr). Definitions are given in earlier reports. Numbers are D/P.

	Period				
Variable	0 - 10	10 - 20	20 - 30	30 - 40	Overall
1 Duration				14/98	
9 Vol at decision time					
10 Peak dbZ at decision time					
11 Echo top - max					
12 Echo top - max ROI					
13 Echo top - mean					
18 Depth - max					
19 Depth - max ROI					
20 Depth mean				27/90	
25 Volume - max				132/95	
26 Volume max ROI			198/98	485/98	
27 Volume - time int				139/97	
28 Volume - mean				137/96	
33 Mass tot - max				94/90	
34 Mass tot - max ROI			129/90	440/95	
35 Mass tot - time int				108/97	
36 Mass tot - mean				107/97	
41 Mass A.C. - max				136/90	
42 Mass A.C. - max ROI				517/93	
43 Mass A.C. - time int				165/95	
44 Mass A.C. - mean				165/95	
49 Area 3 - max			49/91	88/97	54/95
50 Area 3 - max ROI			97/97	257/100	54/96
51 Area 3 - time int			52/90	84/96	
52 Area 3 - mean		44/91		81/93	
57 Area cutoff - max				105/98	43/91
58 Area cutoff - max ROI			100/95	463/100	38/92
59 Area cutoff - time int				112/94	
60 Area cutoff - mean				111/97	
65 Rflux 3 - max				57/90	
66 Rflux 3 - max ROI				365/100	
67 Rflux 3 - mass				62/96	
68 Rflux 3 - mean				61/95	
73 Rflux cutoff - max				82/94	
74 Rflux cutoff - max ROI				424/100	
75 Rflux cutoff - mass				93/95	
76 Rflux cutoff - mean				93/94	
81 Precip water - max					
82 Precip water - max ROI				495/97	
83 Precip water - time int				87/97	
84 Precip water - mean				86/96	
89 MTI/rain mass - 3				32/95	
90 MTI/rain mass - cutoff				42/92	
91 Mean mass/rain mass - 3					
92 Mean mass/rain mass - cutoff					

permitted tracking velocity of only 60 km/hr, rainflux, echo volume, and mass all suggest significant seeding effects at the 90% level 30 to 40 minutes after treatment. Thus, this comparison reflects the bias of the sample (the seeded storms were chosen for their evidence of a seeding effect). Nevertheless, the main point is that nearly *twice* as many variables in the last window appear significant as the tracking velocity approaches 90 to 100 km/hr. In fact, at high permitted speeds almost all of the 45 variables examined appear to have significant effects in the 30 to 40 minute window. Therefore, it is clear that the choice of the value for the maximum permitted tracking speed parameter can strongly influence seeding effect analyses.

Since the effect of increasing the maximum permitted velocity in the echo tracking programme can markedly increase the apparent statistical significance of the seeding effect indicated by the radar variables, the procedure for selecting this parameter must be carefully specified in advance of a confirmatory rain stimulation experiment. Otherwise multiplicity will enter the analysis and the calculation of true probabilities of significance may be made difficult or impossible. The maximum permitted tracking velocity should also be physically realistic, and it seems reasonable to determine it from the observed winds or some other objective parameter which correlates well with actual storm motion (Battan, 1973; Fernandez, 1989). This is now under study.

5. REFERENCES

BATTAN L J, 1973. Radar Observation of the Atmosphere. U Chicago, 210-211.

BELLON A and AUSTIN G L, 1975: Short-range precipitation forecasting using digital radar recorders. Preprints: 16th Radar Meteorology Conference, AMS Boston, 345-346.

BLACKMER R H and DUDA R D, 1972: Application of pattern recognition techniques to digitized radar data. Preprints: 15th Radar Meteorology Conference, AMS, Boston, 138-143.

BRANDES E A, 1972: The use of digital radar in severe storm detection and prediction. Preprints: 15th Radar Meteorology Conference. AMS Boston, 45-48.

CARTE A E and HELD G, 1977: Variability of hailstorms on the South African Plateau. J. Appl. Meteor., 17, 365-373.

CRANE R K, 1976: Rain cell detection and tracking. Preprints: 17th Radar Meteorology Conference, AMS Boston, 505-509.

DIXON M J, 1977: Proposed Mathematical Model for the Estimation of the Areal Properties of High Intensity Short Duration Storms. Unpublished M Sc Thesis, University of Natal.

DIXON M and MATHER G K, 1986: Radar evaluation of a randomized rain augmentation experiment. Preprints: 10th Planned and Inadvertent Weather Modification Conference, AMS Boston, 139-141.

FERNANDEZ W, 1989. Satellite depiction of the evolution of a West African squall cluster. Weather, 44-1, 29-33.

MADER G, 1979: Numerical study of storms in the Transvaal. S. Afr. Geogr. J., 61, 85-98

MASON-WILLIAMS S, 1984: The Bethlehem Runoff Augmentation Research Project: Past, Present and Future. TR 118, Department of Environment, Affairs, p47.

ROSENFELD D, 1987: Objective method for analysis and tracking of convective cells as seen by radar. J. Atmos. and Ocean. Tech., 4, 422-434.

B. STORM SPEEDS

R C Grosh and C Muller

1. INTRODUCTION

Storm motion was very important to PAWS. Both the definitions of the experimental units via the radar tracking program and radar rain measurement requirements are affected by storm speed. Unfortunately, the nature of storm motion in the Eastern Transvaal has been controversial. This appears to have been partly the result of an idiosyncrasy in a computer program. In the past the program used to track and calculate average storm properties for PAWS determined the average case speed to be about 2 km/hr. Long experience with rain storm tracking and motion (Grosh, 1971, 1973a and b, 1974, 1975a and b, 1977a and b, 1978a, b and c, 1984, 1985; Changnon *et al.*, 1975; Morgan *et al.*, 1975) immediately suggested to the new CSIR PAWS directorate that an erroneous calculation was being reported by the computer and this was promptly confirmed by a cursory examination of a handful of PAWS storm track plots in Pretoria. Two years later, coincident with the initiation of this study, the tracking program was finally re-examined by CloudQuest and it was immediately found that echo volume weighting was used in the averaging and that this contributed to the obviously too slow results. When the volume weighting was removed, the average PAWS case speed was calculated by the corrected computer program to be about 13 km/hr. However, this also appeared somewhat suspect as other storm motion studies both at Nelspruit and in the nearby Highveld, reported distinctly faster average echo speeds of about 22 to 30 km/hr for typical storms (Dixon, 1977; Kelbe, 1984; Mason-Williams, 1984; Mader, 1979; Carte and Held, 1978). See Table 1.

Table 1. Echo speeds from studies in the Eastern Transvaal.

	Dixon (Nelspruit)	Mader (Highveld)	Carte & Held (Highveld)
Number of cases	98	1861	86
Speed km/hr	22	25	30

Mader's results must be given the most attention, as he made measurements of 1861 storms. The maximum instantaneous echo area of these Highveld storms averaged about 80 km^2. The Nelspruit study of Dixon considered 98 long-lived cells (2 hour duration), which moved slower than the more typical smaller cells (Mader, 1979). It is well known that storm speed is very closely related to the winds above cloud base, for winds over 16.2 km/hr (Batten, 1973). Nevertheless, when directional wind shear is present large storms tend to move much slower than ambient winds (up to 24 km/hr slower in Oklahoma) and may have a strong propagative component related to the generation of new feeder towers on their flanks especially at lower wind speeds (<16.2 km/hr) when propagation dominates storm motion.

The averaged wind in the cloud bearing layer (up to 200 mb) normally provides the best correlation with storm velocity. At nearby Pretoria, winds for these levels are also greatly in excess of the current storm motion program results, as the monthly 700 mb to 200 mb winds averaged ~47 km/hr (see Table 2). Given that Newton and Fankhauser (1964) have shown that small storms such as those studied by PAWS (maximum echo areas averaged about 120 km^2) move within about 5 km/hr of the average wind below 200 mb, there is good reason to expect that many PAWS cases move much faster than 13 km/hr.

Table 2. Scalar average steering level wind speeds (km/hr) at Pretoria during the convective season.

	Oct	Nov	Dec	Jan	Feb	Mar	Ave
700 mb	27.0	25.6	20.5	19.1	19.4	18.7	22
500 mb	45.4	38.2	29.2	22.0	22.7	26.6	30.7
300 mb	77.0	67.3	58.7	41.0	43.6	53.6	56.9
200 mb	102.6	90.4	82.4	60.1	58.3	73.8	77.9
AVE							47

Furthermore, there is a remarkable order of magnitude difference between the currently reported average (13 km/hr) and the *maximum permitted* speed (90 km/hr) used by the tracking program to establish cell continuity between the successive radar images used for storm case definition. Thus, further research was required and CSIR undertook a study of 50 PAWS case tracks which were on hand to to attempt to provide more clarity on this issue.

2. PROCEDURE

Computer plots of the location and areal evolution of the radar echoes for twenty-five seeded and twenty-five non-seeded cases had been obtained for an earlier study of the Nelspruit tracking programme (Grosh and Muller, 1988). A maximum permitted tracking speed of 80 km/hr was used by the echo tracking program which determined the X and Y coordinates of the plots. Plots for the standard maximum tracking speed (90 km/hr) were not available. However, plots for maximum permitted speeds of 60 and 100 km/hr were available but not used in the primary analysis. The plots for the 80 km/hr maximum potential tracking speed were selected because they were close to the speed used "routinely" by CloudQuest, but could not be accused of favouring higher calculated speeds relative to the standard procedure using the 90 km/hr maximum. The choice of 100 km/hr for the maximum permitted speed input parameter to the tracking program would have favoured faster estimated actual storm speeds from the program calculations.

The measuring procedure manually determined the distance between the centroids of the starting and ending points of the echo plots on a detailed point by point basis. Each data point is separated in time by about 5 to 8 minutes. Thus, a set of many length measurements was integrated to calculate each storm speed. The speed is determined by dividing this length by the echo duration. There was good agreement between the storm speeds measured by the two analysts employed to provide quality control. The individual track speeds are thought to be accurate to within about ±3 km/hr.

3. RESULTS

The mean speed of the 50 tracks is about 23.4 km/hr (Table 3), which compares well with the average 700 mb (steering level) wind speed for these cases, based on the Nelspruit morning soundings (20.2 km/hr).

Table 3. Mean speed of 50 PAWS storm case plots obtained manually from plots generated by a computer tracking program which defined cases with the maximum tracking speed parameter set to 80 km/hr.

	Seed	No-seed	Both
Mean	23.7	23.1	23.4
S.D.	9.5	10.1	9.7

The standard deviation of the echo track speeds can be used (by multiplying by N/(N-1)=50/49) to provide an ("unbiased") estimate of the population variance of $(9.9)^2$. Thus, the mean value theorem indicates that the sample mean value (23.4 km/hr) should be within about 1.4 km/hr ($=9.9/\sqrt{50}$) of the true mean speed.

4. DISCUSSION

However, the 25 case samples were not drawn randomly from the experimental data set. Nevertheless, as the 25 cases in each group represent 60% and 33% of the total number of unseeded and seeded cases, respectively, they are likely to be representative and this appears to be confirmed by the close agreement between the seed and no seed sample means (23.7 vs 23.1 km/hr).

A number of the computer plotted echo paths were unusual (jumping, irregularly turning, or looping back on themselves). The distinctly irregular storms constitute up to about 25% of the unseeded sample. These will be examined further at a later time. However, it must be noted that a few of the paths were so unusual (e.g. u-shaped or jumping large distances between scans) that their validity requires careful consideration. The seeded cases had much more regular tracks. Examination of the tracks obtained by computer tracking the storms with the maximum permitted velocity parameter set to 60 km/hr did not have the effect of reducing the number of large jumps which were caused by missing scans or unusual tracks, but did decrease the path lengths of some apparently normal tracks (linear with uniform distances between images) significantly.

5. CONCLUSION

This study has lead to a much improved estimate of the mean PAWS storm case velocity by the CloudQuest tracking programme, 13 km/hr. However, based on the estimates of the present study and the earlier work of Mader and Dixon, a storm speed of about 25 km/hr seems the most likely average value to apply to PAWS calculations (rounding to the nearest 5 km/hr). At slowest, the present study and that of Dixon can be used to support a speed near 20 km/hr as well. In addition, all the manual echo tracking studies, the steering wind speeds and the small standard deviation (1.4 km/hr) of the mean estimated from the present large sample (N = 50) suggest that slower storm speed averages are unlikely to have general validity for the relatively small PAWS storm cases. In spite of all the above reasons, the conflict with the result of the improved CloudQuest tracking programme has not been resolved, as it is difficult to envision a further computational error in the tracking programme. Thus, further tracking research appears necessary. For the present, it is concluded that a broad range (15 to 25 km/hr) of storm speeds may be expected in the Eastern Transvaal.

6. REFERENCES

BATTAN L J, 1973. Radar Observation of the Atmosphere. University of Chicago Press , 211.

CARTE A E and HELD G, 1978. Variability of hailstorms on the south African plateau. J. Appl. Meteor., 17 (3), 365-373.

CHANGNON S A, MORGAN G M, ACHTEMEIER G L, TOWERY N G and GROSH R C, 1975. Design of a hail suppression project for Illinois. J. Appl. Meteor., 14, 771-780.

DIXON M, 1977. M Sc Thesis, University of Natal.

GROSH R C, 1971. Satellite Cloud Photographs as a Hydrologic Tool for Remote Tropical Regions. Thesis, University of Wisconsin, Department of Meteorology.

GROSH R C, WEINMAN J A and VAN SCHERPENZEEL C W, 1973a. Cloud photographs from satellites as a hydrological tool in remote equatorial regions. J. Hydrol., 19, 147-161.

GROSH R C and SEMONIN R G, 1973b. Moisture budgets and wind fields of thunderstorms passing over an urban area in the Midwest. Preprints: Severe Local Storms Conference, AMS, Boston, 130-137.

GROSH R, STRUEBING W, MUELLER E A and MORGAN G M, 1975a. Dual wavelength observations of the hail and tornado-producing thunderstorms on 3 April 1974 in Central Illinois. Preprints: 16th Weather Radar Conference, Houston, AMS, Boston, 49-52.

GROSH R C and MORGAN G M, Jr., 1975b. Radar-thermodynamic hail day determination. Preprints: 9th Conference on Severe Local Storms, AMS, Boston, 454-459.

GROSH R C, 1977a. Relationship between severe weather and echo tops in Central Illinois. Preprints: Tenth Conference on Severe Local Storms, AMS, Boston, 231-238.

GROSH R C, 1977b. Satellite-observed urban cloud distributions. Preprints: Conf. Planned and Inadvertent Weather Modification, AMS, Boston, 45-48.

GROSH R C, 1978a. A local severe rainstorm. Preprints: Conference on Flash Floods - Hydrometeorological Aspects. AMS, Boston, 70-79.

GROSH R C, 1978b. Operational Prediction of Severe Weather, Ill. State Water Survey, Tech. Letter 28, 3pp.

GROSH R C, 1978c. Lightning and precipitation - the life history of isolated thunderstorms. Preprints: Conference on Cloud Physics and Atmospheric Electricity. AMS, Boston, 614-617.

GROSH R C, 1984. Radar Meteorology. UN/WMO Working Paper No. 4, 130pp.

GROSH R C, MASSAMBANI O and BRIGUENTI NETO J, 1985. Brazilian convective precipitation: Evolution study with the Bauru Radar. Preprints: Conference on Flash Floods. AMS, Boston.

KELBE B E, 1984. Cumulus cloud characteristics of the Eastern Transvaal Highveld. Water SA, 10 (23), 81-90.

MADER G N, 1979. Numerical study of storms in the Transvaal. South African Geographical Journal, 61 (2), 85-98.

MASON-WILLIAMS S, 1984. The Bethlehem runoff augmentation research project: Past, present and future. Dept. Environ. Affairs, HRI, TR 118, 69pp.

MORGAN G M, GROSH R C, ACHTEMEIER G L, STRUEBING W and BRUNKOW D A, 1975. Radar studies of severe storms observed on 3 April 1974 in Central Illinois. Preprints: Conference on Severe Local Storms, AMS, Boston, 178-179.

NEWTON C W and FANKHAUSER J C, 1964. On the movements of convective storms, with emphasis on size discrimination in relation to water-budget requirements. J. Appl. Meteor.,3-6, 651-668.

VI. STATISTICAL ANALYSES

It is essential that rain stimulation experiments which are statistically evaluated by the original experimenters receive independent confirmation. CSIR/DATATEK was subcontracted for that purpose. Their analyses of the PAWS data are summarised in the following section.

OVERVIEW OF THE STATISTICAL ANALYSES OF THE RADAR DATA FROM THE NELSPRUIT CLOUD SEEDING EXPERIMENT

Jacqueline S Galpin

SUMMARY

This report gives an overview of the statistical analyses carried out at CACDS on the data which arise from a randomized experiment carried out between 1984 and 1987. In this experiment, storms were given one of three treatments: "seed and sample", "no seed and sample" or "no seed and no sample". The hypotheses investigated concern differences between these treatments for 250 "track properties" (variables related to changes in storms over a fixed time period). The investigations indicate that there are a number of track properties for which differences are significant. These differences arise mainly between the two no seed treatments, and also occur in the time period before any treatment is applied. This indicates the presence of an inadvertent bias in the data set, which appears to be mainly due to storms of higher than average volume being assigned to the no seed and sample group than to the other groups.

Differences taking this bias into account are investigated by means of analysis of covariance techniques. Several differences between treatments are found after correcting for bias, particularly in the first ten minutes after decision time, although significant differences still occur before decision time.

1. INTRODUCTION

This report provides an overview of the statistical investigations carried out between 1987 and 1989 into the PAWS randomized experiment, using the data from the ground radar at Nelspruit obtained between 1 October 1984 and 1 April 1987. The aim of the PAWS randomized experiment is to investigate the changes taking place within a storm cell on seeding. Three treatments are involved in the experiment. The first is termed "seed and sample" and involves flying through growing turrets on the flanks of the storm, dispensing dry ice pellets (the seeding material used in this experiment). The second treatment is termed "no seed and sample", and consists merely of flying through the rising turrets on the flanks of the storm cell as if seeding were taking place, but without actually seeding. The last treatment is termed "no seed and no sample", and for this treatment the pilot does not penetrate the storm cell, but merely flies near the storm to mark its position.

The analyses carried out at CACDS have been concerned only with the data from the ground radar and not with data from the cloud base aeroplane, nor with the microphysical data obtained during passes through the storm cells. No description is thus given of the procedures or data involved in these two activities.

As an overview report, this report summarizes seven reports by CACDS on different analyses, and discusses the final results obtained, dispensing with historical changes between versions of the data set and the like. It is intended that the report should be sufficiently comprehensive to inform those not interested in the finer details, of the structure and constraints of the data collected, and of the conclusions that can be drawn from it. To this end, all statistical questions raised in the other reports are discussed briefly here.

The previous reports summarized in this report are:

CKOMP 88/7: Preliminary analysis of radar data concerning the Nelspruit cloud seeding experiment, by J S Galpin;

CKOMP 89/18: Interim report of the analyses of covariance of the PAWS data, by J S Galpin and I Auret;

CKOMP 89/25: Special PAWS request for regression analyses, by J S Galpin and I Auret;

CKOMP 89/26: Further analyses of randomization tests; by J S Galpin and M B Mare;

CKOMP 89/27: Interim report on the updated radar data set, by J S Galpin, M B Mare and I Auret;

CKOMP 89/32: Report on the application of Automatic Interaction Detection to the Nelspruit cloud seeding experiment, by I Auret and J S Galpin;

CKOMP 89/33: Final report on analyses of covariance on the Nelspruit data set, by J S Galpin, M Mare and I Auret.

These reports will henceforth be referred to by number only. The references will indicate where further detail on the analyses and discussions should be sought.

The history of the statistical analyses began with the data set being obtained from the Nelspruit researchers in October 1987. Some time was spent in converting the data and programs to run on the CSIR computers, and in familiarization with the data set. Randomization tests were then performed to look for differences between the three treatments applied, for each of the 250 variables, in different time periods around "decision time" or "time zero" (the time at which treatment allocation was done, and application begun). All pairwise combinations of the three treatments were also examined, as opposed to the seed versus no seed comparison made by the Nelspruit researchers (Simpson Weather Associates and Cansas International Corporation, 1986). Differences were found between all three treatments, with many of the differences being between the two no seed groups. In addition, there was a significant difference on the storm volume before the application of the treatment, indicating an inadvertent bias in the data, despite the precautions of randomization. Several analyses were then performed using the statistical procedure of analysis of covariance, to test for differences between pairs of treatments, after adjusting for the biases. These initial analyses examined changes in the time periods 0 to 10, 10 to 20, 20 to 30, 30 to 40, 0 to 20, 0 to 30 and 0 to 40 minutes, as well as in the period ten minutes before decision time.

It was decided at this stage to suspend analyses of the time periods 0 to 20, 0 to 30 and 0 to 40 minutes, as some of the storms in these data sets did not last more than 15 minutes after decision time, a factor that could contaminate the analyses. These analyses, reported on in CKOMP 88/7, examined a slightly different data set from that examined by the Nelpruit researchers, being one from which all storms without an echo before decision time had been removed, in order to allow for testing of bias.

Later examination of the randomization test results led to discrepancies being noticed between the results obtained by the Nelspruit researchers and those at CACDS. Investigation revealed that the initial data set obtained was possibly incorrect, there having been a change in the tracking speed at which the tracking algorithm was run. A fresh data set was thus obtained in December 1988, and investigated as to the possible sources of differences. Although some differences were found, these were not major, and it was realised that the initial indication of a discrepancy was due to a misunderstanding of the reports by the Nelspruit researchers. However, it was decided that the previous analyses should be re-done on the new data set. Little reference will thus be made in this report to results obtained on the old data set; emphasis being on the new data set. It was also decided that the analyses should include not only those for the three combinations of the pairs of treatments mentioned above, but also the combination of seed versus no seed treatments, and that both the data set with storms without pre-decision time echo omitted and the data set without this restriction, should be examined.

Further analyses of covariance were then performed. While the initial analyses of covariance were done for pairs of treatments, it was decided now to perform three way analyses of covariance, simultaneously comparing all three treatments. One reason for switching to the three way model is that the estimated treatment mean for the seed and sample treatment (say) obtained from the comparison of the seed and sample and no seed and sample treatments will differ slightly from the adjusted treatment mean obtained from the comparison of the seed and sample and no seed and no sample treatment, due to the random error component of the data points. Use of the three way model allows a single estimate of each of the three treatment means to be obtained. These may then be followed up by two way comparisons, as a multiple testing procedure to find out where the differences actually lie.

As the analysis of covariance procedure used assumes the bias adjustment made to be linear, and that no interactions exist between covariates, Automatic Interaction Detection (AID) procedures were used to check these assumptions. Certain regression analyses were also performed at the request of the Scientific Director of the project.

The layout of this report is as follows: the structure of the data set is described in section 2, together with a description of the experimental procedures relevant to the analyses; the statistical background to the randomization tests, the analyses of covariance, and the AID procedures are discussed in section 3; the results obtained from these procedures and from the regression analyses performed at the request of the Scientific Directors of the project, are reported on in section 4; and the conclusions reached by the various analyses are summarized and drawn together in section 5.

2. EXPERIMENTAL PROCEDURES AND STRUCTURE OF THE DATA SET

The data under discussion arise from experiments conducted around Nelspruit during the seeding seasons of 1984/85, 1985/86 and 1986/87, where each season lasts from 1 October to 1 April. All days were considered eligible for the experiment, except Sundays, public holidays, and days on which essential equipment was not functioning. It is assumed that these days are missing at random, as the Nelspruit researchers state that no meteorological reason can be anticipated as to why these days should be either more or less favourable for seeding than other days.

2.1 Definition of Experimental Unit

The experimental unit used is the medium-sized, isolated multicellular storm, where a storm is defined as "any contiguous volume all of which exhibits reflectivity in excess of a threshold value" (Simpson Weather Associates and Cansas International Corporation, 1986, volume 4, page 3-12). The use of a storm as experimental unit is different to a number of other weather modification experiments, in which days are chosen as the experimental units, each day being declared as experimental or non-experimental. The aim of the latter experiments has mainly been in testing whether rainfall is increased by seeding. As previously mentioned, the aim of the current investigation concerns the changes taking place in the storm cell after seeding, with the specification that not all storms are of interest, but only the medium sized storms of the type that may be expected to produce about 1 mm of rain per hour at cloud base. These storms are characterized by having radar reflectivities greater than 30 dBz. Isolated cells are used as they are easy to track, changes will readily be visible, and in order that there may be no contamination from other experimental storms.

2.2 Experimental Procedures

Data obtained from the Weather Bureau concerning the synoptic situation as well as data obtained from a balloon ascent are used to decide whether the day is a "go" day or a "no-go" day. This information is supplemented by reflectivity values obtained from the radar, which is activated on "go" days, usually between 9 and 10 am. This latter information is generated by a radar sweep of the area, the sweep being done at 3 , followed by a volume scan (described in detail below). For economic reasons, the seeding aeroplane (Learjet) is only launched if two storm cells with closed contours of greater than 30 dBz, containing reflectivities of 40 dBz or more, are found within the experimental area. This is defined as being within 100 km of the radar site, but not within 10 km of the radar or over foreign territories.

After take-off, the Learjet flies to one of the storm cells identified by the radar as an experimental possibility. A visual inspection of the storm cell is carried out before it is decided that the storm cell should become part of the experiment. Storm cells eligible for the experiment are defined as those having "reasonable cloud dimensions, that is, good width to height proportions and not excessively sheared", having well-defined bases, and having one or more cloud turrets actively growing through the -10°C level (this implying that attempts are made not to include decaying storm cells in the experiment). They are further required to be separated from other cells already included in the experiment by at least 35 km (20 nautical miles). According to the Nelspruit researchers, tests have been carried out on the pilots involved in the experiment as to the possibility of different decision rules being followed by the pilots, and an assurance has been given that the pilots give the same decision in almost all cases. As no decision has at this stage been made as to the experimental treatment to be applied, any bias arising from this subjective procedure may be expected to be independent of the conclusions drawn from the experiment, provided that the pilots are consistent in their decisions.

Further restrictions on the data arising from the tracking algorithm are that the reflectivity should remain above 30 dBz, the volume should be a minimum of 3 cubic kilometers and the maximum speed of movement should be under 90 km/hour. Other restrictions on the data include a limitation on the quality of the radar signal that leads to storms further than 80 km from the radar being dropped, and a possible initial bias that leads to storms with a volume greater than 750 cubic kilometers being excluded.

To summarize, the experimental unit is a medium-sized, isolated multicellular storm with

i) volume between 3 and 750 cubic kilometers,

ii) minimum radar reflectivity always above 30 dBz,

iii) "reasonable cloud dimensions", such as good width to height proportion, not excessively sheared and having a well-defined base,

iv) having cloud turrets actively growing through the -10°C level,

v) speed of movement less than 90 km/hour,

vi) being separated by at least 20 nautical miles from other experimental storms,

vii) first being recorded between 9am and 5 pm, and

viii) being between 10 and 80 km from the Nelspruit radar, but not over foreign territory.

The population from which these units are drawn is the population of such storms occurring on days characterized by not being Sundays or public holidays or days on which essential equipment malfunctioned, being classified as "go" days, and being days having at least two storms with closed 30 dBz contours enclosing a 40 dBz reading occurring simultaneously.

2.3 Treatment Allocation and Application

If the storm cell passes the visual inspection, the time is recorded (and termed the decision time) and the radar operator is informed that an experiment is declared. In the first two seasons under discussion, the radar operator then opened a sealed envelope, and informed the crew as to the experimental treatment to be applied. During the third season a read-only chip was installed in the Learjet, and the treatment selection was obtained by pressing a button, which indicated that the storm should be either sampled or not sampled. The seed/no seed part of the treatment was then done without the pilots' knowledge, the chip controlling whether the dry ice was released from the bin or not, the tell-tale rattling sound being obscured by a horn. This was done to guard against bias arising from the possibility that the pilot may fly in a different way when simulating seeding. It is assumed that the correct treatment was in fact applied.

In the case of "no seed and no sample" the pilot flies in the vicinity of the storm cell for a few minutes, in order to assist in the radar identification of the storm cell. In the case of either "seed and sample" or "no seed and sample", the pilot penetrates all rapidly growing turrets on the flank of the storm between the -5 and -15°C isotherms on the flank of the storm. If the treatment was "seed and sample", the seeding material is dispensed while the Learjet is within the turret, and the treatment period continues until either 120 seconds of seeding has taken place (which uses approximately 23 kg of dry ice), or until no more rapidly rising turrets are available. For the "no seed and sample" treatment, the pilot flies through the turrets as if seeding, and for the same period as if seeding was taking place, but without dispensing any seeding material.

On completion of treatment application to one experimental storm, the aircraft moves to another possible cell, which must be separated from the first cell by at least 20 nautical miles, edge-to-edge, and again applies the above procedure. When insufficient fuel remains for completion of another "seed and sample" run, the aircraft lands. It is possible for the plane to fly further missions, after refuelling. The final data set has up to 4 experimental storms on a day.

After the treatment has been applied to the experimental storm, it is tracked by radar until its peak reflectivity drops below 30 dBz, or until it passes outside the range of the radar.

The sealed, numbered envelopes contain a prespecified list of treatments, provided by the Water Research Commission in Pretoria. These treatment allocations were obtained by generating a random sequence of treatment allocations, subject to certain specifications. The first is that there is an 50% probability of choosing the "seed" treatment, and a 50% chance of choosing the "no seed" treatments. The "no seed" treatments are further split approximately 50/50 according to the "sample" and "no sample" portions of the treatment. Acceptable sequences thus consist of about 50% "seed and sample" treatments, 25% "no seed and sample", and 25% "no seed and no sample", generated in a random order. According to the Nelspruit researchers, further restrictions were also placed on acceptable sequences, for example that the sequence did not contain any runs of 7 or more occurrences of the same treatment allocation. Several acceptable sequences were generated, each containing 150 treatment allocations, with between 70 and 80 "seed" sequences. One of these sequences was then chosen by officials of the Water Research Commission, and the treatment sequence was placed into numbered, sealed envelopes. The Nelspruit researchers were not informed as to which sequence was chosen.

A possible problem arises with the amount of seeding material dispensed while flying through the growing turrets. The PAWS report indicates that the 23 kg of seeding material may be dispensed over a period of 40 minutes, with 60% of the material having been dispensed, on average, within 15 minutes. Not all seeding material is dispensed in all cases - if no more rising turrets occur, seeding is stopped. Thus the amount of material received by a storm cell may vary from storm to storm, as may the rate of dispensing, and thus the period over which seeding takes place. This problem may also occur in the "no seed and sample" treatment. It implies that there may be many more than three treatments applied, the only treatment that does not vary from storm to storm being the "no seed and no sample" treatment.

2.4 Data Description

The raw data for this experiment consists of the radar data obtained from each volume scan.

Volume Scan

The volume scan consists of radar sweeps at increasing vertical angles in steps from 3° to 50°. In the horizontal plane the scan may be a full 360 scan, or may be a sector scan, in which the radar reverses direction after completion of the required sector before stepping up to the next vertical angle of scan. The sector scan is used in cases where the only storm cells lie in one sector of the sky, and is used to save time by not sweeping large areas of blue sky. The scan at elevation 3° is always a full 360° scan, and may be used to check that no storms have appeared in areas not being swept. A full 360° volume scan takes 8.5 minutes, while the average scan frequency is stated to be 6 minutes.

There is one possible statistical implication with this eminently practical procedure, and that is that the time between steps in a volume scan and between separate volume scans may vary for the different storms in the experiment. Variation in duration of volume scans implies that the various data points may be obtained with different precisions, for two reasons. Firstly, more data points may be available over a given period on which to base the estimate of change over the period. Secondly, since it is probable that fewer or smaller changes occur during shorter time periods, a volume scan built up over a shorter period will give a more precise reading of the state of the storm at a particular instant in time.

The initial processing of the data (done at Nelspruit) encompasses the removal of blue sky data and the building up of a storm track of the volume scans. The latter is done by first creating the volume scans from the radar readings at each of the scan heights, and then joining these volume scans together to form a track. The algorithm used to track the storm centroid is able to take care of storms merging and splitting. The case tracks are then identified. At this stage, a few of the experimental cases are lost through problems of tracking, seeding having taken place at the -25°C level, etc. It must be assumed that this loss of experimental units is independent of the treatment applied, as no data was made available through which this could be tested. It could presumably be checked by examining the relative numbers of storms with invalid tracks in each of the treatment classes.

Storm Property Variables

The data received from Nelspruit consists of 63 variables concerning reflectivities for each volume scan for each of a number of storms. These records included non-experimental storms. This data is described in detail in Appendix A of CKOMP 88/7. The variables include the volume weighted centroid (in the x, y and z directions); the reflectivity weighted centroid; the top and base of the storm (at 30 dBz); the volume and 3° area, total and in 11 dBz ranges; the mass and peak reflectivity in 12 heights above ground level; the area, mean reflectivity and rain flux at 3° and at the cutoff altitude (6 km); the mean and peak reflectivity; the height of the peak refelectivity; and the maximum height of the 45 dBz echo. For convenience, a list of these variables is reproduced in Appendix A.

One possible problem with this data is a result of the unavoidable 3 limit on the bottom of the scan range - at 10 km, 3° relates to a height of 0,52 km, while at a distance of 100 km the height is 5,2 km. As the base of the cloud can be below this height, this implies that the estimate of the height of the base of the storm will be affected by the distance of the storm from the radar. This also implies that the variables relating to 3° (such as area, area in a certain dBz range, rain flux, etc.), relate to different parts of a storm depending on the distance of the storm from the radar. This statement also applies to all other variables based on the volume scan. Another implication is, however, that the mass, volume and peak reflectivities cannot be obtained for the lower parts of storms that are further away, so that the mass, etc. of such storms may be under-estimated. For some variables the 3 restriction may be less important, for example it may only be serious if changes occurring below this altitude are important. It is stated in the PAWS report (volume 4, page 3-14) that the -10°C altitude at which seeding takes place occurs at approximately 6 km above ground level, which may imply that one is more interested in the part of the storm above 3.

Track Property Variables

As previously mentioned, this experiment is concerned with changes taking place in certain time periods after seeding. The basic radar variables described above are thus processed over a given time period to give "track property" variables. The first time period of interest is the 10 minutes before decision time to decision time (-10 to 0). Values of track properties in this period should be independent of the treatment, as no treatment has yet been applied, so that comparisons of variables over the three treatment groups can be used to check for bias.

Each of the 260 track properties is calculated by interpolation of the values of the 63 basic radar variables described in the previous section, with the interpolation taking place between the volume scans near each end of the time period of interest. A description of how each of these variables is calculated by the track-properties program is given in CKOMP 88/7, where it is stated whether linear or logarithmic interpolation is used. For convenience, a list of these variables is given in Appendix B.

Variables in the first and last groups (groups 1 and 11), other than variable 1 (the duration of the storm above 30 dBz in the time period of interest) relate mainly to values at decision time, to synoptic conditions of the day and to mesoscale conditions. Both groups are thus independent of the time period being examined, and are termed control properties in the PAWS report. The latter group is also fixed for all experimental cases on a particular day.

Several variables are highly correlated with each other, for example the mean and maximum of most variables have a (linear) correlation of at least

90%. Similar variables in different groups also correlate highly, an example being the maximum rates of increase for most variables. Other variables correlating highly are the echo top and depth, and the persistence and maximum ratio. The volume at decision time (property 9) is also highly correlated with such properties as mean and maximum volume, mean and maximum total mass, mean and maximum mass at cutoff, area at 3and at cutoff, precipitable water, etc. Property 10, the peak dBz at decision time, is also highly correlated with the peak dBz total, mean dBz total, percentage volume as a function of dBz, "delta vertical centroid", etc.

3. BACKGROUND TO THE STATISTICAL PROCEDURES USED

As previously mentioned, the statistical techniques used so far in the analyses of the radar data set are those of randomization testing, analysis of covariance, and automatic interaction detection. A brief description of these techniques is given in sections 3.1, 3.2 and 3.3 respectively.

3.1 Randomization Testing

The statistical methods of analysis of weather modification data recommended by the Statistical Task Force (Brillinger, Jones and Tukey, 1978) are those based on randomization tests (sometimes also called re-randomization). These are not really tests in themselves, but a method of obtaining the significance of a test by means of a randomization procedure. Any hypothesis may be tested by means of a randomization test, using any appropriate test statistic. These methods obviate many of the assumptions usually needed in statistical analyses that cannot be made for weather modification data, such as those of the independence of observations, of shapes of distributions, or of the data having been obtained by simple random sampling.

Randomization tests are most easily described by examining the case where two treatments have been applied to a set of subjects, and the hypothesis to be tested concerns the difference of some statistic, for example the mean, maximum or variance, between the two groups. To illustrate the procedures, consider the one sided hypothesis that the mean of the measurements from the n subjects given treatment 1 is higher than that of the m subjects given treatment 2, which is equivalent to the hypothesis that the difference of the means of treatments 1 and 2 is positive. Under the null hypothesis, there is no difference between the two treatments, so that it makes no difference which treatment is assigned to each subject. Thus, if one were to scramble the data, and regard the first n observations as resulting from treatment 1 and the rest from treatment 2, one should obtain a similar result for the difference-of-means statistic to that obtained originally, if the null hypothesis is true. This will then form another observation from the distribution of the difference-of-means statistic. One can then do a number of such "scramblings" or re-randomizations, and look at how many of the differences of means exceed or equal that obtained in the actual experiment. This percentage will give the probability of the test value being exceeded by chance.

Using all possible permutations of the treatment assignment to obtain the probability, while giving an exact p-value, is not feasible except for experiments involving small sample sizes (there are 3 628 800 possible permutations of a sample of size 10, and many more for the data under analysis). Fortunately, Edgington (1987) shows that the p-value may validly be estimated using a random sample of this full population set.

The method of obtaining the random sample used in the PAWS reports is the same as that used to generate the original sequence. However, the experimental observations being analysed are not really obtained from this definition, due to some experimental units having been lost after assignment of the treatment (owing to invalid storm tracks, storms merging or splitting, etc.). This does not actually cause a severe problem, in that a subset of the random selections from the population of acceptable schemes will consist of those without the missing observations. A further problem is that such a randomization will not necessarily comply with the further length-of-run restrictions that were placed on the string composition.

Another problem is that, when the re-assignment is done, the numbers of observations allocated to each of the treatments will differ for the different re-randomizations (see CKOMP 88/7 for a detailed discussion). This is then a problem in estimating the probability of exceeding the test statistic value by chance alone, as one is comparing numbers of differing precisions. This problem may be circumvented by using what may be termed a "marginal" set, namely the set of permutations of the experimental treatments such that n1 observations are allocated to treatment 1, n2 to treatment 2 and n3 to treatment 3, where n1, n2 and n3 are the numbers of cases that received each treatment in the data set. This is also a valid set of re-randomizations as all these possibilities are included among the full set of valid re-randomizations.

The randomization scheme used here is used to test all pairwise hypotheses, and not just the seed versus no seed comparison. The scheme thus uses different re-randomizations for each hypothesis, the re-randomizations involving only observations arising from the application of the pair of treatments under consideration. This is in contrast to those used by the Nelspruit researchers.

The initial application of the randomization testing procedure was to each variable in the data set individually. However, although it is commonly stated that one would expect to find 5% of the tests significant by chance alone if one is performing the tests at the 95% level, this is not always true, unless the tests are independent. In the case of the analyses reported here, that is definitely not true, as the 250 variables are highly correlated. It is obvious that, if there is a significant difference in, for example, the mean echo top of the storm, it is very likely that the maximum echo top, and the maximum ratio for the echo top are also significant. In the most extreme situation of perfectly correlated variables, one would expect all tests to be significant (or nonsignificant). All that can be said is thus that the number of tests significant by chance alone can be expected to lie between 5 and 100. The level at which the hypothesis testing is done must thus be adjusted to obtain a test at a true 95% level.

The alternative to considering this problem as being one in which 250 individual hypotheses are being tested, is to consider the test as being of the joint hypothesis that none of the 250 variables differ significantly, as opposed to the alternative hypothesis that at least one of the variables differs significantly. This test is based on the union-intersection principle (Gabriel, 1979), in which the distribution of the maximum of the 250 variables is used. In terms of randomization testing, one thus obtains the maximum for the test statistic over the 250 variables at each re-randomization, and uses this distribution as the basis for the comparison with the values found for the test statistics in the actual experiment. All variables for which the statistic is larger (or larger in absolute value) than this maximum are then significant at the 5% level. (The test using the absolute value is of course the two sided test, that is the test of no difference. A test using the actual value of the test statistic is a one-sided test, testing for an increase.)

3.2 Analyses of Covariance

As has been mentioned, the results of the randomization tests show that there are significant differences, mainly between the two no seed treatments, and indicate that the difference in volume arises even in the before decision time period. This difference thus appears to be due to an inadvertent initial bias between the samples allocated to the different treatments.

A partial examination of such differences could be carried out through the examination of pairwise plots of the data. However, the sheer volume of the plots to be examined is prohibitive. In addition, it is very possible that the bias may not lie just in the relation between 2 variables, but may lie in a relation of more than two variables, and may thus not be visible on pairwise plots. Examination of plots is also a somewhat subjective procedure. An alternative procedure was thus employed, namely the analysis of covariance.

In this procedure, the means of the treatment groups are compared for some track property, after correcting for the effect of the "covariates" or "correcting" properties. In order to clarify the object of this technique, consider the following hypothetical example (which may or may not make sense meteorologically), using just two treatments. Suppose that we are examining the change in echo top height of the seed and sample cases versus the no seed and no sample cases, in the 10 minutes after decision time. It may be that the changes in echo top height as a result of seeding are highly affected by the initial volume of the storm, with the rate of change of echo top height depending linearly on the initial volume. "Adjusting" the echo top height for the initial volume may then allow one to see clearly whether seeding has had an effect or not. Although this example uses only one "correcting" variable or covariate, the method also caters for the use of several variables.

The analysis of covariance model used in these analyses is that where all three treatments are taken into account. One representation of this model is:

$$y = \mu_1 + \mu_2 + \mu_3 + \beta_1(x_{1,i} - \bar{x}_1) + \beta_2(x_{2,i} - \bar{x}_2) + \dots + \beta_p(x_{p,i} - \bar{x}_p) + \epsilon_i,$$

where y_i represents the value of the dependent variable under consideration for the i'th case, the μ's represent the adjusted treatment means, the β's are the (linear) regression coefficients of the p predictor variables, the $x_{i,j}$'s are the values of these predictor variables for the i'th case, the $\bar{x}$'s are the corresponding means of these values, and ϵ_i is the random component for the i'th case.

Tests can then be carried out as to the significance of the differences between the three adjusted means (μ_1, μ_2 and μ_3). In many cases (where there is sufficient data, compared to the number of covariates included) one can also test the hypothesis that the same regression line can be used for all three treatments.

Comparing the three means allows identification of whether there is a significant difference between the treatment means, but not as to where the difference lies, should the difference be significant. This can be examined by considering covariance analyses using only two variables at a time.

As the covariates used are correlated among themselves, the coefficients of the regressions will change, sometimes greatly, depending on which variables are in the equation. Thus the elimination of variables should be done using a method in which nonsignificant variables are eliminated from the equation in a stepwise fashion. Several criteria may be used in choosing the final equation - significance of individual terms, drop in explanatory power of the equation, etc. An examination for outliers should also be performed.

There are two drawbacks to the analysis of covariance, however, which are not shared by the plotting procedure. The first is that, even though one could use different regression lines for the different treatments, the correction performed is basically that of linear regression, so that quadratic or other nonlinear effects are not taken into account. The second is that the procedure only looks at means. If the data come from a skewed distribution (as many of the variables in this study appear to), this is not necessarily a statistic of interest. These assumptions may be checked using the automatic interaction detection methods.

3.3 Automatic Interaction Detection (AID)

This is actually a family of methods, used for analyzing data sets consisting of a large number of observations (Hawkins and Kass, 1982). The aim of these techniques is to classify the data into mutually exclusive homogeneous subsets describing a (continuous or categorical) dependent variable in terms of (categorized) values of the predictor variables. No assumptions are made as to the structure of the relationships, whether linear or otherwise, or as to the presence or absence of interactions. The main aim of applying the AID procedure in this case is to examine the appropriateness of an analysis of covariance by determining the presence of interaction terms and non-linearity, and the identification of outliers.

In this technique, each predictor variable is considered in turn as to its ability to explain the variation in the dependent variable. This is done by dividing the dependent variable into groups, based on categories of the predictor variable. A splitting and merging process (based on t tests) is used to get the best combination of the possible categories, with the criterion being that the variation of the dependent variable values within each group should be as low as possible (with the major part of the variation thus lying between the groups). Once the best predictor for the first split has been chosen, and the split implemented, each subgroup is considered separately in the same way as before, all predictor variables again being considered. A tree structure is thus formed, with the dependent variable being split into smaller and smaller groups until no further splitting will lead to significant improvement. This tree can be used as a non-parametric method for predicting the dependent variables from the predictor variables. The tree also gives an indication of what the best variables are for predicting the dependent variable, and whether different variables are needed for predicting low values of the dependent variable to those needed for predicting high values, etc.

The member of the AID family most appropriate for the current analysis is Extended Automatic Interaction Detection or XAID, (Heymann, 1981), which has been developed for the case of a continuous dependent variable. It is also able to handle smaller data sets than the other methods (the minimum recommended size of data set is 50). The current data set is too small for the other methods to be useful. However, XAID detects only a change in location and supposes that the data are normal and equally precise.

As previously mentioned, these techniques require the predictor variables to be categorized. This was done by examining the distribution of values for each predictor variables, and taking the lowest 25% of the observations to be the first category, the next lowest 25% the second category, and so on, to form four categories.

A more detailed description of the technique is given in CKOMP 89/32.

4. DATA ANALYSES

The data sets analysed are, as already mentioned, those derived from the Nelspruit radar data set, as obtained in December 1988. Both the "three condition" and the "four condition" data sets are analysed, the "three condition" data set being that with the post-experimental stratification of all storms being less than 750 cubic kilometers in size, being between 10 and 80 kilometers from the radar, and with temperature ratio partition greater than 2. The "four condition" data set has the further restriction that all storms have an echo in the before decision time period. The numbers of observations in the data sets, for each of the time periods, and for each of the treatments, are shown in table 1. Under the heading "Treatment", 1 denotes seed and sample, 2 denotes no seed and sample, and 3 denotes no seed and no sample.

Table 1 Numbers of observations.

Four condition data set

		Treatment 1	2	3
T	-10 to 0	38	20	27
I	0 to 10	38	20	27
M	10 to 20	37	20	25
E	20 to 30	34	19	22
	30 to 40	27	17	17

Three condition data set

		Treatment 1	2	3
T	-10 to 0	38	20	27
I	0 to 10	40	21	28
M	10 to 20	39	21	26
E	20 to 30	38	24	23
	30 to 40	31	22	17

The reason for the initial use of the four condition data set for randomization testing was the great importance of testing for bias. It is not possible to test for bias unless there are observations present in the before decision time period. However, there has been some literature indicating that it is precisely these cases, which are rapidly growing storms, where the greatest effect of cloud seeding is apparent. For this reason, both data sets have been examined in the randomization testing analysis. Examination of means for the different treatments and time periods (after decision time), given in Appendix E of CKOMP 89/26, indicates, however, that including these cases results in a decrease in the mean value for most variables.

4.1 Randomization Testing

The test statistics used for randomization testing, the separate randomization tests for each variable and the randomization testing taking the multiplicity of tests into account are discussed under separate headings below.

Tests Used in this Report

A number of test statistics have been used in the analyses. Among these are the test statistics used in the PAWS reports, namely the arithmetic and geometric means, the standard deviation, the skewness and the maximum and minimum, of each variable. The kurtosis has also been listed in some of the tables in some of the reports, but has not been discussed. The definition of the geometric mean differs somewhat from that defined in the Nelspruit analyses, being defined as zero if any of the values involved is negative. (See CKOMP 88/7 for more details on these statistics).

A further blanket test for differences in distribution is included in this study, namely the Kolmogorov-Smirnov (KS) two sample test. This test essentially computes the cumulative distribution functions for each of the two sets of sample data, and looks at the maximum absolute difference between the two cumulative distribution functions. This can be stated formally as:

$$KS = \max|F(x) - G(x)|$$

where $F(x)$ and $G(x)$ denote the sample cumulative distribution functions of the two samples, and the points x over which the maximum is taken are the points forming the two data sets. (Strictly speaking, x ranges over the set of all values that the variable can take on, but changes in the function $|F(x) - G(x)|$ can occur only at the actual values present in the two samples.) This test covers all the possibilities of difference in mean, standard deviation, skewness, kurtosis, maximum, minimum etc.

As stated, the Kolmogorov-Smirnov test used here is based on the maximum absolute difference, and is thus a two sided test, testing for any difference in distribution and not just an increase. This is in contrast to the tests used in the Nelspruit analyses, which are one-sided tests, testing for an increase in the statistic. While it may be sensible to test for an increase in mean or maximum in seeding or sampling, it is not clear whether it is sensible to test for an increase in variance, skewness or minimum.

Another reason why the KS test is used is that it is a non-parametric test and is less affected by a few outlying points. This contrasts with the statistics used in the Nelspruit study, which are all highly affected by even a single very outlying point. The reason why this is undesirable is, of course, that one is looking for changes that affect all (or at least most) of the storms given a certain treatment, and is not interested in differences in changes due to only one or two storms. Unfortunately, the KS test is not totally robust against such points, and may thus still give a significant result due to only a few points. Alternatively, it is possible that a significant difference may be obscured by the presence of a few outlying points.

Randomization Tests

The initial analyses, discussed in CKOMP 88/7, included analyses of the data set without the restriction on the initial volume being less than 750 cubic kilometers, and the temperature ratio partition being greater than 2, for the data set with all cases without readings in the period 10 minutes before decision time to decision time (-10 to 0) being removed. It was found that the presence of very large volume storms (there are nine storms with initial volume greater than 750 cubic km), led to skew distributions of the variables, and bias between the treatments. These cases were thus dropped. The bias, however, did not disappear completely. Stratifying on the temperature ratio partition, which removes the graupel only cases, was found to result in a great change in the results, (see CKOMP 88/7), with a number of variables now becoming significant. These indicated the possible presence of both a seeding and a sampling effect, with a possible bias again being found. It was decided to implement the temperature ratio partition stratification.

For the new data set, CKOMP 89/27 gives full details of the randomization tests (based on a sample size of 1 000) of each of the 250 variables (for each of the hypotheses of seed and sample versus no seed and sample, seed and sample versus no seed and no sample, no seed and sample versus no seed and no sample, and seed versus no seed). Variables significant on any of the test statistics are listed in Appendix B of that report for the three condition data set, and Appendix C for the four condition data set, separately for each of the 10 minute time periods. These tables show a large number of variables to be significant on the various tests, with a number of variables also being significant in the before decision time period. This may be due to either bias, or to chance effects, the latter being made more probable because of the large number of hypotheses being tested.

Joint Randomization Testing

CKOMP 89/27 also reports on the results for the randomization testing taking the multiplicity of the tests and the correlation between the variables into account. As one uses the maximum of the test statistic over the different variables as criterion in this procedure, it is obvious that any test statistic used for such a test must be scale-invariant. Thus one cannot use the maximum as a test statistic, as the scales of volume, rainflux, rates of increase, etc., vary greatly. Two test statistics were thus chosen for this analysis - the Kolmogorov-Smirnov (K-S) statistic, as an overall test of change of distribution, and the t-test, as a test of change of mean. As the Nelspruit analyses test for an increase in mean, this test was also done in those terms, and is thus a one sided test. The K-S test is a two-sided test. This analysis was done for both the three and four condition data sets. Results of this test are listed in Table 2.

A single asterisk in this table indicates significance at the 10% level, a double asterisk significance at the 5% level, and a treble asterisk significance at the 1% level. Where significances differed between the two data sets, they were higher on the four condition data set - these are indicated by the extra stars in brackets. Test 1 represents seed and sample, test 2 is no seed and sample, and test 3 is no seed and no sample. Tests of seed versus no seed (test 4) were also performed, but only one variable was significant (variable 237 on 20 to 30).

Table 2 Variables significant on multiple testing

(a) On both three and four condition data sets

Time period	Test	K-S	Mean
-10 to 0	1 vs 3	191 *	-
	2 vs 3	9 **	-
		-	69 **
0 to 10	2 vs 3	9 **	-
		27 **(*)	27 *(*)
		28 **(*)	28 *(*)
			33 *(*)
		35 ***	35 **(*)
		36 ***	36 **(*)
		-	43 *(*)
		-	65 *(*)
		67 **	67 **
		68 **	68 **
		-	75 *(*)
		-	76 *(*)
			81 **(*)
		83 ***	83 **(*)
		84 ***	84 **(*)
		115 *(*)	115 **
		117 *	117 *(*)
		121 **	121 *(*)
		-	126 *(*)
		128 *	128 **(*)
		135 **	-
		-	140 *
			142 *(*)
		149 **	149 *(**)
		201 ***	201 ***
		202 ***	202 **(*)
		-	203 **(*)
		206 *(*)	206 **(*)
			208 **
		221 *	-
		226 **	

(continued)

10 to 20	2 vs 3	9 **	-
		59 *(*)	-
		60 *(*)	-
		116 *	116 *(*)
			121 *(*)
			128 *(*)
		-	149 *(*)
			206 *(*)
			208 *(*)
		226 *	
		228 **	228 *(**)
30 to 40	1 vs 3	155 *	-

(b) Three condition data set only

Time period	Test	K-S	Mean
0 to 10	1 vs 3	-	164 *
	2 vs 3	-	143 *
30 to 40	1 vs 3		160 *

(c) Four condition data set only

Time period	Test	K-S	Mean
0 to 10	1 vs 3	-	33 *
	2 vs 3	-	25 **
		33 **	
		-	41 *
		-	44 **
		-	51 *
		-	52 *
		-	58 *
		-	73 *
		81 **	
		-	119 **
		142 *	-
		-	147 **
		-	207 **
		208 *	
		223 *	-
			226 **
		-	228 **

(continued)

10 to 20	1 vs 3	-	25 *
	2 vs 3	-	25 *
		-	27 *
		-	28 *
		-	43 *
		-	44 *
		-	65 *
		81 *	81 *
		83 *	83 *
		84 *	84 *
		-	115 **
		-	119 *
		121 *	
		-	126 *
		128 **	
		-	133 **
		-	135 **
		-	147 *
		-	201 **
		202 **	202 **
		-	203 *
		206 **	
		-	207 *
		208 **	
		-	221 **
		-	222 **
		223 *	223 **
			226 **
		-	227 **
20 to 30	1 vs 3	133 *	-
	2 vs 3	9 **	-
	1 vs 4	-	237 **
30 TO 40	2 VS 3	9**	-

It can be seen from table 2 that almost all significant variables are significant for the test of no seed and sample versus no seed and no sample (i.e. a fly-through effect). However, it can be seen that variable 9, the volume at decision time, differs significantly in the before decision time period. Many of the variables that differ in the post-decision time period are related to volume, so that these differences could be due to an unanticipated bias.

4.2 Analyses of Covariance

Analysis of covariance is a complicated procedure, as has been illustrated with this data set. Firstly, the covariates have to be chosen, as well as their form (linear, quadratic, etc.). There are thus concerns over the correctness of these assumptions, as well as concerns over distributional assumptions. These latter can be removed by doing the analysis within a randomization testing framework. However, a significant difference between the adjusted treatment means does not imply that the analysis is finished. Some check must also be carried out that the bias correction has been adequately done, but that over-compensation has not taken place. The only way of doing this is by detailed examination of the regression equation and of the residuals, and of the plausibility of the results.

Initial Analyses of Covariance

In the initial analyses reported on in CKOMP 88/7, a number of the analyses of covariance proved significant (73 for the period 0 to 10 minutes), with the majority of the tests being significant when comparing either the seed and sample and no seed and no sample treatments, or the two no seed treatments. Many of these significant analyses are for variables found to be significant during the re-randomization tests, thus indicating that even after taking into account possible (linear) relationships with the control variables, there are differences in treatment means. Some variables, however, become non-significant (indicating that the significance was due to bias), while the opposite also holds - several previously non-significant variables are now significant (indicating that the bias previously obscured the significance).

At this stage it was deemed advisable to check some of the assumptions (linearity, lack of interactions, and absence of outliers).

XAID Analyses

Due to the large amount of work involved in setting up an running an AID and the time constraints, only a few, selected variables of meteorological importance (as chosen by R. Grosh and G. Mather) were used as input to the XAID analysis. The dependent variables investigated are variable 67 (Mass rainflux at 3°), variable 68 (Mean rainflux at 3°), variable 75 (Mass rainflux at cutoff). and variable 6 (Mean rainflux at cutoff), while predictor variables are the twenty control properties: variables 1 to 10 and 241 to 250, and several variables of meteorological interest: such as the values of the dependent variables before decision time, as well as variables 11,13, 20, 27, 28, 40, 51, 52, 59, 60, 84, 95, and 102.

The values of the predictor variables are those of data recorded before decision time. The dependent variable is chosen from corresponding storms in any of the four ten minute periods following the decision time. It is important to note that the data used from the before and after decision time periods must be from the same storm, implying the deletion of all storms without pre-decision time echo, as in the four condition data set.

In the analyses using the twenty control track properties as predictors, the initial volume at decision time appears as the most important factor influencing post-decision time rain flux. Analyses of the augmented set of predictor variables chosen on meteorological grounds, showed that the area at decision time and the initial rain flux value of the cloud at decision time contributes most towards the produced rain flux after the application of the treatment. Transformation of the data to the logarithmic scale (indicated as the variances of the dependent variable increased with the mean) resulted in the initial volume as well as the mean precipitable water in the cloud before decision time contributing most to the subsequent measured rain flux. After adjusting the data for the initial volume the mean x coordinate of the storm (track property 5), the CCL temperature (track property 244) and the cumulative 3° area time integral (track property 246) are the most important predictors.

No first level partitioning due to treatment occurs but several cases of lower significance appear in the 10-20 and 20-30 minute periods after decision time. There are thus indications of a treatment effect, but they are not of major significance and could well be affected by bias in the data.

Several interactions, outliers and non-linearities are present, but as they are not of major significance, it seems that the assumptions for the analysis of covariance are reasonable. However, as only a few predictor variables were examined, conclusions cannot be drawn for the entire data set.

The results are given in detail in CKOMP 89/32.

- Seeding Material Examinations

As mentioned above, concern was also felt that the "seed and sample" treatment is not in fact a single treatment, in that the amount of seeding material dispensed differs from storm to storm. So does the number of turrets that are penetrated in order to dispense this material, and the time spent flying through the turrets. Attempts were initially made to analyse these variables together with the other variables in the analyses of covariance, despite the fact that the only legal covariates are those independent of the treatment. It was hoped that these analyses would show whether an adjustment for these variables was in fact necessary. However, the high correlation of these variables with the treatments resulted in nonsensical results (the estimates of the adjusted treatment means for the no seed and sample treatment were large but negative for all variables - a physical impossibility). Deletion of these variables from the analyses of covariance yielded more sensible results.

An alternative check as to the importance of the seeding material amount was then carried out by testing the significance of these variables for the seed and sample data, and significance of the other two variables was checked using the no seed and sample data set. The analyses showed no significant relation to these three parameters in most cases.

Further Analyses of Covariance

A further analysis consisted of again performing analyses of covariance for all non-control variables (that is, track properties 11 to 240), with the predictor variables being examined being the control properties (track properties 1 to 10 and 241 to 250) on the new data set. Tests were then carried out as to the significance of the differences between the three adjusted means (μ_1, μ_2 and μ_3), using randomization testing. Where there is sufficient data, compared to the number of covariates included, a test of the hypothesis that the same regression line can be used for all three treatments was also included. The hypothesis was accepted in almost all cases where a significant difference in means was found. Cases where the analysis indicated that different regression lines were appropriate still need to be investigated.

Several of these analyses of covariance gave significant results (confirmed by randomization tests), when all predictor variables were included in the equation, and these results are listed in table 3 (for the three condition data set) and table 4 (for the four condition data set), together with the estimates of the adjusted treatment means. (The randomization significance is also given.) The results for the analysis for seed versus no seed (for the three condition data set) are given in table 5.

Even though some of the covariates in these analyses are non-significant, the estimates of adjusted treatment means will be unbiased. However, if one wishes to interpret the regressions, it is sensible to remove non-significant variables. The question of possibly omitted covariates has not been addressed, nor has the question of interactions or of quadratic or higher order effects. However, those variables examined by means of AID indicate that the overriding effect is a linear effect, with interactions being present in a weak form. The residual plots examined do not indicate the presence of nonlinear (quadratic or cubic) effects.

Table 3 Variables for which the analysis of covariance is significant (Three condition data set)

		-10 to 0 minutes		
Variable	Significance	Mean 1	Mean 2	Mean 3
25	.016	255.20	226.23	238.79
29	.034	6.565	9.006	7.797
69	.005	6.379	9.630	6.782
85	.014	6.191	8.587	8.274
103	.037	5.659	5.739	3.084
110	.007	5.597	2.489	2.581
169	.031	0.621	1.190	0.804
		0 to 10 minutes		
14	.036	4.736	5.690	2.517
47	.025	0.036	-0.002	-0.374

(continued)

48	.013	0.305	0.306	0.090
58	.012	0.057	0.052	0.021
61	.016	6.009	6.035	2.993
64	.001	0.285	0.281	0.065
74	.044	0.248	0.214	0.034
77	.002	5.112	5.676	1.471
79	.017	0.034	0.049	-0.352
80	.002	0.309	0.302	0.056
103	.043	5.378	3.803	2.445
122	.027	4.478	5.632	2.142
143	.002	5.165	5.879	1.375
145	.034	0.015	0.020	-0.099
164	.023	1.158	0.579	0.511
185	.023	1.803	1.318	2.842
201	.042	36.493	36.798	35.934
202	.040	37.059	37.429	36.530
216	.005	32.461	32.767	32.534
217	.004	32.411	33.198	32.618
220	.003	-0.000	0.002	0.000
230	.029	0.003	0.001	0.003
		10 to 20 minutes		
119	.022	51.868	52.809	49.188
121	.018	49.956	50.924	46.905
126	.037	39.930	40.423	38.499
135	.047	39.349	39.996	37.801
140	.044	40.190	40.097	36.780
149	.027	5593.0	5668.8	3912.8
169	.014	0.569	0.238	0.251
184	.046	1.186	0.509	0.876
202	.026	36.684	36.976	35.984
222	.048	37.683	37.829	36.614
		20 to 30 minutes		
129	.009	2.026	4.320	5.396
131	.034	-0.028	-0.008	0.012
		30 to 40 minutes		
151	.005	3.279	.441	1.373
159	.018	0.065	-.045	-.029
160	.025	.111	.046	.031

TABLE 4 Variables for which the analysis of covariance is significant (Four condition data set)

		-10 to 0 minutes		
Variable	Significance	Mean 1	Mean 2	Mean 3
25	.016	255.20	226.23	238.79
29	.034	6.565	9.006	7.797
69	.005	6.379	9.630	6.781
85	.014	6.191	8.587	8.274
103	.037	5.659	5.739	3.084
110	.007	5.597	2.489	2.581
169	.031	0.621	1.190	0.804
		0 to 10 minutes		
25	.021	315.20	309.60	244.74
26	.044	0.265	0.285	0.107
27	.013	43.050	44.021	35.342
28	.015	259.16	265.21	213.40
31	.048	0.098	0.103	-0.158
32	.012	0.254	0.258	0.103
39	.038	0.059	0.078	-0.247
40	.018	0.278	0.275	0.102
47	.019	0.023	-0.013	-0.404
48	.006	0.306	0.315	0.075
58	.015	0.057	0.054	0.020
61	.019	5.948	5.726	2.981
64	.001	0.293	0.283	0.059
77	.005	5.038	5.391	1.324
79	.012	0.036	0.034	-0.371
80	.002	0.321	0.305	0.047
87	.044	0.073	0.116	-0.206
88	.049	0.278	0.282	0.128
89	.048	0.428	0.274	0.188
119	.046	53.043	54.212	51.904
121	.028	51.179	51.871	49.665
122	.017	4.591	5.357	2.046
124	.037	-0.010	0.023	-0.049
125	.043	0.040	0.061	0.019
126	.044	40.722	41.317	39.878
143	.003	5.011	5.731	1.281
145	.029	0.017	0.019	-0.104
164	.039	1.121	0.652	0.480
172	.047	-0.363	-0.503	-0.655
185	.014	1.763	1.417	2.924
201	.023	36.551	36.831	36.011
202	.022	37.125	37.495	36.628
206	.049	4.645	4.825	4.254
207	.032	5.127	5.349	4.755
216	.003	32.460	32.783	32.530
217	.001	32.406	33.230	32.581
220	.002	-0.000	0.002	0.000
230	.031	0.003	0.002	0.004

(continued)

Variable	Significance	10 to 20 minutes		
		Mean 1	Mean 2	Mean 3
119	.021	51.926	53.064	49.182
121	.016	50.006	51.187	46.893
126	.021	39.956	40.630	38.481
128	.040	38.766	39.479	37.458
133	.020	40.602	41.639	39.035
135	.022	39.322	40.362	37.820
140	.042	40.235	40.262	36.673
149	.023	5614.8	5695.4	3801.9
167	.044	1511.0	1543.8	1228.9
169	.015	0.561	0.247	0.241
202	.013	36.699	37.069	35.945
221	.039	36.733	37.259	35.965
222	.020	37.670	38.073	36.619
226	.024	4.322	4.872	3.740
227	.024	4.878	5.412	4.313
228	.022	3.777	4.250	3.097
234	.013	0.001	0.000	0.001
239	.040	0.007	0.002	0.004
		20 to 30 minutes		
129	.015	2.115	3.504	5.544
131	.038	-0.031	-0.016	0.012
138	.031	-0.038	-0.015	0.017
147	.036	5796.3	6334.5	4070.6
237	.010	35.472	33.042	33.706
		30 to 40 minutes		
151	.012	3.251	0.745	1.276

TABLE 5 Tests for seed versus no seed variables significant on the three condition data set

Variable	Significance	-10 to 0 minutes	
		Mean 1	Mean 2
25	.045	253.33	235.14
29	.017	6.566	[illegible].277
85	.006	6.246	8.336
110	.001	5.557	2.561
113	.032	5.424	-1.719
160	.031	0.119	0.057
169	.017	0.618	0.977
184	.039	1.581	2.337

(continued)

		0 to 10 minutes	
Variable	Significance	Mean 1	Mean 2
94	.048	1.222	0.680
103	.018	5.325	3.070
105	.047	-0.005	-0.042
164	.010	1.155	0.542
172	.027	-0.376	-0.578
174	.012	0.002	0.001
216	.005	32.452	32.642
217	.005	32.389	32.885
220	.009	-0.000	0.001
		10 to 20 minutes	
12	.050	2.348	1.416
142	.046	38.715	35.178
145	.036	-0.033	-0.145
164	.031	0.758	0.399
169	.002	0.570	0.245
184	.033	1.201	0.700
239	.020	0.007	0.003
		20 to 30 minutes	
124	.038	-0.047	-0.003
129	.004	2.054	4.824
131	.029	-0.027	0.001
143	.046	2.319	4.193
145	.027	-0.143	-0.005
237	.013	35.225	32.881
239	.039	0.008	0.002
		30 to 40 minutes	
104	.020	3.829	2.069
159	.008	0.065	-0.038
160	.005	0.111	0.040
214	.048	0.000	0.001

Since it is not possible to address these questions for all variables involved, it was decided to choose a few variables of particular interest, and to investigate these in depth. The variables chosen as dependent variables were variables 52 (mean area at 3°) and 68 (mean rain flux at 3°) A number of variables were considered as covariates - track properties 1 to 10 and 241 to 250 as before, as well as 36, 52 68, 84 and 149 from the before decision time period. These combinations were also examined as single variable regressions, and are described in the next section.

With respect to the analyses of covariance, it was found that there was no significant difference between the adjusted treatment means for these variables, although the regression part of the analysis of covariance was significant. Plots did not give any indication of a requirement for a quadratic or higher effect, although this is still being investigated.

4.3 Regression Analyses Requested by the Scientific Director

Linear regression relationships for certain variables (13, 20, 28, 36, 52, 60, 68, 76, 84, 95, 102) of the PAWS data were investigated (on the old data set), and are reported on in CKOMP 89/25. The aim of the investigation was to see if the total post-decision time response can be predicted from the pre-decision time responses, and to see if this relationship differs between seeded and unseeded storms. Reasonably good regressions exist for the predictor variables mean area at 3°, mean mass for the whole storm, mean volume, mean area at cut-off and mean precipitable water, but no significant differences were found between the regression relationships for the different treatments. Suitable transformations of the data and removal of possible outliers did not improve the fit of the model, or change the significance due to treatment.

Simple linear regression relationships (predicting the dependent variable from one predictor variable only) were also investigated for the variables involved in the detailed analysis of covariance investigations, as is mentioned above (thus being on the new data set). The regressions were again estimated allowing for separate intercept and slope terms for the different treatments, but, as before, the test as to whether separate slopes and intercepts were needed proved nonsignificant. These results are discussed fully in CKOMP 89/33.

5. CONCLUSIONS

The analyses have shown that there is a bias in the data set, with the volume in particular differing between the three treatment groups. In view of this, and as most variables correlate highly with volume, it is not possible to state that the other variables that differ significantly between the treatments do so because of the treatment effect.

The analyses of covariance, used to test for differences between the treatment means after the bias has been taken into account, show several variables to be significant, particularly in the 0 to 10 minute period. However, several variables in the before decision time period are also significant, indicating that the analyses of covariance have not been totally successful in adjusting for bias.

6. REFERENCES

1. Brillinger D R, Jones L V and Tukey J W. Statistical Task Force to the Weather Modification Advisory Board. 1978. The Management of Weather Resources. Volume II: The role of statistics.

2. Edgington, E S, 1987. Randomization Tests. Marcell Dekker.

3. Gabriel K R, 1979. Some statistical issues in weather experimentation. Communications in Statistics - Theory and Methods, A8(10), pp975-1015.

4. Hawkins and Kass (1982). Automatic Interaction Detection. In Hawkins D M (ed.) (1982). Topics in Applied Multivariate Analysis. Cambridge University Press, Cambridge.

5. Heymann C, 1981. XAID - An Extended Automatic Interaction Detector. SWISK 28, National Research Institute for Mathematical Sciences, CSIR.

6. Simpson Weather Associates and Cansas International Corporation, 1986. Program for Atmospheric Water Supply, 1983-1986 Final Report.

APPENDIX A

BASIC RADAR VARIABLES

1	Centroid X	
2	Centroid Y	
3	Centroid Z	
4	Reflectivity weighted centroid Z	
5	Top	
6	Base	
7	Volume	Total
8	Volume	< 20 dBz
9	Volume	20 - 25 dBz
10	Volume	25 - 30 dBz
11	Volume	30 - 35 dBz
12	Volume	35 - 40 dBz
13	Volume	40 - 45 dBz
14	Volume	45 - 50 dBz
15	Volume	50 - 55 dBz
16	Volume	55 - 60 dBz
17	Volume	60 - 65 dBz
18	Volume	65+ dBz
19	Area at 3 deg	
20	Mean reflectivity at 3 deg	
21	Rain flux at 3 deg	
22	Area at cutoff altitude	
23	Mean reflectivity at cutoff altitude	
24	Rain flux at cutoff altitude	
25	Area at 3 deg	< 20 dBz
26	Area at 3 deg	20 - 25 dBz
27	Area at 3 deg	25 - 30 dBz
28	Area at 3 deg	30 - 35 dBz
29	Area at 3 deg	35 - 40 dBz
30	Area at 3 deg	40 - 45 dBz
31	Area at 3 deg	45 - 50 dBz
32	Area at 3 deg	50 - 55 dBz
33	Area at 3 deg	55 - 60 dBz
34	Area at 3 deg	60 - 65 dBz
35	Area at 3 deg	65+ dBz
36	Mass	Ground level - 2500 m
37	Mass	2500 - 4000 m
38	Mass	4000 - 5500 m
39	Mass	5500 - 7000 m
40	Mass	7000 - 8500 m
41	Mass	8500 - 10 000 m
42	Mass	10 000 - 11 500 m
43	Mass	11 500 - 13 000 m
44	Mass	13 000 - 14 500 m
45	Mass	14 500 - 16 000 m
46	Mass	16 000 - 17 500 m
47	Mass	17 500+m
48	Peak reflectivity	Ground level - 2500 m
49	Peak reflectivity	2500 - 4000 m
50	Peak reflectivity	4000 - 5500 m
51	Peak reflectivity	5500 - 7000 m
52	Peak reflectivity	7000 - 8500 m

53	Peak reflectivity	8500 - 10 000 m
54	Peak reflectivity	10 000 - 11 500 m
55	Peak reflectivity	11 500 - 13 000 m
56	Peak reflectivity	13 000 - 14 500 m
57	Peak reflectivity	14 500 - 16 000 m
58	Peak reflectivity	16 000 - 17 500 m
59	Peak reflectivity	17 500+m
60	Mean reflectivity	
61	Peak reflectivity	
62	Height of peak reflectivity	
63	Maximum height of 45 dBz echo	
64	Track number	

APPENDIX B
TRACK PROPERTIES

GROUP 1 - GEOMETRY, TIME
1 Duration of storm
2 Time of origin
3 Speed of movement
4 Direction of movement
5 Mean X coordinate
6 Mean Y coordinate
7 Mean range
8 Envelope decision time
9 Volume at decision time
10 Peak dBz at decision time

GROUP 2 - TOP, DEPTH, VOLUME, MASS
11 Echo top - maximum
12 Echo top - maximum rate of increase
13 Echo top - mean
14 Echo top - time to maximum
15 Echo top - time to maximum rate of increase
16 Echo top - persistence
17 Echo top - maximum ratio
18 Depth - maximum
19 Depth - maximum rate of increase
20 Depth - mean
21 Depth - time to maximum
22 Depth - time to maximum rate of increase
23 Depth - persistence
24 Depth - maximum ratio
25 Volume - maximum
26 Volume - maximum rate of increase
27 Volume - time integral
28 Volume - mean
29 Volume - time to maximum
30 Volume - time to maximum rate of increase
31 Volume - persistence
32 Volume - maximum ratio
33 Mass for whole storm - maximum
34 Mass for whole storm - maximum rate of increase
35 Mass for whole storm - time integral
36 Mass for whole storm - mean
37 Mass for whole storm - time to maximum
38 Mass for whole storm - time to maximum rate of increase
39 Mass for whole storm - persistence
40 Mass for whole storm - maximum ratio
41 Mass above cutoff altitude - maximum
42 Mass above cutoff altitude - maximum rate of increase
43 Mass above cutoff altitude - time integral
44 Mass above cutoff altitude - mean
45 Mass above cutoff altitude - time to maximum
46 Mass above cutoff altitude - time to maximum rate of increase
47 Mass above cutoff altitude - persistence
48 Mass above cutoff altitude - maximum ratio

GROUP 3 - AREA, RAIN, PRECIPITATION, RATIOS
49 Area 3 degrees - maximum
50 Area 3 degrees - maximum rate of increase
51 Area 3 degrees - time integral
52 Area 3 degrees - mean
53 Area 3 degrees - time to maximum
54 Area 3 degrees - time to maximum rate of increase
55 Area 3 degrees - persistence
56 Area 3 degrees - maximum ratio
57 Area cutoff - maximum
58 Area cutoff - maximum rate of increase
59 Area cutoff - time integral
60 Area cutoff - mean
61 Area cutoff - time to maximum
62 Area cutoff - time to maximum rate of increase
63 Area cutoff - persistence
64 Area cutoff - maximum ratio
65 Rain flux 3 degrees - maximum
66 Rain flux 3 degrees - maximum rate of increase
67 Rain flux 3 degrees - mass
68 Rain flux 3 degrees - mean
69 Rain flux 3 degrees - time to maximum
70 Rain flux 3 degrees - time to maximum rate of increase
71 Rain flux 3 degrees - persistence
72 Rain flux 3 degrees - maximum ratio
73 Rain flux cutoff - maximum
74 Rain flux cutoff - maximum rate of increase
75 Rain flux cutoff - mass
76 Rain flux cutoff - mean
77 Rain flux cutoff - time to maximum
78 Rain flux cutoff - time to maximum rate of increase
79 Rain flux cutoff - persistence
80 Rain flux cutoff - maximum ratio
81 Precipitable water - maximum
82 Precipitable water - maximum rate of increase
83 Precipitable water - time integral
84 Precipitable water - mean
85 Precipitable water - time to maximum
86 Precipitable water - time to maximum rate of increase
87 Precipitable water - persistence
88 Precipitable water - maximum ratio
89 Mass time integral/rain mass - 3 degrees
90 Mass time integral/rain mass - cutoff
91 Mean mass/rain mass - 3 degrees
92 Mean mass/rain mass - cutoff

GROUP 4 - VERTICAL CENTROIDS
93 Vertical centroid - maximum
94 Vertical centroid - maximum rate of increase
95 Vertical centroid - mean
96 Vertical centroid - time to maximum
97 Vertical centroid - time to maximum rate of increase
98 Vertical centroid - persistence
99 Vertical centroid - maximum ratio
100 Z weighted vertical centroid - maximum
101 Z weighted vertical centroid - maximum rate of increase

102 Z weighted vertical centroid - mean
103 Z weighted vertical centroid - time to maximum
104 Z weighted vertical centroid - time to maximum rate of increase
105 Z weighted vertical centroid - persistence
106 Z weighted vertical centroid - maximum ratio
107 Delta vertical centroid - maximum
108 Delta vertical centroid - maximum rate of increase
109 Delta vertical centroid - mean
110 Delta vertical centroid - time to maximum
111 Delta vertical centroid - time to maximum rate of increase
112 Delta vertical centroid - persistence
113 Delta vertical centroid - maximum ratio

GROUP 5 - SPARE
114 Discriminant function
115 Mass of the 3 degree rain flux/area time integral at 3 degrees
116 Rain flux at 3 degrees at the beginning of the time period of interest
117 Rain flux at 3 degrees at the end of the time period of interest

GROUP 6 - REFLECTIVITY
119 Peak dBz whole storm - maximum
120 Peak dBz whole storm - maximum rate of increase
121 Peak dBz whole storm - mean
122 Peak dBz whole storm - time to maximum
123 Peak dBz whole storm - time to maximum rate of increase
124 Peak dBz whole storm - persistence
125 Peak dBz whole storm - maximum ratio
126 Mean dBz whole storm - maximum
127 Mean dBz whole storm - maximum rate of increase
128 Mean dBz whole storm - mean
129 Mean dBz whole storm - time to maximum
130 Mean dBz whole storm - time to maximum rate of increase
131 Mean dBz whole storm - persistence
132 Mean dBz whole storm - maximum ratio
133 Mean dBz 3 degrees - maximum
134 Mean dBz 3 degrees - maximum rate of increase
135 Mean dBz 3 degrees - mean
136 Mean dBz 3 degrees - time to maximum
137 Mean dBz 3 degrees - time to maximum rate of increase
138 Mean dBz 3 degrees - persistence
139 Mean dBz 3 degrees - maximum ratio
140 Mean dBz cutoff - maximum
141 Mean dBz cutoff - maximum rate of increase
142 Mean dBz cutoff - mean
143 Mean dBz cutoff - time to maximum
144 Mean dBz cutoff - time to maximum rate of increase
145 Mean dBz cutoff - persistence
146 Mean dBz cutoff - maximum ratio
147 Maximum height 45'S - maximum
148 Maximum height 45'S - maximum rate of increase
149 Maximum height 45'S - mean
150 Maximum height 45'S - time to maximum
151 Maximum height 45'S - time to maximum rate of increase
152 Maximum height 45'S - persistence
153 Maximum height 45'S - maximum ratio

154 Height peak dBz - maximum
155 Height peak dBz - maximum rate of increase
156 Height peak dBz - mean
157 Height peak dBz - time to maximum
158 Height peak dBz - time to maximum rate of increase
159 Height peak dBz - persistence
160 Height peak dBz - maximum ratio

GROUP 7 - MASS=F(HEIGHT)
161 Mass=f(height) : mean - mean
162 Mass=f(height) : mean - maximum
163 Mass=f(height) : mean - minimum
164 Mass=f(height) : mean - maximum rate of increase
165 Mass=f(height) : mean - maximum rate of decrease
166 Mass=f(height) : standard deviation - mean
167 Mass=f(height) : standard deviation - maximum
168 Mass=f(height) : standard deviation - minimum
169 Mass=f(height) : standard deviation - maximum rate of increase
170 Mass=f(height) : standard deviation - maximum rate of decrease
171 Mass=f(height) : -skew - mean
172 Mass=f(height) : -skew - maximum
173 Mass=f(height) : -skew - minimum
174 Mass=f(height) : -skew - maximum rate of increase
175 Mass=f(height) : -skew - maximum rate of decrease
176 Mass=f(height) : mode - mean
177 Mass=f(height) : mode - maximum
178 Mass=f(height) : mode - minimum
179 Mass=f(height) : mode - maximum rate of increase
180 Mass=f(height) : mode - maximum rate of decrease

GROUP 8 - PEAK(DBZ)=F(HEIGHT)
181 dBz=f(height) : mean - mean
182 dBz=f(height) : mean - maximum
183 dBz=f(height) : mean - minimum
184 dBz=f(height) : mean - maximum rate of increase
185 dBz=f(height) : mean - maximum rate of decrease
186 dBz=f(height) : standard deviation - mean
187 dBz=f(height) : standard deviation - maximum
188 dBz=f(height) : standard deviation - minimum
189 dBz=f(height) : standard deviation - maximum rate of increase
190 dBz=f(height) : standard deviation - maximum rate of decrease
191 dBz=f(height) : -skew - mean
192 dBz=f(height) : -skew - maximum
193 dBz=f(height) : -skew - minimum
194 dBz=f(height) : -skew - maximum rate of increase
195 dBz=f(height) : -skew - maximum rate of decrease
196 dBz=f(height) : mode - mean
197 dBz=f(height) : mode - maximum
198 dBz=f(height) : mode - minimum
199 dBz=f(height) : mode - maximum rate of increase
200 dBz=f(height) : mode - maximum rate of decrease

GROUP 9 - %VOLUME=F(DBZ)
201 %Volume=f(dBz) : mean - mean
202 %Volume=f(dBz) : mean - maximum
203 %Volume=f(dBz) : mean - minimum

204 %Volume=f(dBz) : mean - maximum rate of increase
205 %Volume=f(dBz) : mean - maximum rate of decrease
206 %Volume=f(dBz) : standard deviation - mean
207 %Volume=f(dBz) : standard deviation - maximum
208 %Volume=f(dBz) : standard deviation - minimum
209 %Volume=f(dBz) : standard deviation - maximum rate of increase
210 %Volume=f(dBz) : standard deviation - maximum rate of decrease
211 %Volume=f(dBz) : -skew - mean
212 %Volume=f(dBz) : -skew - maximum
213 %Volume=f(dBz) : -skew - minimum
214 %Volume=f(dBz) : -skew - maximum rate of increase
215 %Volume=f(dBz) : -skew - maximum rate of decrease
216 %Volume=f(dBz) : mode - mean
217 %Volume=f(dBz) : mode - maximum
218 %Volume=f(dBz) : mode - minimum
219 %Volume=f(dBz) : mode - maximum rate of increase
220 %Volume=f(dBz) : mode - maximum rate of decrease

GROUP 10 - %3 DEGREES AREA=F(DBZ)
221 %Area=f(dBz) : mean - mean
222 %Area=f(dBz) : mean - maximum
223 %Area=f(dBz) : mean - minimum
224 %Area=f(dBz) : mean - maximum rate of increase
225 %Area=f(dBz) : mean - maximum rate of decrease
226 %Area=f(dBz) : standard deviation - mean
227 %Area=f(dBz) : standard deviation - maximum
228 %Area=f(dBz) : standard deviation - minimum
229 %Area=f(dBz) : standard deviation - maximum rate of increase
230 %Area=f(dBz) : standard deviation - maximum rate of decrease
231 %Area=f(dBz) : -skew - mean
232 %Area=f(dBz) : -skew - maximum
233 %Area=f(dBz) : -skew - minimum
234 %Area=f(dBz) : -skew - maximum rate of increase
235 %Area=f(dBz) : -skew - maximum rate of decrease
236 %Area=f(dBz) : mode - mean
237 %Area=f(dBz) : mode - maximum
238 %Area=f(dBz) : mode - minimum
239 %Area=f(dBz) : mode - maximum rate of increase
240 %Area=f(dBz) : mode - maximum rate of decrease

GROUP 11 - CONTROL
241 Average mixing ratio for the lowest 60 mb
242 Cloud condensation level temperature
243 Buoyancy at 500 mb
244 Temperature at cloud condensation level/buoyancy at 500 mb
245 Number of tracks for the day
246 Cumulative 3 degrees area time integral for the day
247 Maximum volume of any storm for the day
248 Maximum rate of increase of volume for the day
249 Maximum tops of any storm for the day
250 Maximum dBz of any storm for the day